

UNCLASSIFIED

AD NUMBER
AD913771
NEW LIMITATION CHANGE
TO Approved for public release, distribution unlimited
FROM Distribution authorized to U.S. Gov't. agencies only; Test and Evaluation; 31 AUG 1973. Other requests shall be referred to Air Force Avionics Laboratory, Attn: NVA-698DF, Wright-Patterson AFB, OH 45433.
AUTHORITY
AFAL ltr, 21 Sep 1978

THIS PAGE IS UNCLASSIFIED

AFAL-TR-73-260

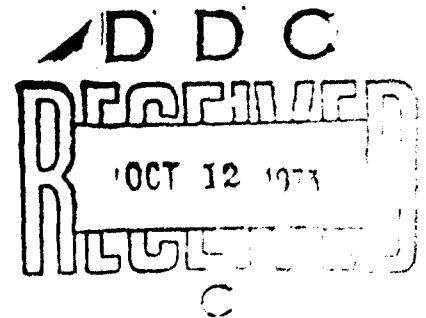
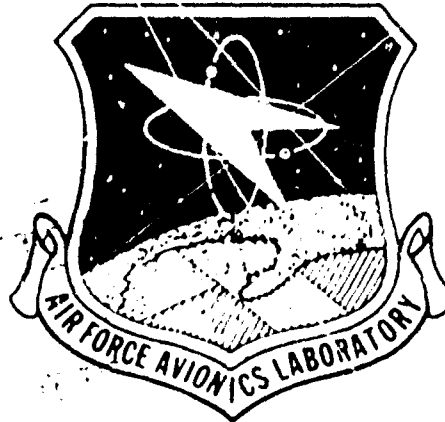
PERFORMANCE SYNTHESIS OF
ELECTRO-OPTICAL SENSORS

Frederick A. Rosell
Robert H. Willson

WESTINGHOUSE DEFENSE AND ELECTRONIC SYSTEMS
Systems Development Division
Baltimore, Maryland

TECHNICAL REPORT
AFAL-TR-73-260

August 1973



Distribution limited to United States government agencies only; test and evaluation; 31 August 1973. Other requests for this document must be referred to Air Force Avionics Laboratory (HVA-698DP), Wright-Patterson Air Force Base, Ohio 45433

AIR FORCE AVIONICS LABORATORY
Air Force Systems Command
Wright Patterson Air Force Base, Ohio

NOTICE

When Government drawings, specifications, or other data are used for any purpose other than in connection with a definitely related Government procurement operation, the United States Government thereby incurs no responsibility nor any obligation whatsoever; and the fact that the Government may have formulated, furnished, or in any way supplied the said drawings, specifications, or other data, is not to be regarded by implication or otherwise as in any manner licensing the holder or any other person or corporation, or conveying any rights or permission to manufacture, use, or sell any patented invention that may in any way be related thereto.

Copies of this report should not be returned unless return is required by security considerations, contractual obligations, or notice on a specific document.

**PERFORMANCE SYNTHESIS OF
ELECTRO-OPTICAL SENSORS**

**Frederick A. Rosell
Robert H. Willson**

Distribution limited to United States Government agencies only;
test and evaluation 31 August 1973. Other requests for this
document must be referred to Air Force Avionics Laboratory
(NVA-698DF), Wright Patterson Air Force Base, Ohio 45433

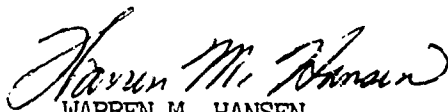
FOREWORD

This program involved the refinement of mathematical models and performance of psychophysical experiments as part of the continuation effort of the 698DF development project for a high-resolution low-light-level television system for tactical airborne application. These studies have led to a better understanding of motion and MTF effects of electro-optical sensors and the use of the results can lead to more realistic system specifications and a reduced need for costly laboratory and flight testing of systems.

The Air Force Project Director on this program was Frank A. McCann, AFAL/NVA(698DF). The Westinghouse effort was conducted principally by Frederick A. Rosell and Robert H. Willson. The program was performed by the Westinghouse Systems Development Division, Baltimore, Maryland, under Air Force Contract F33615-70-C-1461.

This report was submitted by Frederick A. Rosell and Robert H. Willson.

This technical report has been reviewed and is approved for publication.



WARREN M. HANSEN
Acting Deputy Director
Navigation & Weapon Delivery Division

ABSTRACT

This effort is a continuation of the Performance Synthesis Study, Electro-Optical Sensors reported in Technical Report AFAC-TR-72-229, dated August 1972. Analytical models were further developed and refined to include image motion and aperturing effects. Psychophysical experiments were performed as tests of the theories and it was found that the theory is reasonably accurate. A concept of balanced resolution is defined which combines a system's performance for both aperiodic and periodic imagery. The question of a single figure of merit for a system is also discussed.

TABLE OF CONTENTS

<u>Section</u>	<u>Page</u>
I INTRODUCTION AND SUMMARY	1
II RANGE ANALYSIS AND MODEL UPDATE.	9
2.1 The Sensors Model and Observer Requirements.	9
2.2 Passive Television Imaging System.	27
2.3 Active Television Imaging Systems.	45
2.4 Effects of Image Motion.	49
2.5 The Balanced Resolution Concept.	75
III DISPLAY SIGNAL-TO-NOISE RATIO FUNDAMENTALS	81
3.1 The Elementary Model	81
3.2 The Effect of Finite Apertures on Image Detail	99
3.3 Effect of Apertures on Signal-to-Noise Ratio	118
IV EFFECTS OF IMAGE MOTION.	121
4.1 Psychophysical Experiments Involving Image Motion.	122
4.2 Analysis of Sensor Motion Data	129
V PSYCHOPHYSICAL EXPERIMENTS INVOLVING SENSOR MTF.	139
VI FIGURE OF MERIT.	167
6.1 MTF Related Image Quality Parameters	168
6.2 Signal-to-Noise Ratio Related Image Quality Parameters	175
REFERENCES	180

LIST OF ILLUSTRATIONS

<u>Figure</u>		<u>Page</u>
1	Location of Points of Noise Insertion Relative to the MTF's.	14
2	Video Output Waveforms for a Single Isolated Bar and a Repetitive Bar Pattern.	18
3	Levels of Object Discrimination. Object Area to be Used in the SNR_D Calculations is Δy by L	22
4	Equivalent Bar Pattern Criteria for Object Identification.	22
5	Probability vs Normalized SNR_{DI} . For Any Probability Value. Obtain SNR_{DI} from Table 3 for 50% Probability. Find Value of k for Desired Probability and Multiply Value of SNR_{DI} by k to Obtain New Values of SNR_{DI}	26
6	MTF and MTF Related Function for the Assumed Sample System.	29
7	Display Signal-to-Noise Ratio vs Spatial Frequency for the Assumed System at Various Average Input Photocathode Currents for Bar Pattern Images.	30
8	Display Signal-to-Noise Ratio vs Spatial Frequency for the Assumed System at Various Average Input Photocathode Currents for Aperiodic Images.	31
9	Threshold Resolution vs Average Input Photocurrent for the Assumed System with Input Image Modulation Contrast of 1.0	33
10	Threshold Resolution vs Average Input Photocurrent for the Assumed System with Input Modulation of 0.1	34
11	Threshold Angular Resolution vs Average Input Photocurrent for the Assumed System with Various Input Image Modulation Contrasts. Threshold Resolution is Based on the Balanced Resolution Concept. Angle Corresponds to One Line Width	38

<u>Figure</u>		<u>Page</u>
12	Ratio of Apparent to Inherent Contrast vs Range for Various Values of Sky-to-Ground Ratio for a Meteorological Visibility of 10 Nautical Miles.	42
13	Ratio of Image Contrast at Range R to that at Range Zero for a Meteorological Visibility of 20 Nautical Miles and Sky-to-Ground Ratios of 1.4 and 7.0	42
14	Threshold Resolution vs Range for a Meteorological Visibility of 20 Nautical Miles and Sky-to-Ground Ratios of 1.4 and 7.0	43
15	Threshold Angular Resolution vs Range for a Meteorological Visibility of 20 Nautical Miles and Sky-to-Ground Ratios of 1.4 and 7.0	43
16	Threshold Angular Resolution for Bar Patterns vs Range for the Assumed TV Camera as a Function of Input Image Contrast for a 20 nmi Visibility and a Sky/Ground Ratio of 1.4	44
17	Threshold Angular Resolution for Bar Patterns vs Range for the Assumed TV Camera as a Function of Input Image Contrast for a 20 nmi Visibility and a Sky/Ground Ratio of 7.0	44
18	Average Input Photocurrent for the Assumed System vs Range for an Average Scene Reflectivity of 0.3	47
19	MTF and MTF Related Quantities for the 16/16/16 mm I-EBSICON Camera Used in the Assumed System	48
20	Display Signal-to-Noise Ratio vs Spatial Frequency for the Assumed Active System for an Inherent Image Contrast of 0.5 and a Visibility of 20 nmi. Calculations are based on the Aperiodic Image Model.	50
21	Display Signal-to-Noise Ratio vs Spatial Frequency for the Assumed Active Systems for an Inherent Image Contrast of 0.5 and a Visibility of 20 nmi Calculations Based on the Periodic Image Model.	51
22	Threshold Resolution in Lines/Pict. Ht. for the Assumed Active System vs. Range. Inherent Image Contrast is 0.5	52

<u>Figure</u>		<u>Page</u>
23	Threshold Resolution in Angular Subtense of a Single Line vs Range for the Assumed Active System. Inherent Contrast is 0.5.	52
24	Effect of Image Motion on Bar Patterns of Various Spatial Frequencies.	56
25	Modulation Transfer Function Due to Linear Image Motion Plotted to Second Zero for Various Bar Pattern Velocities Expressed in Terms of Time for Pattern to Transverse Picture Width.	58
26	Spatial Frequency and the Corresponding Angular Motion for the Assumed System for which the Signal Modulation is Zero as a Function of Bar Pattern Motion (Linear).	59
27	Modulation Transfer Function Due to Linear Image Motion vs Spatial Frequency Normalized to the Cut-Off Frequency.	60
28	Modulation Transfer Function for Linear Image Motion . . .	61
29	Waveforms of Image Displacement and Velocity vs Time . . .	61
30	Modulation Transfer Function vs Bar Pattern Spatial Frequency for Sinusoidal Motion of Peak Amplitude of 100, 50, and 25 Microradians per Exposure Time for the Assumed System	63
31	Cut-Off Frequency and the Angular Subtense of Cut-Off Frequency Line Width vs the Peak-to-Peak Angular Amplitude of Sinusoidal Motion	64
32	Modulation Transfer Function for Sinusoidal Motion vs Spatial Frequency Normalized to the Cut-Off Frequency.	65
33	Modulation Transfer Function for Sinusoidal Image Motion	65
34	Modulation Transfer Function for the Assumed System with Random Image Motion of RMS Amplitude 25, 50, and 100 Microradians per Exposure Time	67
35	Cut-Off Spatial Frequency and Angular Subtense of Corresponding Period for the Assumed System as a Function of the RMS Angular Motion per Exposure Time. Angular Subtense is Shown as Solid Line.	68

<u>Figure</u>		<u>Page</u>
36	Modulation Transfer Function vs Spatial Frequency Normalized to the Cut-Off Frequency for Random Image Motion.	69
37	Modulation Transfer Function for Random Image Motion. . . .	69
38	Modulation Transfer Function for Static System and Scene and for System with Scene in Random Motion of RMS Amplitude 50 Microradians with 660 mm Focal Length Lens	70
39	Threshold Resolution vs Input Photocurrent for the Assumed Sensor with a Static Scene and with Random Motion of the Sightline of Magnitude 25 and 40 μ rad. $C_M = 0.3$	70
40	Threshold Angular Resolution vs Input Photocurrent for the Assumed Sensor with a Static Scene and with Random Motion of the Sightline of Magnitude 25 and 50 μ rad. $C_M = 0.3$	71
41	Threshold Angular Resolution vs Input Photocathode Current Based on the Periodic, Aperiodic and the Average Calculated for the Threshold Resolution in Lines/Pict. Ht. $C_M = 0.1$	72
42	Threshold Angular Resolution vs Input Photocathode with a Random Motion of Amplitude 50 microrad RMS for a WAV and NAV. $C_M = 0.1$	73
43	Ratio of Threshold Angular Resolution in NAV to that in WAV with Random Sightline Motion of Amplitude 50 microrad RMS. $C_M = 0.1$	73
44	Threshold Angular Resolution vs Input Photocurrent Based on the Periodic, Aperiodic and the Average Calculated for Threshold Angular Resolution in Microradians. $C_M = 0.1$	78
45	Corrected Probability of Detection vs SNR_{DI} Required for Rectangular Images of Size 4×4 , 4×64 , 4×128 and 4×180 Lines.	86
46	Threshold SNR_{DI} vs Bar Pattern Spatial Frequency for Display-to-Observer Viewing Distance of $14'$, $28''$ and $56''$	87
47	Threshold Video SNR vs Bar Pattern Spatial Frequency for a Video Bandwidth of 10^7 Hz	88

<u>Figure</u>		<u>Page</u>
48	Effect of an Aperture on a Point and Line Source Image	90
49	Schematic of the Input-Output Relationship for an Aperture.	96
50	Illustration of the Effect of an Aperture of Effective Duration $x_0/\alpha = 1.0$ on a Rectangular Input Image in Both the Space and Fourier Domains for $x_0/\alpha = 2.0$	97
51	Fourier Spectra of Unit Amplitude Rectangular Input Pulses of Duration $x_0/\alpha = 8$ and 4. Also shown is the Optical Transfer Function for a Gaussian Impulse Response of Effective Duration $x_0/\alpha = 1.0$	99
52	The Effect of a Gaussian Impulse Response on (-) Unit Amplitude Rectangular Input Pulses of Duration 16, 8, 4, and 1. Output Waveshape is Shown as Dashed Curve. . . .	99
53	Relative Output Pulse Amplitude vs the Width of a Unit Amplitude Rectangular Pulse after Filtering by a Gaussian Aperture of Effective Duration $x_0/\alpha = 1.0$	100
54	Equivalent Output Pulse Width vs the Width of a Unit Amplitude Rectangular Input Pulse of Width x_0/α After Passing Through a Gaussian Aperture of Equivalent Width $x_0/\alpha = 1.0$	101
55	Increase in Noise Perceived by an Observer Due to an Increase in Effective Image Size Due to an MTF Preceding a Point of Noise Insertion	103
56	Signal and Noise Diagram for the Case of an Aperiodic Image with Noise Added Subsequent to an Aperture.	104
57	Normalized Function $F(N)/F(0)$ vs Spatial Frequency and ΔB_N the Noise Equivalent Bandwidth	107
58	(a) Aperture Following a Point of Noise Insertion, and (b) Functional Noise Diagram for (a).	112
59	Apertures Which Both Follow and Precede Points of Noise Insertion	116
60	Schematic of an EBSICON Camera Tube	119
61	Experimental Set Up for Motion Experiments.	122

<u>Figure</u>		<u>Page</u>
62	Corrected Probability vs Display Signal-to-Noise Ratio for Target Recognition-Speed 10 Sec/Picture Height; Tank \circ , Truck \square , Derrick \bullet , Radar Truck \diamond , Televised Images at 875 Lines, 25 Frames/Sec, $D_V/D_H = 3.5$	124
63	Relative Response vs Spatial Frequency for Motion Experiment \square Static Case with Blower on, \circ Pure Motion, 10 Sec/Picture Height for a Frame Time 1/25 Sec.	128
64	Relative Response vs Spatial Frequency--Measured for 10 Sec/Picture Height \blacksquare , Theoretical \bullet	128
65	Static Amplitude Response for WX 31841.	131
66	Dynamic Amplitude Response for Pattern Speed of 60 Second/Picture Width \square $V_T = 20V$, \blacksquare $V_T = 7.5V$ for WX 31841--Solid Curve Static Case, \bullet Theoretical. . . .	132
67	Dynamic Amplitude Response for Pattern Speed of 20 Seconds/Picture Width \square $V_T = 20V$, \blacksquare $V_T = 7.5V$ for WX 31841--Solid Curve Static Case, \bullet Theoretical. . . .	132
68	Dynamic Amplitude Response for Pattern Speed of 10 Seconds/Picture Width \square $V_T = 20V$, \blacksquare $V_T = 7.5V$ for WX 31841--Solid Curve Static Case, \bullet Theoretical. . . .	133
69	Build Up Lag \bullet , Delay Lag \circ As a Function of Target Voltage for WX 31911	134
70	Gamma, γ for Different Target Voltages for WX 31911.	134
71	Dynamic Sensitivity for 100% Contrast Pattern, $V_T = 20$ volts \circ static, \bullet 60 Sec/P.W., \square 20 Sec/P.W., \blacksquare 10 Sec/P.W., \diamond 5 Sec/P.W. Bandwidth 12 MHz.	136
72	Dynamic Sensitivity for 100% Contrast Pattern, $V_T = 7.5$ volts \circ Static, \bullet 60 Sec/P.W., \square 20 Sec/P.W., \blacksquare 10 Sec/P.W., \diamond 5 Sec/P.W. Bandwidth 12 MHz.	136
73	Dynamic Sensitivity for 35% Contrast Pattern, $V_T = 20$ volts \circ Static, \blacksquare 10 Sec/P.W., Bandwidth 12 MHz.	137
74	Dynamic Sensitivity for 35% Contrast Pattern, $V_T = 7.5$ volts, \circ Static, \blacksquare 10 Sec/P.W., Bandwidth 12 MHz.	137

<u>Figure</u>		<u>Page</u>
75	Experimental Set-Up for the Televised Camera Generated Imagery	140
76	Modulation Transfer Functions for Case A ● , Case B ○ , and Case C □ . Lens and Camera Combined	141
77	Bar Patterns of Variable Aspect, Isolated Bars and Isolated Circles Used for Experiments	142
78	Bar Patterns of Constant Aspect Used for Experiments. . . .	143
79	Exp. No. 1 and 2. Threshold SNR_{DI} for ● Original Data and Present Data ○ Minimum Illumination Back- Ground □ 1 ft-Lambert Background--Constant Aspect Pattern Case A MTF.	148
80	Exp. No. 2 Probability of Bar Pattern Recognition Versus Display Signal-to-Noise Ratio for Case A MTF, 1 ft-Lambert Monitor and 1 ft-Lambert Back- ground Bar Pattern Spatial Frequency ○104, ● 200, □ 329, ■ 396, ◇ 482, ◆ 635 AF 5 Bar.	148
81	Exp. No. 3 Threshold SNR_{DI} for ● Original Data and Present Data 1 ft.-Lambert Background ○ Normal, □ Very Critical Threshold Judgment--Constant Aspect Pattern Case A MTF.	141
82	The Display Signal-to-Noise Ratio Experiment.	150
83	Exp. No. 4 Threshold SNR_{DI} for Electronically Generated Squares ○ New Data, □ Old Data.	151
84	Exp. No. 5 Probability of Bar Pattern Recognition Constant Aspect Bars--Case B MTF Spatial Frequency ○ 104, ● 200, □ 329, ■ 396, ◇ 482, ◆ 635	153
85	Exp. No. 5 Threshold SNR_{DI} for Constant Aspect Bar Patterns Case B MTF	153
86	Exp. No. 6 Probability of Bar Patterns Recognition for Case C, Constant Aspect Bar Patterns Spatial Frequency ○ 104, ● 200, □ 329	154
87	Exp. No. 6 Threshold SNR_{DI} for Case C, Constant Aspect Patterns	154
88	Threshold SNR_{DI} for AF 5 Bar Pattern Case A ● , Case B ○ , Case C □ MTF's	155

<u>Figure</u>		<u>Page</u>
89	Probability of Bar Patterns Recognition for Constant Length Bar Patterns--Case A MTF.	156
90	Exp. No. 7 Comparison of Threshold SNR_{DI} for Case A MTF, ● Constant Length, ■ Constant Aspect Bar Patterns	157
91	Exp. No. 7 and 8 Comparison of Threshold SNR_{DI} for Constant Length Bar Patterns Case A ○, Case C □ MTF's.	157
92	Exp. No. 9 and 10 Threshold SNR_{DI} for Isolated Bars for Case A ○, Case C □ MTF's, ◇ Electronically Generated Squares.	158
93	Exp. No. 11 and 12 Threshold SNR_{DI} for Isolated Circles for Case A ○, Case C □ MTF's, ◇ Electronically Generated Squares	159
94	Photographs of Models Used for Recognition Experiments--Upper Left, Tank; Upper Right, Van Truck; Lower Left, Half Truck with Antenna; and Lower Right, Derrick Half Truck.	160
95	Exp. No. 13 Tactical Target Recognition for Case A MTF ○ Tank, ● Derrick, □ Truck, ◇ Radar Truck.	162
96	Exp. No. 14 Tactical Target Recognition for Case C MTF ○ Tank, ● Derrick, □ Truck, ◇ Radar Truck.	163
97	Waveform of Derrick Half Truck Along the Horizontal as a Function of Vertical Position of Scan Lines	164
98	Two Modulation Transfer Functions. Curve A illustrates a High, Low Frequency Response while Curve B illustrates a High, High Frequency Response.	167
99	MTF, Equivalent Bandwidth N_b and Noise Equivalent Bandwidth, N_e vs Spatial Frequency for a Typical 40/40/25 I-EBSICON Camera Tube	168
100	Output Waveshape (-) for a Step Function Input (---). Shape of Output Waveshape, $\Delta g_1 / \Delta x_1$ is used to Find Image Acutance	172
101	Display Signal-to-Noise Ratio Obtainable (-) and Required (---) for Two Light Levels as a Function of Spatial Frequency	176

LIST OF TABLES

<u>Table</u>	<u>Page</u>
1 Levels of Object Discrimination.	21
2 Johnson's Criteria for the Resolution Required per Minimum Object Dimensions vs Discrimination Level.	21
3 Best Estimate of Threshold SNR_{DI} for Detection, Recognition and Identification of Images	25
4 Assumed TV and Scene Parameters.	28
5 Typical Values of the Sky-to-Ground Ratio.	40
6 Values a/A and SNR_V Used for Motion Experiment	124
7 Parameters Used in Calculating SNR_D for Aperiodic Target	126
8 Value of N_{eT} and N_{eL} and Overall N_{eLT} for Three Cases. . . .	141
9 Line Numbers and Rev Aspect for Various Patterns	144
10 Experimental Conditions.	147

1.0 Introduction and Summary

The objectives of the Performance Synthesis Study — Electro-Optical Sensors — performed under Air Force Contract Number F33615-70-C-1461 are to determine the fundamental limitations of long range air-to-ground detection, recognition and identification of tactical military targets, to determine methods of realizing maximum range performance through optimum spatial, temporal and electrical filtering of the received image signals and to devise methods of predicting maximum range performance taking into account the parameters of real targets, backgrounds, illumination sources, atmospherics and sensory systems. The results are to be applicable to all imaging sensors whether passive or active and are to include low-light-level television, forward-looking infrared scanners and direct view light amplifiers.

The current effort is a continuation of the programs previously reported in Ref. 1 (Technical Report AFAL-TR-71-137, May 1971) and Ref. 2 (Technical Report AFAL-TR-72-229). As before, the approach taken is to devise analytical models to describe sensory system performance including the observer as an integral part of the system. Psychophysical experiments are performed to obtain the necessary constants of the observers to quantitatively evaluate the analytical models. Through these efforts, it is hoped to promote a better understanding of the operation of electro-optical sensors, guide the further development of systems components, improve methods of sensory system

performance and reduce the necessity of costly laboratory and flight evaluation of prototype systems.

In the previous efforts reported, the early emphasis in analysis and experimentation was on images of simple or regular geometry such as rectangles and bar patterns. Real images of tactical objects were also considered with a concerted effort to correlate the discernability of bar patterns with various levels of real object discrimination -- particularly real object recognition and identification. Some success with the equivalent bar pattern approach was realized as noted in Ref. 2. However, further efforts were, and still are, required.

The discernability of an image projected onto the photosurface of an electro-optical sensor and ultimately displayed to an observer is limited by the sensor's sensitivity to the received radiation and by noises generated either in the primary photoconversion process or in subsequent signal processing. Also, the image's discernability is limited by finite sensor apertures that decrease the image modulation. Preliminary efforts to account for the effects of these apertures were reported in Ref. 1. The theory, then presented, though leading to reasonable system predictions was intuitively unsatisfying. An advanced theory was presented in Ref. 2 that was more satisfying but still had deficiencies -- particularly in the treatment of aperiodic (rectangular) images.

Concurrent with the effort reported in Ref. 2, a separate effort was undertaken under Air Force Contract Number F33615-70-C-1461 by Sendall and Rosell to analyze FLIR and TV on a common basis. In this program, the aperiodic image treatment was considerably improved due in

large part to Sendall. These advances in the modeling are reported herein in some detail. While much of the ground work for the present models must be attributed to Otto Schade, Sr., the translation of the theory to practice has not proved trivial.

The performance synthesis program as presently constituted is a relatively small program. Specifically, it involves the part time efforts of the authors and the not inconsiderable efforts of many motivated and dedicated Westinghouse engineers who volunteer their efforts in the tedious psychophysical experimentation.

In each of the continuation efforts, there has been an effort to focus on the most critical problems involved in the image discrimination task. In this most recent effort, we have elected to concentrate on the areas of image aperture effects and image motion which are closely allied problems.

In the early days of airborne television, wide fields of view were the rule. Typically, viewfields were $30^{\circ} \times 40^{\circ}$ which are comparable within a factor of 2, to the viewfield of the unaided eye. Scene resolution observed on the display was also comparable to that which could be observed by the unaided eye in the daytime. With passage of time, viewfields have become ever narrower, with fields of view as small or smaller than 1° becoming usual. Under many conditions, the TV augmented observer's resolution of scene detail substantially exceeds that which he can resolve directly. While narrower fields of view have led to longer scene object detection ranges, range cannot be extended indefinitely by simply reducing viewfield. In the more modern systems, the resolution of scene detail is limited not by the lens or TV camera,

but by sightline instability. In TV practice, the effect of sightline instability is to blur the image during the TV image exposure time. These sightline instability effects are analytically considered in some detail in Section 2. Psychophysical experiments using moving images were performed and the results are reported in Section 4. In the psychophysical experimentation, recognition experiments were performed using images moving laterally across the field of view. The primary effect of the motion was to degrade resolution in the horizontal leaving the vertical unchanged (except for some vibration induced in the camera sightline due to the motion apparatus). Efforts were made to model the motion effects. Some apparent success is noted but the efforts must be considered preliminary. Moving image experiments represent a high level of difficulty. In any given experiment, it is difficult to separate the effects of motion interacting with the exposure time from the effects of motion on sensor lag. Also, it is difficult to both define and measure signal levels using complex imagery. However, the initial efforts reported herein are essential to obtain a feel for the magnitude of the problems involved and to form a base for further effort.

To lay the groundwork for the modulation transfer function experiments, we develop the theory of apertures in great detail in Section 3. This includes the latest treatment of the effects of apertures on aperiodic images. In the evolution of the sensor models, aperiodic and periodic images are separately treated. Using these models, it is found that simple aperiodic images can be detected at much longer ranges

than periodic images both in principle and in practice. Preliminary efforts were made to develop a "balanced" resolution concept as discussed in Section 2. The balanced resolution concept is felt to have merit when based on the average angular scene resolution (rather than the average limiting resolution based on threshold spatial frequency). The preferred averaging technique weights the periodic model more heavily which is felt to be in the right direction.

The detailed theory of apertures developed in Section 3 is used to update the model of Section 2 and, as we noted, to serve as a foundation for the MTF related psychophysical experimentation having to do with both image motion and fixed sensor apertures. The theory of the effect of apertures is well developed and mathematically rigorous. However, the observer is an integral part of the system and the mathematical rigor must therefore include the human element and thus the theory must be confirmed through psychophysical experiments. To our knowledge, experiments to confirm the theory have not been performed except to show first order effects.

The psychophysical experimentation reported in Section 5 is devoted to modulation transfer function effects. Different MTF characteristics were obtained by defocusing of the camera's objective lens. Specified in terms of Schade's noise equivalent passband, N_e , the best MTF had an N_e of 252 and the poorest had an N_e of 69. The experiments made with constant aspect and constant length bar patterns appear to indicate that the current theory yields results that are somewhat pessimistic for MTF's with low N_e (poor MTF). Experiments with isolated bars and circles indicate that the theory

correctly accounts for the MTF effects. Using images of real objects (vehicles), it was found that the results predicted on the basis of theory are again pessimistic but to a lesser extent than that predicted for the periodic patterns. The periodic theory of apertures thus appears to need further work.

For many years, researchers in the optical field have sought a single unit figure of merit for sensory systems. Whether such a unit has much in the way of practical merit is open to debate but in the quest, a better understanding of the parameters that determine image quality should evolve. In Section 6, a number of the figures of merit previously proposed are reviewed. Most of the figures of merit involve some integral of the modulation transfer function or equivalently, the integral of the point spread function. A primary difference between various measures is the weight applied to the functions before integrating.

Most of the figures of merit do not include sensitivity or signal-to-noise as a parameter. Thus a sensor with a very high figure of merit may be far inferior to one with a low figure in a given application. For example, a very high resolution vidicon would be inferior to a low resolution ILLTV when a night scene is to be viewed. When signal-to-noise ratio is included as a parameter, the figure of merit usually ceases to be a single number but rather, becomes a function. In recent work, attempts have been made to include sensitivity and noise in the figure of merit. The concept is to integrate the area between the signal curve and the noise curve (with signals and noises expressed as a function of spatial frequency). The principal deficiency of

this scheme is the problem of selecting the low frequency limit.

It is clear that finding a single figure of merit for a sensory system is highly unlikely. The figure of merit will undoubtedly be a function and will include both sensitivity and resolution parameters. The threshold resolution vs photosurface irradiance characteristic of a sensor, used extensively by television designers, is a figure-of-merit function based on bar pattern inputs. This characteristic includes the sensor sensitivity, MTF and noise parameters but the characteristic may not be in the most useful form and it has not been related to a picture quality criterion. A figure of merit based on the threshold resolution characteristic has been proposed by Schade and will be discussed in the follow-on efforts.

2.0 Range Analysis and Model Update

In this section, we shall review the efforts made during the current program to improve the analytical electro-optical-sensor-augmented observer model and show the practical application of the model to imaging systems. In Section 2.1, the sensor model and observer requirements, as previously reported in Refs. 1 and 2 and updated in this report, are discussed. The model is applied to a passive electro-optical imaging system in Section 2.2 and to an active electro-optical imaging system in Section 2.3. In these sections, the scene is assumed to be stationary relative to the sensor. In Section 2.4, the effects of relative image motion on overall system performance will be taken into account to the extent that these effects are now understood. In all of these analyses, the emphasis is in determining the range at which specific scene objects can be detected, recognized and identified under varying scene and atmospheric conditions. In Section 2.5, a balanced resolution concept is discussed.

2.1 The Sensor Model and Observer Requirements

The analysis and experimentation discussed in this report and the two which preceded it are based on the concept that signal-to-noise ratio can be associated with a scene object after it has been imaged by a lens and phototransduced by a photosensitive surface. The image is then further processed by the electro-optical system. In this processing, signal-to-noise ratio is lost. Knowing the system parameters, the amount lost can be readily calculated for images of simple or regular geometric shape.

Eventually, the sensor recreates a visible light image on a display which may be directly viewed by an observer. With good design, the electro-optical sensor displays the image with sufficient size and luminance to insure that the observer will not be acuity or light-level limited. If this is the case, the system determines the image signal-to-noise ratio and not the observer's eye except that, due account must be taken of the ability of the observer to integrate over the area of the image and to integrate over a period of time.

In the elementary sensory system model reviewed in Section 3.1, it is assumed that the displayed image is signal limited by the image's size and irradiance level and further limited by noises generated either in the scene photon-to-sensor-photoelectron conversion process or by the system itself. Then, it is shown that the image's discernability can be further reduced by the sensor's finite apertures. By finite apertures, we mean those elements or processes in the sensor which cause a blurring of the image. In an ideal sensor, a point object would be imaged as a point on the display. In a real system, the lens causes the point to become a blur circle in the image plane due to diffraction, lack of focus and aberration effects. The image may then be further blurred by fiber-optic faceplates, electron lens defects, phosphor particles, lateral spread in charge storage targets and the finite diameters of electron beams. Some blurring effects are intentionally introduced. For example, the horizontal resolution in a TV camera may be video bandwidth limited and the display beam may be intentionally defocused in the vertical to minimize the raster structure. These blurring effects on the image are quantitatively described in terms of the optical transfer functions of individual

system elements and are taken into account in analyzing the image signal-to-noise ratios.

The observer is an integral part of a real time imaging system and the system's overall performance must take the observer's requirements into account. For simplicity, we divide the total imaging problem into three parts which are: the properties of the scene, the capability of the imaging system and the requirements of the observers. The ability of the observer to resolve imaged scene detail is determined by matching the signal-to-noise ratio of an image appearing on the output of the electro-optical sensor's display to that required by the observer to discern the image at a given level of detail.

The properties of the scene will be discussed in the next two sections. In this section, we will concentrate on the sensor and observer requirements. We note first that the lens images the scene on the input photosurface which converts the scene photons to photoelectrons. The rate at which the photoelectrons are generated can be described in terms of a current, i . In the development of the elementary model, it was found that the signal-to-noise ratio of an image appearing on the display of a typical television camera could be written as

$$\text{SNR}_D = \left[\frac{t}{\alpha} \left(\frac{a}{A} \right) \right]^{\frac{1}{2}} \frac{2G_M G_i i_{av}}{[eG^2 i_{av} + I_p^2 / 2\Delta f_V]^{\frac{1}{2}}} \quad (1)$$

where t is the integration time of the observer's eye, a is the image area, α is the picture aspect ratio (W:H), A is the total effective

photosurface area, C_M^* is the image modulation contrast, G is the pre-storage gain of the TV camera tubes gain storage target, i_{av} is the average photocurrent, e is the charge of an electron, I_p^2 is the mean square system (preamplifier) noise added subsequent to the readout of the image by the electron beam and Δf_V is the video bandwidth. In deriving the above equation, it was assumed that the image area, a , is large relative to the overall system blur circle, that the photoelectron image is amplified by an amount, G , before being stored and read out, and that the only sources of noise are the photoelectron noise and the preamp noise, both of which are white in character. When the above conditions prevail, the above equation applies equally well to the detection of simple geometric shapes such as squares or rectangles and to bar patterns. For squares or rectangles, a is the area of the square or rectangle while for bar patterns, a is the area of a single bar. The areas, a , have some restrictions but these restrictions can generally be neglected for the usual class of imaging tasks.

Simple rectangular objects against a uniform background are designated as aperiodic objects while a bar pattern is designated as a periodic object in the direction transverse to the bars. Whether periodic or aperiodic, it is often an analytical convenience to describe the dimensions of the object's image in terms of dimensionless reciprocals, i.e., if the image dimensions are Δx by Δy and if the image plane height is Y , then we define

$$* C_M = (i_{\max} - i_{\min}) / (i_{\max} + i_{\min}).$$

$$N = \frac{Y}{\Delta x} \frac{\text{lines}}{\text{picture height}}, \quad (2)$$

$$N_Y = \frac{Y}{\Delta y} = \frac{Y}{\epsilon \Delta x} = \frac{N}{\epsilon}, \quad (3)$$

where ϵ is equal to the ratio $\Delta y/\Delta x$. The quantity N , when used to describe a bar pattern has the form of a spatial frequency which is a convenience when performing Fourier analysis of the image in the frequency domain.

With Eqs. (2 and 3),

$$\text{SNR}_D = \frac{1}{2} \frac{3V}{p [2\Delta f_V]^2} \quad (4)$$

In the above, the image is a function of x and y . In the following, we will assume that the x and y variables of the image, and of the apertures which blur the image are independent and separable so that the images can be independently analyzed in the x and y directions.

Suppose that the imaging system has two principal apertures, the lens and the camera tube's gain storage target. Let the modulus of the lens' optical transfer function be $|R_{OL}(N)|$ and that of the target be $|R_{OT}(N)|$. The quantities $|R_{OL}(N)|$ and $|R_{OT}(N)|$ are known as the modulation transfer functions or MTFs. The lens MTF precedes the point of photoelectron noise insertion (at the photosurface) while the target follows the point of photoelectron noise insertion but precedes the point of preamplifier noise insertion as shown in Fig. 1.

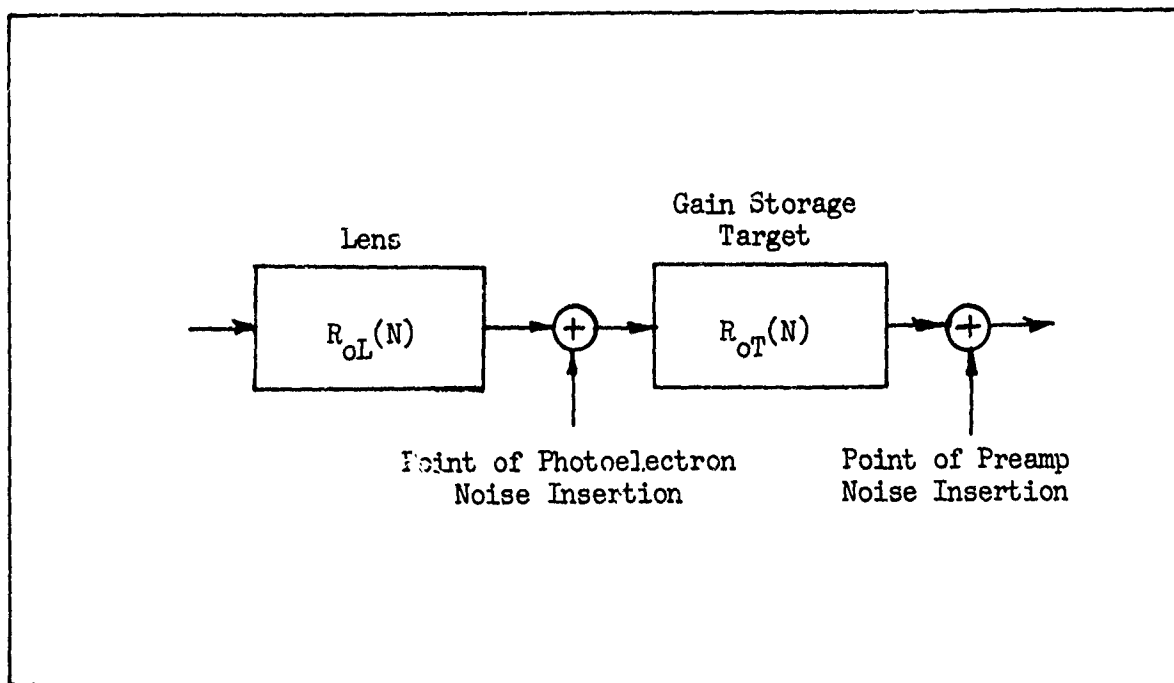


Fig. 1 Location of Points of Noise Insertion Relative to the MTFs.

If the input image is aperiodic, both the lens and target MTFs will increase the noise perceived by the observer. However, the magnitude of the increase depends upon the location of the MTF relative to the point of noise insertion. The lens increases the photoelectron and the preamp noises by the same factor since it precedes both noise insertion points. However, the target filters or bandlimits the photoelectron noise since it follows its point of noise insertion. Thus, the target MTF has a relatively greater effect on the preamp noise than on the photoelectron noise.

The noise increase factor for aperiodic images is given approximately by

$$\xi_{xLT} \cdot \xi_{yLT} = \left[1 + \left(\frac{\delta_L}{\Delta x_i} \right)^2 + \left(\frac{\delta_T}{\Delta x_i} \right)^2 \right]^{\frac{1}{2}} \cdot \left[1 + \left(\frac{\delta_L}{\Delta y_i} \right)^2 + \left(\frac{\delta_T}{\Delta y_i} \right)^2 \right]^{\frac{1}{2}}, \quad (5)$$

where Δx_i and Δy_i are in units of picture heights and, δ_L and δ_T are the noise equivalent apertures defined by the equations

$$\delta_L = \frac{1}{N_{eL}} = \frac{1}{\int_0^\infty |R_{oL}(N)|^2 dN}, \quad (6)$$

$$\delta_T = \frac{1}{N_{eT}} = \frac{1}{\int_0^\infty |R_{oT}(N)|^2 dN}. \quad (7)$$

Note that by Eqs. (2, 3, 6 and 7), Eq. (5) may be written in the equivalent form

$$\xi_{xLT} \cdot \xi_{yLT} = \left[1 + \left(\frac{N}{N_{eL}} \right)^2 + \left(\frac{N}{N_{eT}} \right)^2 \right]^{\frac{1}{2}} \cdot \left[1 + \left(\frac{N}{\epsilon N_{eL}} \right)^2 + \left(\frac{N}{\epsilon N_{eT}} \right)^2 \right]^{\frac{1}{2}}. \quad (8)$$

In the above, it is assumed that the sensor MTF is the same in both the x and y directions. The filtering effect of the target on the photoelectron noise is given by

$$\Gamma_{xT} \cdot \Gamma_{yT} = \frac{\xi_{xLT} \cdot \xi_{yLT}}{\left[1 + \left(\frac{\delta_L}{\Delta x} \right)^2 + 2 \left(\frac{\delta_T}{\Delta x} \right)^2 \right]^{\frac{1}{2}} \cdot \left[1 + \left(\frac{\delta_L}{\Delta y} \right)^2 + 2 \left(\frac{\delta_T}{\Delta y} \right)^2 \right]^{\frac{1}{2}}}, \quad (9)$$

or equivalently,

$$\Gamma_{xT} \cdot \Gamma_{yT} = \frac{\xi_{xLT} \cdot \xi_{yLT}}{\left[1 + \left(\frac{N}{N_{eL}} \right)^2 + 2 \left(\frac{N}{N_{eT}} \right)^2 \right]^{\frac{1}{2}} \cdot \left[1 + \left(\frac{N}{\epsilon N_{eL}} \right)^2 + 2 \left(\frac{N}{\epsilon N_{eT}} \right)^2 \right]^{\frac{1}{2}}}. \quad (10)$$

These results are incorporated into the Eq. (4), as follows

$$\text{SNR}_D = \left[\frac{t_s}{\alpha} \right]^{\frac{1}{2}} \cdot \frac{1}{(\xi_{xLT} \cdot \xi_{yLT})^{\frac{1}{2}} N} \frac{2C_M G_T i_{av}}{\left[G_T^2 e \Gamma_{xT} \Gamma_{yT} i_{av} + \frac{I_p^2}{2\Delta f_V} \right]^{\frac{1}{2}}} \quad (11)$$

As we discussed above, the noise increase factors affect the photoelectron noise and the preamp noise equally but the target exerts a filtering action on the photoelectron noise. We note, however, that the target increases the perceived photoelectron noise more than it filters it.

A bar pattern is periodic in one direction and aperiodic in the other. Assume that the bar pattern is periodic in the x direction. In the periodic x direction, the primary effect of the lens and target will be to decrease the signal modulation and leave noise unchanged. However, as before, the target will exert a filtering effect on the photoelectron noise. The decrease in signal modulation is given by the square wave flux factor, $R_{SF}(N)$. The square wave flux factor is related to the overall system MTF, $|R_{OS}(N)|$, by the formula,

$$R_{SF}(N) = \frac{8}{\pi^2} \sum \frac{|R_{OS}(kN)|}{k^2}, \text{ for } k \text{ odd.} \quad (12)$$

The purpose of this calculation is to convert the signal waveform to a mean signal, i.e., SNR_D is proportional to the mean signal-to-rms noise ratio not the peak-to-peak or rms signal.

The targets filtering action on the photoelectron noise in the

periodic direction is given by

$$\beta_{xT} = \int_0^N \frac{|R_{oT}(N)|^2}{N} dN . \quad (13)$$

Using Eqs. (12 and 13) in Eq. (4), we obtain

$$SNR_D = \left[\frac{t_s}{\alpha} \right]^{\frac{1}{2}} \frac{R_{SF}(N)}{(\xi_{yLT})^{\frac{1}{2}N}} \frac{2G_M G_T i_{av}}{[G_T^2 e \Gamma_{yT} \beta_{xT} i_{av} + I_p^2 / 2\Delta f_V]^{\frac{1}{2}}} . \quad (14)$$

In the above, we have observed that the image is aperiodic in the y direction so that the noise increase factor is

$$\xi_{yLT} = \left[1 + \left(\frac{N}{\epsilon N_{eL}} \right)^2 + \left(\frac{N}{\epsilon N_{eT}} \right)^2 \right]^{\frac{1}{2}} , \quad (15)$$

and the noise filtering factor is

$$\Gamma_{yT} = \frac{\xi_{yLT}}{\left[1 + \left(\frac{N}{\epsilon N_{eL}} \right)^2 + 2 \left(\frac{N}{\epsilon N_{eT}} \right)^2 \right]^{\frac{1}{2}}} , \quad (16)$$

for the y direction. Ordinarily, the bars in the pattern are quite long ($\epsilon \gg 1$) relative to their spacing so that the noise increase and filtering factors in the y direction can be neglected (but not always).

The Eqs. (11 and 14) are used to determine the image signal-to-noise ratio obtainable from the sensor for images of simple or regular geometry. In the previous effort (Ref. 2), it was postulated that the detectability of these simple geometric images could be correlated with the detectability, recognizability and identifiability of real images by suitably selecting an equivalent simple image.

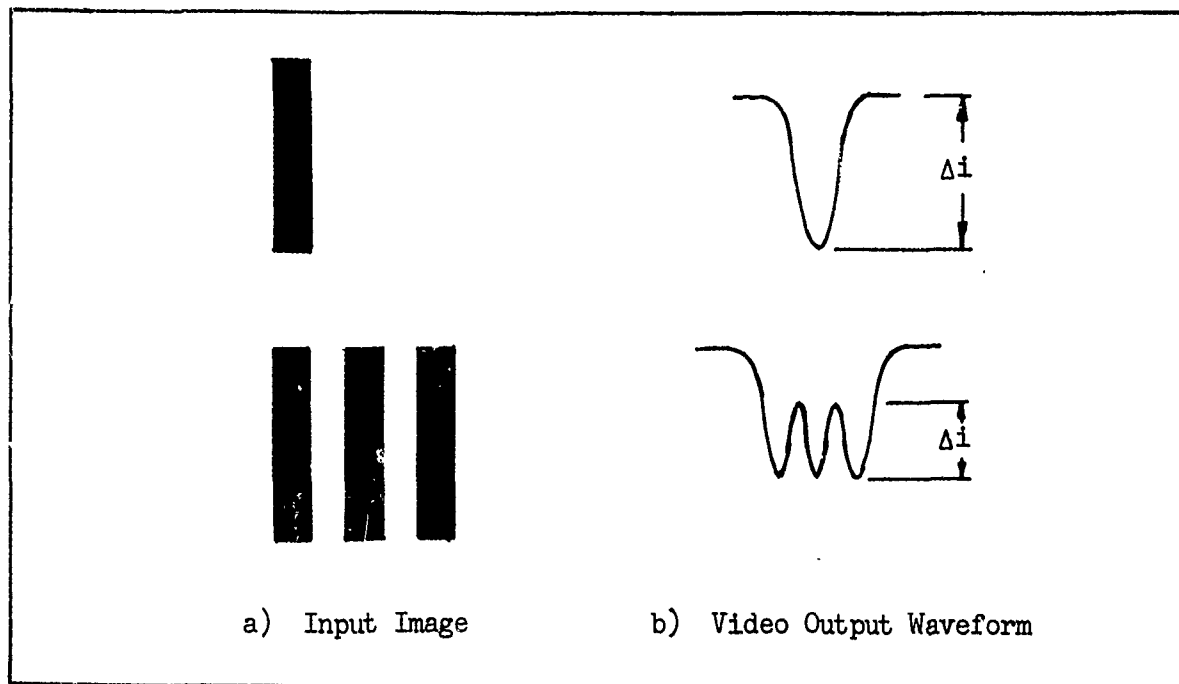


Fig. 2 Video Output Waveforms for a Single Isolated Bar and a Repetitive Bar Pattern.

In Fig. 2a, an isolated single bar is shown along with a bar pattern. The width of the single bar is equal to the width of the bars or spaces in the bar pattern. The expected waveform of the images traverse to their width is shown as they might appear in the video channel in Fig. 2b. Although the irradiance level of the single bar is the same as for the bar pattern, the incremental signal, Δi , is larger for the single bar than for bars within the bar pattern due to the sensor's modulation transfer function. We have postulated in the past, that an observer, in detecting the presence of a bar pattern, must detect the presence of a single bar in the bar pattern. We have found that this postulate is reasonable and that the signal-to-noise ratio needed by the observer to detect the presence of an isolated bar is approximately the same as the signal-to-noise ratio needed to detect the bar in the bar pattern.

However, as was illustrated in Fig. 2, the signal obtainable from the sensor is larger for the isolated bar than it was for the bar in the bar pattern.

Thus, the SNR_D as calculated using aperiodic objects using Eq. (11) can be expected to be larger than the SNR_D using Eq. (14). This will be of consequence as we attempt to correlate the detectability of real scene object with the detectability of simple geometric test objects.

A real scene hardly ever consists of periodic or isolated aperiodic objects. An example of an isolated aperiodic object is an aircraft imaged against a clear sky background. A recently plowed or cultivated field might qualify as a periodic scene object. When the object qualifies as an isolated aperiodic object, the Eq. (11) is directly applicable and similarly the Eq. (14) qualifies when the scene is periodic. In general, specific scene objects are neither periodic or aperiodic (in the sense that we are using aperiodic) but somewhere in between. In the foregoing paragraph, we observed that SNR_D calculated on the basis of an aperiodic object will be larger than the SNR_D calculated for a periodic object. In turn, we will see that system "resolution" will be higher for the aperiodic object than for the periodic object when resolution is specified in terms of the smallest bar width that can be discerned.

In the previous effort (Ref. 2), it was proposed that levels of object discrimination, i.e., detection, orientation, recognition and identification be established along the lines suggested by Johnson (Ref. 3). In this scheme, a scene object is replaced by an equivalent bar pattern. The bar pattern was to be constructed with bar length equal to the length of the object and with bar widths equal to the object's minimum

dimension divided by a factor k_d . The factor k_d is small for low levels of object discrimination such as simple detection or orientation and larger for high levels of discrimination such as recognition or identification. The definitions of the levels of discrimination are given in Table 1 and the discrimination factors, k_d , are tabulated in Table 2. The principal discrimination levels are detection, recognition and identification. The equivalent bar patterns corresponding to these discrimination levels are illustrated schematically in Fig. 3 and the geometric relations from a systems viewpoint for the identification case are illustrated in Fig. 4.

We note that the replacement of an object by an equivalent bar pattern for the detection case involves substantial changes in the detection concept. For an aperiodic object, the SNR_D is based on the total area of the object's image. With the equivalent bar pattern notion, the SNR_D is calculated on the basis of $1/2$ the area. Secondly, for an aperiodic object, the SNR_D is calculated using Eq. (11) while with the equivalent bar pattern approach, SNR_D is calculated using Eq. (14). Again, we note that even for objects of the same image area, SNR_D calculated on the basis of Eq. (11) will be higher than SNR_D calculated on the basis of Eq. (14). On the other hand, the isolated aperiodic case, while it does occur, is unrealistic when used to predict the detectability of the usual terrestrial object amid a low to moderately cluttered background. When objects in severe clutter are to be detected; resolution calculated even on the basis of Eq. (14) for the periodic pattern may be too high. For some situations, it may be necessary to recognize an object to detect it.

<u>Classification of Discrimination Level</u>	<u>Meaning</u>
Detection	An object is present.
Orientation	The object is approximately symmetrical or unsymmetrical and its orientation may be discerned.
Recognition	The class to which the object belongs may be discerned (e.g., house, truck, man, etc.).
Identification	The target can be described to the limit of the observer's knowledge (e.g., motel, pick-up truck, policeman, etc.).

Table 1 Levels of Object Discrimination.

<u>Discrimination Level</u>	<u>Discrimination Factor, k_d, in terms of the Number of Resolution Lines Required per Minimum Object Dimension (TV Lines)</u>
Detection	2.0 ± 1.0 $- 0.5$
Orientation	2.8 ± 0.8 $- 0.4$
Recognition	8.0 ± 1.6 $- 0.4$
Identification	12.8 ± 3.2 $- 2.8$

Table 2 Johnson's Criteria for the Resolution Required per Minimum Object Dimension vs Discrimination Level.

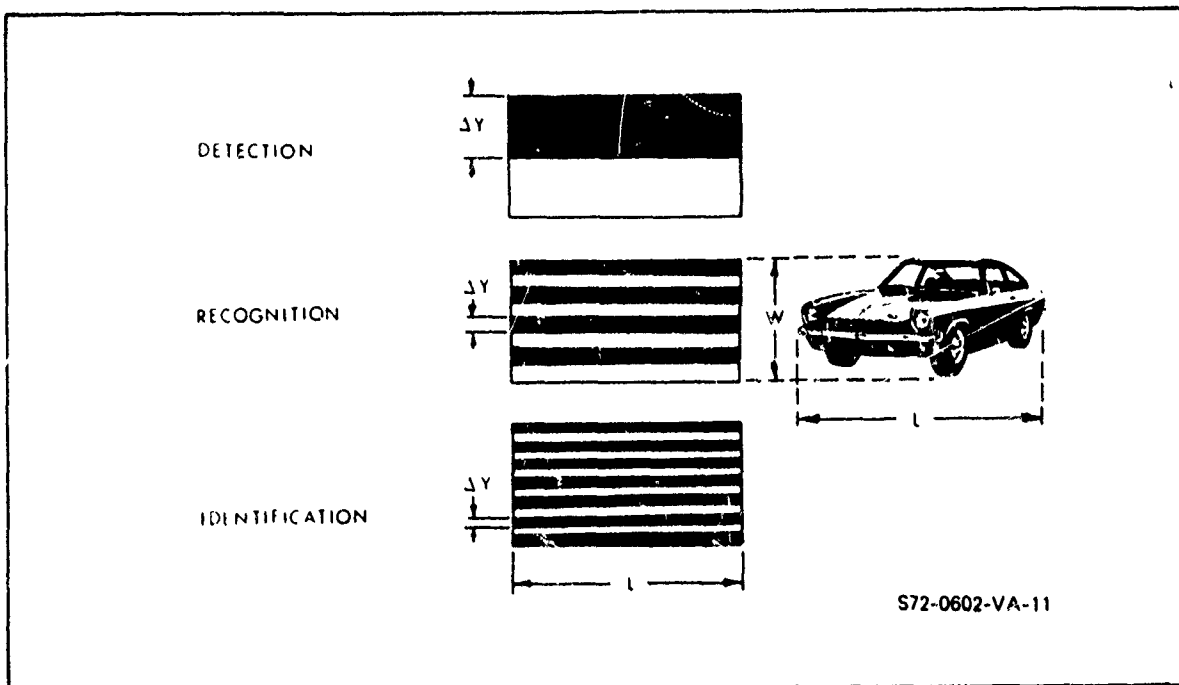


Fig. 3 Levels of Object Discrimination. Object Area to be Used in the SNR_D Calculation is Δy by L .

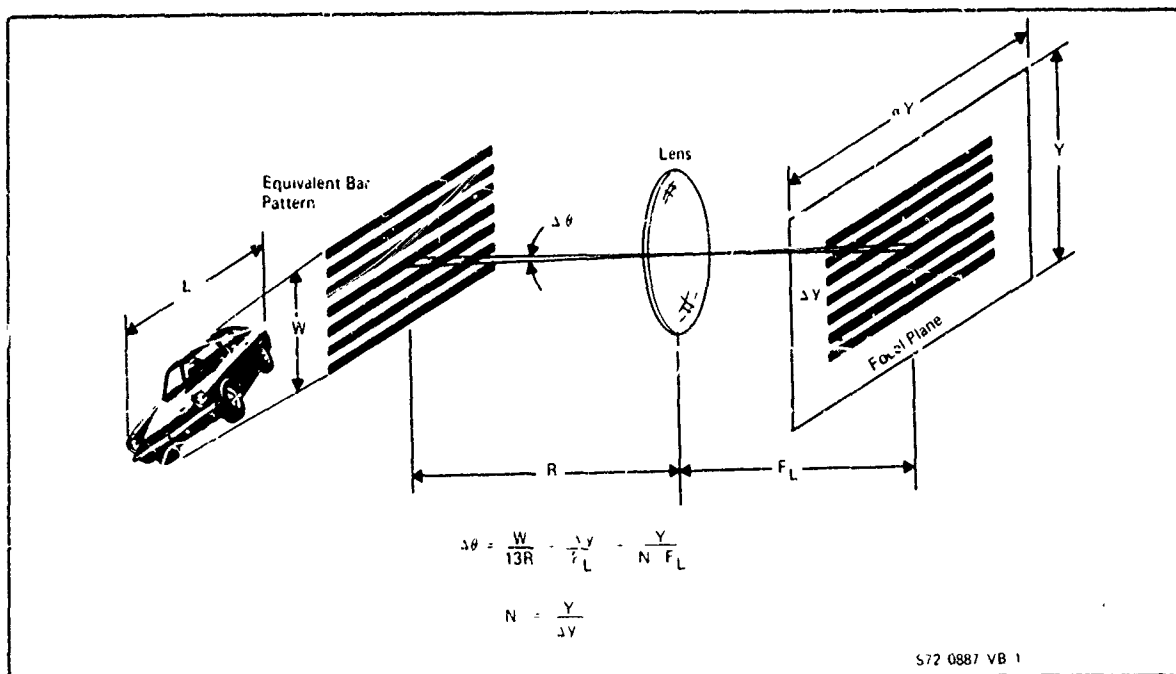


Fig. 4 Equivalent Bar Pattern Criterion for Object Identification

For the recognition case, we face a dilemma similar to the detection case. To recognize an object, it is probable that the objects outline must be discerned with a fairly high degree of clarity. However, the outline is by no means periodic but the prediction of an object's recognizability and identifiability of real scene objects, such as vehicles were correlated with the detectability of an equivalent bar pattern. The correlation, based on the threshold SNR_D required by the observer appeared surprisingly good and perhaps too good because of a difference in the method of calculating signal as we noted at the time. In the case of the real object, we calculated the threshold signal-to-noise ratio on the basis of the peak signal excursion above (or below) background while for the equivalent bar pattern, we used the signal excursion within the bar pattern structure as noted in Fig. 2b. Had we calculated SNR_D for the real object on the basis of the mean signal excursion rather than the peak signal above background, the SNR_D at threshold would have been smaller for the real object.

When the visual task is to detect a truly aperiodic object, such a water tower against the horizon sky, the analysis is clear cut, as noted before. The aperiodic Eq. (11) is used. For more complex scenes or levels of discrimination we suggested in Ref. 2, as a possible compromise, a dual resolution criterion wherein the resolution is first calculated on the basis of an aperiodic object and then on the basis of a periodic object. The overall system resolution is then estimated to be the arithmetic average of the periodic and aperiodic object resolution. It is tentatively proposed that the total object areas are to be chosen in the following manner. Suppose the equivalent scene object

is a rectangle of area equal to the area of the real object, of width approximately equal to the object's minimum dimension and of length approximately equal to the area of the real object's area divided by its width.

However, the SNR_D , and in turn, the resolution, is calculated for an area equal to the width of the equivalent area divided by the discrimination factor of Table 2. For detection, in a moderately cluttered area, the object area, for purposes of calculation, is the equivalent object width divided by 2, times the equivalent object length. This is true for both the periodic and aperiodic image calculation when the dual criterion is used. Similarly, for recognition, the object area for calculation purposes, is the equivalent object width divided by 8, times the equivalent object length.

In calculating resolution, we match the image signal-to-noise ratio obtainable from the sensor to that required by the observer. This usually involves a trial and error or a graphical solution to determine scene object resolution thresholds. A somewhat simpler approach might be to average the SNR_D 's calculated on the periodic/aperiodic bases and calculate resolution thresholds on the average. This could be a good approximation.

The detection of simple aperiodic objects such as squares and rectangles can be precisely predicted. Similarly, we can predict the detectability of periodic bar or sine wave patterns with high accuracy. It can, however, be correctly inferred that the extension of the theory of detection of simple periodic or aperiodic objects to real scene objects is an unprecise art needing considerable further work.

Discrimination		k_d TV Lines per Minimum	Threshold SNR_{DI} for Spatial Frequency (Lines/Pict. Ht.) of			
<u>Level</u>	<u>Background</u>	<u>Dimension</u>	<u>100</u>	<u>300</u>	<u>500</u>	<u>700</u>
Detection	Uniform*	1	2.8	2.8	2.8	2.8
Detection	Clutter	2	4.8	2.9	2.5	2.5
Recognition	Uniform	8	4.8	2.9	2.5	2.5
Recognition	Clutter	8	6.4	3.9	3.4	3.4
Identification	Uniform	13	5.8	3.6	3.0	3.0

* Treated as an Aperiodic Object.

Table 3 Best Estimate of Threshold SNR_{DI} for Detection, Recognition and Identification of Images.

Fortunately, the sensitivity of the equations to the various alternative criteria, when real scene parameters are taken into account, is not large so that reasonable predictions result.

We observed that to obtain resolution predictions, it is necessary to determine observer signal-to-noise ratio requirements. A large number of psychophysical experiments were performed to determine these observer requirements for various visual tasks and were reported in Ref. 2. Further work in this area has been undertaken and is reported in this document. In Ref. 2, the threshold signal-to-noise ratios required by the observer for various levels of object discrimination were experimentally determined using the equivalent bar pattern approach and are noted in Table 3. We note once again that the threshold signal-to-noise ratio values indicated were based on the equivalent bar pattern approach and apply to

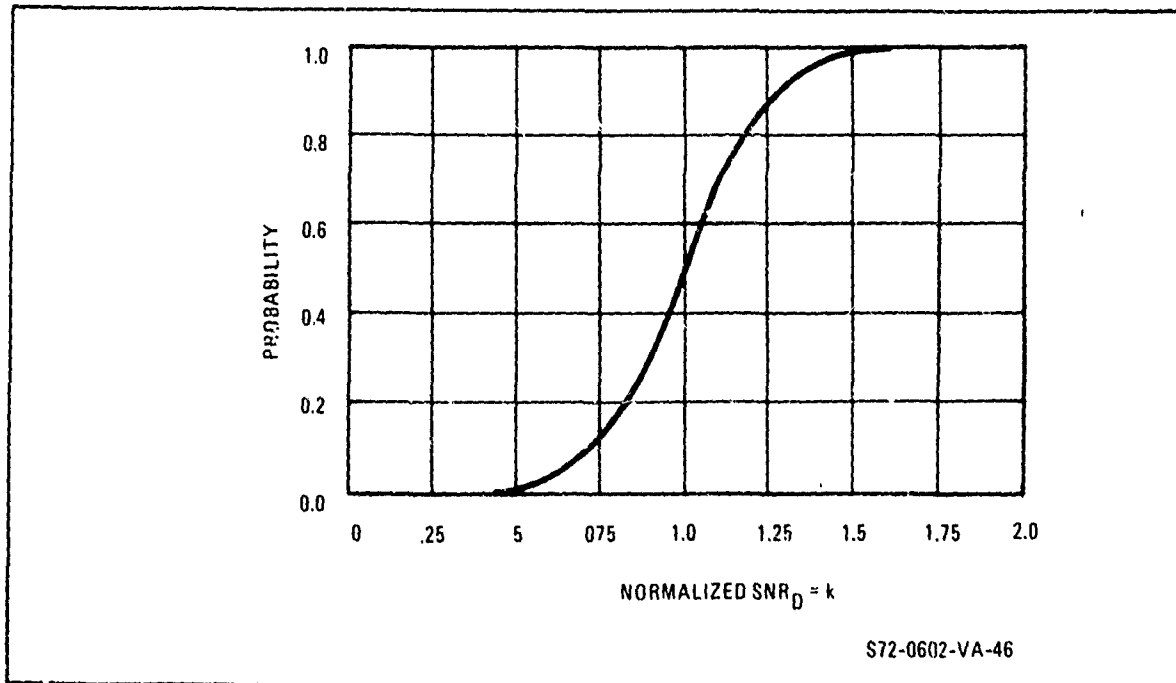


Fig. 5 Probability vs Normalized SNR_{DI} . For Any Probability Value, Obtain SNR_{DI} from Table 3 for 50% Probability. Find Value of k for Desired Probability and Multiply Value of SNR_{DI} by k to Obtain New Value of SNR_{DI} Required.

a fixed observer viewing distance to displayed picture height ratio of 3.5:1 which penalizes the detection of low frequency bar patterns. We also noted in Ref. 2 that the signal-to-noise ratio calculated for the recognition and identification of real objects was performed in a somewhat different manner than for the equivalent bar pattern with the probable result that the SNR_D values of Table 3 are too high. This inequity will be compensated in part by use of the dual periodic-aperiodic image calculation approach.

Again, we note that the resolution prediction equations are not of great sensitivity to the signal-to-noise ratio thresholds. For first cut calculations, we shall assume that the observer requires a signal-to-noise ratio of 3.0 to detect either an aperiodic or periodic object at the 50% level of probability and, that this number is

relatively independent of the equivalent bar pattern's spatial frequency. For other values of probability, the threshold signal-to-noise ratio should be increased by the factor shown in Fig. 5.

With the understandings developed above, we progress to examples of range prediction starting first with the passive scene imaging case followed by the active image case. Initially, we will consider the relative scene camera motion to be zero and then discuss motion as a factor.

2.2 Passive Television Imaging System

A passive imaging system is one which images a scene lighted only by natural scene sources such as the sun, moon, sky or stars. To illustrate the analysis of a passive system, we will consider a specific television telescope with parameters as given in Table 4. This system is primarily intended for daylight use but twilight capability is desired. The level of object discrimination required is the recognition of scene objects which are of essentially square geometry. We will first assume that the scene is stationary and that no atmosphere intervenes between the scene and observer. Then the case of restricted visibility will be considered and later, in Section 2.4, we will consider relative sensor-to-scene motion.

The TV systems MTF and MTF related parameters are given in Table 4 and Fig. 6. The principal MTFs are those of the lens and the camera tube target. Using Eq. (14), the SNR_D is calculated for the periodic equivalent bar pattern and plotted in Fig. 7. Similarly, the SNR_D is calculated using the aperiodic Eq. (11) and are plotted in Fig. 8.

LENS

Field-of-View	$1.13^{\circ} \times 0.85^{\circ}$
Focal Length	660 mm
T/Stop	10
MTF	Fig. 10
Noise Equiv. Bandwidth (N_e)	330 Lines/Pict. Ht.

CAMERA TUBE

Type	16/16 mm EBSICON
Photocathode	
Type	S-25
Responsivity	3.2 mA/W (2854°K Source)
Effective Area	$1.28 \times 10^{-4} \text{ M}^2$
Gain-Storage Target	
Type	Silicon Diode Matrix
Diameter	16 mm
Gain	2 to 2000 (Variable)
Max Average Signal Current	3×10^{-7} Amperes
MTF	Fig. 10
Noise Equiv. Bandwidth	170 Lines/Pict. Ht.

VIDEO PROCESSOR

Preamplifier Noise	6×10^{-9} Ampere
Video Bandwidth	6×10^6 Hz

SCENE

Object Geometry	Square
Level of Discrimination	Recognition
Equivalent Bar Ht. to Width Ratio (ϵ)	8
Irradiance	Variable
Average Reflectivity	0.15

Table 4 Assumed TV and Scene Parameters.

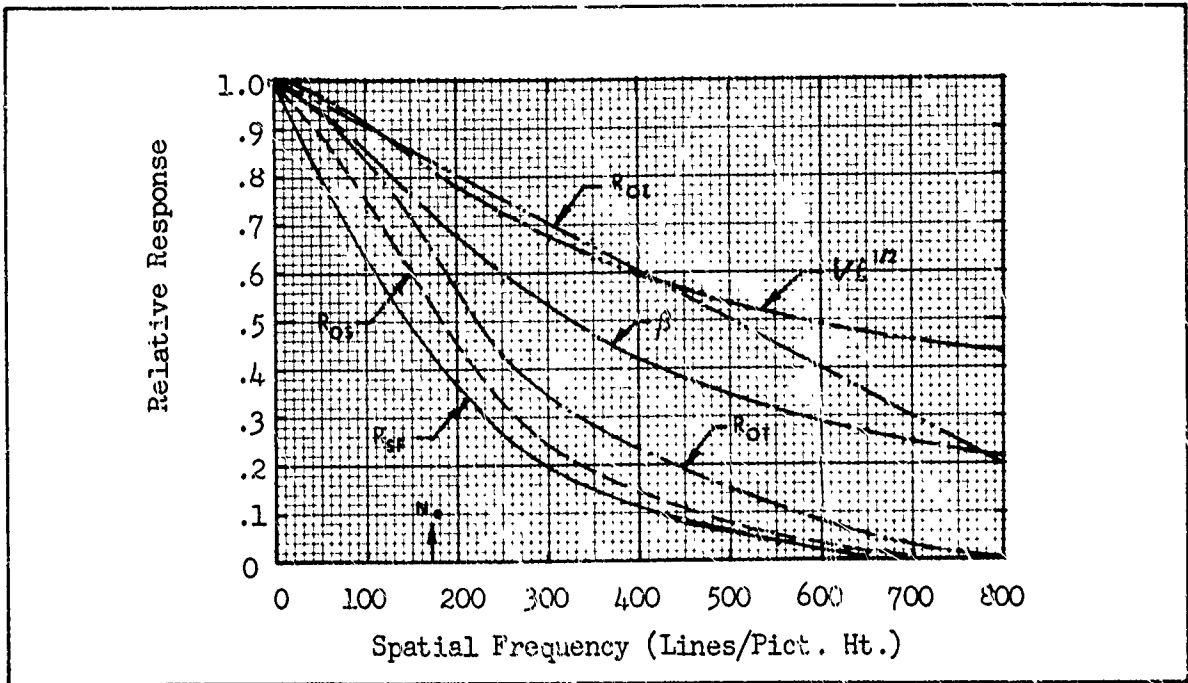


Fig. 6 MTF and MTF Related Functions for the Assumed Sample System.

These curves represent the image signal-to-noise ratio obtainable from the sensor. On the same curves, we show the observer's signal-to-noise ratio thresholds. The observer's threshold SNR_{DT} , as we noted in the previous section is approximately constant and independent of the input image contrast. As scene object contrast is reduced, the SNR_D obtainable from the sensor decreases. However, for analytical convenience, it is assumed that the observer's SNR_{DT} increases as the object contrast decreases, i.e.,

$$SNR_{DT} \text{ (for Object Contrast, } C_M) = \frac{SNR_{DT} \text{ (for } C_M = 1.0)}{C_M} . \quad (17)$$

This assumption greatly reduces the number of curves to be drawn.

The intersection of the SNR_D and SNR_{DT} curves gives the threshold

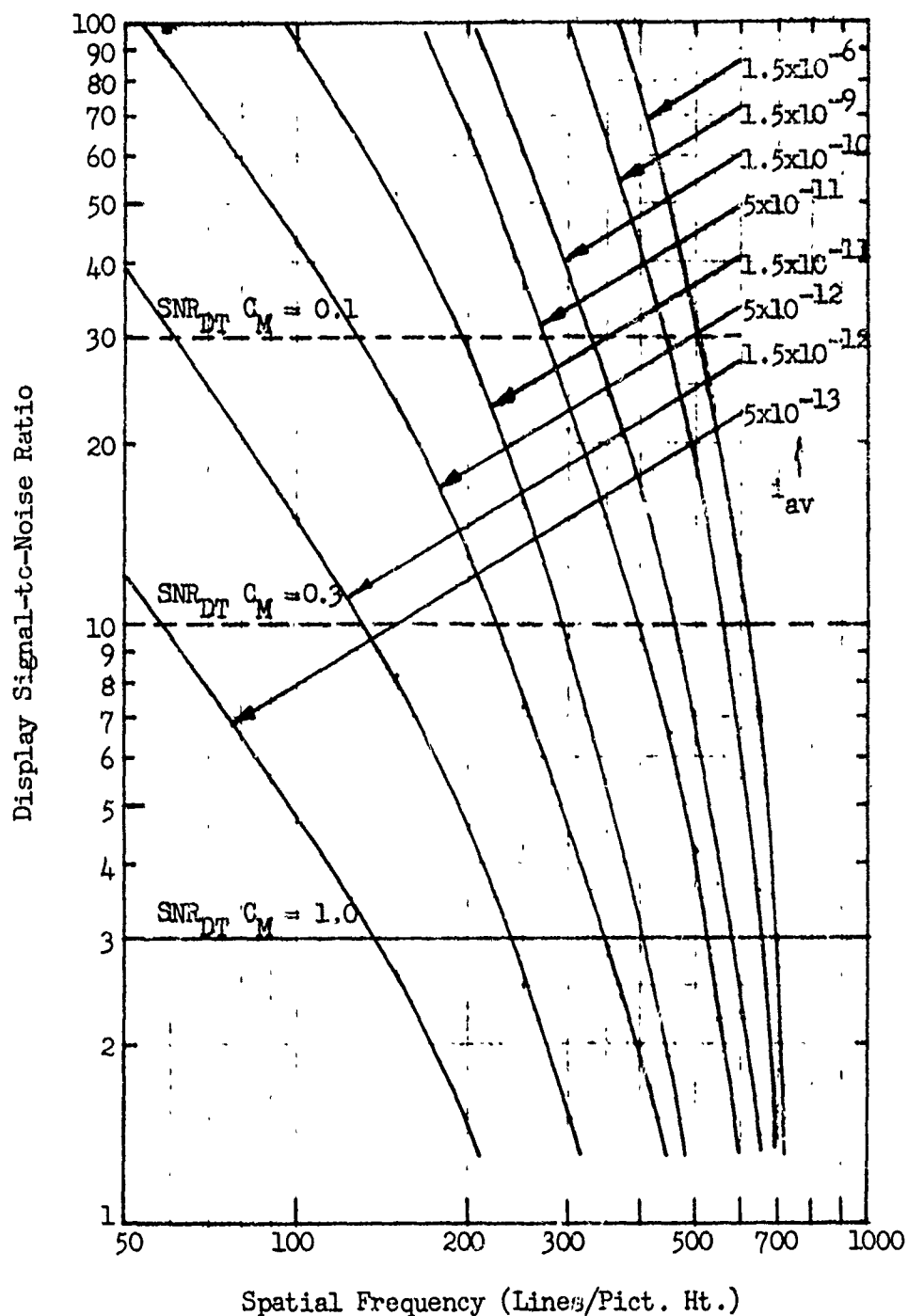


Fig. 7 Display Signal-to-Noise Ratio vs Spatial Frequency for the Assumed System at Various Average Input Photocathode Currents for Bar Pattern Images.

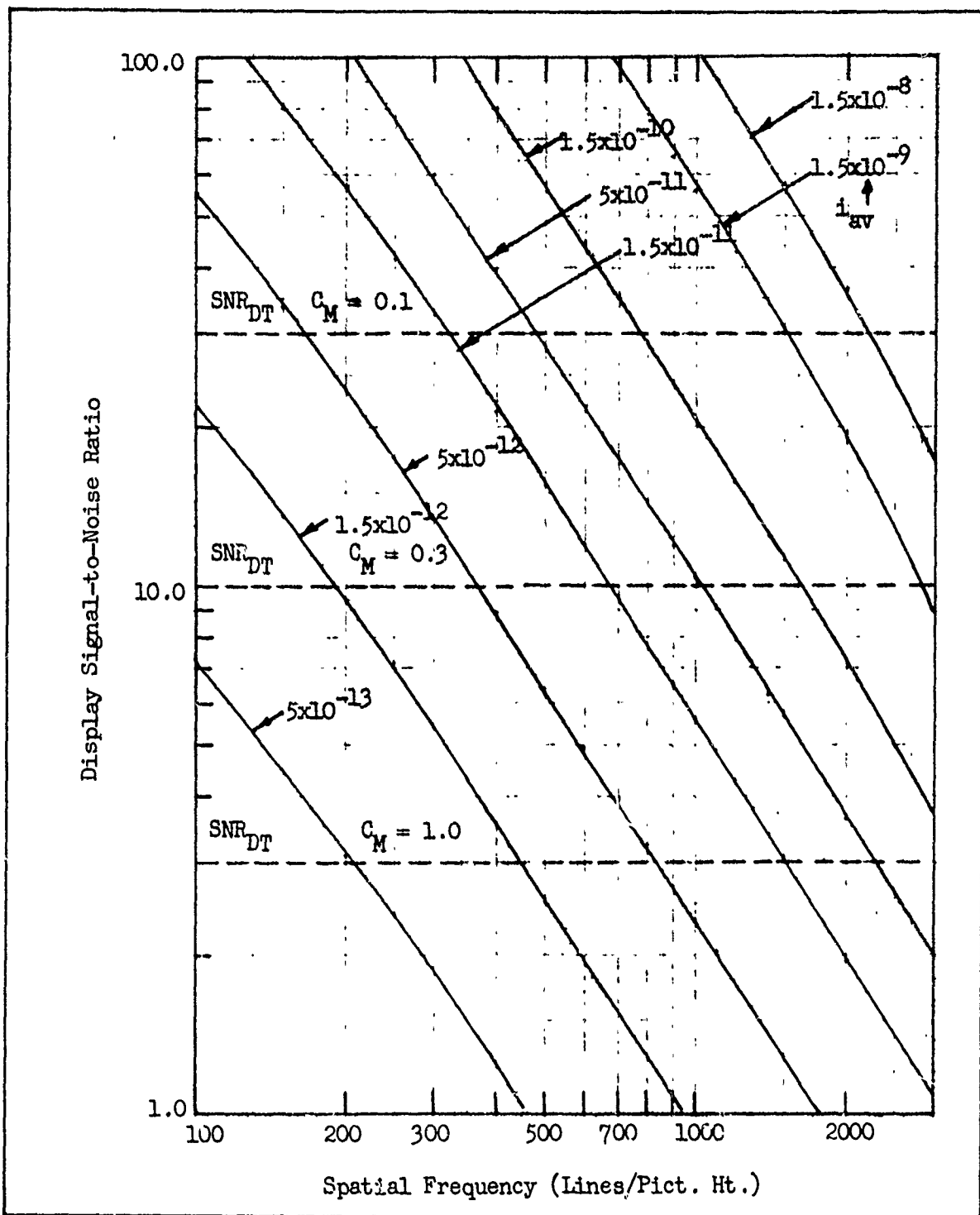


Fig. 8 Display Signal-to-Noise Ratio vs Spatial Frequency for the Assumed System at Various Average Input Photocathode Currents for Aperiodic Images.

resolution vs input photocurrent curves shown in Fig. 9 and 10. The very high resolution numbers associated with the aperiodic objects may appear startling at first, but as will be shown in Section 5, resolutions of the order predicted are in fact realized in real systems. It is seen that the MTF of the sensor has a much smaller effect on aperiodic images than on periodic images.

We have proposed that the system resolution be the average of the resolution calculated on the basis of the aperiodic object and the periodic object. A similar concept has been proposed by Schade (Ref. 4) which he refers to as balanced resolution. Schade notes that aperiodic objects are more frequently observed in nature than periodic objects but he weights the periodic and aperiodic resolution estimates equally as we have tentatively suggested. The method of weighting is considered open to revisions in the future and as discussed in Section 2.5.

Using the balanced resolution concept, the range predicted for sensors will substantially increase. On the other hand, we note that range estimates made previously on the basis of the equivalent bar pattern (or periodic model) seemed to correlate reasonably well with observed ranges in many cases. However, this cannot be construed as an indication of the superiority of the periodic resolution model as opposed to the balanced (aperiodic/periodic) model. The reason for the apparent superiority of the equivalent bar pattern (periodic) approach is that in previous systems analysis it has been usual, more often than not, to ignore a considerable number of image degrading effects including

- 1) sensor time constants

resolution vs input photocurrent curves shown in Fig. 9 and 10. The very high resolution numbers associated with the aperiodic objects may appear startling at first, but as will be shown in Section 5, resolutions of the order predicted are in fact realized in real systems. It is seen that the MTF of the sensor has a much smaller effect on aperiodic images than on periodic images.

We have proposed that the system resolution be the average of the resolution calculated on the basis of the aperiodic object and the periodic object. A similar concept has been proposed by Schade (Ref. 4) which he refers to as balanced resolution. Schade notes that aperiodic objects are more frequently observed in nature than periodic objects but he weights the periodic and aperiodic resolution estimates equally as we have tentatively suggested. The method of weighting is considered open to revisions in the future and as discussed in Section 2.5.

Using the balanced resolution concept, the range predicted for sensors will substantially increase. On the other hand, we note that range estimates made previously on the basis of the equivalent bar pattern (or periodic model) seemed to correlate reasonably well with observed ranges in many cases. However, this cannot be construed as an indication of the superiority of the periodic resolution model as opposed to the balanced (aperiodic/periodic) model. The reason for the apparent superiority of the equivalent bar pattern (periodic) approach is that in previous systems analysis it has been usual, more often than not, to ignore a considerable number of image degrading effects including

- 1) sensor time constants

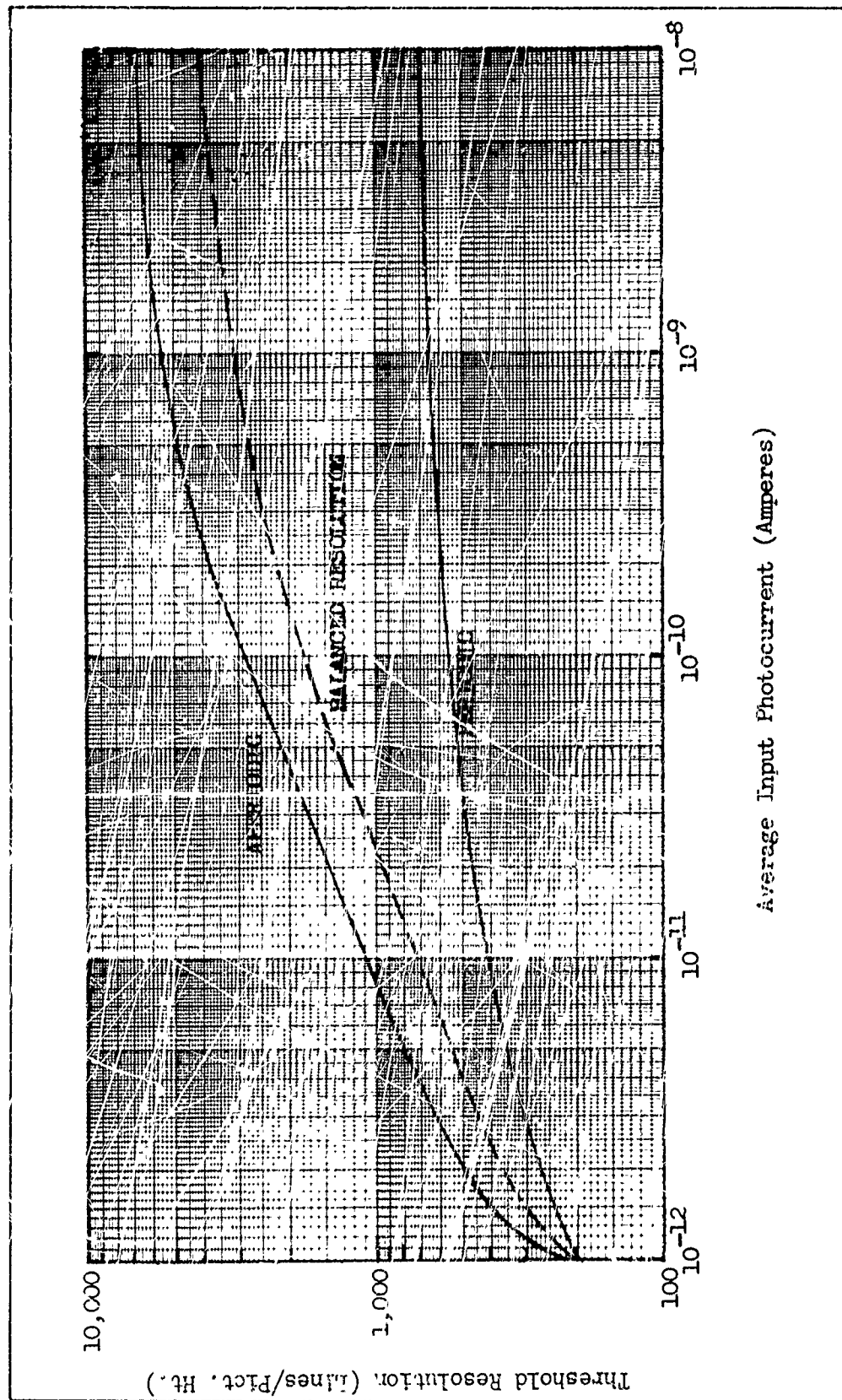


Fig. 9 Threshold Resolution vs Average Input Photocurrent for the Assumed System with Input Image Modulation Contrast of 1.0.

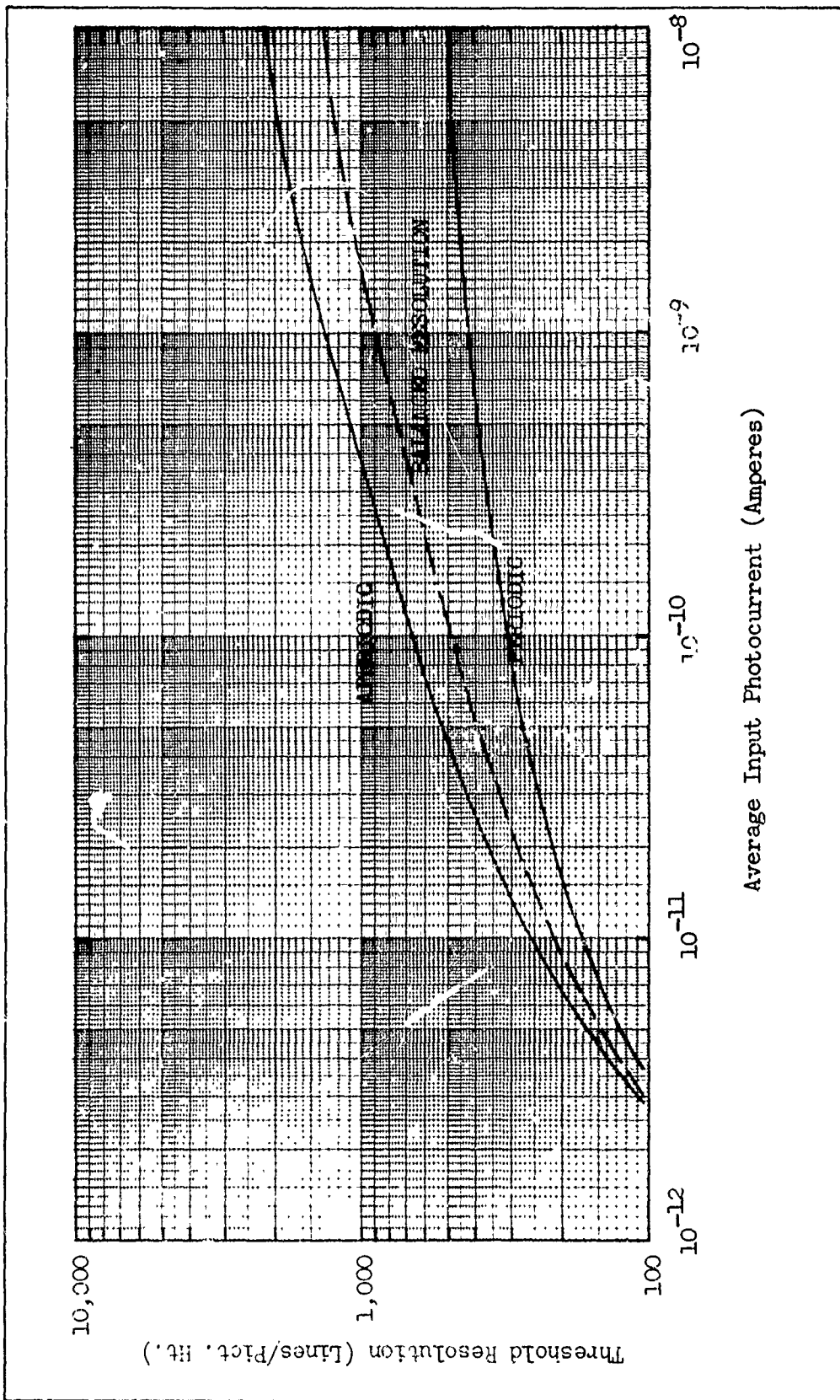


Fig. 10 Threshold Resolution vs Average Input Photocurrent for the Assumed System with Input Modulation Contrast of 0.1.

- 2) line-of-sight instability
- 3) MTF in the vertical direction
- 4) observer limitations
- 5) display dynamic range limitations
- 6) system degradation in the field
- 7) certain MTF losses such as that due to aerodynamic boundary layers, atmospheric turbulence, windows and the like

The point is that the pessimistic nature of the periodic model undoubtedly compensates for the neglect of many other system defects. As we will see, including some of the effects above in the periodic model would cause range predictions to fall far below the ranges measured.

In the above, we have used the input photosurface current as a parameter. This can be related to the input photosurface irradiance through the integral relation

$$i = \int_0^{\infty} \sigma(\lambda) A E(\lambda) d\lambda \quad , \quad (18)$$

where $\sigma(\lambda)$ is the spectral responsivity of the photosurface, A is its effective area, and $E(\lambda)$ is its irradiance. For specific sources, such as a tungsten lamp, sunlight, etc., we can use the approximation

$$i = \sigma_B A E_B \quad , \quad (19)$$

where σ_B is the specific responsivity to a specific source irradiance E_B . We will use this approximation recognizing its limitations.

The average input photosurface irradiance E_{pav} is related to the average scene irradiance E_s through the formula

$$E_{pav} = \frac{\rho_{av} E_s}{4T^2} \quad , \quad (20)$$

for a diffusely reflecting surface of average reflectivity, ρ_{av} , and a lens of T stop = T where T is the ratio

$$T = F_L / D \sqrt{\tau_o} \quad , \quad (21)$$

with F_L equal to the lens focal length, D equal to the lens diameter and τ_o equal to the lens transmittance.

The sensor resolution is given in terms of "lines per picture height" which, being dimensionless, is a convenience in the sensor analysis since image size can undergo several changes in the various sensor image and reimaging steps. By use of dimensionless units, MTF scale changes need not be made. From a systems viewpoint, the system's threshold angular resolution is of more interest. Knowing the threshold resolution, N , in lines per picture height, the threshold angular resolution, $\Delta\theta$, can be easily calculated using the formula

$$\Delta\theta = \frac{Y}{N \bullet F_L} \quad , \quad (22)$$

where Y is the effective input photocathode height and F_L is the lens focal length. $\Delta\theta$ is interpreted as the angular subtense of a single bar of spatial frequency N .

We averaged the threshold resolutions calculated for the periodic

and aperiodic images as plotted in Fig. 9. Then i_{av} is converted to E_s , the highlight scene irradiance using the combination of Eqs. (19 and 20), i.e.,

$$E_s = \frac{4T^2}{\rho_{av}} \cdot \frac{i_{av}}{\sigma A} \quad (23)$$

In the calculation, the parameters of Table 4 were used. The scene irradiance if given in Watts/m² can be approximately related to an equivalent scene illuminance level given in ft-candles by multiplying the Watts/m² by 2. Finally, the averaged threshold resolution, expressed in angular terms is plotted vs input photocurrent in Fig. 11. The use of angular units has the merit of being independent of the scene object's linear dimensions.

Before proceeding, we note that the gain used in Eqs. (11 and 14) is a variable. For very high scene irradiance levels, the sensor gain is reduced to about 2. As the scene irradiance is reduced, the sensor gain is increased until it reaches its maximum value (2000 for the sensor assumed).

The resolving power of a real imaging system will be degraded by the atmosphere intervening between the scene and observer. The amount of degradation will be primarily a function of the scene-to-camera range, the meteorological visibility, the sky condition and the sky-to-ground brightness ratio. These factors are discussed in some detail in (Ref. 2) but will be briefly reviewed here.

The meteorological visibility is a function of the number and sizes of particles in the air and its effect on scene object detectivity

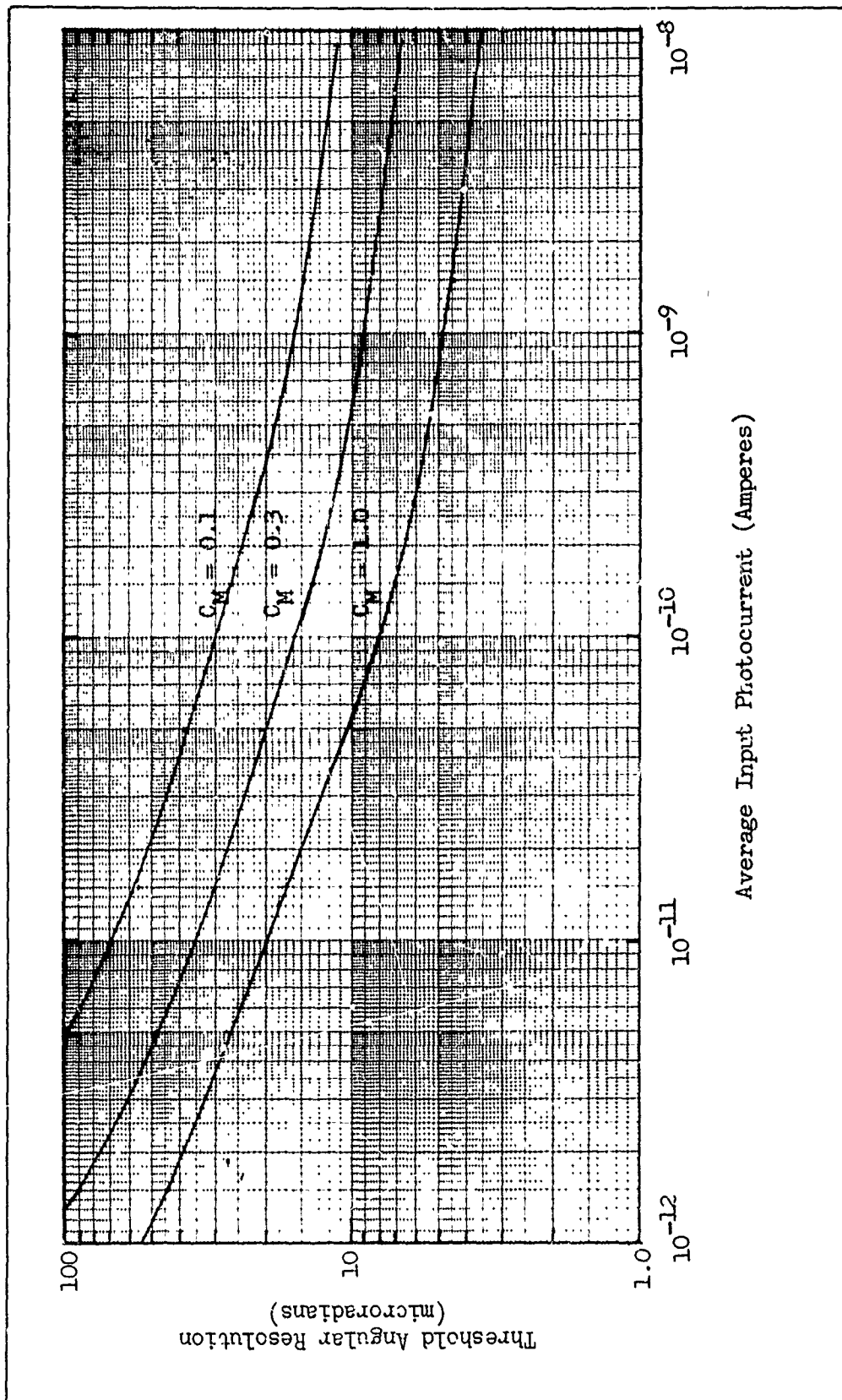


Fig. 11 Threshold Angular Resolution vs Average Input Photocurrent for the Assumed System with Various Input Image Modulation Contrasts. Threshold Resolution is Based on the Balanced Resolution Concept. Angle Corresponds to One Line Width.

is, to a certain extent, a function of the directivity and the type of scene light. Subjectively, the visibility is described by terms such as exceptionally clear, very clear, clear, haze and fog. Semiquantitatively, the visibility is described by the maximum range at which a large black object viewed against the horizon sky becomes barely perceptible when its apparent contrast in the visible spectrum at the observer's location drops to 2%.

For the case of a black object viewed against the horizon sky, the ratio of apparent contrast, i.e., the objects contrast at range, R , to the inherent contrast at range zero, is

$$\frac{C_R}{C_0} = e^{-\sigma R} , \quad (24)$$

where σ is the atmospheric extinction coefficient. The primary effect of the atmosphere in this case is to increase the object's brightness leaving the background (sky) brightness unchanged. In the air-to-ground surveillance case, the atmosphere increases the brightness of both the object and the background so that the equation for contrast reduction becomes

$$\frac{C_R}{C_0} = \frac{1}{[1 - \frac{S}{G}(1 - e^{-\sigma R})]} , \quad (25)$$

where S/G is the ratio of the brightness of the horizon sky to that of the grounds. For a clear sky

$$\frac{S}{G} \sim \frac{0.2}{\rho} , \quad (26)$$

<u>Sky Condition</u>	<u>Ground Condition</u>	<u>S/G</u>
Clear	Fresh Snow	0.2
Clear	Desert	1.4
Clear	Forest	5.0
Overcast	Fresh Snow	1.0
Overcast	Desert	7.0
Overcast	Forest	25.0

Table 5 Typical Values of the Sky-to-Ground Ratio.

where ρ is the background reflectivity. For an overcast sky

$$\frac{S}{G} \sim \frac{1}{\rho} , \quad (27)$$

Middleton (Ref. 5) gives the typical values of Table 5. The case of $S/G = 1$ for the downlook case is identical to the case of viewing an object against the horizon sky. When $S/G < 1.0$, as for fresh snow under a clear sky, contrast degradation is less than for viewing against the horizon sky and conversely, it is greater when $S/G > 1.0$.

Curves of C_R/C_0 are shown in Fig. 12 as a function of range for various values of S/G . It is seen that C_R/C_0 falls off very rapidly for S/G large. These curves were drawn for a visibility of 10 nmi.

In Table 5, it was noted that with a clear sky and a desert background, $S/G = 1.4$ while with the same background under an overcast sky, $S/G = 7.0$. Assuming a 20 nmi visibility (very clear) C_R/C_O is plotted for $S/G = 1.4$ and 7 in Fig. 13. It is seen that the image contrast, C_R , falls off much more quickly for an overcast sky ($S/G = 7.0$) than it does for a clear sky ($S/G = 1.4$). In both cases, the same scene is being viewed.

Suppose that a bar pattern is used as a test object in the flight evaluation of the equipment. Including the effect of atmospherics, the SNR_D Eq. (14) applies except that

$$C_M = C_{M0} / [1 - S/G(1 - e^{-\sigma R})] , \quad (28)$$

where C_{M0} is the object contrast at zero range. At a given scene light level, the signal, being contrast dependent, becomes range dependent in turn as shown in Fig. 14. With no atmosphere, i.e., a vacuum, the TV camera resolution would be independent of range as shown by the dashed line. With a real atmosphere of 20 nmi visibility, the sensor resolution drops from 620 lines to about 460 lines at 40,000 feet viewing a desert scene under clear sky conditions. Under overcast sky, the resolution drops from 620 to 300 lines. The equivalent curves expressed in terms of angular resolution are shown in Fig. 15. Also, the effect of the atmosphere and the sky-to-ground ratio on other values of contrast are shown in Figs. 16 and 17.

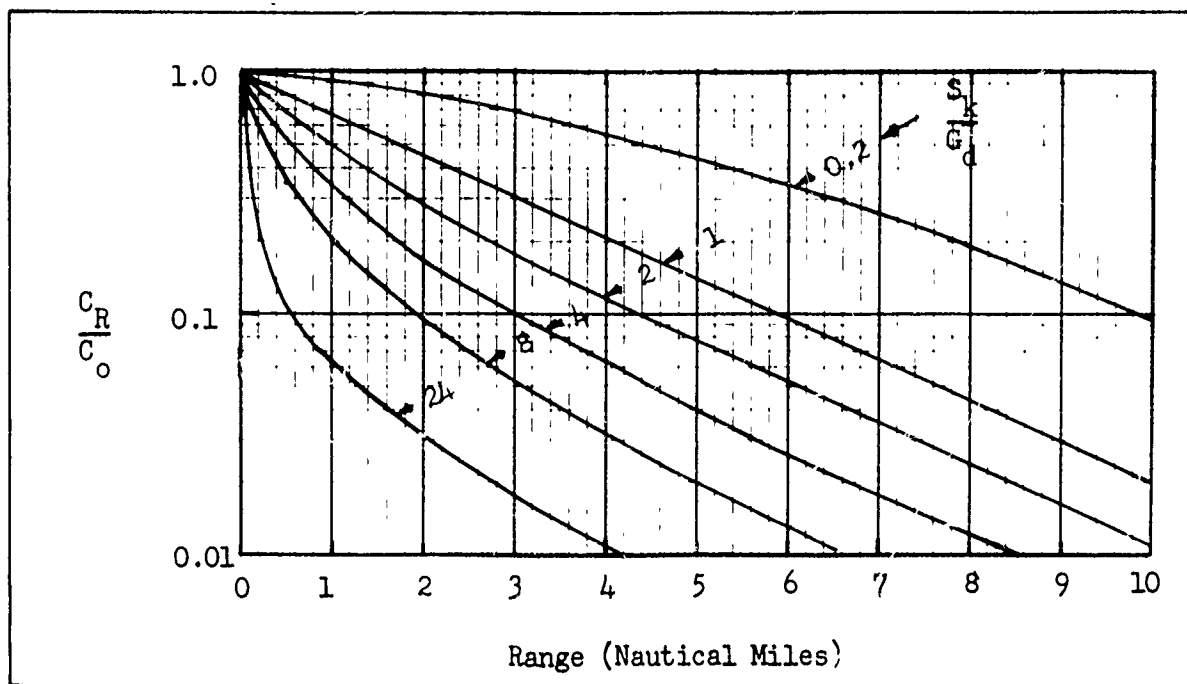


Fig. 12 Ratio of Apparent to Inherent Contrast vs Range for Various Values of Sky-to-Ground Ratio for a Meteorological Visibility of 10 Nautical Miles.

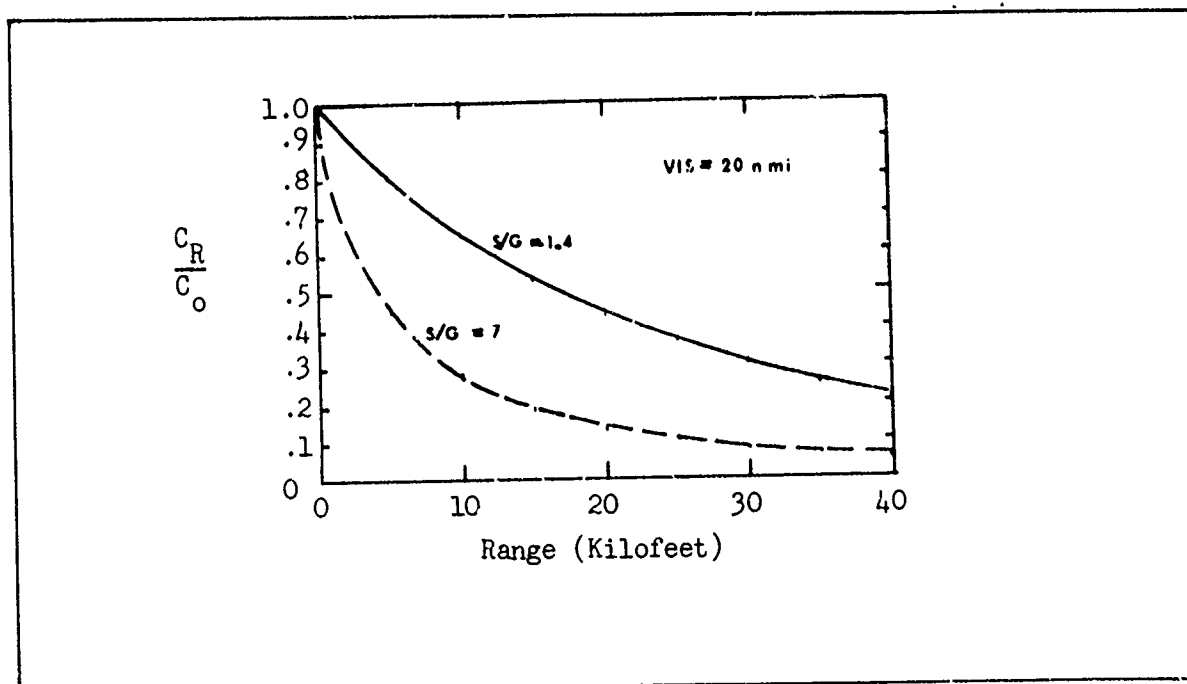


Fig. 13 Ratio of Image Contrast at Range R to that at Range Zero vs Range for a Meteorological Visibility of 20 Nautical Miles and Sky-to-Ground Ratios of 1.4 and 7.0.

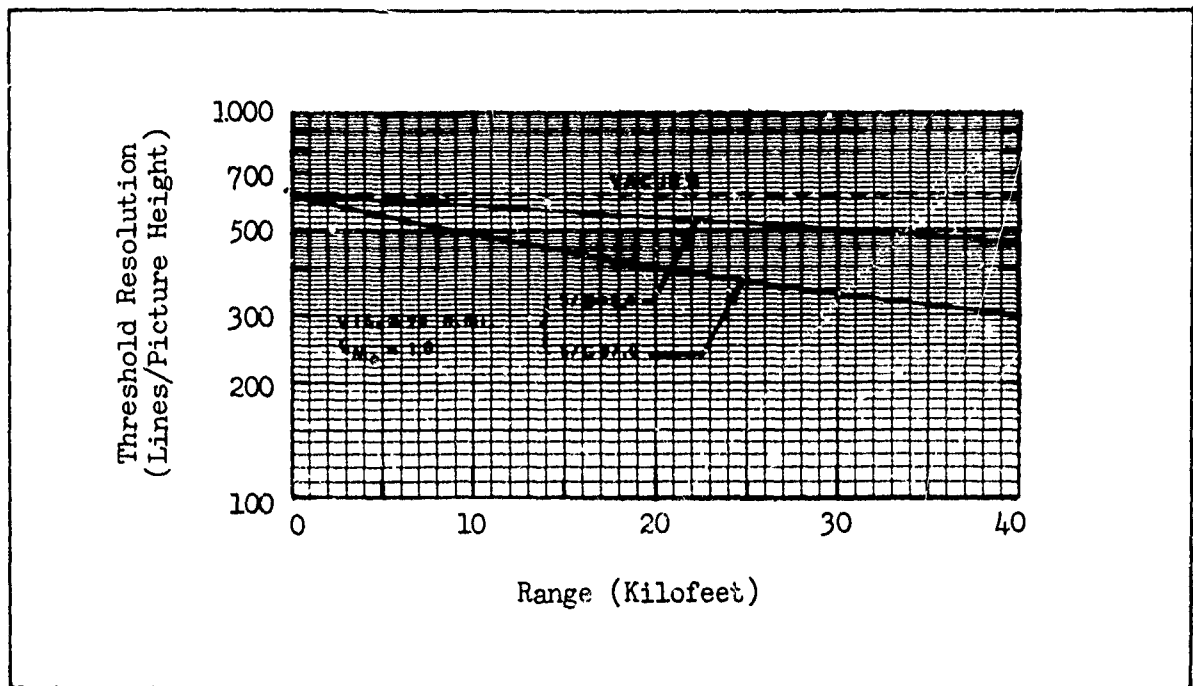


Fig. 14 Threshold Resolution vs Range for a Meteorological Visibility of 20 Nautical Miles and Sky-to-Ground Ratios of 1.4 and 7.0.

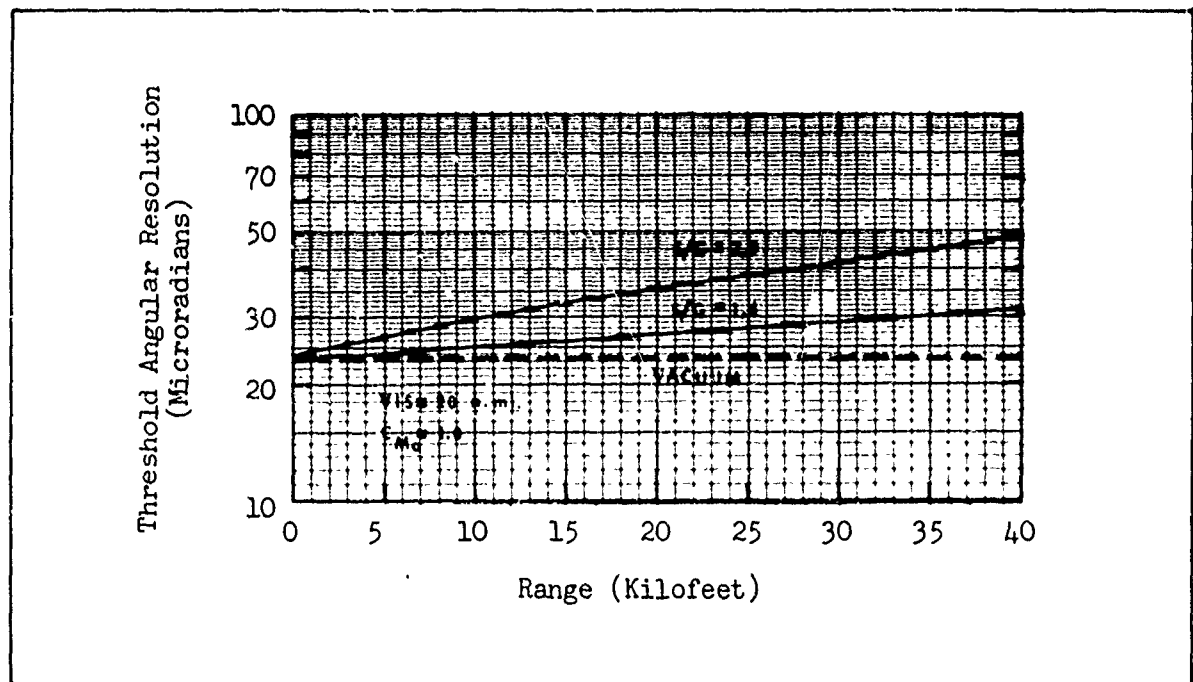


Fig. 15 Threshold Angular Resolution vs Range for a Meteorological Visibility of 20 Nautical Miles and Sky-to-Ground Ratios of 1.4 and 7.0.

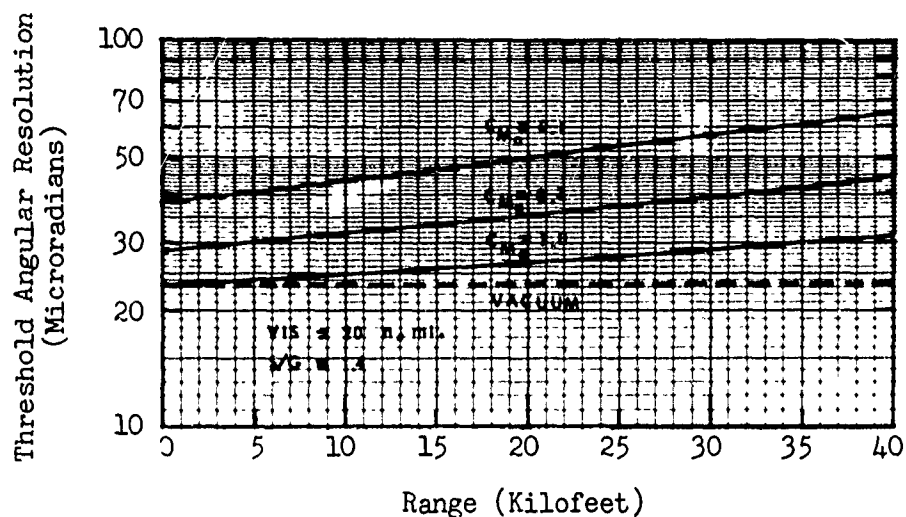


Fig. 16 Threshold Angular Resolution for Bar Patterns vs Range for the Assumed TV Camera as a Function of Input Image Contrast for a 20 nmi Visibility and a Sky/Ground Ratio of 1.4.

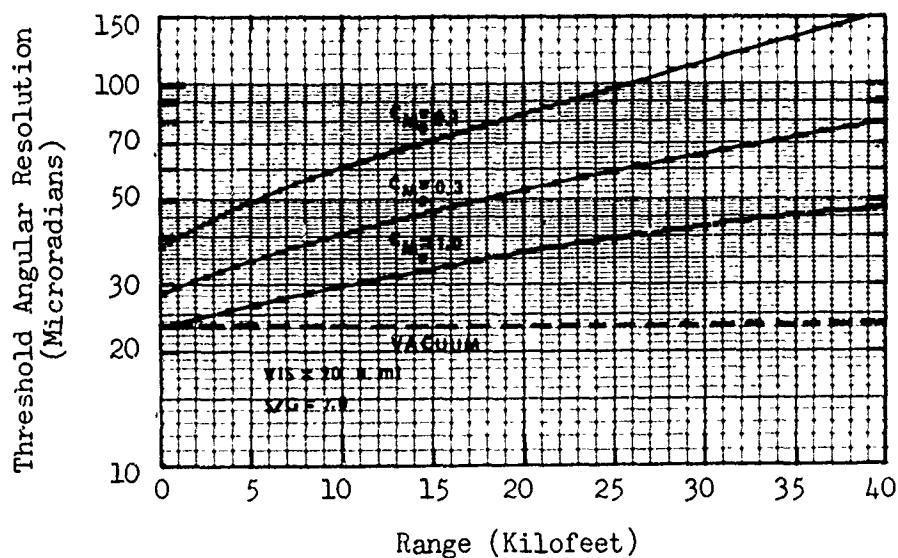


Fig. 17 Threshold Angular Resolution for Bar Patterns vs Range for the Assumed TV Camera as a Function of Input Image Contrast for a 20 nmi Visibility and a Sky/Ground Ratio of 7.0.

The atmosphere may also have a modulation transfer function due to thermal gradients, inversion layers, etc. These are most serious for ground based TV telescopes but do affect air-to-ground viewing as well. These effects are noted but not analyzed further herein.

2.3 Active Television Imaging Systems

An active imaging system is one which images a scene lighted by an auxiliary system source. In the case of interest here, the auxiliary source is located near the television telescope. A simple search light qualifies as an auxiliary source but the trend in recent sophisticated systems is to use a pulsed laser which may be range gated to eliminate atmospheric backscatter. The analysis of active television systems of the range gated variety has been treated in some detail in Ref. 2 but will be reconsidered using the updated model.

The system parameters will be identical to those considered in the previous section with the primary change being the addition of a 40 watt system source (sometimes called an illuminator), an image intensifier and an electronic exposure gate for the TV camera. The system source is of the GaAs variety which provides 0.85 micron radiation in 2 μ s bursts. The photoresponse of the input photocathode is taken to be 2.5×10^{-2} A/W and the intensifier gain is presumed to be 20 (ratio of current in the TV camera tube to that in the intensifier). For first order analysis, The Eqs. (11 and 14) will be used as for the passive case. The principal differences from a systems viewpoint are that the inherent scene contrasts will tend to be higher, the atmosphere will have a much smaller effect on the apparent scene contrast but may severely decrease scene irradiance.

An active system, used only during the night hours, will usually be limited by a low scene irradiance and photoelectron noise rather than by preamplifier noise as is the case for a daylight system. Since light levels are low, the designer of an active system seeks high sensitivity and low sensor lag rather than a large signal storage capability as the daylight system designer does.

The actual scene irradiance is given by the relation

$$E_s = P_o \exp(-\sigma R) / \omega R^2, \quad (29)$$

where P_o is the source power (watts), σ is the atmospheric extinction coefficient, ω is the solid angle irradiated (sr), and R is the slant range from camera to scene. The average sensor irradiance level assuming a diffuse scene is obtained from

$$E_{pc} = \frac{\rho_{av} P_o \exp(-2\sigma R)}{4T^2 \omega R^2}, \quad (30)$$

where ρ_{av} is the average scene reflectivity and T is the lens T/stop (equal to the lens f-number divided by the square root of the lens' transmittance). Note that the atmosphere decreases the scene irradiance on both its trip to the scene and its return. The input photosurface current, i_{av} , is given by

$$i_{av} = \frac{\rho_{av} S A P_o \exp(-2\sigma R)}{4T^2 \omega R^2}, \quad (31)$$

where S is the photosurface responsivity (A/W) and A is its effective area. The above photocurrent is plotted in Fig. 18 for 3 values of

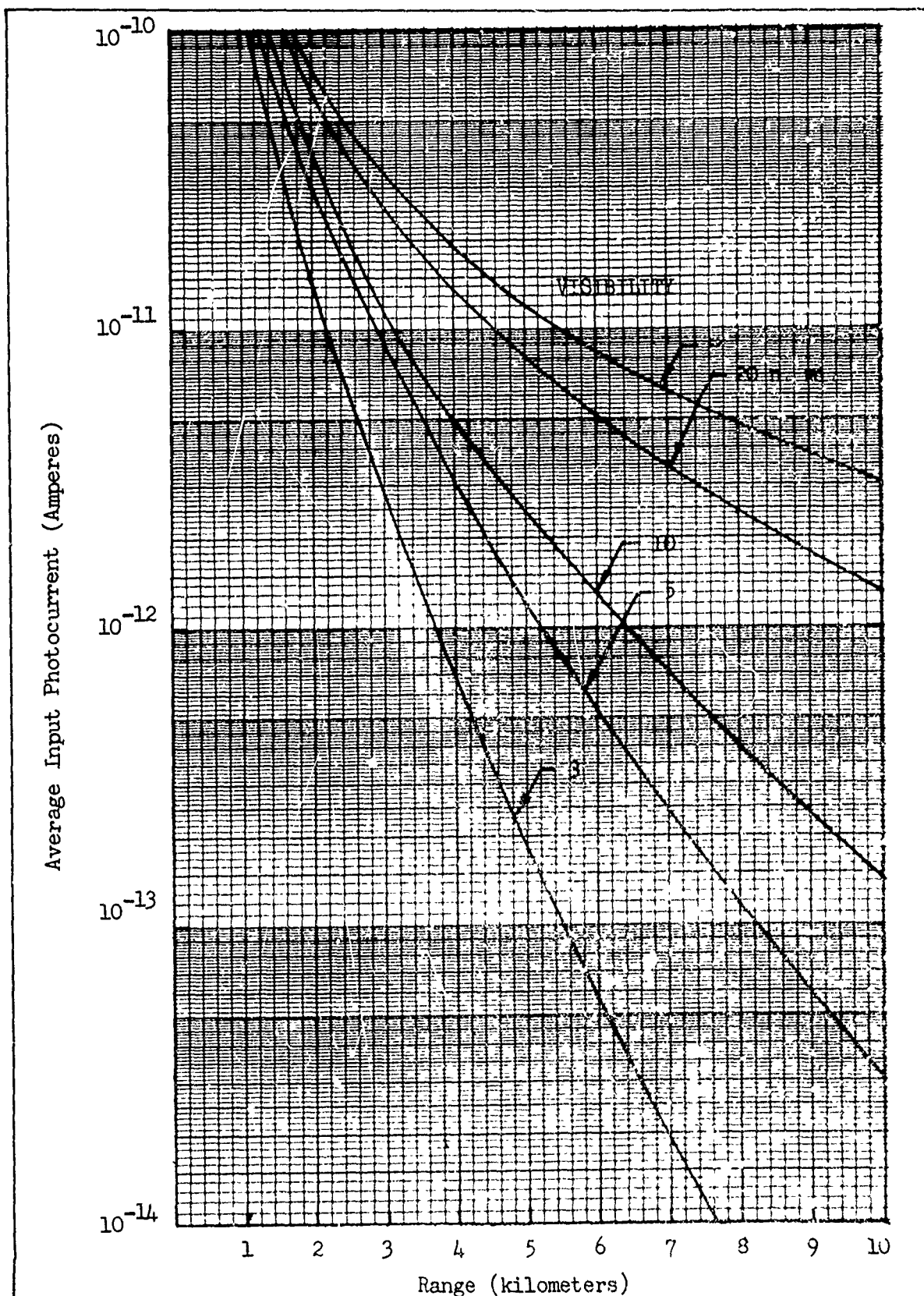


Fig. 18 Average Input Photocurrent for the Assumed System vs Range for an Average Scene Reflectivity of 0.3.

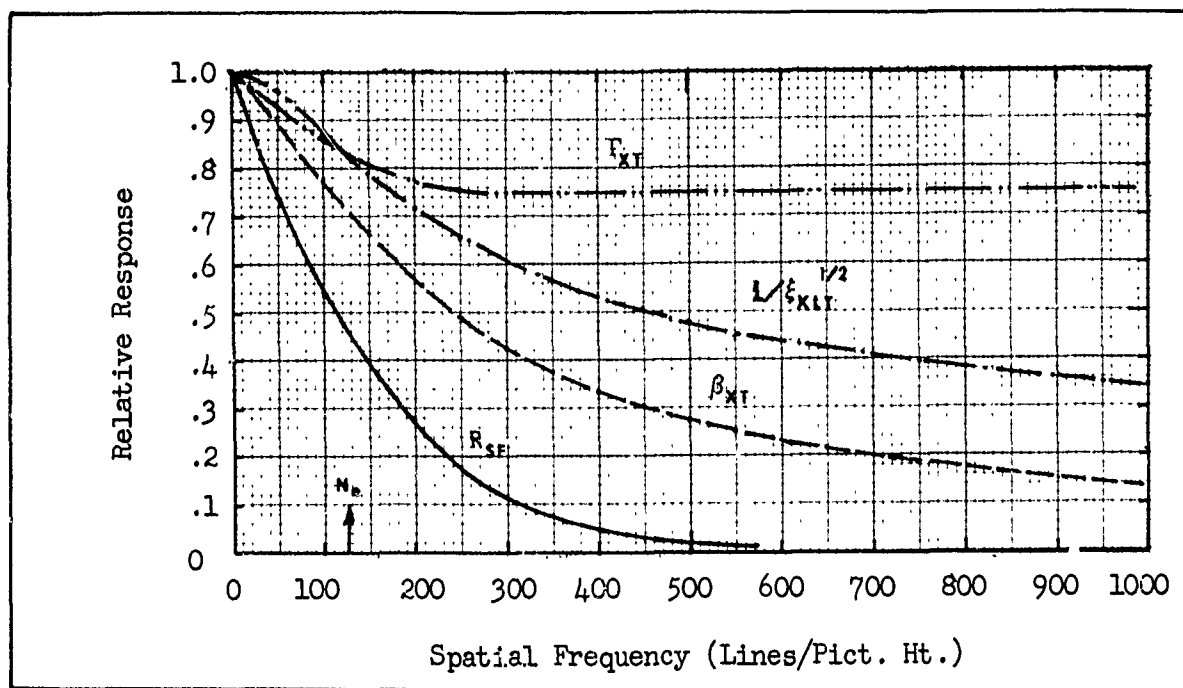


Fig. 19 MTF and MTF Related Quantities for the 16/16/16 mm I-EBSICON Camera Used in the Assumed System.

visibility (sea level, horizontal path assumed). From these curves, it is possible to make some resolution vs range estimates directly. A typical 16 mm I-EBSICON camera tube, operated at full gain saturates with input photocurrents near about 5×10^{-11} Ampere. For high scene contrasts, it is possible to image with currents as low as 10^{-13} A while, for moderately low contrasts, 10^{-12} A may be required. For the moderately low contrast case, the range at which a reasonably good image will be obtained will vary from about 3.5 to 15 kilometers depending upon the visibility.

The MTF and MTF related quantities are shown in Fig. 19. As can be seen, the intensifier has an appreciable effect on the overall square wave flux response. Because of the high gain of the intensifier and camera tube ($\sim 40,000$), the Eqs. (11 and 14) reduce to

$$\text{SNR}_D = \left[\frac{t\epsilon}{\alpha} \right]^{\frac{1}{2}} \cdot \frac{1}{N} \cdot \frac{2C_M(i_{av})^{\frac{1}{2}}}{[e\xi_{xLT}(N)\Gamma_{xT}(N)\xi_{yLT}(N)\Gamma_{yT}(N)]^{\frac{1}{2}}}, \quad (32)$$

for aperiodic objects and for periodic objects

$$\text{SNR}_D = \left[\frac{t\epsilon}{\alpha} \right]^{\frac{1}{2}} \cdot \frac{R_{SF}(N)}{N} \cdot \frac{2C_M(i_{av})^{\frac{1}{2}}}{[e\xi_{yLT}(N)\Gamma_{yT}(N)\beta_{xT}(N)]^{\frac{1}{2}}}. \quad (33)$$

These SNR_D values are plotted in Figs. 20 and 21 for an inherent object contrast of 0.5 and a meteorological visibility of 20 n. miles. The meteorological visibility determines the average photocurrent as given by Eq. 31. The threshold resolution vs range is plotted in Fig. 22 in terms of bar pattern spatial frequency and in terms of angular subtense of a single bar in Fig. 23. It is seen that the aperiodic resolution dominates as was noted in the passive imaging case but the difference between periodic and aperiodic resolution is not as pronounced. Note that as range increases, the resolution predicted on the periodic model basis approaches that predicted on an aperiodic model.

In the above, we neglected the loss of image contrast due to a finite laser pulse width and a finite range gate interval. These effects are discussed in some detail in Ref. 2.

2.4 Effects of Image Motion

We have seen that the resolution of scene detail can be limited by the ambient light level, system generated noises and by the atmosphere. To these limitations, we now add relative scene motion. The effects of image motion are to cause the image to blur in a manner analogous to the blur caused by an added system aperture. Indeed,

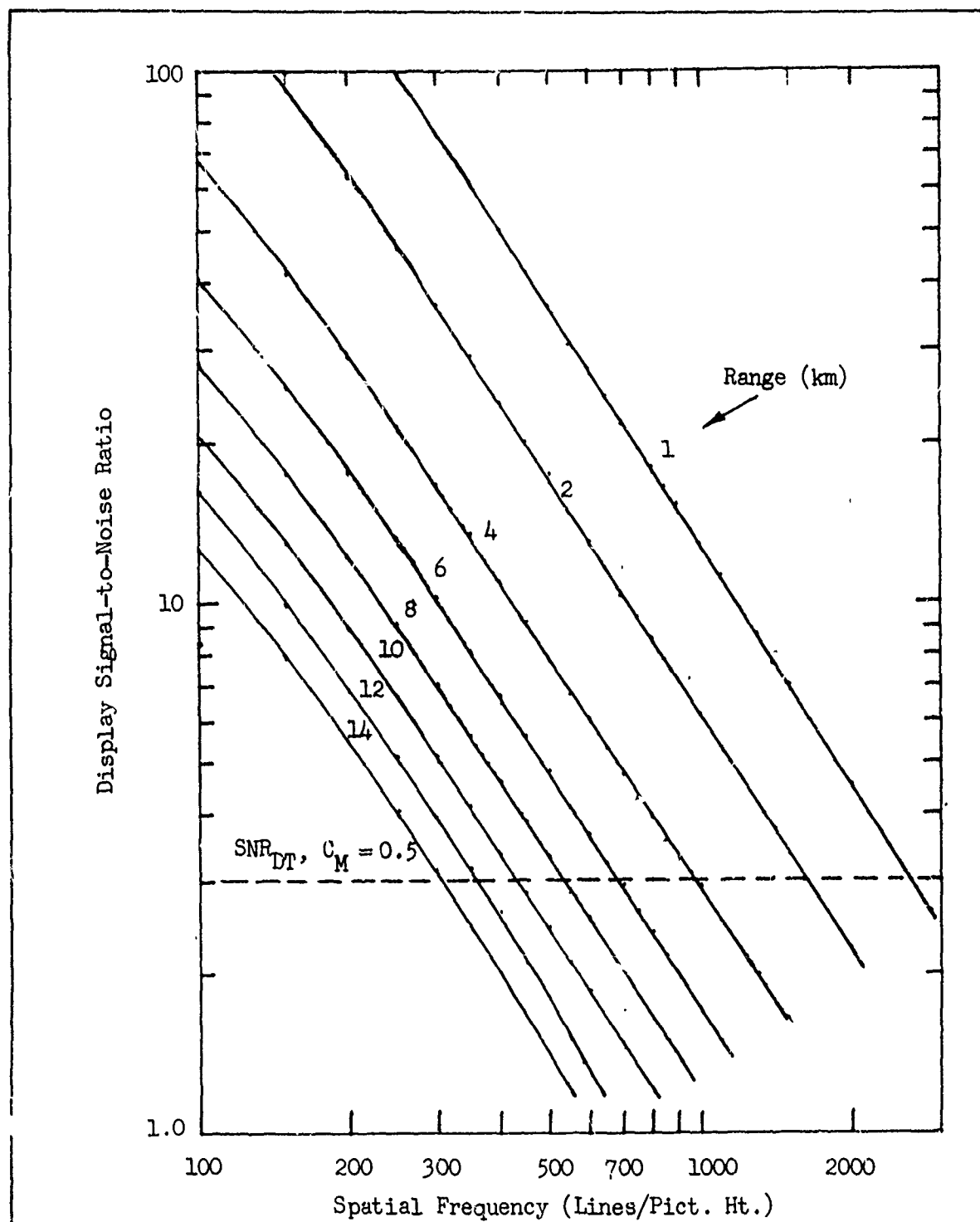


Fig. 20 Display Signal-to-Noise Ratio vs Spatial Frequency for the Assumed Active System for an Inherent Image Contrast of 0.5 and a Visibility of 20 n. mi. Calculations are based on the Aperiodic Image Model.

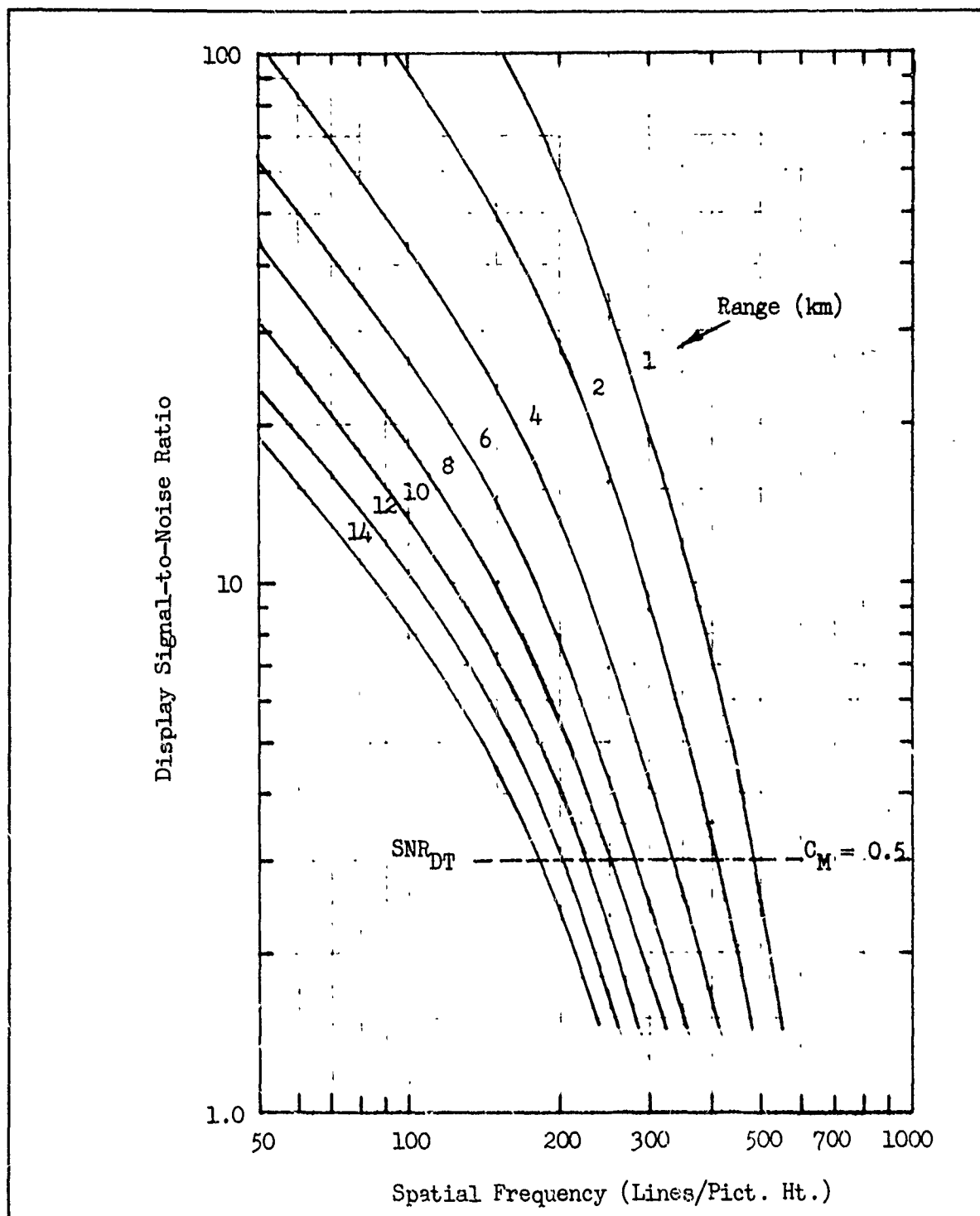


Fig. 21 Display Signal-to-Noise Ratio vs Spatial Frequency for the Assumed Active System for an Inherent Image Contrast of 0.5 and a Visibility of 20 n. mi. Calculations Based on the Periodic Image Model.

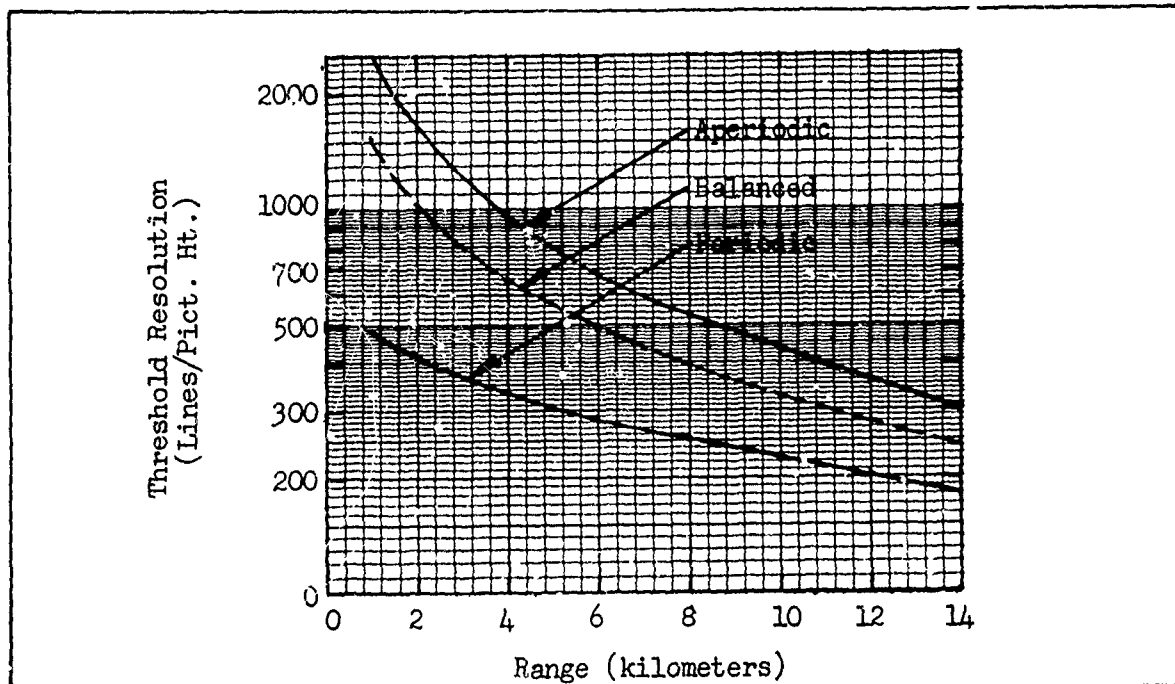


Fig. 22 Threshold Resolution in Lines/Pict. Ht. for the Assumed Active System vs Range. Inherent Image Contrast is 0.5.

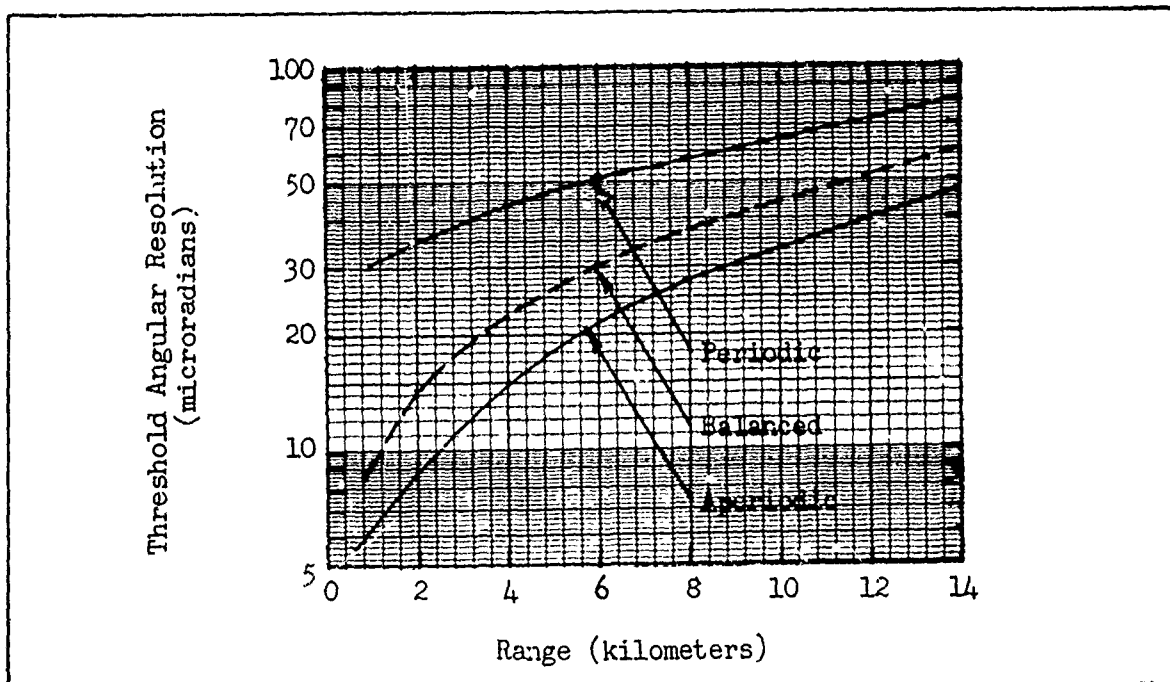


Fig. 23 Threshold Resolution in Angular Subtense of a Single Line vs Range for the Assumed Active System. Inherent Image Contrast is 0.5.

motion effects can often be described in terms of a modulation transfer function.

One effect of image motion is to induce image lag effects due to the TV system's read-in and read-out time constants. These effects are light level dependent; being most pronounced at the lower light levels. We shall consider these effects following the discussion of the effects of exposure time.

Relative scene motion may be caused by machinery within the TV camera enclosure (such as blowers or pumps) by noise in motion sensors such as gyros, by platform perturbations such as aircraft vibration or by the forward motion of the platform as occurs in flight. This relative image motion is a problem because the TV camera has an exposure time.

Typically, the television camera has an exposure time of $1/30$ second although, under high light levels, the effective exposure time may be reduced to near the field time of $1/60$ second. This reduction in effective exposure time is due to the readout of both fields by the electron beam during a single scan of the charge storage surface. The result is low resolution pictures, presented displaced by one line from one field to the next. The resultant picture resolution is higher than that of either field alone but probably not as high as it would be if the picture on each field were independent from the other. These effects have been noted but lack quantitative measure. For the purposes of this discussion, the TV exposure time will be assumed to be $1/30$ second unless otherwise noted.

Except for the usual effects due to scanning, the exposure or frame time of a television camera is directly analogous to the exposure time of

a photographic camera. A photographer, taking even stationary scene pictures, must be very careful to avoid jiggling his camera when using exposure times of the order of $1/30$ second. Ordinarily, he will prefer to use $1/100$ to $1/200$ second exposure times to avoid camera motion problems. When photographing action scenes, exposure times are usually reduced further to about $1/500$ second or less. It is noted that the effect of image blur due to relative scene or camera motion may be worse for a single photographic exposure than it is for cinematography or for television where several blurred pictures, slightly displaced, may combine in the observer's eye to form an overall image of greater clarity as in the television case where both fields are readout in a single field as discussed above. Again, these effects have not been quantitatively investigated to the author's knowledge.

Given a stationary camera, the relative scene motion is a function of the distance of the scene from the camera. It is clearly more difficult to photograph a 60 mph car passing across the camera viewfield at a range of 10 feet than it is at 1000 feet. In the usual airborne reconnaissance system, ranges are very long -- typically, 5000 to 50,000 feet and the scene motion is relatively negligible. However, the camera's line-of-sight is continually being perturbed by the aircraft's velocity, the ambient vibration of environment, and the mechanisms required to slew, point and stabilize the line-of-sight. In general, the line-of-sight will be in continuous motion of some kind. Even when a ground point is being perfectly tracked, only one point in the image will be stationary -- all other points in the viewfield will be in relative angular motion. Many of these effects have been discussed in considerable detail in Ref. 2.

Consider an aircraft in straight and level flight. Let a TV camera view the ground with a fixed depression angle. Then the line-of-sight to the fixed ground point will rotate as the aircraft flies toward it. The image of the point will travel from the bottom of the picture to the top. For changes in the sightline which are not too large, the rate of image motion is approximately linear. Alternatively, the line-of-sight may oscillate about the ground point with reasonably constant amplitude and frequency due to mechanical resonances, or oscillate with random amplitudes and frequencies due to noises generated by the inertial sensors or due to other noises transmitted by the mechanical structure.

The eye can track scene objects which are moving at very high angular rates compared to the angular rates which the television camera will tolerate without losing significant scene resolution. Thus, for our purposes, we can concentrate on the motion-induced sensor effects. It is also clear that to blur an image, the image's motion must be comparatively large during an exposure time. However, the term large is relative to the size of the image detail to be resolved. The amount a small object can move without being blurred beyond recognition is also small.

The effects of image motion on scene resolution has been analytically treated for a number of simple but quite common cases (Ref. 6). These are linear motion, sinusoidal vibration of constant amplitude, and sinusoidal vibration of random amplitude. These will be discussed below. As one would intuitively expect, linear motion is the least degrading and random motion is the most.

In photographing or televising an object passing across a field of view, a sharp picture will be obtained only if the angular rate of

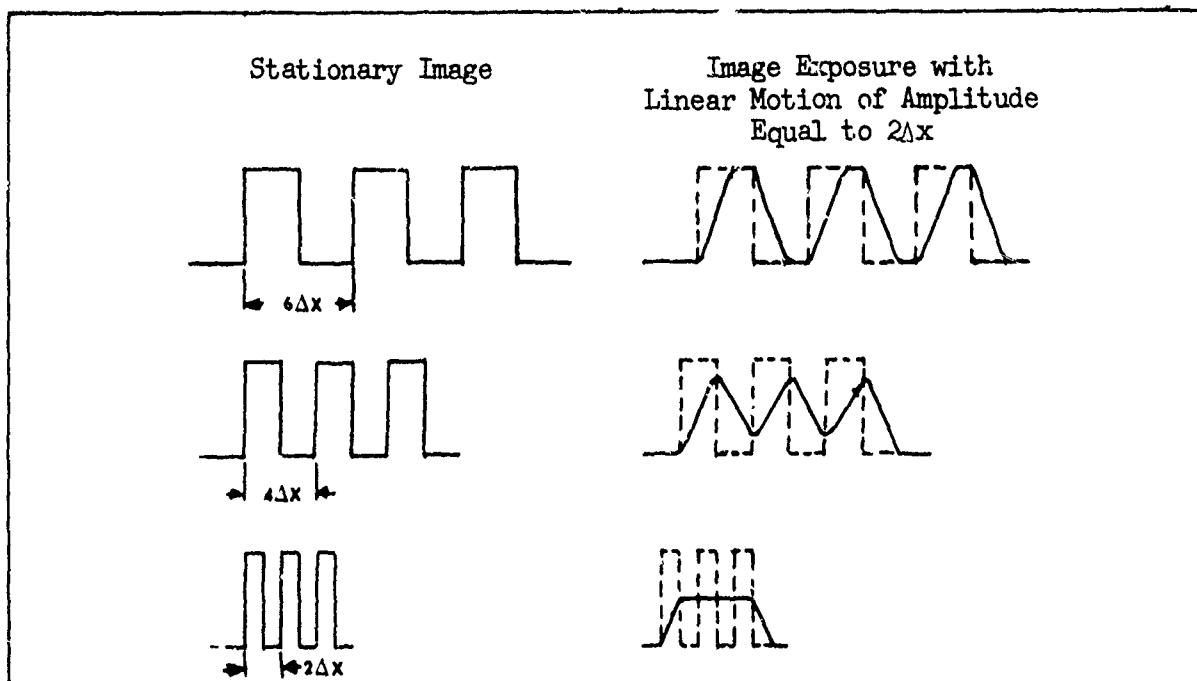


Fig. 24 Effect of Image Motion on Bar Patterns of Various Spatial Frequencies.

the object is small relative to the object's angular detail during the exposure time. As the object's angular rate increases, the object's image begins to blur with fine details being the first to disappear. Suppose that the object is a bar pattern as shown in Fig. 24. If the coarse pattern of period $6\Delta x$ moves a distance $2\Delta x$ during an exposure time, the intensity waveform in the exposed image, though of the same amplitude, becomes trapezoidal. If the bar pattern spacing becomes smaller, so that the period is $4\Delta x$, the exposed image's amplitude within the bar pattern is reduced and the waveshape tends toward sinusoidal. With a bar pattern of period equal to the distance moved during the exposure time, i.e., $2\Delta x$, the exposed image becomes a uniform grey, i.e., there is no modulation in the exposed image and the bar pattern structure disappears.

It is customary in TV engineering to express the image resolution

at the input photocathode in terms of a spatial frequency with units of lines per picture height. That is, if the bar (or sine wave) spacing is Δx (period of $2\Delta x$) and if the picture height is Y , then the spatial frequency, N , is equal to

$$N = \frac{Y}{\Delta x} \frac{\text{lines}}{\text{picture height}} \quad (34)$$

By analogy with the above discussion, it is seen that if the image motion is 2 lines in an exposure time, then the output image modulation becomes zero.

As shown in Ref. 2, the effect of linear image motion can be described in terms of a modulation transfer function given by

$$R_o(N) = \frac{\sin(\pi N v_i t_f / 2Y)}{\pi N v_i t_f / 2Y} \quad (35)$$

for v_i equal to the pattern speed in mm/sec, Y equal to the picture height and t_f equal to the frame or exposure time. In laboratory measurements, it is common to specify the bar pattern velocity in terms of the number of seconds, t_s , required for one bar in the test pattern to traverse the field of view. Using this specification, the pattern velocity becomes

$$v_i = \frac{4Y}{3t_s} \quad (36)$$

(for a picture aspect ratio of 4/3). Now,

$$R_o(N) = \frac{\sin(2\pi N t_f / 3t_s)}{2\pi N t_f / 3t_s} \quad (37)$$

This MTF is plotted in Fig. 25 for various pattern velocities. The

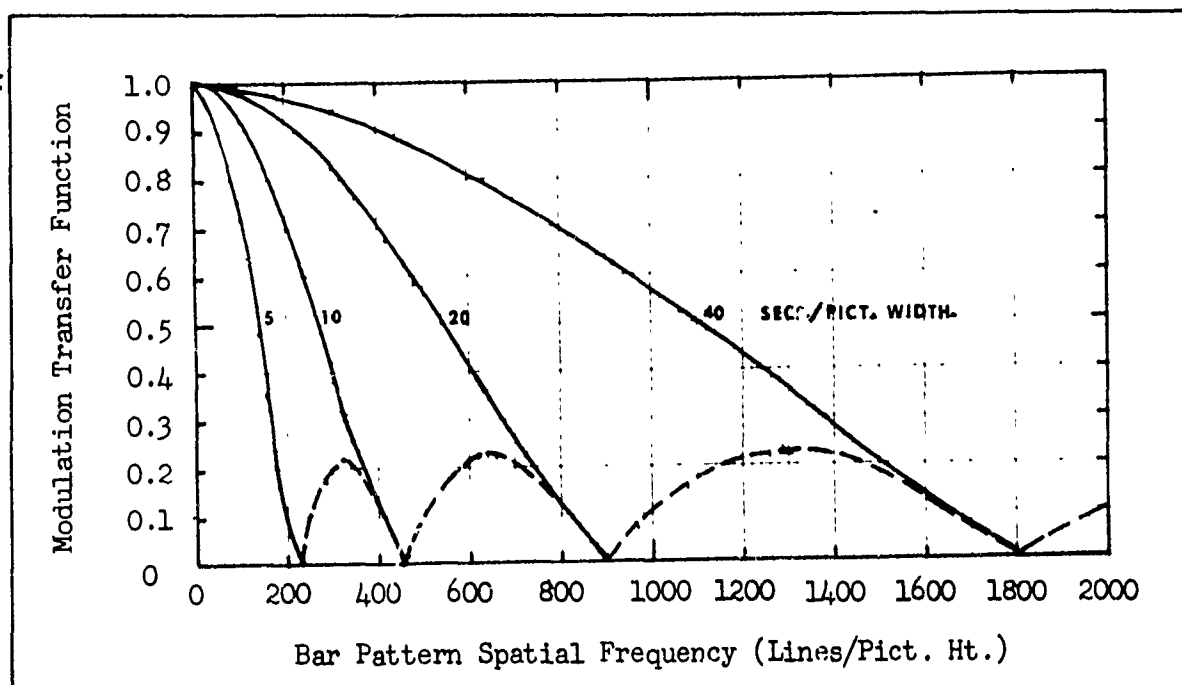


Fig. 25 Modulation Transfer Function Due to Linear Image Motion Plotted to Second Zero for Various Bar Pattern Velocities Expressed in Terms of Time for Pattern to Traverse Picture Width.

response is seen to go to zero and then increase again as shown by the dashed lines. The increase in response after the first zero results when the bar pattern motion exceeds 2 lines/exposure time. The response is negative indicating a phase reversal, i.e., the black lines appear as white on the display and conversely. While a signal modulation results, it is not generally useful and is called false resolution. The spatial frequency at which the response first goes to zero is given by

$$N_c = \frac{3}{2} \frac{t_s}{t_f} \quad (38)$$

and is plotted in Fig. 26. The angular motion per frame time corresponding to N_c is also plotted in the same figure for the assumed daylight system of Section 2.2.

If it is desired to resolve a certain spatial frequency, say 225

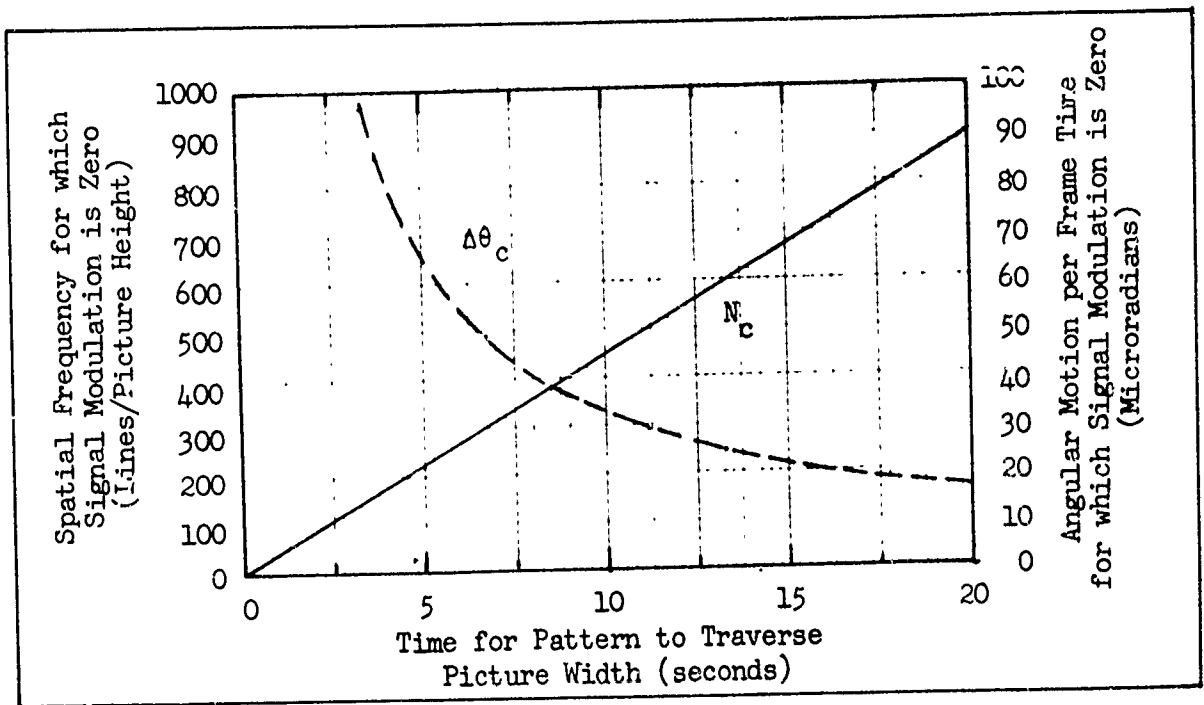


Fig. 26 Spatial Frequency and the Corresponding Angular Motion for the Assumed System for which the Signal Modulation is Zero as a Function of Bar Pattern Motion (Linear).

lines, the pattern velocity must be less than 5 seconds per picture width, for at that velocity, the signal modulation decreases to zero.

How much less, depends upon the loss in signal modulation that can be tolerated. For example, if the MTF must be 0.5 or better at 225 lines, the cut-off frequency N_c must be increased. In Fig. 27, we plot MTF vs N/N_c . For 0.5 response, N/N_c is about 0.6 and thus to obtain 0.5 response at $N = 225$ lines, N_c must be increased to $225/0.6$ or 375 lines and the motion from Fig. 26 must be less than about 8.5 sec/picture width.

In yet another description, we let $\Delta x_v = v_i t_f$ be the distance moved per exposure time and since $\Delta x = Y/N$, then

$$\begin{aligned}
 R_o(N) &= \frac{\sin(\pi \Delta x_v / 2 \Delta x)}{\pi \Delta x_v / 2 \Delta x} \\
 &= \frac{\sin(\pi n_v / 2)}{\pi n_v / 2}
 \end{aligned} \tag{39}$$

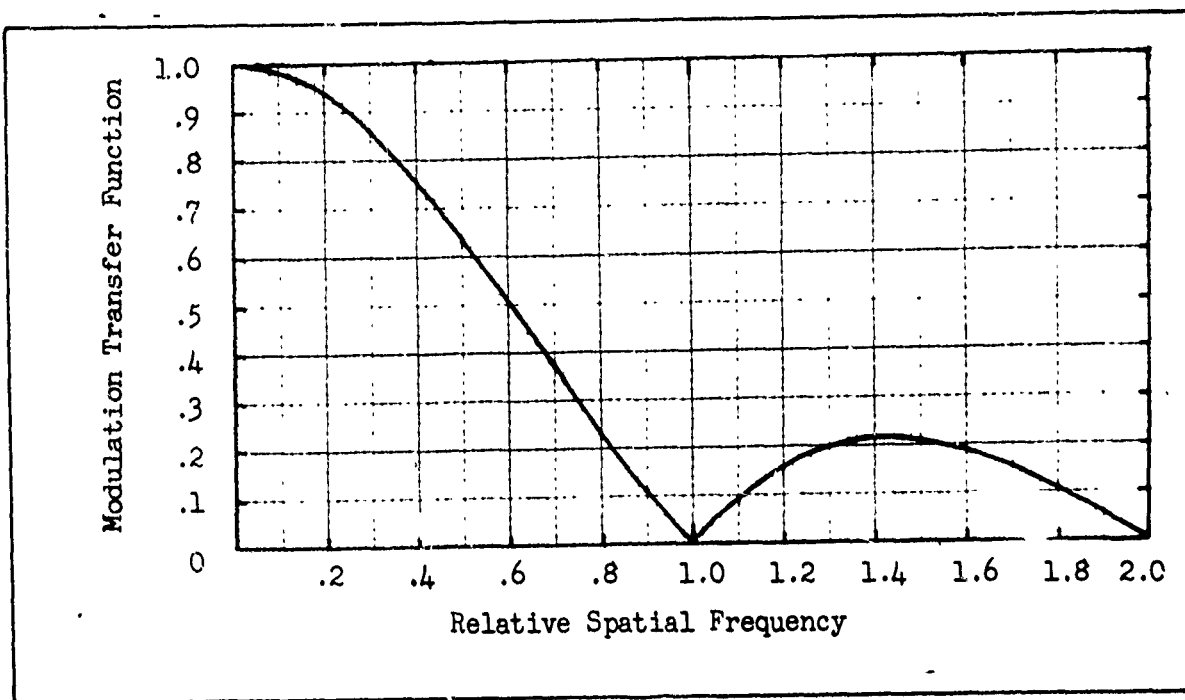


Fig. 27 Modulation Transfer Function Due to Linear Image Motion vs Spatial Frequency Normalized to the Cut-Off Frequency.

where n_v is the number of lines the pattern moves in an exposure time. This MTF is plotted in Fig. 28. It is seen that if the bar pattern moves one line per integration time, the MTF drops to 63% while for $1\frac{1}{2}$ lines, the MTF is 29%.

In most air-to-ground surveillance tasks, a ground point must be quite precisely tracked. The linear motion MTF argument can be used to conclusively show this need. Assuming a ground point is tracked, linear motion should not be much of a factor but its discussion is still worthwhile because it is the easiest to understand.

Sinusoidal image motion of constant amplitude can result from resonances in the mechanical structure. The form of the motion is shown in Fig. 29. The MTF for sinusoidal motion has been derived

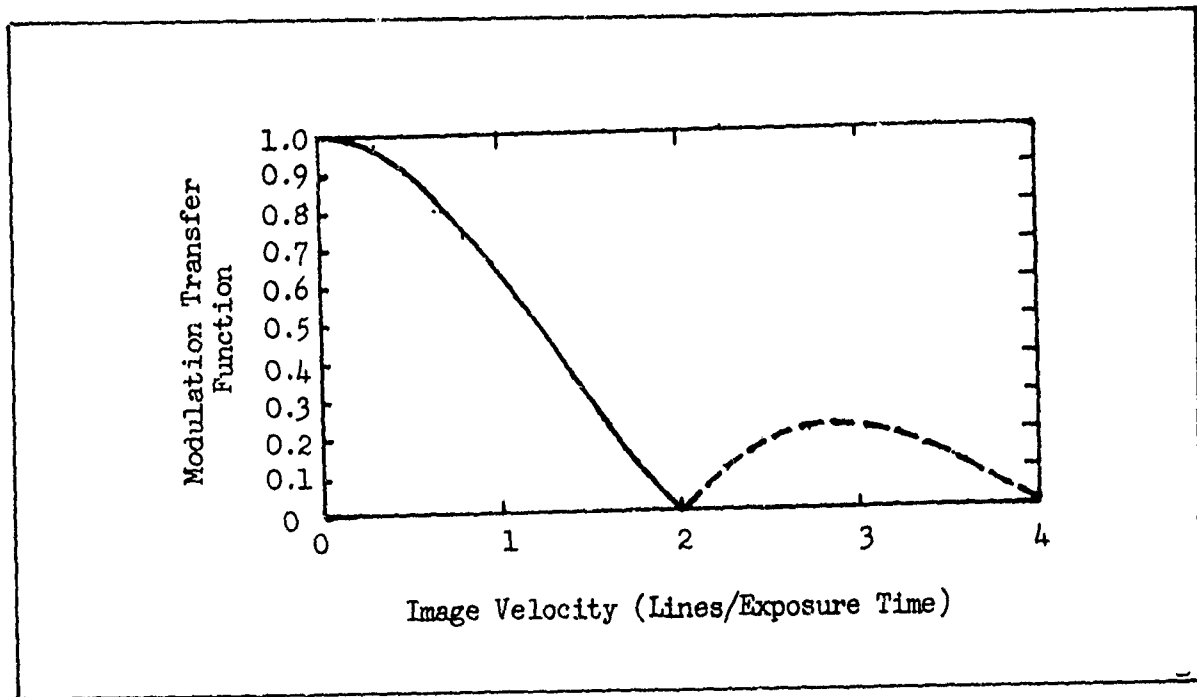


Fig. 28 Modulation Transfer Function for Linear Image Motion.

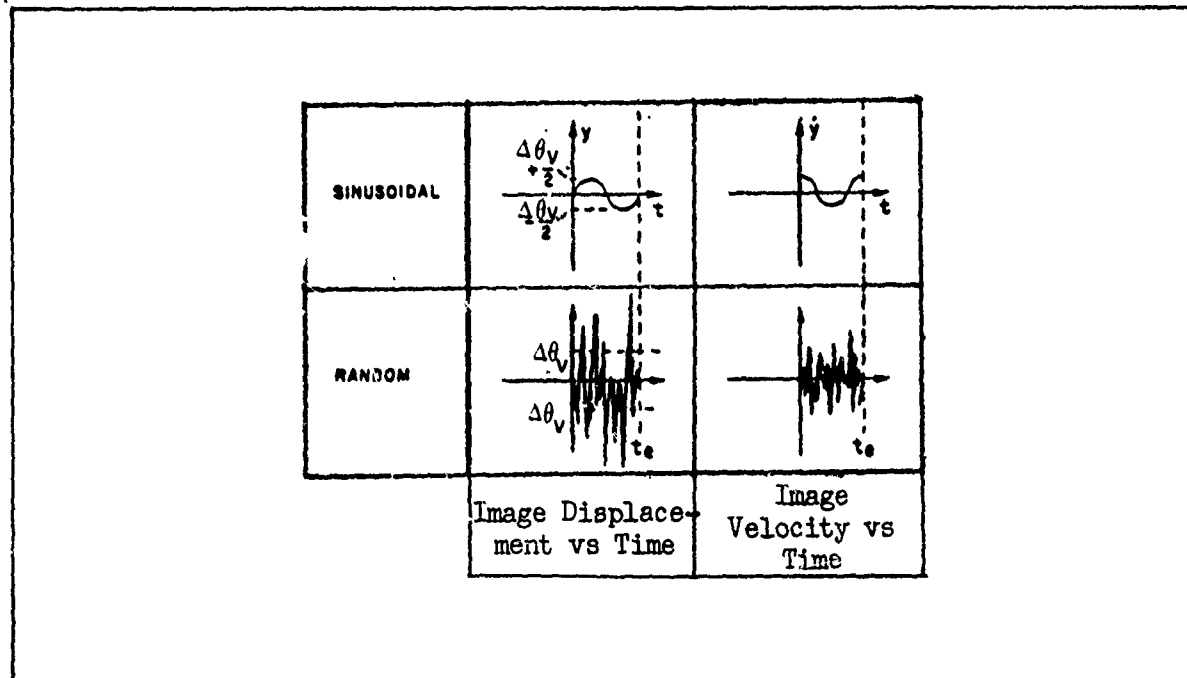


Fig. 29 Waveforms of Image Displacement and Velocity vs Time.

for the special case where the beginning of a cycle coincides with the beginning of the exposure time and ends at the end of the exposure time. The effect will be the same whether one cycle or an integral number of cycles occur within the exposure time — the MTF is a function only of the spatial frequency of the sinusoid and its amplitude. The MTF is

$$R_o(N) = J_o\left(\frac{AN}{2Y}\right), \quad (40)$$

where J_o is a Bessel function of zero order, A is the peak-to-peak amplitude of the motion in mm and Y is the picture height also given in mm. For the assumed system, the amplitude, A , may be written as $F_L \cdot \Delta\theta_v$ where F_L is the lens focal length and $\Delta\theta_v$ is the peak-to-peak angular motion. Then,

$$R_o(N) = J_o\left(\frac{F_L \Delta\theta_v N}{2Y}\right). \quad (41)$$

This function is plotted in Fig. 30 for $\Delta\theta_v = 25, 50$ and 100 microradians. Again, a negative (false resolution) response can be discerned.

Next, we note that the cutoff spatial frequency, i.e., the spatial frequency at which the response goes to zero in Fig. 30 is given by

$$N_c = 1.53 N_v, \quad (42)$$

where N_v is the amplitude of the motion measured in lines per picture height. Alternatively, in angular terms

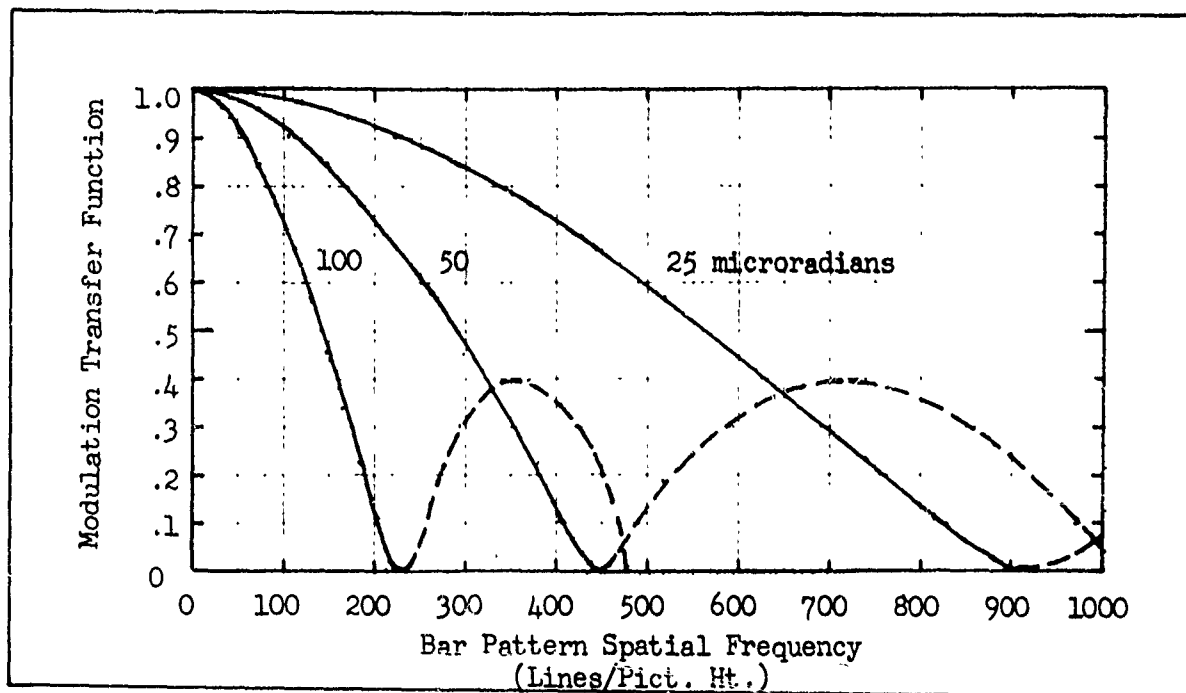


Fig. 30 Modulation Transfer Function vs Bar Pattern Spatial Frequency for Sinusoidal Motion of Peak Amplitude of 100, 50 and 25 microradians per Exposure Time for the Assumed System.

$$\Delta\theta_c = \frac{\Delta\theta_v}{1.53} \quad , \quad (43)$$

and

$$N_c = \frac{Y}{F_L \cdot \Delta\theta_c} = \frac{1.53Y}{F_L \cdot \Delta\theta_v} \quad . \quad (44)$$

These last two functions are plotted in Fig. 31. To illustrate, suppose the peak-to-peak sinusoidal motion is 100 microradians per exposure time. Then $\Delta\theta_c$, the angular subtense of a bar in the bar pattern for which the signal modulation is zero is 62.8 microradians. For our assumed system, 62.8 microradians translates to a TV camera resolution of 222 lines per picture height.

In normalized form, the modulation transfer function becomes

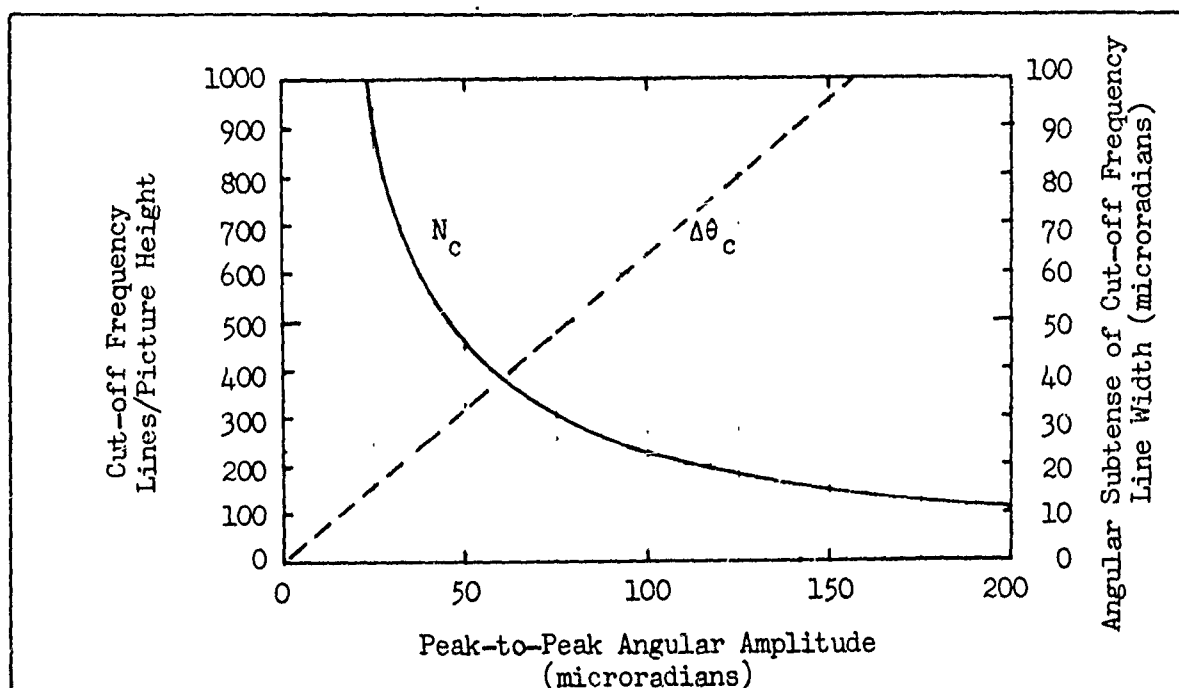


Fig. 31 Cut-off Frequency and the Angular Subtense of Cut-off Frequency Line Width vs the Peak-to-Peak Angular Amplitude of Sinusoidal Motion.

$$R_o(N) = J_o\left(\frac{1.53\pi}{2} \cdot \frac{N}{N_c}\right), \quad (45)$$

which is plotted in Fig. 32. This curve can be used in a manner analogous to Fig. 27 to determine the value of the modulation transfer factor at a spatial frequency below the cutoff value.

Finally, the modulation transfer function is shown in Fig. 33 as a function of the peak-to-peak motion given in terms of the number of lines the motion subtends at the spatial frequency in question. It is seen that if the bar pattern motion is 1 line per exposure time, the MTF drops to 47% and drops to zero for motion of the order of 1.5 lines per exposure time.

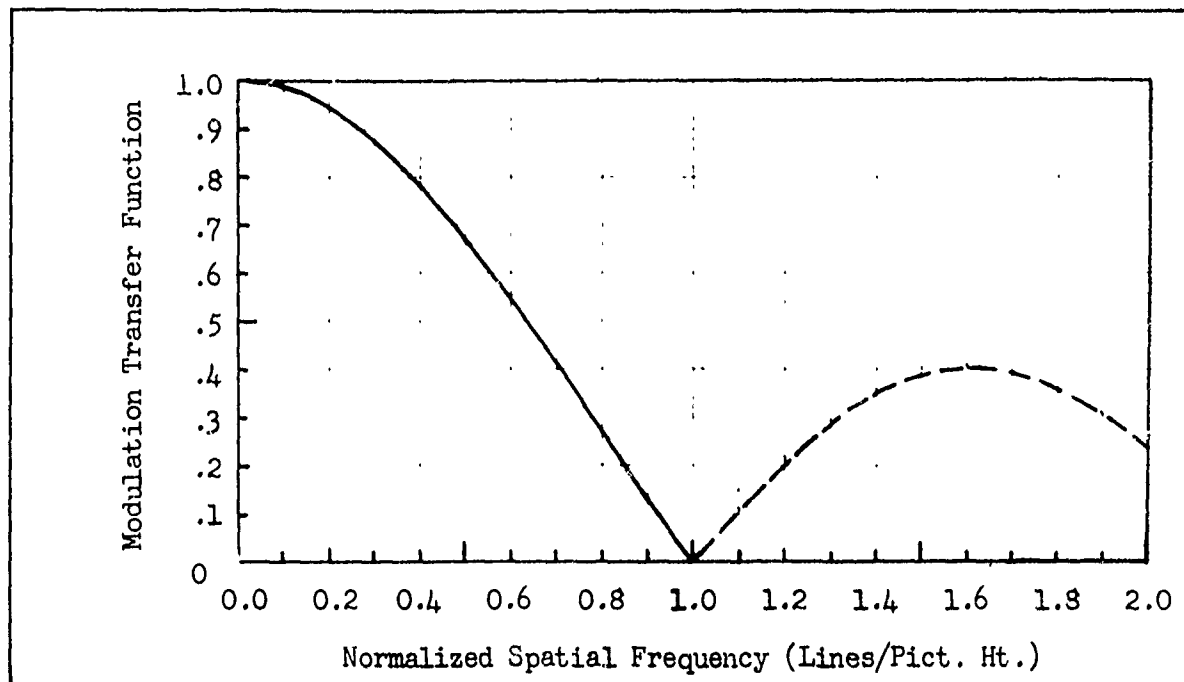


Fig. 32 Modulation Transfer Function for Sinusoidal Motion vs Spatial Frequency Normalized to the Cut-off Frequency.

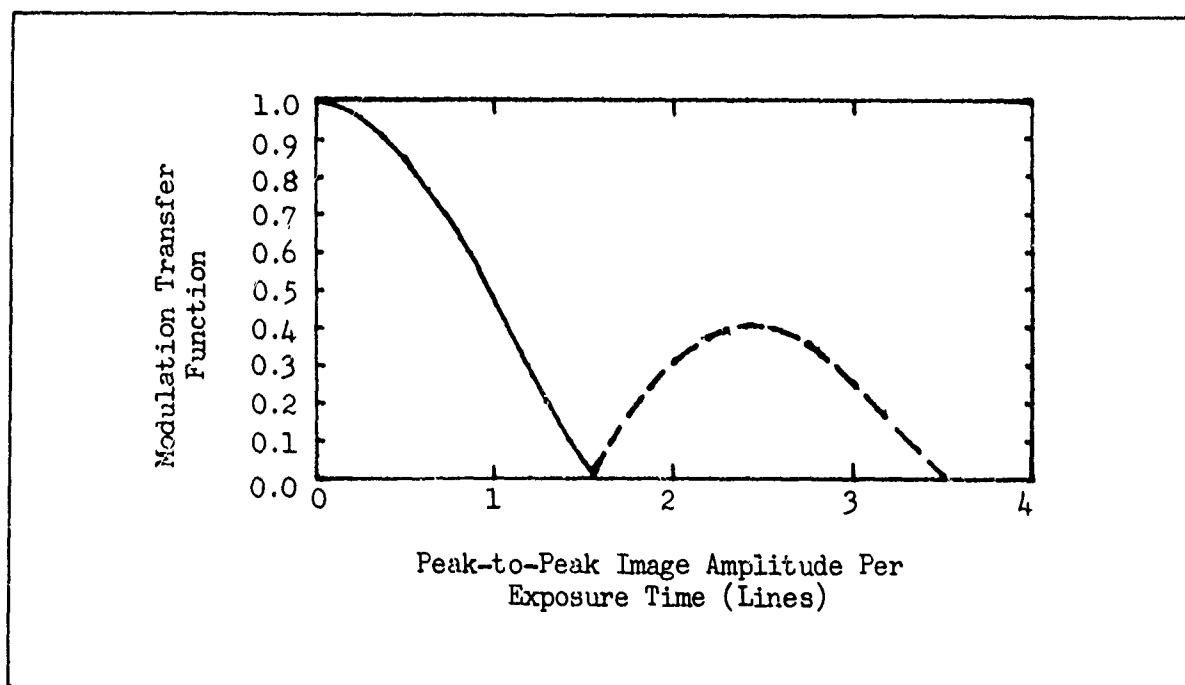


Fig. 33 Modulation Transfer Function for Sinusoidal Image Motion.

It is seen in Fig. 30 that image motion of any particular spatial frequency has an effect at all other spatial frequencies. It may happen that the line-of-sight will vibrate at 2 or more frequencies (or be such that it can be decomposed into a small number of discrete frequencies). In this case, the overall MTF effect can probably be estimated by taking the product of the MTF's associated with the various frequencies.

Random motion is perhaps the most commonly encountered in practice. For this case, the MTF is given by

$$MTF = \exp\left[-\frac{1}{2}\left(\frac{\pi AN}{Y}\right)^2\right] \quad (46)$$

with the terms being as before except that the amplitude, A, is measured in terms of its rms value. As in the sinusoidal motion case, we can write the amplitude A as $F_L \Delta\theta_v$ so that

$$MTF = \exp\left[-\frac{1}{2}\left(\frac{\pi F_L \Delta\theta_v N}{Y}\right)^2\right] \quad (47)$$

This equation is plotted in Fig. 34 for various values of the angular motion amplitude $\Delta\theta_v$.

Since the exponential term does not pass through zero, we arbitrarily define the cut-off spatial frequency as that frequency for which the MTF is 0.02, then

$$N_c = 0.89 N_v \quad , \quad (48)$$

where N_v is the rms amplitude of the motion per frame time measured in

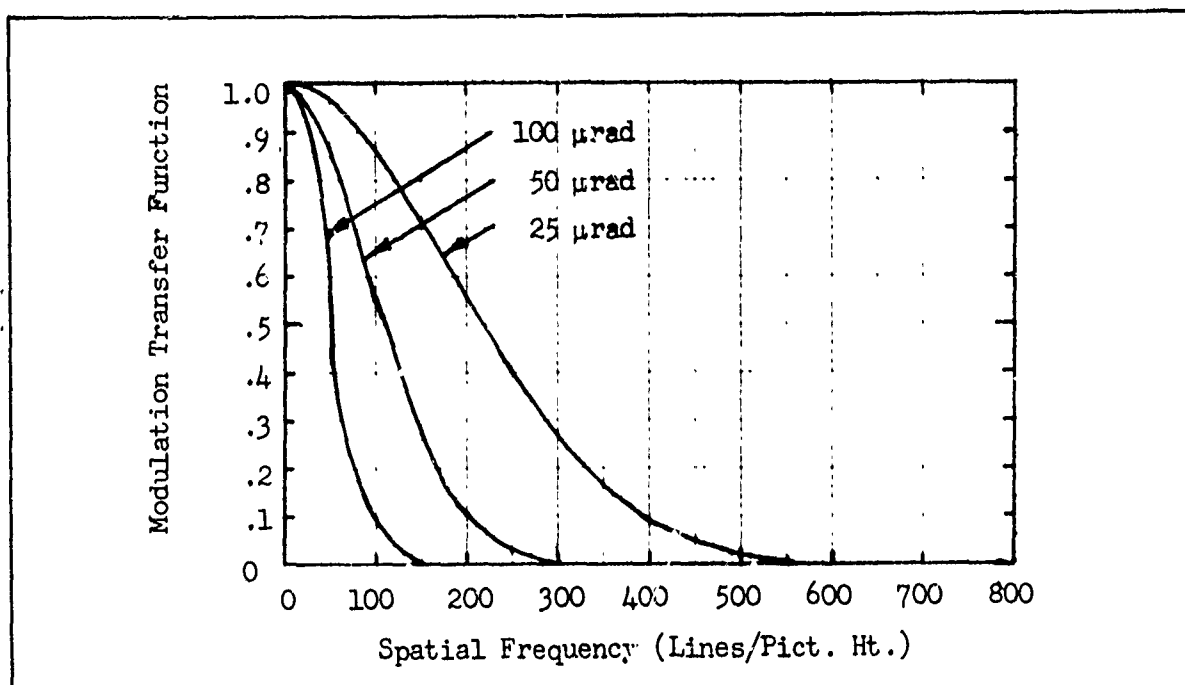


fig. 34 Modulation Transfer Function for the Assumed System with Random Image Motion of RMS Amplitude 25, 50 and 100 microradians per Exposure Time.

lines per picture height.

By analogy to the sinusoidal motion case, we can write

$$\Delta\theta_c = \frac{\Delta\theta_v}{0.89} , \quad (49)$$

and

$$N_c = \frac{0.89Y}{F_L \cdot \Delta\theta_v} , \quad (50)$$

which are plotted in Fig. 35. The MTF normalized to the cut-off frequency is given by

$$R_o(N) = e^{-3.92\left(\frac{N}{N_c}\right)^2} , \quad (51)$$

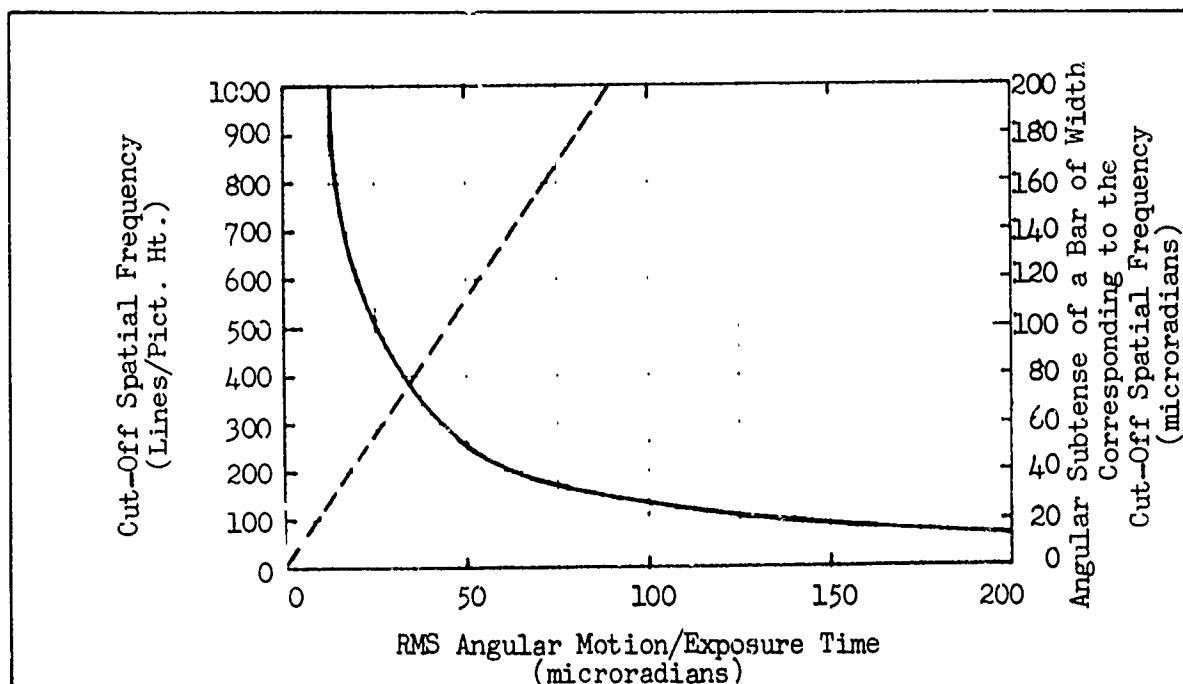


Fig. 35 Cut-off Spatial Frequency and Angular Subtense of Corresponding Period for the Assumed System as a Function of the RMS Angular Motion per Exposure Time. Angular Subtense is Shown as Solid Line.

and is plotted in Fig. 36. Also, the MTF is plotted as a function of the rms image motion amplitude expressed in lines in Fig. 37. Finally, the MTF is shown for the assumed system of Section 2.2 in Fig. 38 together with the effect of a 50 microradian rms motion. As can be seen, the motion MTF completely dominates.

The effect of random motion on system resolution is shown in Fig. 39 in units of lines per picture height and in Fig. 40 in terms of threshold angle. These curves were drawn for an input image modulation of 0.3 and three values of motion (static and 25 and 50 microradians rms). The curves of threshold angle relate most directly to range since range is directly proportional to $\Delta\theta$. With good visibility, reducing the rms motion amplitude by a factor of 2 results in a 50 - 60% range increase.

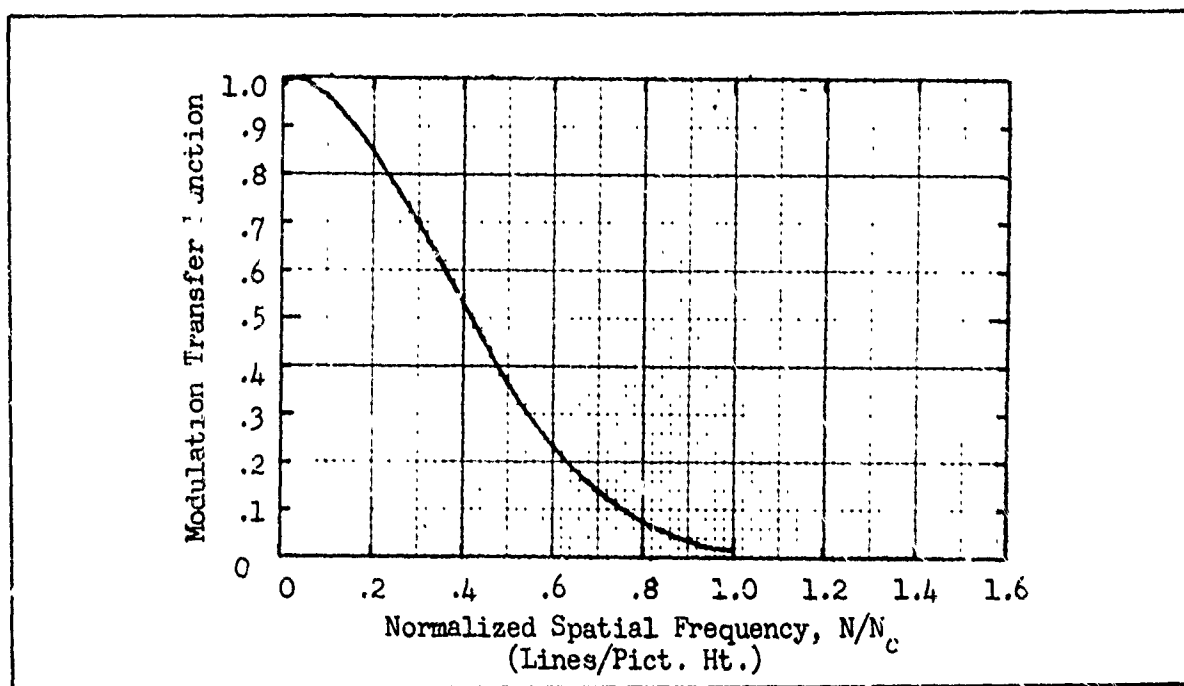


Fig. 36 Modulation Transfer Function vs Spatial Frequency Normalized to the Cut-off Frequency for Random Image Motion.

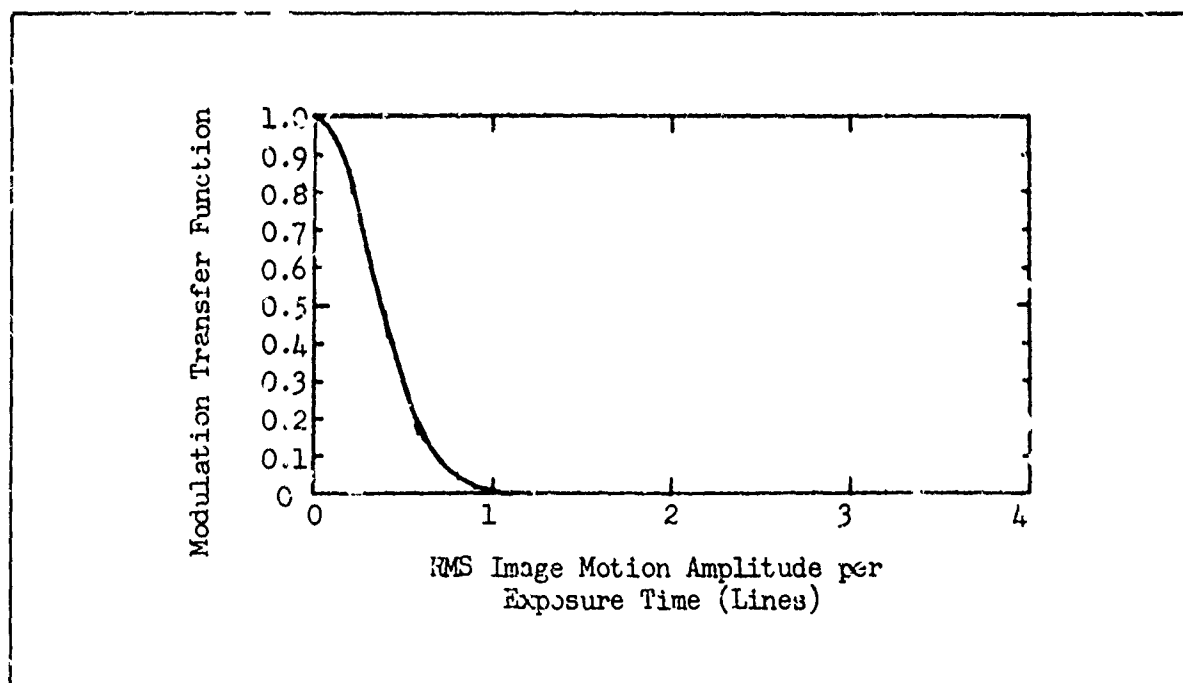


Fig. 37 Modulation Transfer Function for Random Image Motion.

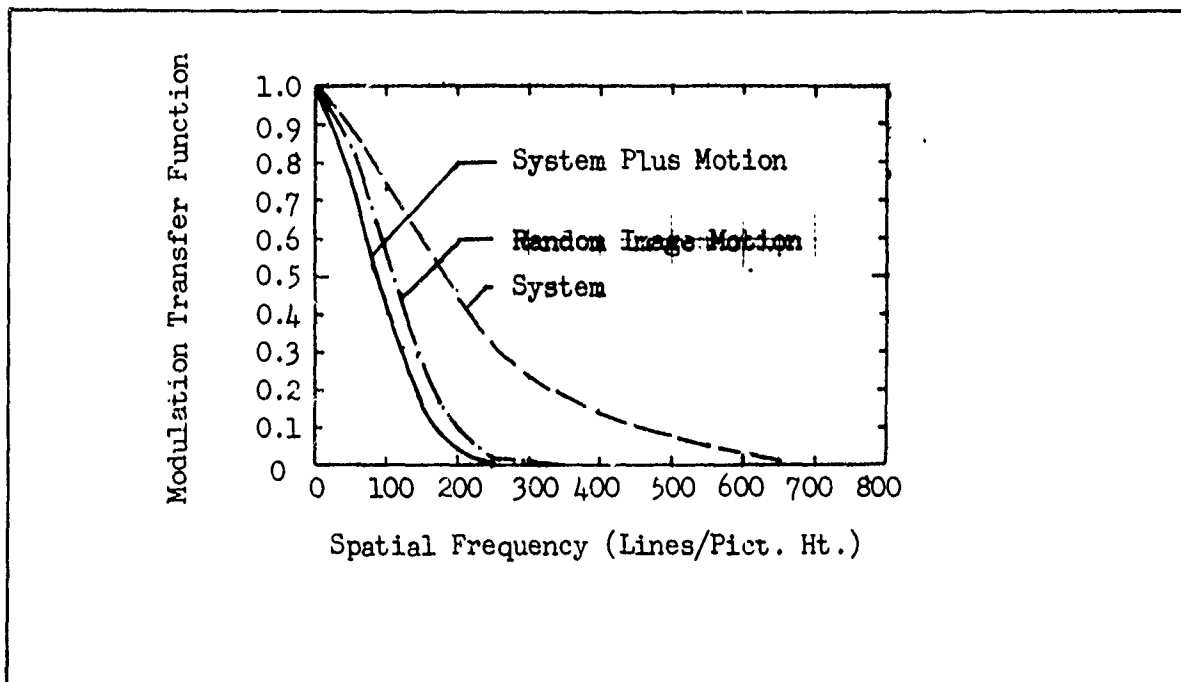


Fig. 38 Modulation Transfer Function for Static System and Scene and for System with Scene in Random Motion of RMS Amplitude 50 microradians with 660 mm Focal Length Lens.

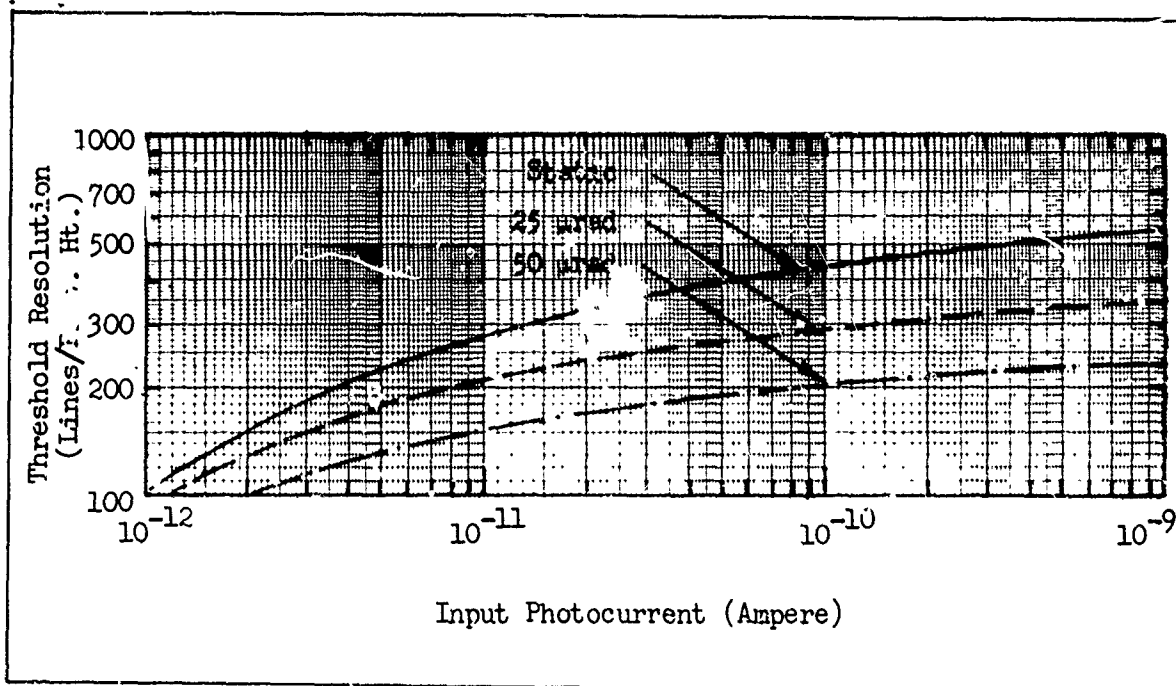


Fig. 39 Threshold Resolution vs Input Photocurrent for the Assumed Sensor with a Static Scene and with Random Motion of the Sightline of Magnitude 25 and 50 μ rad. $C_M = 0.3$.

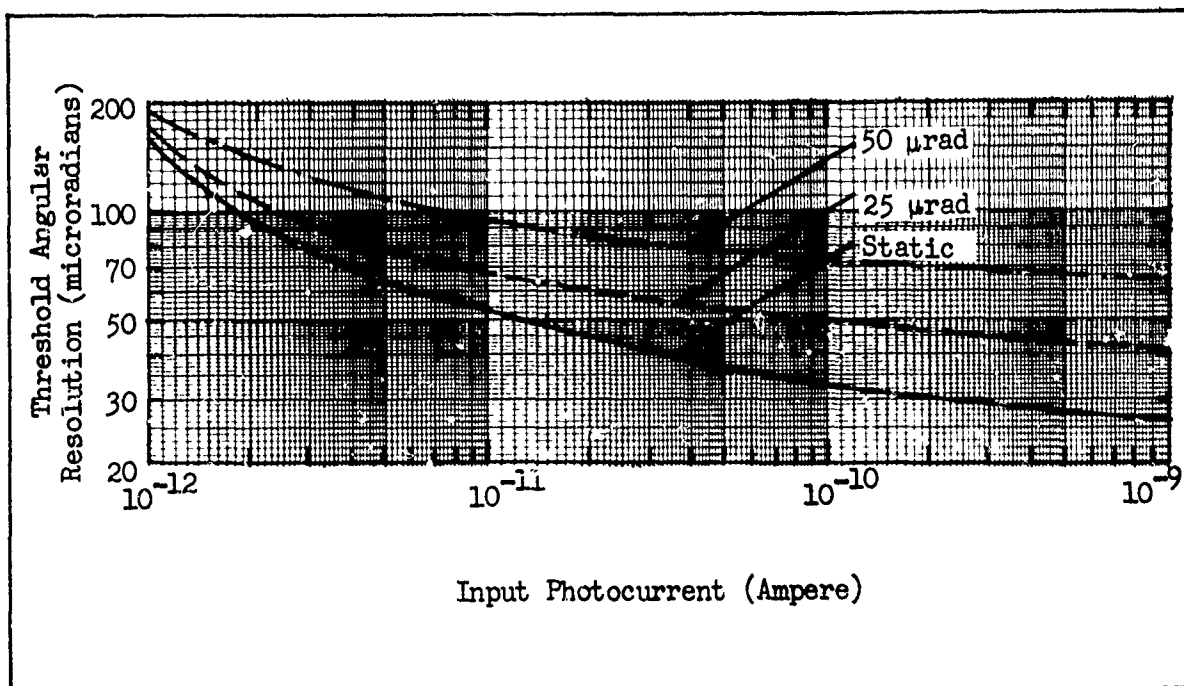


Fig. 40 Threshold Angular Resolution vs Input Photocurrent for the the Assumed Sensor with a Static Scene and with Random Motion of the Sightline of Magnitude 25 and 50 μrad . $C_M = 0.3$.

The angular resolution for the aperiodic and periodic case is shown in Fig. 41. Also shown is the balanced resolution calculated on the basis of the average threshold resolution in lines/pict. ht. These curves were drawn for a random motion of 50 microradian rms amplitude and an input image contrast of 0.1.

In many systems, it is customary to optically zoom the field of view in order to have a wide angle view (WAV) for general navigation and a narrow field of view (NAV) for object recognition. In changing the field of view by say a factor of 4, it is hoped to increase the resolution of scene detail by the same factor. However, in the NAV, the hoped for increase in resolution will not usually be realized because of the more serious effect of motion on the NAV. To show this effect we calculated the limiting resolution for a field of view 4 times larger than

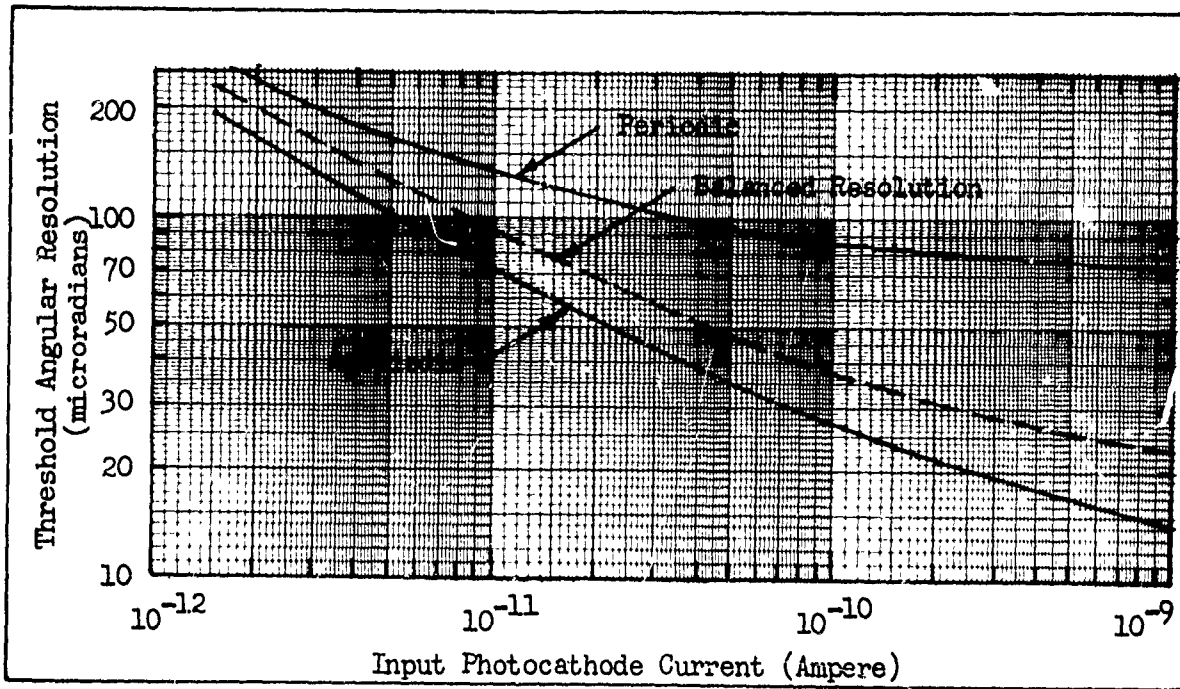


Fig. 41 Threshold Angular Resolution vs Input Photocathode Current Based on the Periodic, Aperiodic and the Average Calculated for the Threshold Resolution in Lines/Pict. Ht. $C_M = 0.1$.

that used in the discussion heretofore with the results shown in Fig. 42. The dashed line, shows the angular resolution in the WAV (about a 4° field of view) and the solid line shows the angular resolution in the NAV (about a 1° field of view). In both cases, the modulation contrast is assumed to be 0.3, the image motion is random of rms amplitude 50 microradians, and the periodic image model was used.

The image appearing on the display is actually 4 times larger in the NAV than in the WAV but the useful magnification, based on threshold angular resolution is much less as can be seen in Fig. 43 where we plot the ratio of angular resolution in the NAV to that in the WAV. At high light levels, the actual effective magnification, when sightline motion is a factor, is only about 2 rather than 4 as ideally expected.

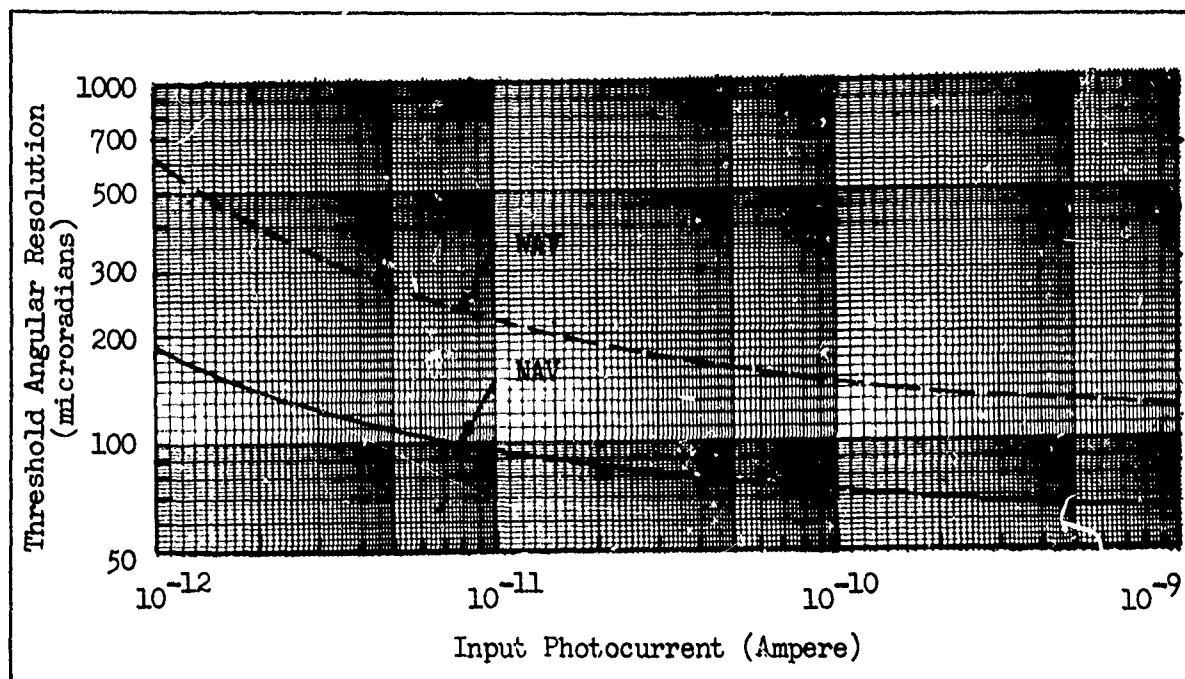


Fig. 42 Threshold Angular Resolution vs Input Photocurrent with a Random Motion of Amplitude 50 microrad RMS for a WAV and NAV. $C_M = 0.1$.

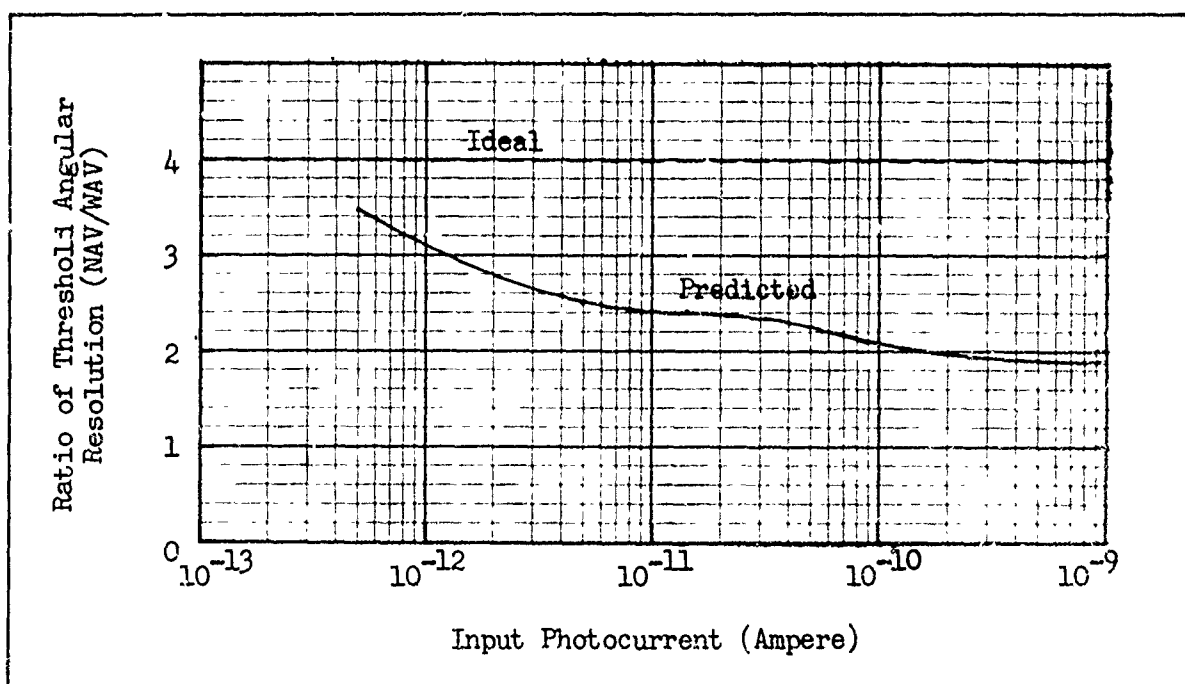


Fig. 43 Ratio of Threshold Angular Resolution in NAV to that in WAV with Random Sightline Motion of Amplitude 50 microrad RMS. $C_M = 0.1$.

The subject of camera time constants will be treated in detail in Section 4 but the results will be briefly reviewed here. The time constants of a camera can be quantitatively thought of as being due to the capacity and resistance of the charge storage surface and the resistance of the reading beam. As an example, consider the EBSICON camera tube which has a photoemissive photocathode and a silicon diode mosaic storage surface. The mosaic is charged by photoelectrons which were accelerated through a large voltage. In the target, the energy of the photoelectron is converted to hole-electron pairs and the electrons are stored in the capacity of the back biased diodes. With proper design, the RC time constant of the diodes is large enough so that the charge will be retained for a number of frame times which implies that the capacitance of the targets is relatively high (for a given R). For readout, the capacitors are discharged through the resistance of the electron beam and for fastest operation, the capacitance of the target should be small. Clearly a tradeoff is dictated between target storage time and readout time constants. At low signal current operation, the resistance of the electron scanning beam is high and the RC time constant of the readout process is higher than that at high signal currents where the beam resistance is low so a number of frames are required to completely read out the charge. This will have the effect of contrast reduction for dynamic imaging.

Target voltage can also markedly influence the process. A large target voltage, which causes the target capacity to decrease, will decrease the RC time constant, whereas with a low target voltage, the target capacity increases and the RC time constant is larger.

As shown in Section 4, the lag introduced by the RC time constant can be appreciable with low target voltages even though the signal levels are high. Other tubes, with lower prestorage gain such as the I-SEC and I-I-Isocon have even greater lag problems. Dynamic MTF measurements have been made but the results do not appear to fully account for the considerable loss in sensitivity at low spatial frequencies. However, this must be interpreted as an inadequate measurement procedure. Image lag effects will be a major concern in the follow-on program. Because of the preliminary nature of the results obtained so far, we do not propose a method of including lag effects into the analysis at this time. The designer is cautioned, however, that the loss in sensitivity due to lag may be as much as a factor of 4 to 100 at low light levels and due account of lag effects should be made in selecting a sensor for a given application.

2.5 The Balanced Resolution Concept

The effort in sensory system modeling for the purpose of predicting the range at which a real scene object can be discerned is to find a simpler equivalent test object that can be used to replace the real scene object. Presumably, a correspondence can be found between the range at which the real scene object can be discerned with the needed clarity and the range at which the equivalent test object can be detected (or resolved). The simpler equivalent test object should be easy to make and fully amenable to analysis. It is, however, clear that no single test object can be found that will be fully equivalent to all real scene objects which are of infinite variety and complexity. On-the-other-hand, if systems design is to be

anything but a trial and error process, equivalent test objects must be found.

The equivalent bar pattern as suggested by Johnson represents one of the first attempts to find a test pattern which can be used in laboratory evaluation and analysis. This approach makes good sense because it imposes a system resolution requirement. This model was further refined and experimentally tested with the results discussed previously in Ref. 2. The principal deficiency in the concept was in defining the method of measuring the image signals in the real object. It was first thought that the average modulation within the real object could be used but this would require some sort of area weighting. In the end, the maximum signal swing was used which is different than the method of measuring signal swing in the bar pattern which is the mean signal.

A bar pattern, being repetitive, is one of the most difficult of the one-dimensional images to detect and hence it is felt that its use will result in pessimistic predictions. However, in the past, range predicted using the equivalent bar pattern has shown reasonable correlation with range measured for real objects imaged against a terrain background. This is in large part due to the neglect of many important system parameters such as the sky-to-ground brightness ratio, sensor time constants, image motion and display-observer interactions. That is, the pessimistic nature of the equivalent bar pattern prediction obscures other system defects which are, more often than not, neglected. As our knowledge of these system defects

increases, it becomes necessary to take these other factors into account. In particular, when an effect is isolated, such as sightline vibration, it is important that the impact of the effect on range be known. Increases in stability, for example, can be quite costly and the desire will be to evaluate the cost of greater sightline stability vs the improvement in range to be expected.

In an attempt to find a better model, the balanced resolution concept was proposed. The first procedure adopted and rather extensively used in the above is to calculate the resolution based on the equivalent bar pattern and then on a single bar of the bar pattern. For a given set of operating conditions, the calculation results in two values of limiting resolution N_1 and N_2 in lines per picture height. The "balanced" resolution N_b was then taken to be

$$N_b = (N_1 + N_2)/2 \quad . \quad (52)$$

The result of this procedure is shown in angular resolution form in Fig. 41. It is seen that the results are dominated by the aperiodic model and will undoubtedly give far too optimistic results. A possibility is to calculate the aperiodic resolution on the basis of an element of size equal in height and width to the bar width in the equivalent bar pattern.

An alternate approach is to calculate the balanced resolution on the basis of the average angular resolution. This is equivalent to averaging

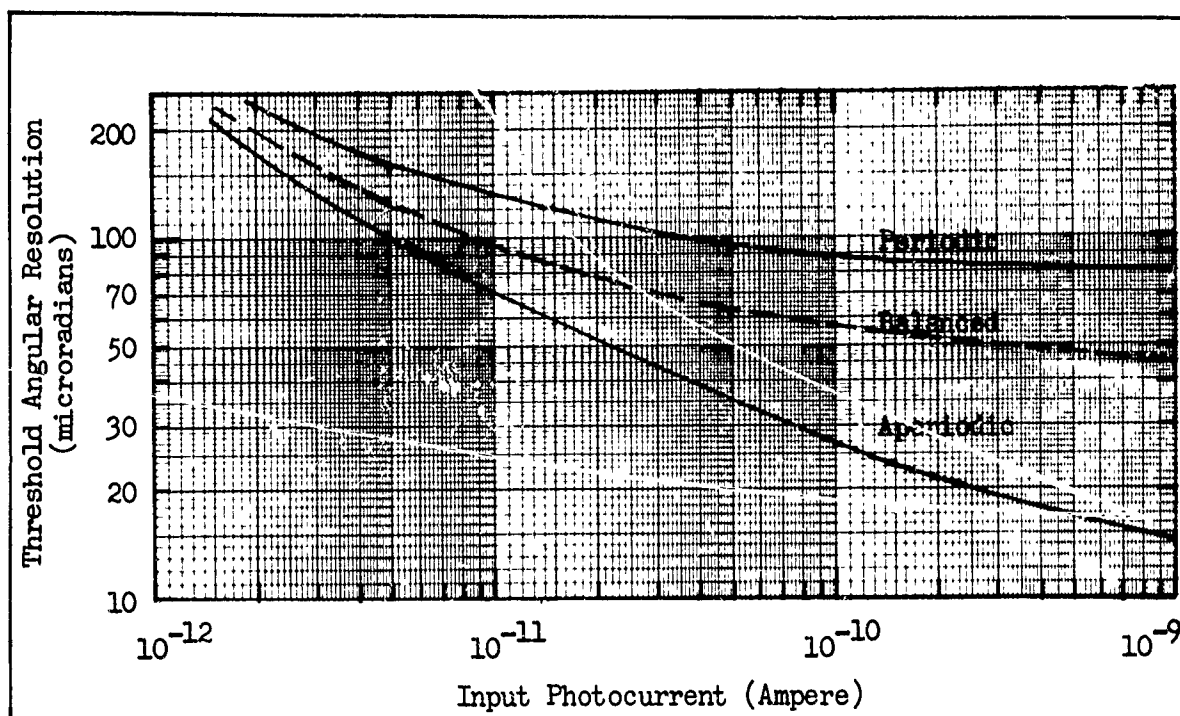


Fig. 44 Threshold Angular Resolution vs Input Photocurrent Based on the Periodic, Aperiodic and the Average Calculated for Threshold Angular Resolution in microradians. $C_M = 0.1$.

$$\begin{aligned}\Delta\theta_b &= (\Delta\theta_1 + \Delta\theta_2)/2 \\ &= \frac{1}{2} \left(\frac{1}{N_1} + \frac{1}{N_2} \right) \quad (53)\end{aligned}$$

This is also equivalent to averaging the ranges calculated using the aperiodic and periodic model. The result of averaging on an angular basis is shown in Fig. 44. As can be seen, averaging on the angle basis biases the result toward the periodic model.

If a choice were to be made at this point in time, we would tend to favor averaging the results on the angle basis because it gives results better than the pessimistic periodic model but not as optimistic as the aperiodic model which is considered to be excessively optimistic for use in recognition or identification models. The search is, of

course, for a weighting function and, in particular, for one which makes use of the currently well known models that we currently have. However, further efforts are needed to justify the weighting function, whatever it may be, on a rational basis. These first preliminary efforts are for the purpose of examining the impact of certain assumptions.

3.0 Display Signal-to-Noise Ratio Fundamentals

In this section, we will discuss the fundamentals of the display signal-to-noise ratio concept starting with the elementary or ideal model and then adding to the model to bring it into closer correspondence with reality. The elementary model takes into account the image's dimensions, signal levels, and noise levels but otherwise assumes that the image is transmitted through the sensory system with perfect spatial fidelity. The elementary model is then refined by including the effects of finite imaging apertures such as the objective lens, reimaging sensors such as an image intensifier, the TV camera tube and etc. The images and the apertures which alter the image's amplitude, shape and position are analyzed by Fourier methods using the methods of communications theory. An attempt has been made to be general and fairly rigorous in these derivations. We are indebted to Robert L. Sendall of Electro-Optical systems for many of the concepts presented particularly in the area of the aperiodic image treatment.

In Sections 4 and 5, we will discuss some preliminary efforts made to verify the theory. As will be seen, the theory adequately predicts first order effects and many second order effects as well. However, second order effects are quite difficult to measure through psychophysical experimentation partly because of the weak functional dependence of the effects and partly because of the statistical nature of the experimentation.

3.1 The Elementary Model

The historical development of the elementary model was noted and the model was derived in Ref. 2. The purpose of this discussion is to review the elementary model and to give further insight with regard

to its meaning and use. The basic formulation assumes a small rectangular image of area, a , amid a much larger background. Suppose the average number of photoelectrons generated by the sensor's photosurface in time, t , due to the image area, a , is n_2 and the number generated by an equally sized comparison area in the background is n_1 . Then the elementary model as derived in Ref. 2 gives the mean signal-to-rms-noise ratio of the image as

$$\begin{aligned} \text{SNR}_{\text{pc}} &= (n_2 - n_1) / [(n_1 + n_2)/2]^{\frac{1}{2}} \\ &= (\dot{n}_2 - \dot{n}_1)at / [(\dot{n}_1 + \dot{n}_2)at/2]^{\frac{1}{2}}, \end{aligned} \quad (54)$$

where \dot{n}_1 and \dot{n}_2 are the photoelectron generation rates in units of electrons per unit area and time. The subscript pc is added to SNR to indicate that this is the SNR at the output of the input photosurface. We define the image modulation contrast as

$$\begin{aligned} C_M &= \frac{\dot{n}_2 - \dot{n}_1}{\dot{n}_1 + \dot{n}_2} \\ &= \frac{\dot{n}_2 - \dot{n}_1}{2\dot{n}_{\text{av}}}, \end{aligned} \quad (55)$$

so that

$$\text{SNR}_{\text{pc}} = \frac{2C_M \dot{n}_{\text{av}} (at)^{\frac{1}{2}}}{[\dot{n}_{\text{av}}]^{\frac{1}{2}}}. \quad (56)$$

In the above derivation, it is assumed that the noise is due to the image photon-to-electron conversion process. When this is the case, the

sensor is said to be photoelectron-noise-limited. For later convenience, the photoelectron rates, \dot{n} , are written in terms of the photocurrents, i , as follows

$$i = \dot{n}eA \quad , \quad (57)$$

where e is the charge of an electron and A is the total effective photosurface area. Now, Eq. (56) becomes

$$SNR_{pc} = \left(\frac{at}{A}\right)^{\frac{1}{2}} \frac{2G_M i_{av}}{[ei_{av}]^{\frac{1}{2}}} \quad . \quad (58)$$

In a typical high performance TV camera tube, the image is next transferred to a gain storage target of gain, G_T , and storage time, t_f , so that

$$SNR_T = \left(\frac{at_f}{A}\right)^{\frac{1}{2}} \frac{2G_T G_M i_{av}}{[G_T^2 ei_{av}]^{\frac{1}{2}}} \quad . \quad (59)$$

Note that the signal, $2G_T G_M i_{av}$, and the photoelectron noise, $[G_T^2 ei_{av}]^{\frac{1}{2}}$, are equally amplified with no net result at this point. In TV, the gain storage target is sequentially scanned line-by-line by an electron beam. It is possible to measure a signal-to-noise ratio in the video channel which is given by

$$SNR_{VO} = \frac{2G_T G_V G_M i_{av}}{\sqrt{2(G_T G_V)^2 ei_{av} \Delta f_V}} \quad , \quad (60)$$

where the subscript 0 in SNR_{V0} refers to the notion that the signal amplitude is not limited by the sensor apertures, G_V is the video amplifier gain, and Δf_V is the video bandwidth. Combining Eqs. (59) and (60), we observe that

$$SNR_D = [2t_f \Delta f_V (\frac{a}{A})]^{\frac{1}{2}} SNR_{V0} \quad . \quad (61)$$

The subscript, D, is added to note that the image signal-to-noise ratio is now referred to the image appearing on a hypothetically perfect display. In the video, the image is frequency upconverted by the electron beam scanning process. In the display, the image frequencies are downconverted by the reverse process, i.e., the electron beam of the cathode ray tube display recreates the original image on the display.

The image area ratio $(\frac{a}{A})$ is dimensionless. This is a convenience in later analysis because the real image area can become larger or smaller as it traverses the system. The use of dimensioned units requires that scale changes be made at each point where the image changes size. But even further, we note that the displayed image can be much larger than the image on the input photosurface. We also note the video gain, G_V , appearing in Eq. (60). By suitably adjusting the d-c level of the display brightness and the video gain, the displayed image can be much brighter and of greater contrast than the image incident on the input photosurface. Thus, in theory, the displayed image can be sufficiently large, sufficiently bright and of high enough contrast

so that the observer's eye, viewing the displayed imagery will be neither acuity, nor contrast, nor displayed-image-brightness limited. If these conditions are met, the SNR_D becomes the SNR_{DI} , the image signal-to-noise ratio generated in the observer's retina provided* that the time, t_f , is changed to the time, t_i , the integration time of the eye.

The above equations represent the image signal-to-noise ratio obtainable from the sensor. The SNR_{DI} required by the observer is determined through psychophysical experimentation as was extensively discussed in Ref. 2. In early work by De Vries (Ref. 7), it was assumed that to be detectable, the image SNR_{DI} must equal or exceed some threshold constant, i.e.,

$$SNR_{DI} \geq K_T = SNR_{DT} \quad . \quad (62)$$

This was verified in Ref. 2 with the typical result shown in Fig. 45 in the form of probability of detection vs signal-to-noise ratio. The threshold signal-to-noise ratio, SNR_{DT} , corresponding to a 50% probability of detection, is very nearly a constant, independent of image size for most of the image sizes of interest (the exceptions are noted in Ref. 2).

As previously noted in Section 2.1, it is hypothesized that an observer must detect the presence of a single bar in a bar pattern to discern the presence of a bar pattern. Thus, Eqs. (59) and (61) apply.

* Assuming continuous presentation of the scene on the display.

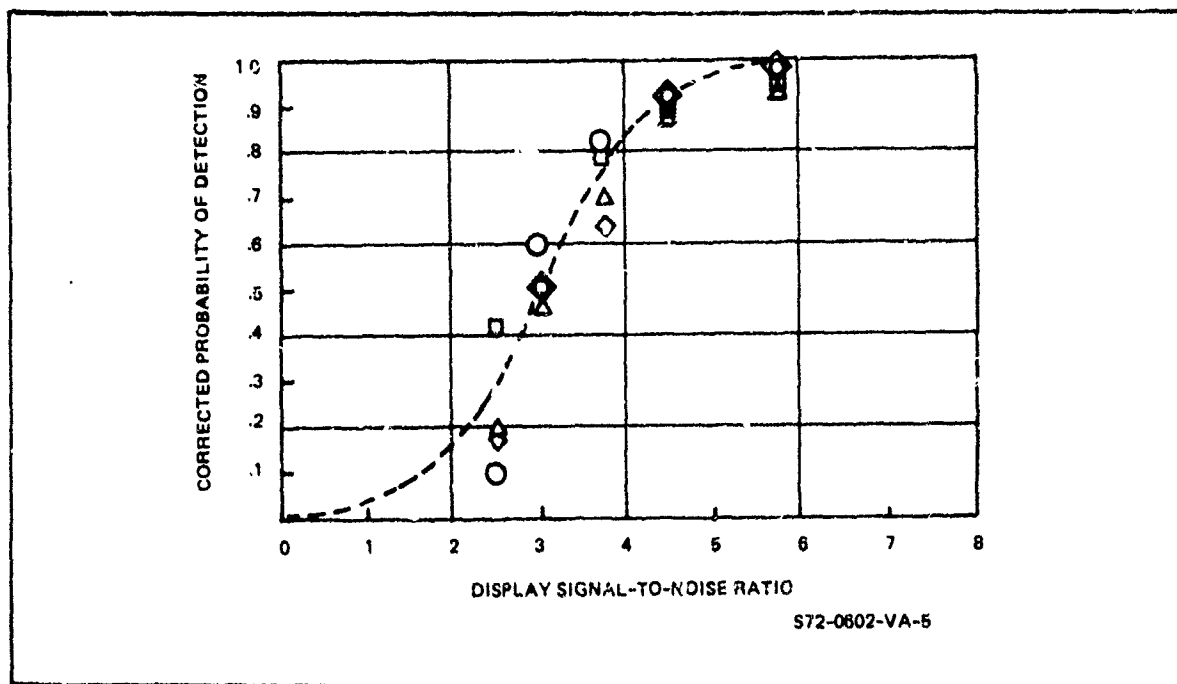


Fig. 45 Corrected Probability of Detection vs SNR_{DI} Required for Rectangular Images of Size $\bigcirc 4 \times 4$, $\square 4 \times 64$, $\triangle 4 \times 128$ and $\diamond 4 \times 180$ lines.

However, it is usual to rewrite Eq. (61) in the form

$$SNR_{DI} = \left[\frac{2t_i e \Delta f_V}{\alpha} \right]^{\frac{1}{2}} \frac{1}{N} SNR_{VO} \quad (63)$$

by use of Eqs. (2) and (3) and the area relation, $A = \alpha Y^2$.

Again, through psychophysical experimentation, the threshold signal-to-noise ratios were determined with the typical result shown in Fig. 46. As for aperiodic images, we note that the SNR_{DT} is approximately a constant over a wide range of spatial frequencies. The equations above apply to the case where the primary noise is that generated in the primary photoconversion process. If a system noise, such as preamp noise of rms value, I_p , in bandwidth Δf_V is added subsequent to the sensor gain, then

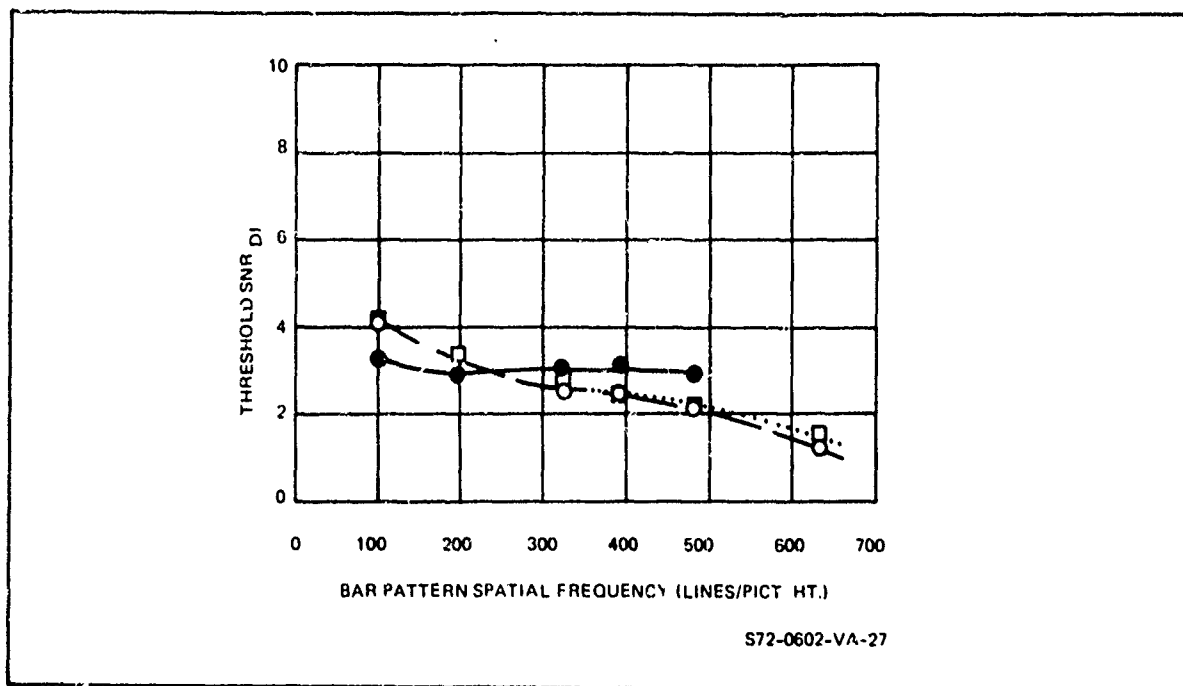


Fig. 46 Threshold SNR_{DI} vs Bar Pattern Spatial Frequency for Display-to-Observer Viewing Distances of ○ 14", □ 28" and ● 56".

$$\text{SNR}_{DI} = \left[\frac{at_i}{A} \right]^{\frac{1}{2}} \frac{2G_T C M_{av}^i}{[G_T^2 e i_{av} + I_p^2 / 2\Delta f_V]^{\frac{1}{2}}} \quad (64)$$

for the aperiodic model and,

$$\text{SNR}_{DI} = \left[\frac{t_i \epsilon}{\alpha} \right]^{\frac{1}{2}} \frac{1}{N} \frac{2G_T C M_{av}^i}{[G_T^2 e i_{av} + I_p^2 / 2\Delta f_V]^{\frac{1}{2}}} \quad (65)$$

for the periodic model. In both cases, the added system noise is assumed to be white.

Before continuing, we note that many analysts and experimenters choose to define the threshold signal-to-noise ratio in terms of the video signal-to-noise ratio, SNR_{VOT}. For the periodic image case, this results in the equation

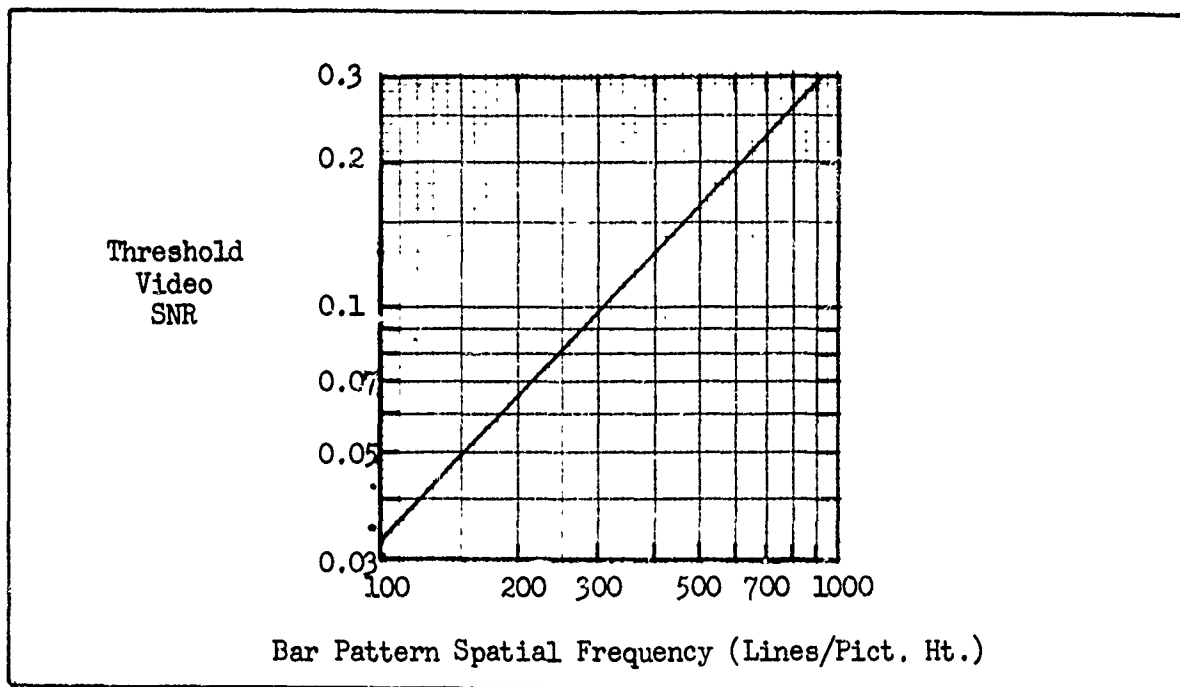


Fig. 47 Threshold Video SNR vs Bar Pattern Spatial Frequency for a Video Bandwidth of 10^7 Hz.

$$SNR_{VO-T} = \frac{N \cdot SNR_{DT}}{\left[\frac{2t_i \epsilon \Delta f_V}{\alpha} \right]^{\frac{1}{2}}} \quad (66)$$

For $t_i = 0.1$ sec, $\epsilon = 5$, $\Delta f_V = 10^7$ Hz and $\alpha = 4/3$, $SNR_{VO-T} = 1.16 \times 10^{-4}$ SNR_{DT} and for $SNR_{DT} = 2.8$, we plot the SNR_{VO-T} in Fig. 47. This curve or some variation of it is sometimes called the "eye modulation demand function." The inference is that as image's spatial frequency increases, the eye "demands" more signal modulation. The use of this curve is generally to be deplored. First of all, if the spatial frequency of the pattern is too high, the observer should be able to move closer to the display and thereby reduce the threshold. But the threshold does not decrease. Furthermore, instead of a single number for a threshold, a curve

becomes necessary. Finally, system parameters become mixed with observer parameters which is an inconvenience when observer-display interactions are to be considered.

With this short review of the elementary model, we proceed to the treatment of finite apertures.

3.2 The Effect of Finite Apertures on Image Detail

If an imaging device were perfect, a point source would appear as a point in the image's plane. If this were so, all images would be transmitted through the device with perfect fidelity. In reality, images will differ from the object in amplitude, shape or phase (position) or all three. These image changes are due to finite imaging apertures such as those associated with a lens, a fiber optic faceplate, an electron scanning beam, a phosphor particle and the like. In the case of a lens, the limiting aperture may be the lens diameter or an iris placed before it. In a fiber-optic faceplate, it is the diameter of the fiber itself. Whatever their form or cause, their effect is to smear image detail in a manner analogous to the filtering of electrical signals by electrical filter networks.

To illustrate the effect of an aperture, consider the point source object of Fig. 48(a). Due to diffraction, chromatic and geometric aberrations, and imperfect focusing, the point will be imaged by the lens as a blur. A line source as shown in Fig. 48(b) will be similarly blurred. An equation representing the image intensity vs the x , y coordinates in the image plane is known as the point spread function or impulse response. For the line, the one-dimensional equation is known as the line spread function. The line spread case corresponds most directly to the

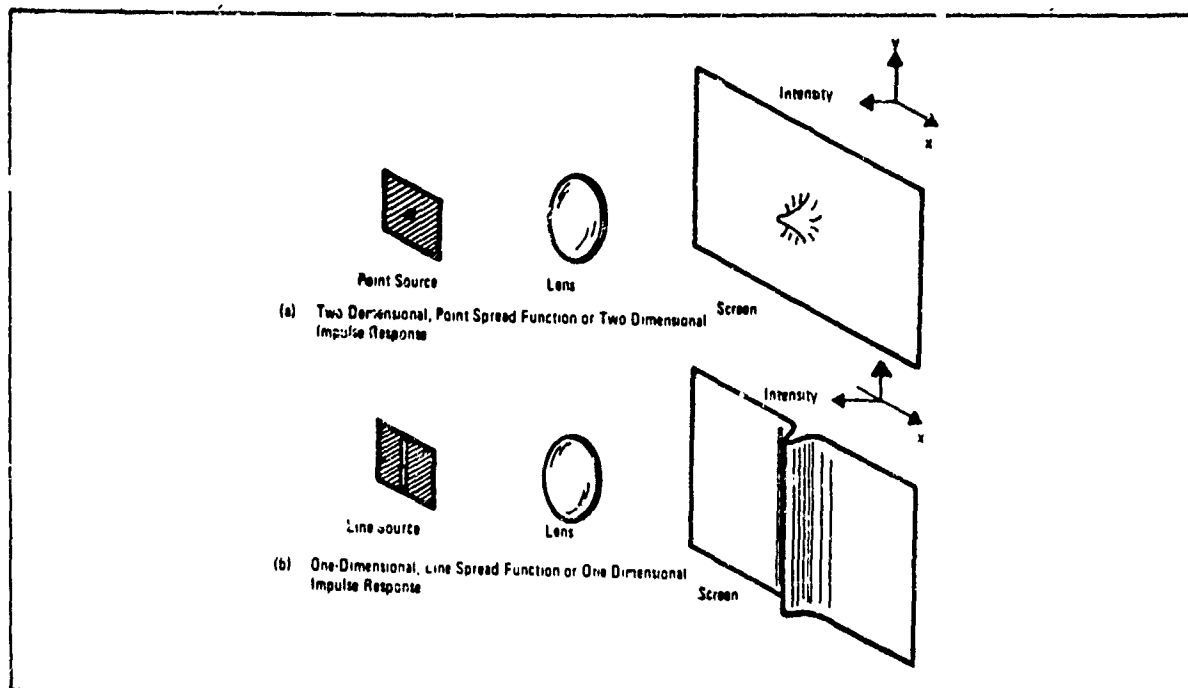


Fig. 48 Effect of an Aperture on a Point and Line Source Image.

radio communications case where the signals vary only in amplitude and time. However, the two-dimensional aspects of a point image do not impose unusual conceptual difficulties.

A linear aperture is one which has a response to several input signals acting simultaneously, that is identical to the sum of the responses that each signal would produce individually. This property of linearity leads to considerable simplification in the mathematical description of such phenomena. In particular, it becomes possible to decompose complicated input signals to simpler signals for which the system response is known and then find the total response by summing the individual responses in linear combination. Furthermore, we can then use Fourier analysis in which the complicated input signals are decomposed to sine and cosine waves.

The Fourier transform of a complex function $f(x,y)$ of two independent

variables, x and y , is given symbolically by $F(k_x, k_y)$ and is defined by

$$F(k_x, k_y) = \iint_{-\infty}^{\infty} f(x, y) \exp[-j2\pi(k_x x + k_y y)] dx dy \quad (67)$$

The complex quantities, k_x and k_y , are referred to as spatial frequencies and are also independent. The original function, $f(x, y)$, can be recovered by taking the inverse Fourier transform as follows

$$f(x, y) = \iint_{-\infty}^{\infty} F(k_x, k_y) \exp[j2\pi(k_x x + k_y y)] dk_x dk_y \quad (68)$$

Some further properties of the Fourier transform are discussed in Reference 8 but a general familiarity with Fourier techniques is assumed.

One of the most important imaging system test objects is the point source. In more glamorous terminology, the point source is known as the Dirac delta function, the unit volume impulse or, the zero order singularity test function. Symbolically, it is designated $\delta_0(x - x_1, y - y_1)$ and has the property of being of infinite amplitude at $xy = x_1, y_1$ and zero everywhere else. Also,

$$\iint_{-\infty}^{\infty} \delta_0(x - x_1, y - y_1) dx dy = 1.0 \quad (69)$$

and, the Fourier transform of $\delta_0(x - x_1, y - y_1)$, is

$$F(k_x, k_y) = 1.0 \quad (70)$$

That is, the frequency response of the Dirac delta function is unity everywhere in frequency space. Thus, the Dirac delta function can be thought of as a point image of infinite amplitude but finite volume in

x, y space and of uniform distribution in spatial frequency space over all frequencies. This frequency distribution is often known as a white spectrum.

The response of any finite aperture, be it a lens, photosurface, electron beam, or whatever, to the Dirac delta function is designated $r_o(x, y)$ in the space domain and $R_o(k_x, k_y)$ in the Fourier spectrum. The quantity $r_o(x, y)$ is the point spread function or impulse response and $R_o(k_x, k_y)$ is known as the optical transfer function, or OTF, or alternatively as the complex-steady-state-frequency response. If either $r_o(x, y)$ or $R_o(k_x, k_y)$ are known, then the aperture's response to any input test signal can be determined, i.e., these functions completely specify the parameters of the aperture. In general, the OTF may be written in the form

$$R_o(k_x, k_y) = |R_o(k_x, k_y)| \exp[j\phi(k_x, k_y)] \quad (71)$$

The quantity $|R_o(k_x, k_y)|$ has been designated the modulation transfer function, or MTF, and $\phi(k_x, k_y)$, the phase transfer function, or PTF.

Whenever image intensity distributions are analyzed by Fourier means, it is the practice to normalize the frequency distribution in the following manner. Suppose the intensity distribution is $g_i(x, y)$, then the normalized spectrum is

$$G(k_x, k_y) = \frac{G_i(k_x, k_y)}{G_i(0, 0)} \quad (72)$$

where

$$G_i(0, 0) = \iint_{-\infty}^{\infty} g_i(x, y) dx dy \quad (73)$$

as can be seen from Eq. (67). The normalization of the spectra by their

"zero frequency" values is partly for convenience but has a fundamental reason. Since intensity is a non-negative quantity, an intensity distribution always has a non-zero "dc-component" or constant background. The visual quality of an image is, to a large extent, dependent on the contrast or relative intensities of the information bearing portions of the image above or below the ever present background and hence, the spectra are normalized by that background (Ref. 8). The OTF is also normalized and has a value of unity at zero frequency. Also, the conjugate of the OTF, $R_o^*(k_x, k_y) = R_o(-k_x, -k_y)$ and, the value of the OTF at frequencies above zero is always less than unity. These conditions are, of course, properties of linear apertures and do not apply to non-linear elements.

It is further noted that while the OTF is always unity at zero frequency, it is not implied that the absolute intensity level of the object is the same as the absolute intensity of the object's image. In the case of a lens, the absolute image intensity level is always less than that of the scene due to the lens' finite entrance aperture; a decrease which is not evident in the OTF because of the way OTF is normalized.

In the general discussion, spatial frequency has been expressed in line pairs per unit distance. Usually, either k_x or k_y are given in line pairs/mm. This is sometimes a convenience in specifying the OTF of a lens which can be used with a number of film formats and because film OTF's are often given in the same units. In more complex systems, where a number of imaging and re-imaging steps may be involved, the line pair/mm units are not so handy. For example, in a low-light-level television

camera, the input image, the image at the output of the intensifier, the image at the gain-storage target and the displayed image may all be a different size. One of the principal merits of describing various aperture responses in the frequency domain is that the overall response of a number of apertures in cascade can be determined by simple multiplication of the individual responses. However, when image magnifications and minifications are involved as in the LLLTV, direct multiplication is not possible — a scale change must be made at each OTF interface.

The scale change complexity, due to changes in picture size, can be avoided by expressing resolution in terms of the picture height. This is true in TV practice where the specific units used are lines or half cycles per picture height. In the following, we will use the TV nomenclature except when otherwise specified. To avoid confusion, we will give the symbol N to resolution expressed in these terms. For this case, the Fourier transform pair equations become

$$F(N_x, N_y) = \iint_{-\infty}^{\infty} f(x, y) \cdot \exp[-j\pi(N_x x + N_y y)] \cdot dx \cdot dy \quad (74)$$

$$f(x, y) = \frac{1}{4} \iint_{-\infty}^{\infty} F(N_x \cdot N_y) \exp[j\pi(N_x x + N_y y)] \cdot dN_x \cdot dN_y, \quad (75)$$

when results are plotted in terms of N , lines per picture height, they can be converted to line pairs per millimeter at any point using the formula

$$k_x = N_x / 2Y, \quad (76)$$

where Y is the picture height in mm.

Another unit of interest is the angular measure, k_θ , which is spatial frequency expressed in line pairs per milliradian which is related to N by

$$k_{\theta x} = \frac{N \cdot F_L}{2000Y} \quad , \quad (77)$$

where F_L is the lens focal length.

To clarify these measures, suppose that a repetitive bar pattern is projected onto an image plane. Let the bar pattern spacing be Δy in mm. The spatial frequency k is the number of cycles, equal to $2\Delta y$ in length which can be fitted into 1 mm. Thus,

$$k = \frac{1}{2\Delta y} \quad . \quad (78)$$

If the picture height is Y mm, N is the number of half cycles equal to Δy in length that can be fitted into Y , i.e.,

$$N = Y/\Delta y \quad . \quad (79)$$

The angular subtense, $\Delta\theta$, of Δy in mr, with a lens of focal length, F_L , is $1000\Delta y/F_L$. The spatial frequency k_θ is the number of cycles of length $2\Delta\theta$ which can be fitted into a milliradian. Thus,

$$k_\theta = \frac{1}{2\Delta\theta} = \frac{F_L}{2000\Delta y} \quad . \quad (80)$$

In general, k_θ will be used only to describe overall sensory system resolution.

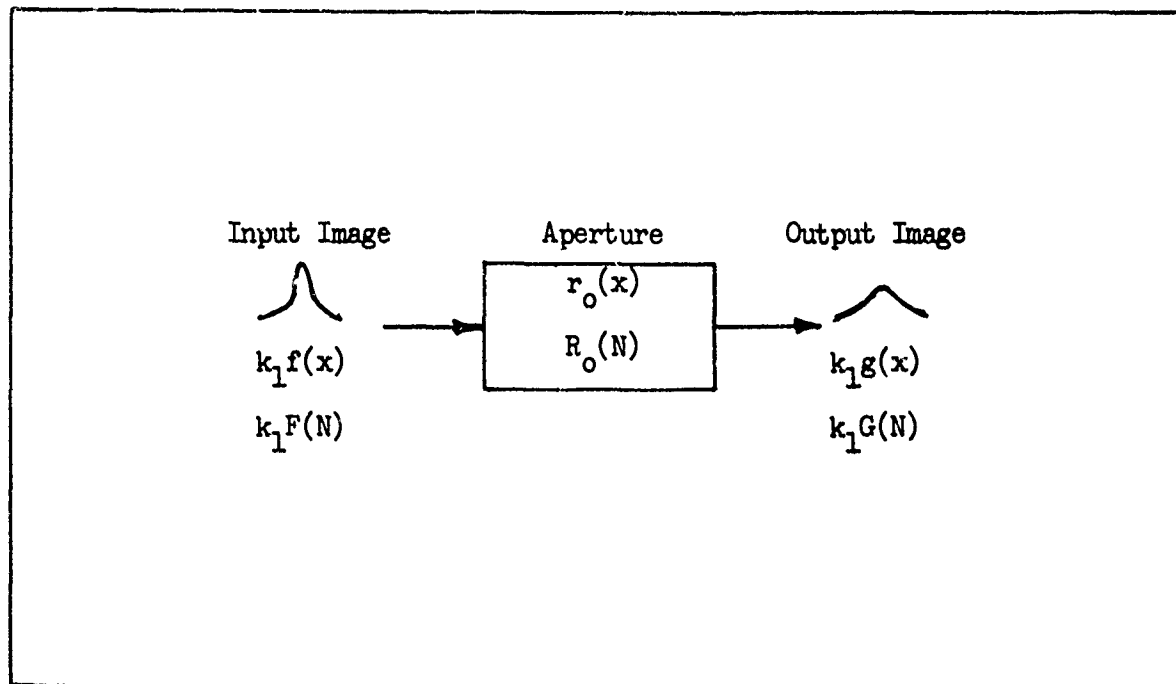


Fig. 49 Schematic of the Input-Output Relationships for an Aperture.

An aperiodic object, as used here, is an isolated object viewed against a uniform background of large extent. For practical purposes, a background can be considered to be of large extent when the object is sufficiently far removed from other objects so that the image of the object, after being smeared out by the apertures through which it passes, does not become additively combined with the smeared out images of other objects in the viewed scene.

The general nomenclature we shall use for analysis of one-dimensional objects is shown in the functional diagram of Fig. 49. In the space domain, the input signal is $k_1 f(x)$, the aperture is $r_o(x)$ and the output is $k_1 g(x)$ where $g(x)$ is the convolution of $r_o(x)$ and $f(x)$, i.e.,

$$g(x) = r_o(x) * f(x) \quad . \quad (81)$$

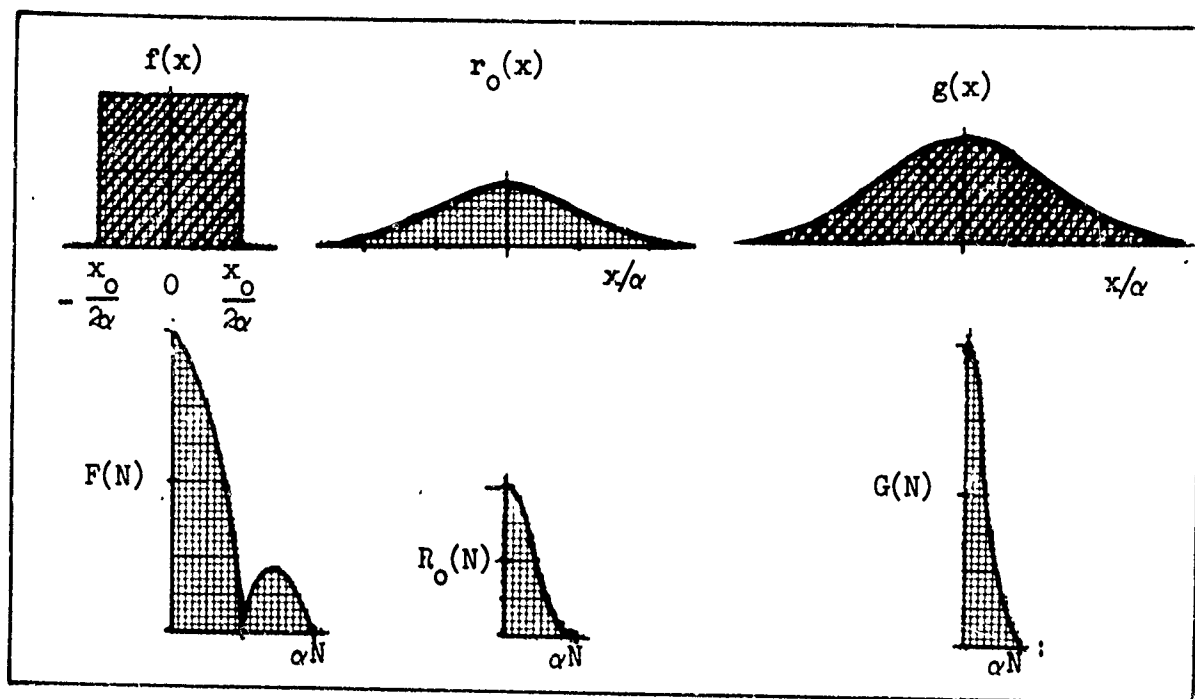


Fig. 50 Illustration of the Effect of an Aperture of Effective Duration $x_0/\alpha = 1.0$ on a Rectangular Input Image in Both the Space and Fourier Domains for $x_0/\alpha = 2.0$.

Similarly in the spatial frequency domain

$$G(N) = R_0(N) \cdot F(N), \quad (82)$$

where $G(N)$, $R_0(N)$ and $F(N)$ are the Fourier transforms of $g(x)$, $r_0(x)$ and $f(x)$. These processes are illustrated graphically in Fig. 50 for the special case of a rectangular input signal and a Gaussian aperture of the mathematical form

$$r_0(x) = \left[\exp\left[-\frac{1}{2}\left(\frac{x}{\alpha}\right)^2\right] \right] / (2\pi\alpha^2)^{\frac{1}{2}}, \quad (83)$$

and

$$R_0(N) = \exp\left[-(\pi\alpha N)^2/2\right]. \quad (84)$$

A unit amplitude rectangular input image can be described by either

$$f(x) = \begin{cases} 0 & x < -\frac{x_0}{2\alpha} \\ 1 & -\frac{x_0}{2\alpha} \leq x \leq \frac{x_0}{2} \\ 0 & x > \frac{x_0}{2\alpha} \end{cases} \quad (85)$$

or

$$F(N) = \frac{x_0}{\alpha} \frac{\sin(\pi N x_0 / 2\alpha)}{(\pi N x_0 / 2\alpha)} \quad (86)$$

The effect of passing the above rectangular image through the Gaussian aperture of Eqs. (83 and 84) above is illustrated in Fig. 50 for the case of $x_0/\alpha = 2$. For this case, the input signal is near the same size as the aperture, so the aperture has a pronounced effect on it.

The Fourier spectra of pulses of width $x_0/\alpha = 8$ and 4 are shown along with $R_0(N)$ for the assumed Gaussian aperture in Fig. 51. It is seen that the MTF should have little effect on the pulse of width 8 but a more pronounced effect on the pulse of width 4. This is in fact the case as can be seen in Fig. 52 where the output wave shapes for various pulses of width $x_0/\alpha = 16, 8, 4$ and 1 are shown. The outputs pulses are plotted as dashed curves while the input pulses are plotted as solid curves. It is seen that as the input pulses become progressively smaller, the first effect is to round the output pulse corners leaving peak amplitude unchanged. As the input pulse approaches the effective width of the point spread function, $r_0(x/\alpha)$, the amplitude decreases as well. The change in pulse amplitude is shown as a function of the input pulse width in Fig. 53. When the input pulse is wide, the effective

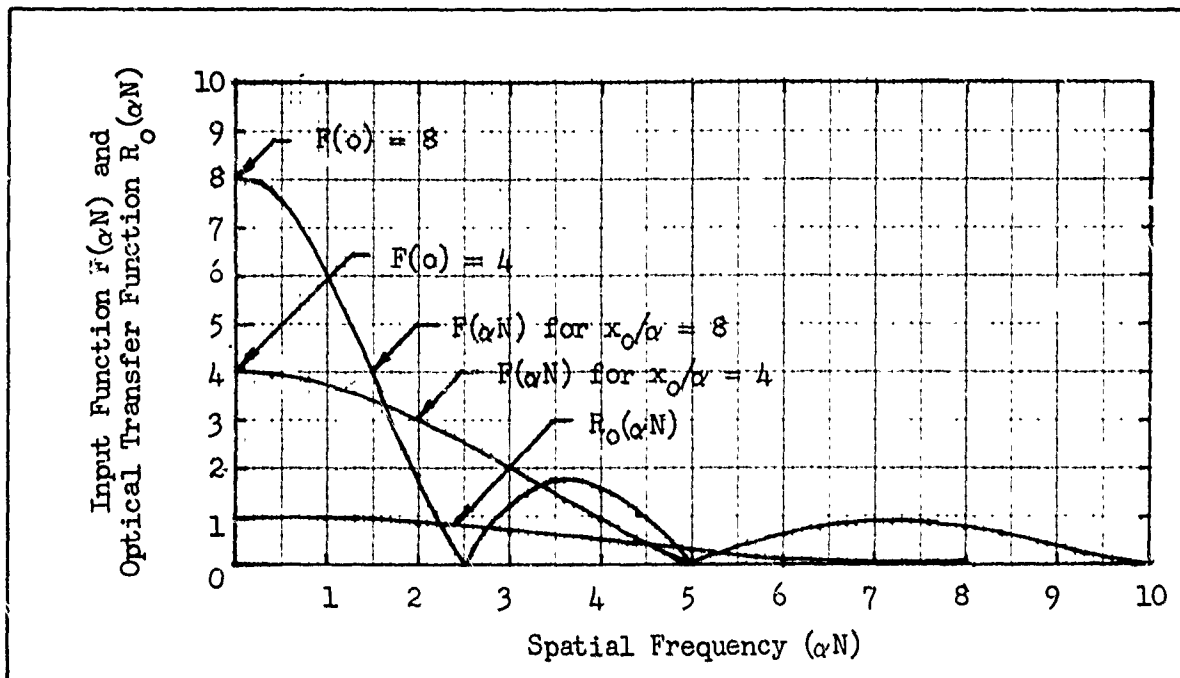


Fig. 51 Fourier Spectra of Unit Amplitude Rectangular Input Pulses of Duration $x_o/\alpha = 8$ and 4. Also shown is the Optical Transfer Function for a Gaussian Impulse Response of Effective Duration $x_o/\alpha = 1$.

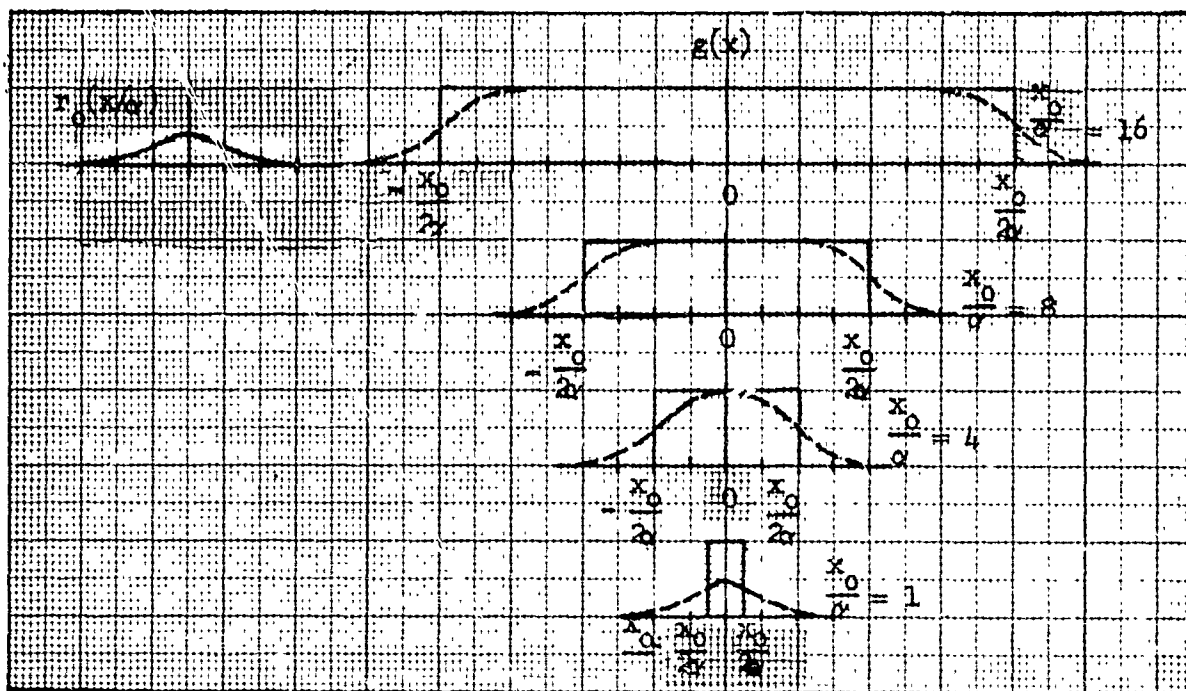


Fig. 52 The Effect of a Gaussian Impulse Response on (—) Unit Amplitude Rectangular Input Pulses of Duration 16, 8, 4, and 1. Output Waveshape is Shown as Dashed Curve.

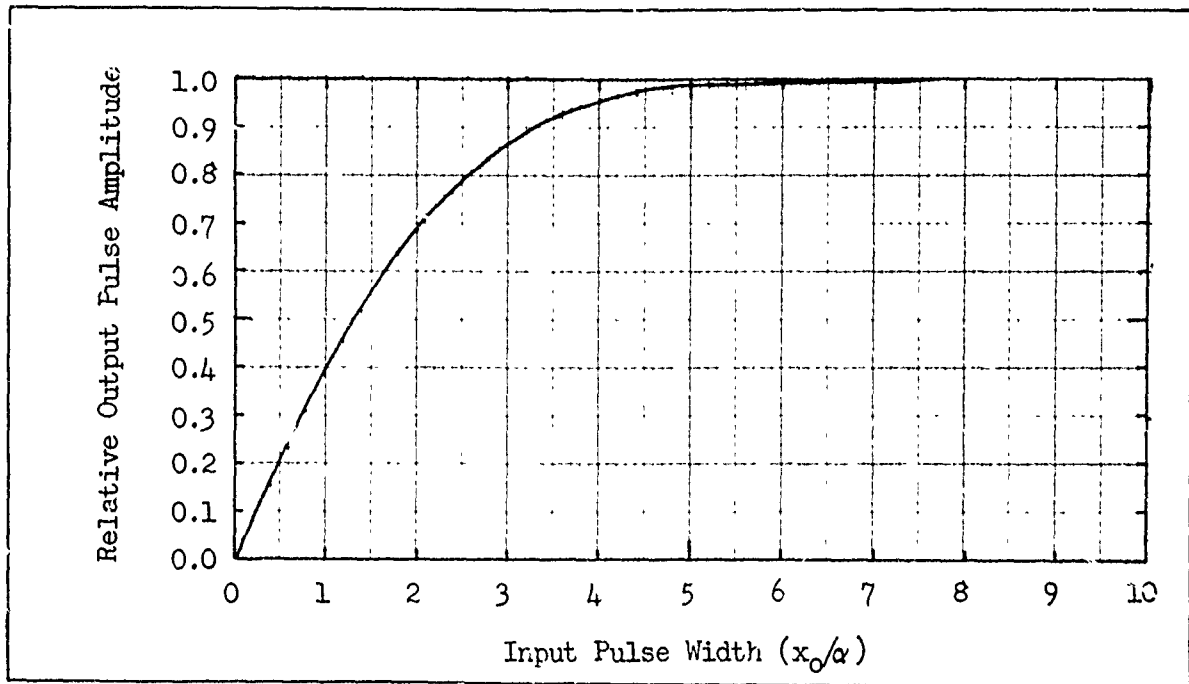


Fig. 53 Relative Output Pulse Amplitude vs the Width of a Unit Amplitude Rectangular Pulse after Filtering by a Gaussian Aperture of Effective Duration, $x_0/\alpha = 1.0$.

width of the output pulse is almost equal to that of the input pulse. As the input pulse becomes very narrow, the effective width of the output pulse becomes very nearly a constant independent of the width of the input pulse as can be seen from the curve of Fig. 54.*

In the elementary theory of imaging, it is assumed that the eye, within certain bounds, can expand its limits of integration as necessary to match the dimensions of a displayed image and that the perceived signal, s_p , will be proportional to the area of the displayed image.

* In plotting the effective width, it was assumed that the width is equal to the width of a rectangle of height equal to the output pulse amplitude and area equal to the output (or input) pulse. This is not the noise integration distance to be discussed later.

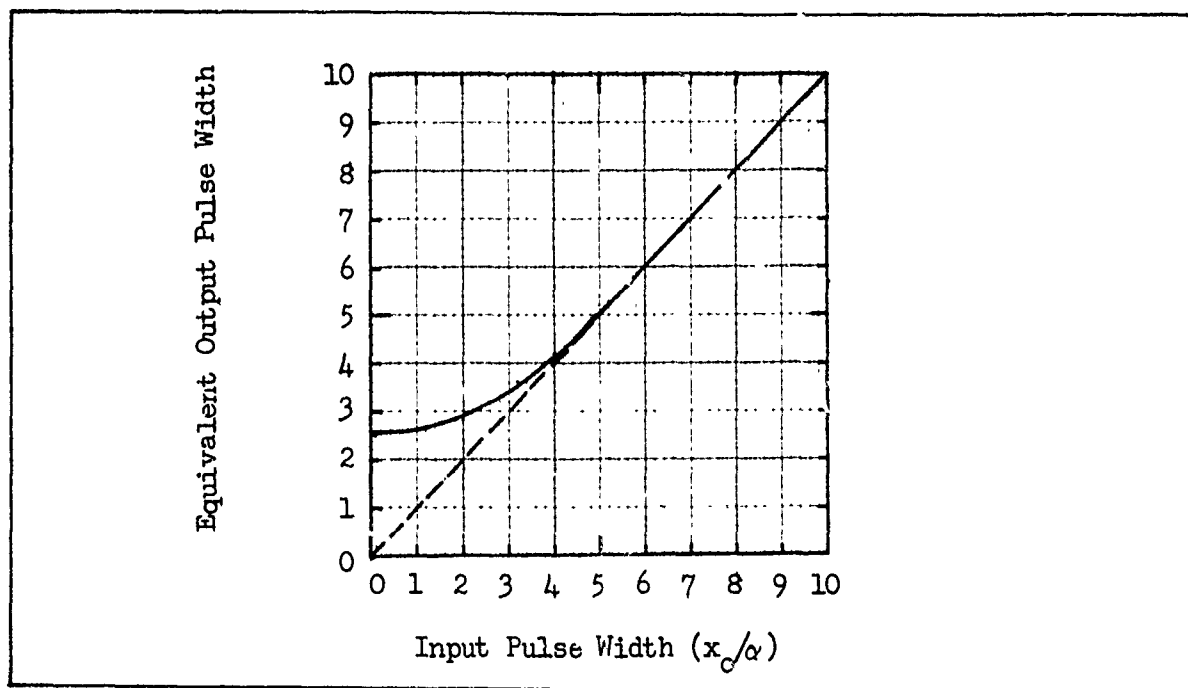


Fig. 54 Equivalent Output Pulse Width vs the Width of a Unit Amplitude Rectangular Input Pulse of Width x_o/α After Passing Through a Gaussian Aperture of Equivalent Width $x_o/\alpha = 1.0$.

Specifically,

$$s_p = k_1 t \int_{-\infty}^{\infty} g(x) dx , \quad (87)$$

where k_1 is the incremental amplitude of the input pulse, and t is the integration time of the observer's eye. Observe that

$$G(N) = \int_{-\infty}^{\infty} g(x) \exp(-j\pi Nx) dx , \quad (88)$$

and that

$$G(0) = \int_{-\infty}^{\infty} g(x) dx . \quad (89)$$

That is, the integral over the output area image is equal to the value of

the Fourier transform of the output image at zero frequency.

We further note that from Eq. (79),

$$G(o) = R_o(o) \cdot F(o) \quad (90)$$

and since $R_o(o)$, the value of the OTF at zero frequency is equal unity by definition, $G(o) = F(o)$ and

$$\begin{aligned} s_p &= k_1 t G(o) \\ &= k_1 t F(o) \\ &= k_1 t \int_{-\infty}^{\infty} f(x) dx \quad . \end{aligned} \quad (91)$$

The implication of the above result is that the area under the output pulse in Fig. 50 is identical to the area under the input pulse as is also shown by the hatched areas in the figure. Thus, if our assumption concerning the spatial integrating capability of the eye is correct, the aperture has no effect on the perceived signal, i.e., as the image is spread out by the aperture, the eye merely expands its limits of integration to include all of the signal.

While the aperture does not affect the perceived signals, it can affect the perception of noise added either prior to or subsequent to an aperture. To begin, assume that noise is added after the image has passed through the aperture as shown in Fig. 55. Suppose the input pulse is rectangular as shown by the dashed lines and that the output pulse is smeared out as shown by the solid curve. In general, the signal must be perceived in the presence of noise. If the pulse had not been smeared out, the eye would then integrate the noise only over the distance x_o . However, with the pulse smeared out, the eye would then integrate the noise

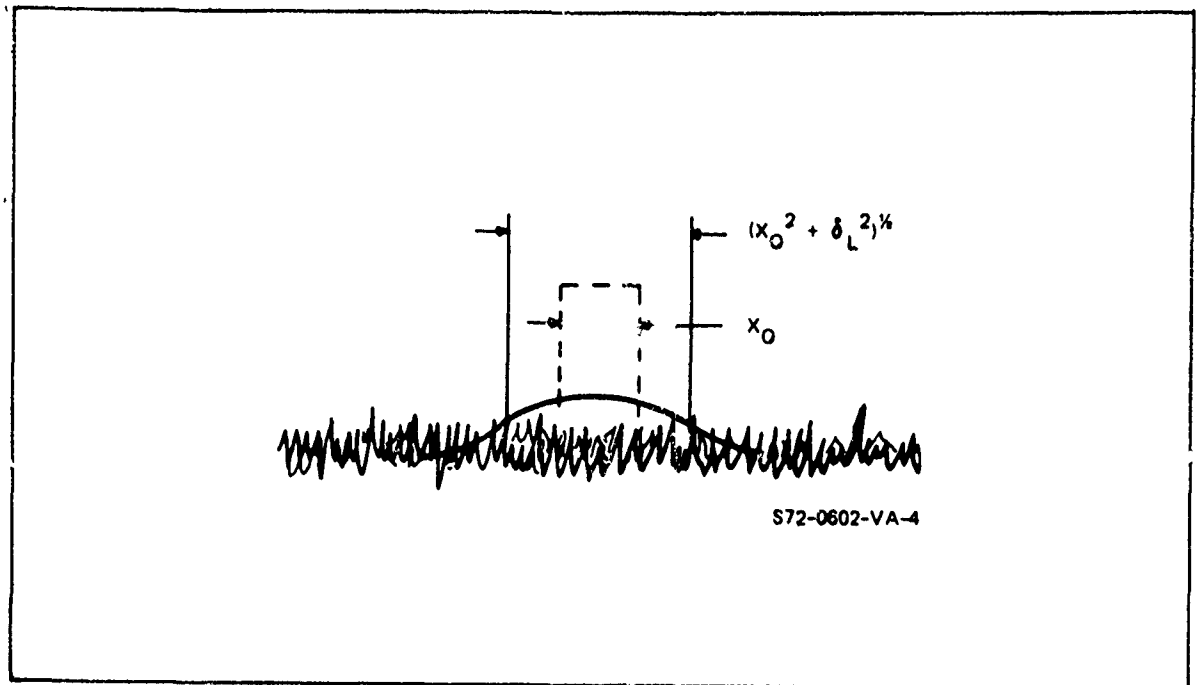


Fig. 55 Increase in Noise Perceived by an Observer due to an Increase in Effective Image Size due to an MTF Preceding a Point of Noise Insertion

over some larger distance; perhaps over an effective distance $(x_0^2 + \delta_L^2)^{1/2}$ as shown. Thus, while the aperture did not decrease the perceived signal, nor add noise of its own, it can increase perceived noise generated elsewhere in the imaging process. We note, for future reference, that the effect of noise added before an aperture is less serious than a noise added after an aperture for in the former case, the aperture also has a filtering effect on the noise.

In the treatment that follows, we shall consider the eye to be a perfect integrator in space. Assume a one-dimensional image with a white noise background of uniform variance $\hat{\sigma}^2$ units per cycle. The noise diagram is as shown in Fig. 56. For the noise model, we will assume the relation

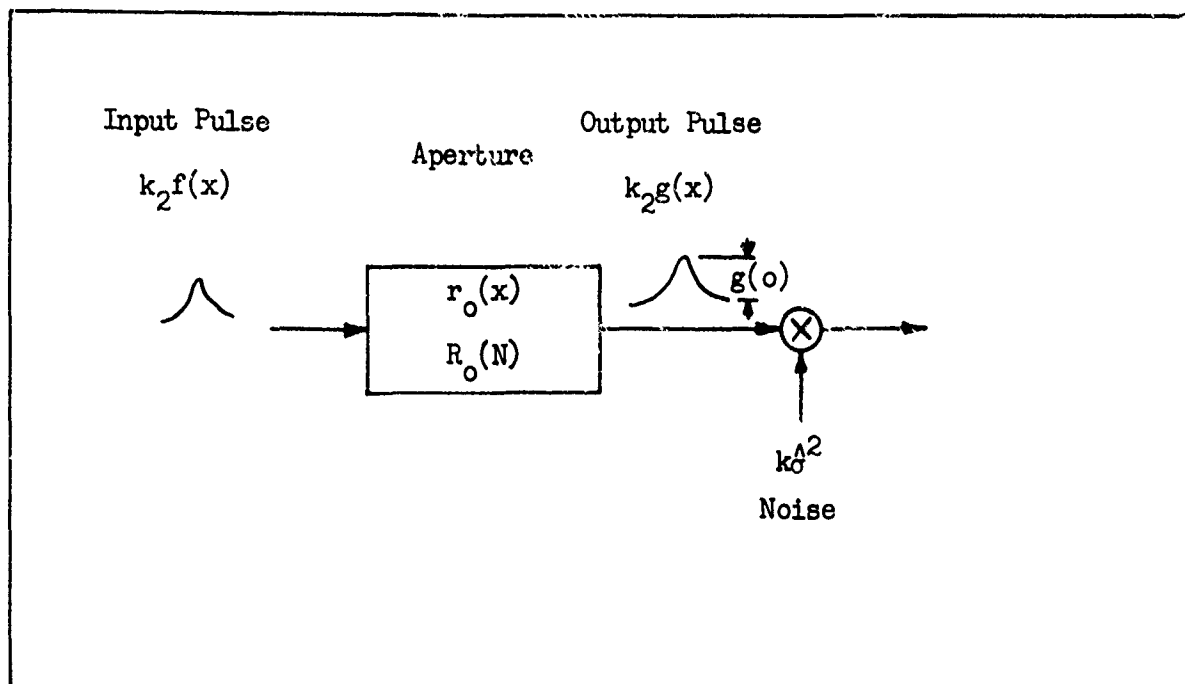


Fig. 56 Signal and Noise Diagram for the Case of an Aperiodic Image with Noise Added Subsequent to an Aperture.

$$\hat{n}_p^2 = (K\Delta)^2 t \delta_o^2 \Delta B_N \quad (92)$$

where K is a unit conversion constant, t is the integration time of the eye, δ_o is the spatial duration of the image and ΔB_N is the noise equivalent spatial bandwidth. The duration variable, δ_o , expresses the notion that the eye integrates the image along the width of the image while ΔB_N expresses the notion that the noise is bandlimited. As will be seen, the output image waveshape itself determines both the duration and the bandwidth of the noise.

We define the duration variable to be the integral of the output image divided by the output pulse amplitude, i.e.,

$$\delta_o = \frac{k_2 \int_{-\infty}^{\infty} g(x) dx}{k_2 g(o)} = \frac{\int_{-\infty}^{\infty} g(x) dx}{g(o)} \quad (93)$$

With these results, we can write

$$\hat{n}_p^2 = (K_G^A)^2 t \frac{|F(o)|^2}{g(o)^2} \frac{\int_0^\infty |F(N)R_o(N)|^2 dN}{|F(o)|^2} \quad (94)$$

which can be simplified to

$$\hat{n}_p^2 = (K_G^A)^2 t \frac{\int_0^\infty |F(N)R_o(N)|^2 dN}{g(o)^2} \quad (95)$$

However, we shall use the previous form of Eq. (94) for illustrational purposes.

Suppose the input image is a rectangular image of the form given by Eq. (85) with $\alpha = 1$. When the input image width x_o is large with respect to δ , the noise equivalent line spread width of the aperture, and as previously noted in connection with Eq. (93),

$$\delta_o = \frac{F(o)}{g(o)} \quad (96)$$

The bandwidth ΔB_N is given by

$$\begin{aligned} \Delta B_N &= \frac{\int_0^\infty |G(N)|^2 dN}{|G(o)|^2} \\ &= \frac{\int_0^\infty |F(N)R_o(N)|^2 dN}{|F(o)|^2} \quad (97) \end{aligned}$$

then $g(o) \approx 1.0$ and $F(o) \approx x_o$ as can be readily seen for the wide input pulse shown in Fig. 52. Also, $R_o(N)$ will be ≈ 1.0 as can be seen for the spectrum of the wide pulse shown in Fig. 51. The result is that the duration variable becomes x_o and the bandwidth term becomes

$$\Delta B_N \approx \int_0^\infty \frac{|F(N)|^2 dN}{x_0^2} . \quad (98)$$

For our unit amplitude rectangular pulse

$$F(N) = \frac{x_0 \sin \pi N x_0 / 2}{\pi N x_0 / 2} \quad (99)$$

and

$$\int_0^\infty \frac{|F(N)|^2 dN}{x_0^2} = \frac{x_0}{x_0^2} = x_0 . \quad (100)$$

Thus, $\Delta B_N = x_0$, and

$$\hat{n}_p^2 = (K\Delta)^2 t x_0^2 \cdot \frac{1}{x_0} . \quad (101)$$

The root mean square noise becomes

$$\hat{n}_p = K\Delta (x_0 t)^{\frac{1}{2}} \quad (102)$$

which is seen to be simply proportional to the square root of the image area as the elementary model would lead us to believe.

For an intuitive feel for this result, we note once more that for images of large width, the duration of the image is the value of $F(N)$ at $N = 0$ as shown in Fig. 51. The bandwidth is determined by normalizing $F(N)$ by dividing by $F(0)$ as shown in Fig. 57. Then the normalized function is squared and integrated to give the noise equivalent bandwidth ΔB_N as is also shown in the figure.

We next consider the case where the input image width becomes small with respect to the width δ_ℓ of the noise equivalent line spread

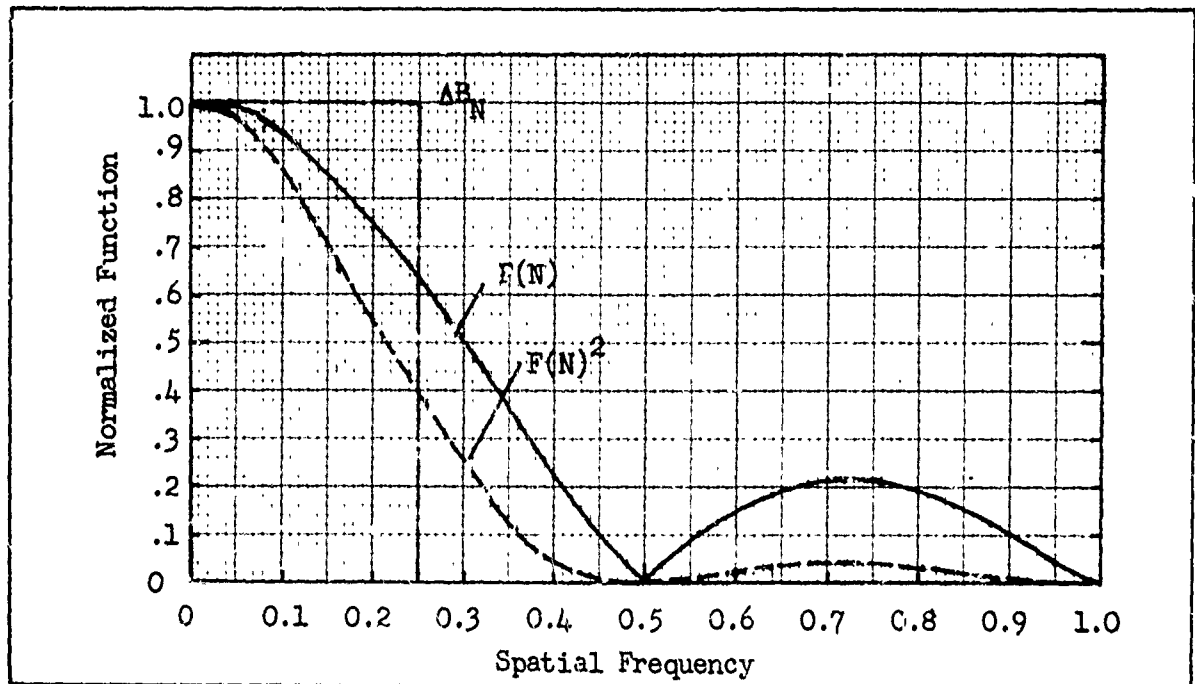


Fig. 57 Normalized Function $F(N)/F(0)$ vs Spatial Frequency and ΔB_N the Noise Equivalent Bandwidth.

function. As the input image width approaches the dimensions of an impulse, $F(N)/F(0)$ becomes numerically equal to unity (the Fourier spectrum of an impulse is a constant over all frequency). Therefore,

$$\begin{aligned}
 g(x) &= F(0) \int_0^{\infty} \frac{F(N)}{F(0)} R_0(N) e^{j\pi N x} dN \\
 &= x_0 \int_0^{\infty} R_0(N) e^{j\pi N x} dN \\
 &= x_0 r_0(x)
 \end{aligned} \tag{103}$$

That is, the output waveshape function takes on the shape of the aperture's impulse response. We observe that

$$g(0) = x_0 r_0(0) \tag{104}$$

Using this result in Eq. (93),

$$\begin{aligned}\delta_o &= \frac{F(o)}{g(o)} = \frac{x_o}{x_o r_o(o)} \\ &= \frac{1}{r_o(o)} .\end{aligned}\tag{105}$$

Thus, the output image duration becomes a constant which is numerically equal to the inverse of the impulse response's amplitude.

This result may become somewhat clearer by noting that the equivalent impulse duration, δ_ℓ , as defined by a rectangle of amplitude equal to $r_o(o)$ and of width δ_ℓ selected so that $r_o(o) \cdot \delta_\ell$ is equal to the area under the impulse response, is numerically equal to

$$\delta_\ell = \frac{\int_{-\infty}^{\infty} r_o(x) dx}{r_o(o)} = \frac{1}{r_o(o)}\tag{106}$$

so that $\delta_o = \delta_\ell$ for the infinitesimally narrow input image.

As we noted above, $F(N)/F(o)$ becomes approximately unity as the input image width approaches an impulse. Hence, the noise equivalent bandwidth becomes simply

$$\Delta B_N = \int_0^N R_o^2(N) dN\tag{107}$$

which is numerically equal to Schades, N_e , the noise equivalent bandwidth, for an aperture. Then, the mean square noise becomes

$$\hat{n}_p^2 \approx (K_G^A)^2 t_{\delta_\ell}^2 N_e\tag{108}$$

The noise equivalent bandwidth, N_e , is equal to

$$N_e = \frac{1}{\delta_e} \quad (109)$$

where δ_e is the noise equivalent aperture. Since δ_e is not far different from δ_l , the rms noise becomes

$$\hat{n}_p \approx (K\hat{A})(t\delta_e)^{\frac{1}{2}} \quad (110)$$

and therefore, the rms noise is proportional to the square root of the noise equivalent aperture as the input image becomes very small.

Again, to develop an intuitive feel for this result, we note that for a small image, the output pulse spectrum assumes the form $x_o R_o(N)$. The noise equivalent bandwidth is determined by squaring $R_o(N)$ and integrating to give ΔB_N in a manner directly analogous to that used in obtaining ΔB_N of Fig. 57.

While the equations above for the limiting cases, (either very large or very small input images) are easy to use, many input images of interest fall between these extremes. To simplify the handling of these cases, we shall assume that both the input image and the aperture have Gaussian waveshapes. Let the Fourier spectrum of the input pulse be

$$\frac{F(N)}{F(0)} = \exp - \frac{\pi}{8} \left(\frac{N}{N_{ex}} \right)^2 \quad (111)$$

and let the aperture's Fourier spectrum be

$$R_o(N) = \exp - \frac{\pi}{8} \left(\frac{N}{N_{el}} \right)^2 \quad (112)$$

The noise equivalent bandwidth for the overall image is given by

$$\begin{aligned}
 N_{eo} &= \int_0^{\infty} \frac{|F(N)R_o(N)|^2 dN}{F(o)^2} \\
 &= \int_0^{\infty} \exp - \left[\frac{\pi}{4} N^2 \left(\frac{1}{N_{ex}^2} + \frac{1}{N_{el}^2} \right) \right] dN \\
 &= \frac{2}{\sqrt{\pi}} \frac{1}{\left[\frac{1}{N_{ex}^2} + \frac{1}{N_{el}^2} \right]^{\frac{1}{2}}} \int_0^{\infty} \exp \theta^2 d\theta \\
 &= \frac{1}{\left[\frac{1}{N_{ex}^2} + \frac{1}{N_{el}^2} \right]^{\frac{1}{2}}} \tag{113}
 \end{aligned}$$

or

$$\frac{1}{N_{eo}} = \left[\frac{1}{N_{ex}^2} + \frac{1}{N_{el}^2} \right]^{\frac{1}{2}} \tag{114}$$

In terms of the noise equivalent apertures,

$$\delta_{eo}^2 = \delta_{ex}^2 + \delta_{el}^2 \tag{115}$$

For Gaussian waveshapes, the overall noise equivalent aperture of a number of apertures in cascade can therefore be determined from the component apertures added in quadrature. Even when the input image waveshapes and

apertures are not Gaussian, the approximation can be used with little error. If the input image is rectangular of duration, x_0 , as in the examples above,

$$\delta_{eo}^2 = x_0^2 + \delta_{el}^2 \quad (116)$$

A further approximation is that the duration variable, δ_o , of Eq. (91) above can also be approximated by δ_{eo} . Then,

$$\hat{n}_p^2 \approx (K\hat{\sigma})^2 t \delta_{eo}^2 \cdot \frac{1}{\delta_{eo}} \quad (117)$$

and

$$\hat{n}_p \approx K\hat{\sigma}(t\delta_{eo})^{\frac{1}{2}} \quad (118)$$

Now suppose first that the input wave shape is rectangular so that $\delta_{ex} = x_0$ and that the physical aperture, δ_{el} , is zero. Then,

$$\hat{n}_p \approx K\hat{\sigma}(tx_0)^{\frac{1}{2}} \quad (119)$$

The ratio of Eq. (118) and the above, is designated the noise increase factor, ξ , i.e.,

$$\begin{aligned} \xi &= \frac{\delta_{eo}}{x_0} = \frac{[x_0^2 + \delta_{el}^2]^{\frac{1}{2}}}{x_0} \\ &= [1 + (\frac{\delta_{el}}{x_0})^2]^{\frac{1}{2}} \quad (120) \end{aligned}$$

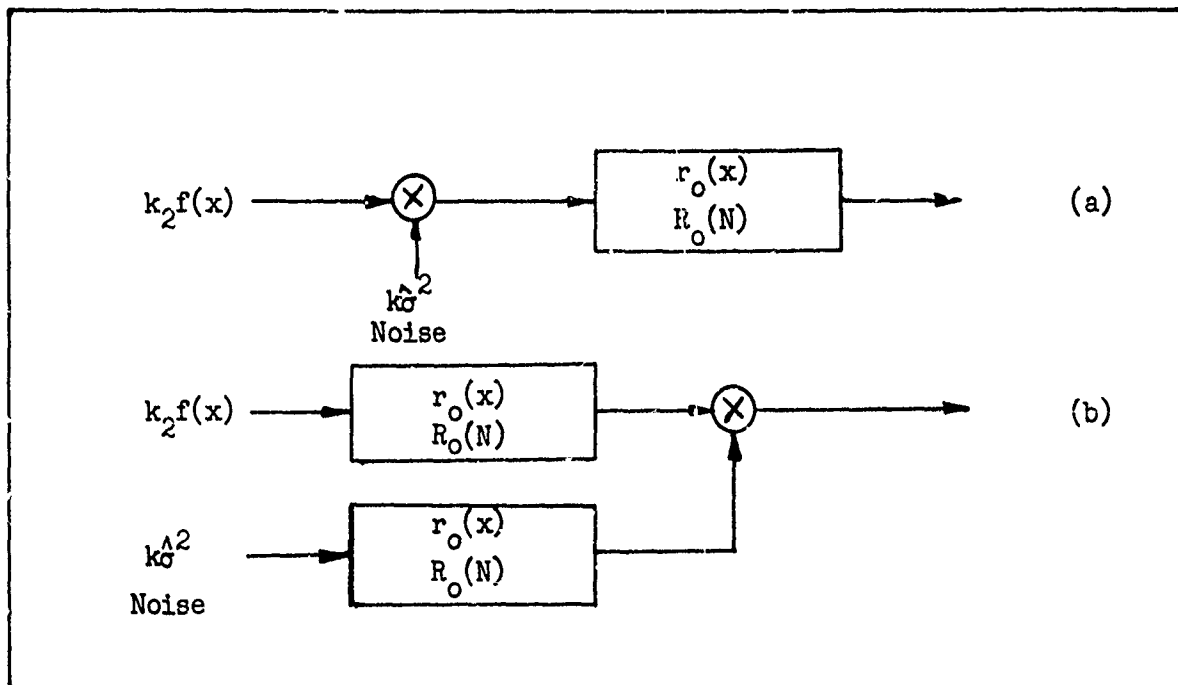


Fig. 58 (a) Aperture Following a Point of Noise Insertion, and
(b) Functional Noise Diagram for (a).

Using this noise increase factor, the Eq. (118) may be written as

$$\hat{n}_p = K\hat{\sigma}(t\xi x_o)^{\frac{1}{2}} \quad (121)$$

which will be a convenience in subsequent analyses.

We next consider the case where the aperture follows the point of noise insertion as shown in Fig. 58(a). In this case, the aperture function, $r_o(x)$, can both increase the perceived noise by increasing the noise integration distance and decrease it by virtue of a filtering action. In the previous case (noise added after the aperture), the

noise in the image is white in character (though spatially bandlimited). In the case now under consideration, the displayed noise will have a finite spectrum due to passing through the aperture.

Conceptually, the processes will be assumed to be of the following nature. The input image is first passed through the aperture so as to increase the noise integration distance. Next, the noise is band pass limited and added to the output signal as shown in the functional noise diagram of Fig. 58(b). For later convenience, we will first assume that the noise source follows the aperture in which case Eq. (91) above applies, i.e.,

$$\hat{n}_p^2 = (K_G)^2 t_{\delta_0}^2 \Delta B_{NW} \quad (122)$$

except that the subscript W has been added to ΔB_N to indicate the white character of the noise. To correct for the finite noise spectrum, we write

$$\begin{aligned} \hat{n}_p^2 &= (K_G)^2 t_{\delta_0}^2 \Delta B_{NW} \cdot \frac{\Delta B_{NF}}{\Delta B_{NW}} \\ &= \Gamma (K_G)^2 t_{\delta_0}^2 \Delta B_{NW} \end{aligned} \quad (123)$$

where Γ is the correction factor for a finite noise spectrum. The noise bandwidth, ΔB_{NW} , is given by

$$\Delta B_{NF} = \int_0^\infty \frac{|G(N)R_o(N)|^2 dN}{F(o)^2}$$

$$= \int_0^{\infty} \frac{|F(N)R_o^2(N)|^2 dN}{F(o)^2} \quad (124)$$

Using the Gaussian aperture approximation as in Eq. (115)

$$\delta_{eF} = [\delta_{ex}^2 + 2\delta_{el}^2]^{\frac{1}{2}} \quad (125)$$

and since $\Delta B_{NF} = 1/\delta_{eF}$,

$$\Delta B_{NF} \approx \frac{1}{[\delta_{ex}^2 + 2\delta_{el}^2]^{\frac{1}{2}}} \quad (126)$$

Also,

$$\Delta B_{NW} = \frac{1}{[\delta_{ex}^2 + \delta_{el}^2]^{\frac{1}{2}}} \quad (127)$$

so that the noise correction factor becomes

$$\Gamma = \frac{[\delta_{ex}^2 + \delta_{el}^2]^{\frac{1}{2}}}{[\delta_{ex}^2 + 2\delta_{el}^2]^{\frac{1}{2}}} \quad (128)$$

It is clear that Γ is a number less than one. Now,

$$\hat{n}_p^2 = (K_G^A)^2 t \delta_o^2 \Gamma \Delta B_{NW} \quad (129)$$

and by analogy to Eq. (121), we can write

$$\hat{n}_p = K_G^A (t \xi \Gamma x_o)^{\frac{1}{2}} \quad (130)$$

The noise increase factor, ξ , is a number larger than one while the noise correction factor, Γ , is less than one. However, the product $\Gamma\xi$ is greater than one. Hence, the effect of an aperture following a point of noise insertion is to increase noise but by an amount less than if the aperture preceded the point of noise insertion.

Before continuing, we note that the general formulation for this case, corresponding to Eq. (99) for the previous case is given by

$$\hat{n}_p^2 = (K_G^A)^2 t \int_0^\infty \frac{|F(N)R_o^2(N)|^2 dN}{g(o)^2} \quad (131)$$

To complete this discussion, we consider the case of two apertures with two points of noise insertion, one noise following the first aperture but preceding the second and, the other noise at the output of the second aperture as shown in Fig. 59. To begin, we assume the two noises to be \hat{n}_{p1} and \hat{n}_{p2} . If the apertures did not exist, then the two noise sources may be assumed to add in quadrature, i.e.,

$$\hat{n}_o^2 = \hat{n}_{p1}^2 + \hat{n}_{p2}^2 \quad (132)$$

If the input image is rectangular with duration x_o and if both noise sources are white, then

$$\hat{n}_o^2 = [(k_1 \hat{\sigma}_1)^2 + (k_2 \hat{\sigma}_2)^2] t x_o \quad (133)$$

Both apertures increase the noise integration distance by an amount ξ where

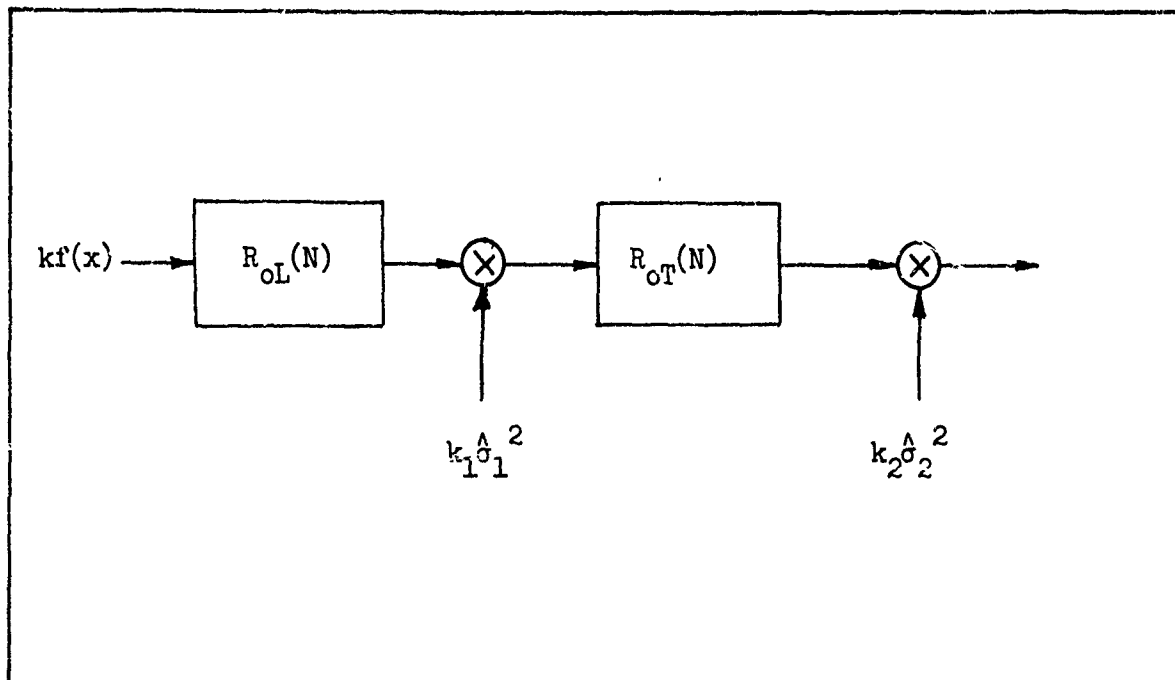


Fig. 59 Apertures Which Both Follow and Precede Points of Noise Insertion.

$$\xi = [1 + (\frac{\delta_{eL}}{x_0})^2 + (\frac{\delta_{eT}}{x_0})^2]^{\frac{1}{2}} \quad (134)$$

where δ_{eL} and δ_{eT} are the noise equivalent apertures of the first and second aperture respectively. Since the first noise source precedes the second aperture, the first noise must be corrected for a finite noise spectrum. The correction factor, Γ , is equal to

$$\Gamma = \frac{\xi_{xLT}}{[1 + (\frac{\delta_L}{x_0})^2 + 2(\frac{\delta_T}{x_0})^2]^{\frac{1}{2}}} \quad (135)$$

and the noise becomes

$$\hat{n}_o^2 = [(k_1 \hat{\sigma}_1)^2 \Gamma + (k_2 \hat{\sigma}_2)^2] t \xi x_0 \quad (136)$$

Both noises are increased by ξ , the noise increase factor, but, the noise which precedes the second aperture is filtered by it.

We turn next to the effect of apertures on periodic images. A one-dimensional pattern such as the conventional bar pattern is aperiodic along the bars and periodic in the direction transverse to the bars. Consequently, the analysis above applies along the bars but changes are needed in the periodic direction. If the input to a linear sensor is periodic, the output will also be periodic. The output and input periods (frequencies) will also be identical.

We suppose first that the MTF precedes the point of noise insertion. Then, the primary effect of the apertures will be to decrease the signal modulation. Since the period, or noise integration distance is unchanged (at least for the higher spatial frequencies) the perceived noise is unaltered as well. According to Schade, the mean signal associated with a bar pattern of spatial frequency N after the bar pattern has passed through an aperture of MTF, $R_o(N)$ is given in terms of a square wave flux response $R_{SF}(N)$ which is numerically equal to

$$R_{SF}(N) = \frac{8}{\pi^2} \sum_{k=1}^{\infty} \frac{|R_o(N)|}{k^2} \text{ for } k \text{ odd.} \quad (137)$$

If the MTF precedes the point of noise insertion, the typical elementary SNR_D equation [see Eq. (4)] becomes

$$SNR_D = \left[\frac{t_s}{\alpha} \right]^{\frac{1}{2}} \frac{R_{SF}(N)}{N} \frac{2C_M G i_{av}}{\left[eG^2 i_{av} + I_p^2 / 2\Delta f_v \right]^{\frac{1}{2}}} \quad (138)$$

In the above, we have ignored the effect of the apertures along the length of the bars.

When the aperture follows a point of noise insertion, the aperture also filters the noise as it did in the aperiodic case. The noise filtering function for the periodic case is given by

$$\beta(N) = \frac{\int_0^N |R_o^2(N)| dN}{N} \quad (139)$$

This factor multiplies only the noises introduced prior to the location of the aperture. For example, the MTF of the sensor $|R_{OT}(N)|$ would usually filter the photoelectron noise of Eq. (139) but not the preamp noise. Then, Eq. (139) becomes

$$SNR_D = \left[\frac{t_e}{\alpha} \right]^{\frac{1}{2}} \frac{R_{SF}(N)}{N} \frac{2G_M G_I i_{av}}{\left[eG^2 \beta(N) i_{av} + I_p^2 / 2\Delta f_v \right]^{\frac{1}{2}}} \quad (140)$$

3.3 Effect of Apertures on Signal-to-Noise Ratio

We have derived and discussed the effect of finite sensor apertures on image waveforms and noise, in some detail. We now combine these effects with the elementary sensor model. For this purpose, we rewrite Eq. (4) below as

$$SNR_{DI} = \left[\frac{t_i \epsilon}{\alpha} \right]^{\frac{1}{2}} \frac{1}{N} \frac{2G_T C_M i_{av}}{\left[G_T^2 e i_{av} + I_p^2 / 2\Delta f_v \right]^{\frac{1}{2}}} \quad (141)$$

which was derived for a sensor with only two noise sources; photoelectron noise and preamp noise. A typical sensor of this type is shown

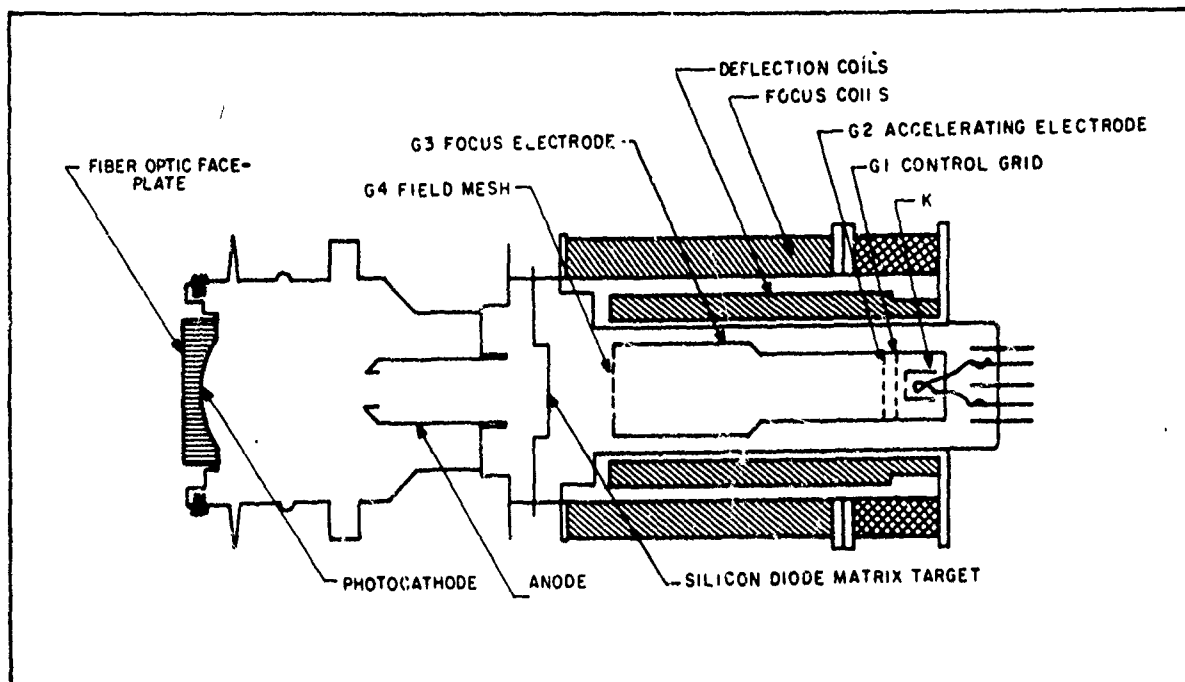


Fig. 60 Schematic of an EBSICON Camera Tube.

in Fig. 60. The lens represents an aperture preceding the point of photoelectron noise insertion (at the input photocathode) while the target follows the photoelectron noise input but precedes the preamp noise introduced at the target lead. The lens MTF is designated $R_{OL}(N)$ and the target MTF is $R_{OT}(N)$.

The effect of the apertures on an aperiodic object is to increase the noise leaving signal unchanged. The lens increases the perceived photoelectron and preamp noise as does the target, but the target also has filtering effect on the photoelectron noise. Quantitatively,

$$SNR_{DI} = \left[\frac{t_i \epsilon}{\alpha} \right]^{\frac{1}{2}} \frac{1}{[\xi_{xyLT}(N)]^{\frac{1}{2}} \cdot N} \cdot \frac{2G_T G_M i_{av}}{[G_T^2 \epsilon \Gamma_{xyT}(N) i_{av} + I_p^2 / 2\Delta f_V]^{\frac{1}{2}}} \quad (142)$$

where $\xi_{xy} = \xi_x \cdot \xi_y$ and ξ is given by Eq. (120) and $\Gamma_{xy} = \Gamma_x \cdot \Gamma_y$ and Γ is given by Eq. (128). For one-dimensional bar patterns, both the lens and target reduce signal modulation while the target has a filtering effect on noise. These effects are included in the equation below as

$$\text{SNR}_{DI} = \left[\frac{t_{ie}}{\alpha} \right]^{\frac{1}{2}} \cdot \frac{R_{SF}(N)}{[\xi_{yLT}(N)]^{\frac{1}{2}} \cdot N} \cdot \frac{2G_T C_M i_{av}}{[G_T^2 e \Gamma_{yT}(N) i_{av} + I_p^2 / 2\Delta f_V]^{\frac{1}{2}}} \quad (143)$$

where $R_{SF}(N)$ is given by Eq. (139).

In this section, a theory of the effects of apertures on image detectability has been presented for stationary images. In the next section, the effects of image motion are included and in section 5, the preliminary attempts to verify the theory of apertures experimentally will be discussed.

4.0 Effects of Image Motion

Except when an object moves relative to a stationary background, relative scene/sensor motion is degrading to image quality. These degrading effects can be divided into three distinct mechanisms; the effect of the motion on the observer directly, the interaction of image motion and camera exposure time, and sensor time constant effects. These various effects were previously considered in Ref. 2 in some detail and will be further considered herein. In general, the effects of image motion on the observer are considered to be nearly negligible for the image motion rates commonly encountered in television practice. The interaction of image motion and exposure time is considered to be quite serious as can be discerned from the analytical treatment in Section 2 of this report. Also, sensor time constants can be limiting to system sensitivity and dynamic range.

In this section, motion experiments were performed to test the validity of certain of the image motion concepts and to gain further insight into the image motion problem. Specifically, psychophysical experiments were performed using moving bar patterns and the complex images (vehicles) used previously in the recognition experiments. The vidicon camera was used to generate the imagery. In these experiments, the light level was high enough so that sensor time constants are nearly negligible and the primary effect of motion is due to exposure time. Finally, further analysis was performed on sensor lag data previously taken for the purpose of improving the analytical sensor models.

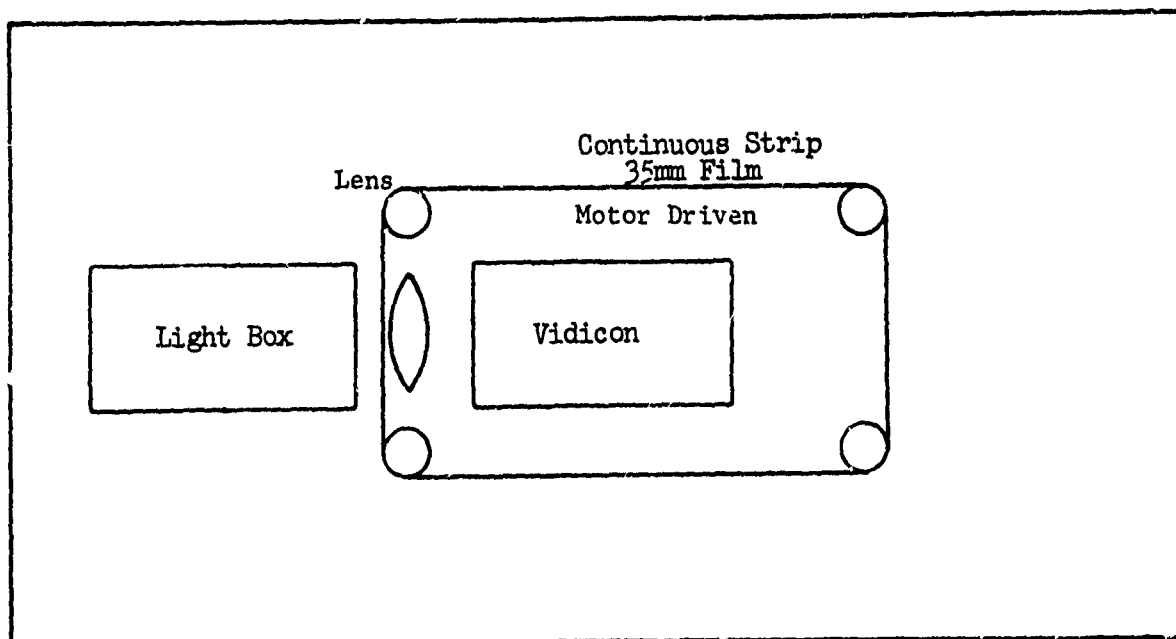


Fig. 61 Experimental Set Up for Motion Experiments

For bar patterns, the current motion MTF model was used (motion effects only--not lag), and it appears to be adequate for the particular case considered. For the vehicular imagery, an aperiodic model was applied with apparent success but the results must be considered tentative. The sensor-lag effects were and still are the most difficult to model although some correlations between observed image degradation and lag measurements are becoming apparent.

4.1 Psychophysical Experiments Involving Image Motion

The experimental set-up which was used for the motion experiments is shown in Fig. 61. A continuous strip of 35mm film was moved, at a constant speed, past the vidicon camera. Speed could be varied from less than 60 seconds per picture width to faster than 5 seconds per picture width. Motion could be either from left-to-right or right-to-left. For the experiments

with vehicle imagery reported here, a film speed of 10 seconds per picture width was used and the motion, as seen on the monitor, went from left to right. Four vehicle images were used, a tank, a van truck, a truck with a radar antenna on top and a mobile derrick with a bulldozer blade. The order of the images on the film was randomly chosen as was the signal-to-noise ratio of the image. Three observers participated in the experiment. A total of 600 data points were taken.

Display signal-to-noise ratio was calculated as follows. The broad area form of the SNR_D equation is used and for convenience it is repeated here as

$$SNR_{DI} = \left[2t \Delta f_V \frac{a}{K_d A} \right]^{\frac{1}{2}} SNR_V \quad (144)$$

where $t = 0.1$, $\Delta f_V = 12.5 \times 10^6$ Hz and SNR_V is the peak-to-peak signal voltage (with image motion) in the image divided by the RMS noise voltage. The value of a/A that was used was the area of the image, a , on the photosurface divided by the active area of the photosurface, A , assuming a perfect lens with no MTF's effects. The factor of K_d in the equation comes from the assumption that we are to calculate SNR_{DI} of an equivalent bar pattern basis, that is, for recognition, the bars are each $a/8$ in area (see Fig. 3 of Section 2). In Table 6, the values of a/A and the unattenuated SNR_V values are listed for the images which were used in this experiment.

In Fig. 62, the calculated values of SNR_D are plotted as a function of corrected probability for the four images. The average SNR_{D-T} value, at the 50% probability level is 5.9. This is 80% higher than that which was obtained for the same targets when stationary.

Target	(a/A)	SNR _v (Zero db Level)
Tank	.000702	1
Derrick	.000514	.95
Truck	.000649	.80
Radar Truck	.000602	.90

Average a/A = .000615

Table 6 Values a/A and SNR_v Used for Motion Experiment

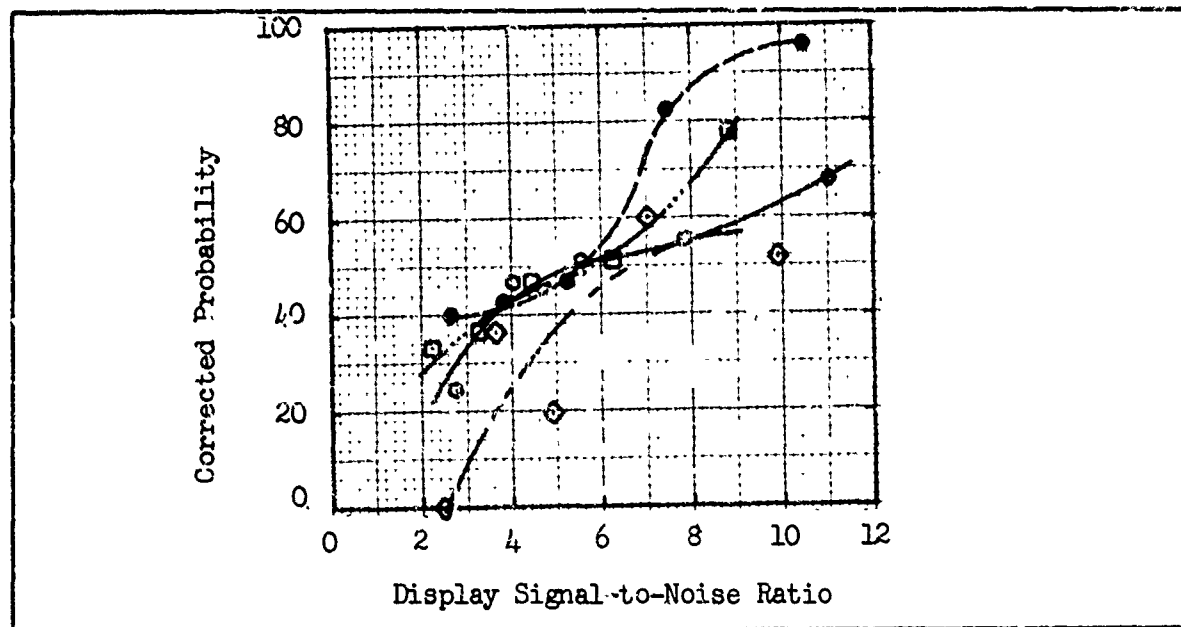


Fig. 62 Corrected Probability vs Display Signal-to-Noise Ratio for Target Recognition - Speed 10 Sec/Picture Height
 Tank ○ , Truck □ , Derrick ● , Radar Truck ◇ , Televised Images at 875 Lines, 25 frames/sec, $D_v/D_H = 3.5$

The above calculations ignored the MTF's associated with the lens, the camera, the interaction of camera exposure time and image motion. In the following these MTF's will be included in the SNR_{DI} calculation by using the aperiodic form of SNR_{DI} as developed in Section 3.

The aperiodic form of SNR_{DI} is

$$SNR_{DI} = \left[\frac{2t \Delta f_V a}{\xi_{x_{LT}} \xi_{y_{LT}} K_d A} \right]^{\frac{1}{2}} SNR_V \quad (145)$$

where $\xi_{x_{LT}}$ $\xi_{y_{LT}}$ account for the increase in the perceived noise due to the spreading of the image by the various MTF's. If the width of the actual image is x_o and the length is y_o , then $\xi_{x_{LT}}$ $\xi_{y_{LT}}$ is given by

$$\xi_{x_{LT}} \cdot \xi_{y_{LT}} = \left[1 + \left(\frac{\delta_L}{x_o} \right)^2 + \left(\frac{\delta_T}{x_o} \right)^2 + \left(\frac{\delta_M}{x_o} \right)^2 \right]^{\frac{1}{2}} \left[1 + \left(\frac{\delta_L}{y_o} \right)^2 + \left(\frac{\delta_T}{y_o} \right)^2 \right]^{\frac{1}{2}} \quad (146)$$

where the subscripts L, T and M refer to the lens, camera tube, and motion respectively. The values of δ_L , δ_T and δ_M are calculated from

$$\delta_L = \frac{1}{N_{eL}} = \frac{1}{\int |R_{oL}|^2 dN} \quad (147)$$

$$\delta_T = \frac{1}{N_{eT}} = \frac{1}{\int |R_{oT}|^2 dN} \quad (148)$$

$$\delta_M = \frac{1}{\int |R_{oM}|^2 dN} \quad (149)$$

and the rest of the terms are as before.

In Table 7, the values of δ_L , δ_T , δ_M , x_o , y_o , $\xi_{x_{LT}}$, and $\xi_{y_{LT}}$ that are used for calculating Eq. (145) are listed. There was some vibration in our experimental set up due to the blower on the light box and an estimate of

Condition	Parameter						
	x_o	y_o	δ_L	δ_T	δ_M	$\xi_{x_{LT}}$	$\xi_{y_{LT}}$
Static	2.53×10^{-3}	4.05×10^{-2}	7.91×10^{-4}	4.11×10^{-3}	0	1.93	1.01
Motion	2.53×10^{-3}	4.05×10^{-2}	1.17×10^{-2}	4.11×10^{-3}	5.34×10^{-3}	5.43	1.05

Table 7 Parameters Used in Calculating SNR_n for Aperiodic Target

the overall MTF of the lens, including this vibration, was made from the static square wave response of the systems with the blower on. This data is shown in Figure 63.

Using the numbers from Table 7, we find that, statically $SNR_{D-T} = 2.2$ whereas dynamically $SNR_{D-T} = 2.5$. The two results are nearly the same and their difference is well within a reasonable experimental error.

To continue, we will show that the measured dynamic pattern square wave response is only slightly smaller than that obtained by multiplying the sensors static square wave response times the sine wave response for linear motion assuming complete sensor integration for one frame time (1/25 sec here). Assume that

$$R_{SQM}(N) = R_O(N) R_{SQ}(N) \quad (150)$$

where $R_{SQM}(N)$ is the dynamic square wave response, $R_{SQ}(N)$ the static square wave response of the sensor, and $R_O(N)$ is the sine wave response due to the interaction of linear motion and the sensor integration.

In reference (2), it was shown that the sine wave response due to the interaction of linear motion and sensor integration is given by

$$R_o(N) = \frac{\sin(\pi N v_i t_f / 2Y)}{\pi N v_i t_f / 2Y} \quad (151)$$

In laboratory measurements, it is the usual practice to specify the bar pattern velocity in terms of the number of seconds, t_s , required for one bar in the test pattern to traverse the long dimension of the field of view. Using this formulation, pattern velocity is

$$v_i = \frac{4 Y}{3 t_s} \quad (152)$$

for our 4/3 aspect picture and Eq. (151) becomes

$$R_o(N) = \frac{\sin(2\pi N t_i / 3 t_s)}{2\pi N t_i / 3 t_s} \quad (153)$$

Eq. (153) is plotted in Fig. 63 as the circled points, \circ , and the measured static square wave response of the camera and lens is shown by the open squares, \square . The product of the two, Eq. (150), is shown by the solid circles, \bullet , in Fig. 64 and the measured dynamic square wave response is shown by the solid squares, \blacksquare , in Fig. 64. As can be seen, the measured and the calculated results are nearly the same. For a given spatial frequency, the measured curve is about .80 times the calculated curve. It is believed that this discrepancy is due to the lag of the vidicon. Lag will be discussed further in the next section. The dynamic square wave pattern response of Eq. (150) is converted to a dynamic sine wave pattern response, R_{oM} , using Eq. (154), successively, starting at high line numbers where R_{SQM} is nearly zero and working down towards lower line numbers.

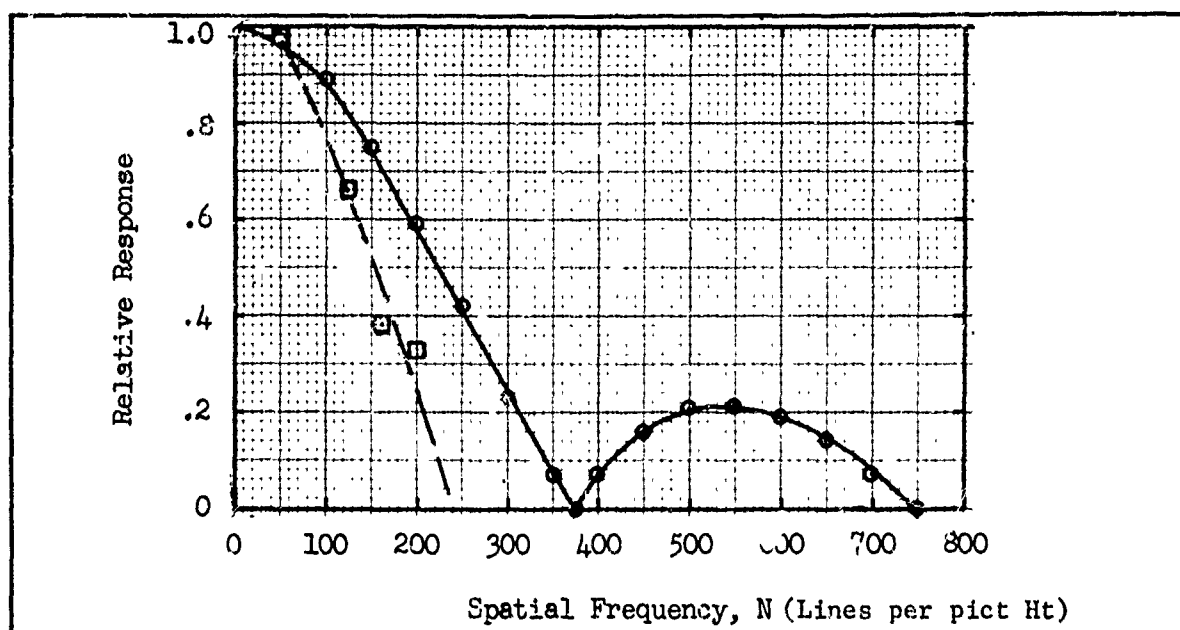


Fig. 63 Relative Response vs Spatial Frequency for Motion
Experiment \square Static Case with Blower on, \circ Pure
Motion, 10 Sec/Picture Height for a Frame Time $1/25$ Sec.

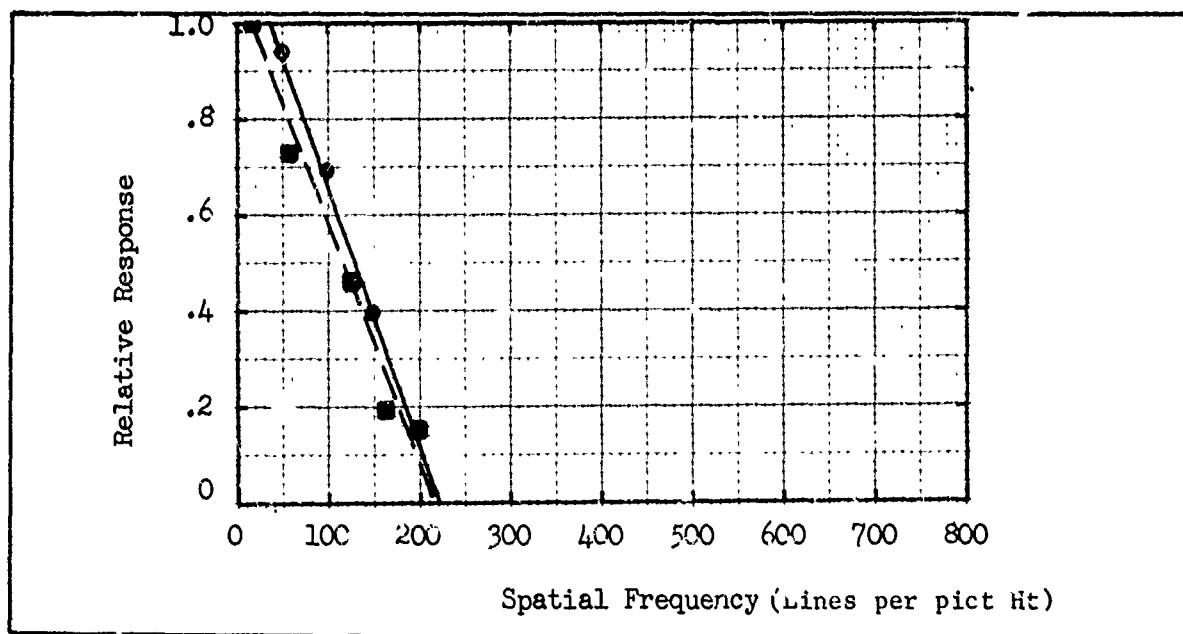


Fig. 64 Relative Response vs Spatial Frequency - Measured
for 10 Sec/Picture Height \blacksquare . Theoretical \bullet

$$R_{QM}(N) = \frac{4}{\pi} \left[R_{SQM}(N) - \frac{1}{3} R_{SQM}(3N) + \frac{1}{5} R_{SQM}(5N) \dots \right] \quad (154)$$

In conclusion, it is seen that by including the MTF for sensor exposure time for linear motion and the effects of MTF of the sensor, as given by ξ_{xLT} and ξ_{yLT} in the SNR_{DI} calculation account nearly totally for motion effects when aperiodic targets are used. Further confirmation of this should be obtained using other speeds but, as of now, the conclusion seems reasonable and will be used. Of course, if the sensor had a great deal of lag, accounting for motion by the above method is inaccurate. More work remains to be done in this area.

4.2 Analysis of Sensor Motion Data

It was seen in the last section that the dynamic square wave response of the laboratory vidicon which was used for the psychophysical experiments was only slightly lower than that predicted by the product of the vidicon's static square wave response and the MTF that is characteristic of an ideal integrating surface. It is of interest to investigate whether such a simple result can be extended to other camera tubes as well. In the following, experimental results confirm that this model can be used for resistive sea silicon diode targeted tubes such as the EBS if the tube is operated at high target voltages (low lag) but the results are seen to be extremely optimistic if the target is operated at low voltages (high lag).

The analysis which follows is an extension of that which was reported in Ref. (2). The measurements were made on a Westinghouse WX-31841 camera tube operated at high (20 volts) and low (7.5 volts) target voltages. At the high target voltage, camera lag is small whereas at low target voltage,

camera lag is high. This tube employs a 40 mm diameter photocathode of the multialkali type, a minifying diode electrostatic image section and a resistive sea type silicon diode array target of 25 mm active diameter with 2,000 diodes per linear inch. The readout beam is magnetically focussed and deflected. The picture aspect ratio was 4/3 (width-to-height). Measurements were made under standard TV scan conditions utilizing two interlaced fields per frame. The preamplifier noise was approximately 12 nA (rms) at a bandwidth of 12 MHz. Measurements were made of the static square wave response, of dynamic square wave response using a moving resolution test chart, of buildup and decay lag, and of the static and dynamic limiting resolution.

Dynamic amplitude response measurements were obtained by imaging a slant burst pattern from an RCA P-200 resolution test chart onto the tube photocathode. The pattern was affixed to a continuous transparent belt that could be run at various speeds across the field of view of the camera tube. The pattern was illuminated from behind and the image adjusted to the proper size. The illumination was adjusted to give a static signal current (in excess of the dark current) of 400nA. The signal modulation of the line bursts was displayed on an oscilloscope and the percent modulation was read directly from the oscilloscope presentation. With this chart, a bandwidth of only 4 MHz was required which resulted in a significant decrease in noise and allowed the direct reading of the oscilloscope with a reasonable accuracy for chart speeds as high as 2.5 seconds per picture width.

Because of the test chart design, it was found necessary to adjust the chart speed for each resolution line number in order to obtain an equivalent single speed corresponding to that which would have been used with a vertical bar chart. Chart speeds were employed that gave equivalent vertical

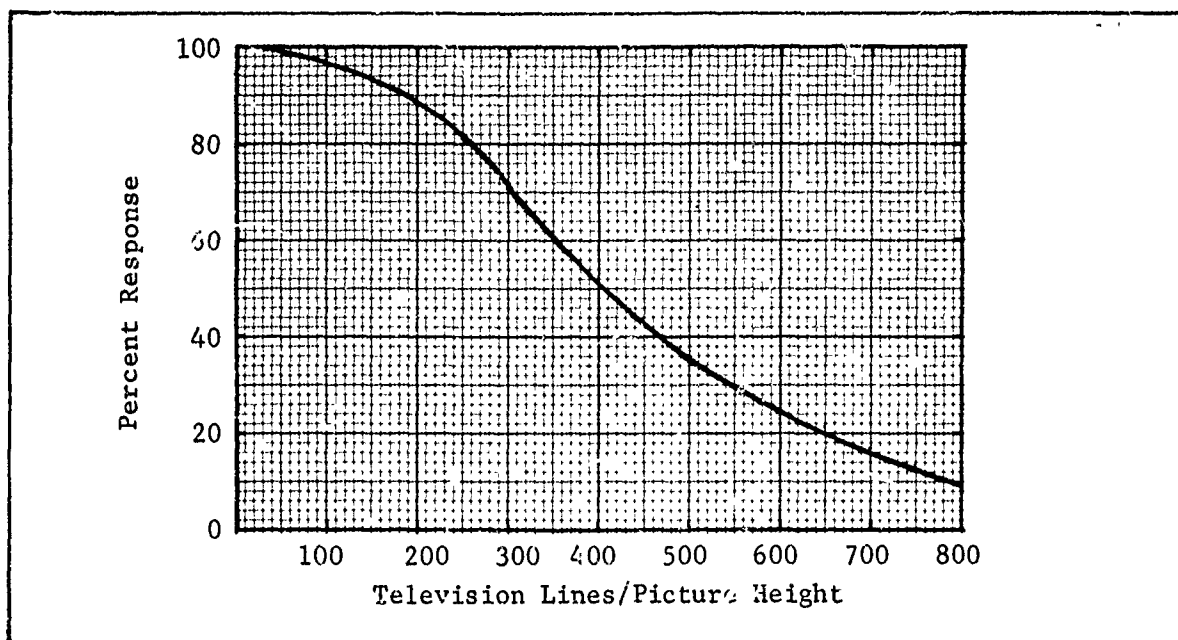


Fig. 65 Static Amplitude Response for WX31841

bar chart speeds of 60 sec/picture width, 20 sec/picture width and 10 sec/picture width. Measurements were made at target voltages of $V_T = 20$ volts and 7.5 volts for resolution line bursts of 100, 200, 400, and 600 TVL per Raster Height.

In Fig. 65, the static square wave response is shown and in Figs. 66, 67, and 68, the dynamic square wave response are shown. Also indicated in the figures are the theoretical curves which were obtained by multiplication of the static square wave response and the motion MTF. For a target voltage of $V_T = 20$ volts, the low lag case (3rd field signal is $\approx 19\%$), the measured data and calculated data are similar for chart speeds of 10 and 20 seconds per picture width (the average difference is 24%), and for 60 seconds, the measured results are within an average of 8% of the predicted numbers. With a target voltage of $V_T = 7.5$ volts, the high lag case (3rd field current is

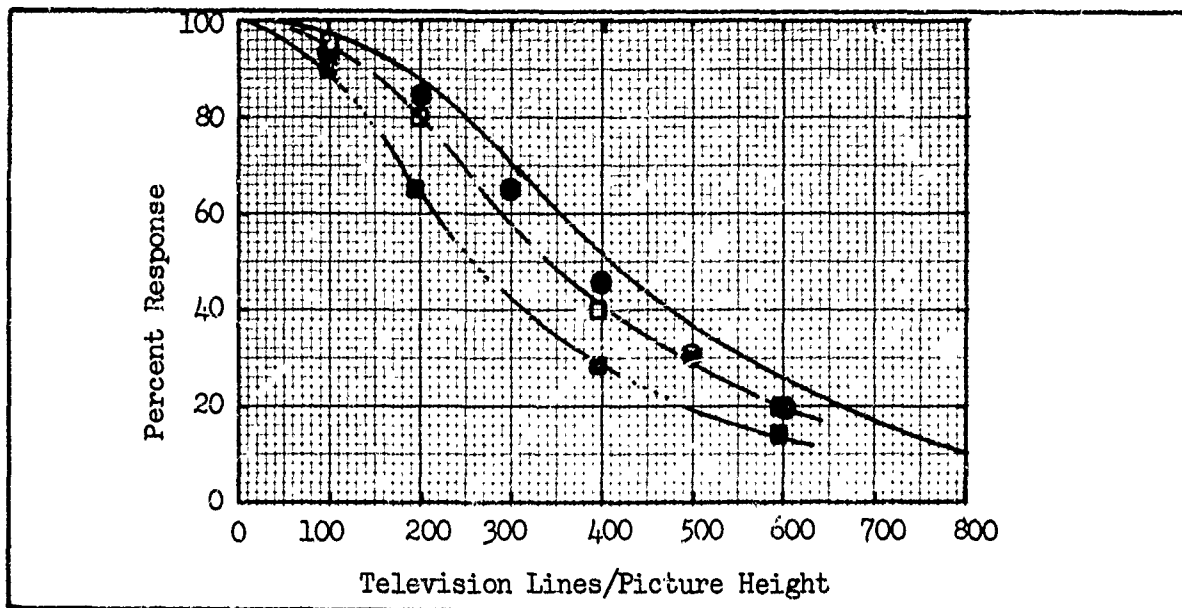


Fig. 66 Dynamic Amplitude Response for Pattern Speed of 60 Second/
Picture Width $\square V_T = 20V$, $\blacksquare V_T = 7.5V$ for WX 31841 - Solid
Curve Static Case \bullet Theoretical

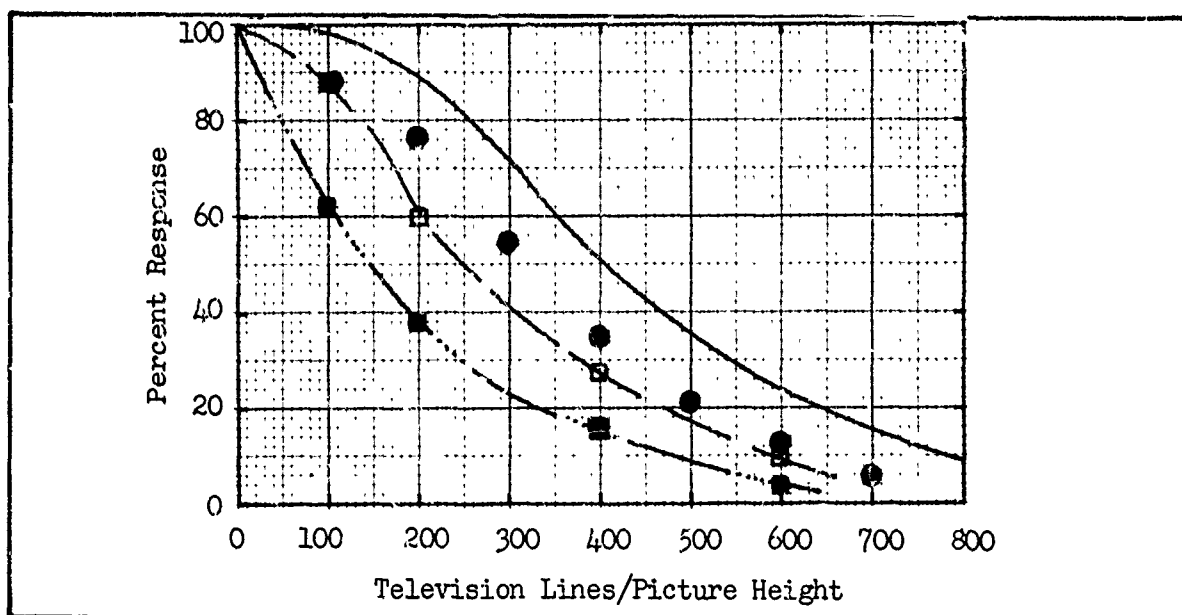


Fig. 67 Dynamic Amplitude Response for Pattern Speed of 20 Seconds/
Picture Width $\square V_T = 20V$, $\blacksquare V_T = 7.5V$ for WX 31841 - Solid
Curve Static Case \bullet Theoretical

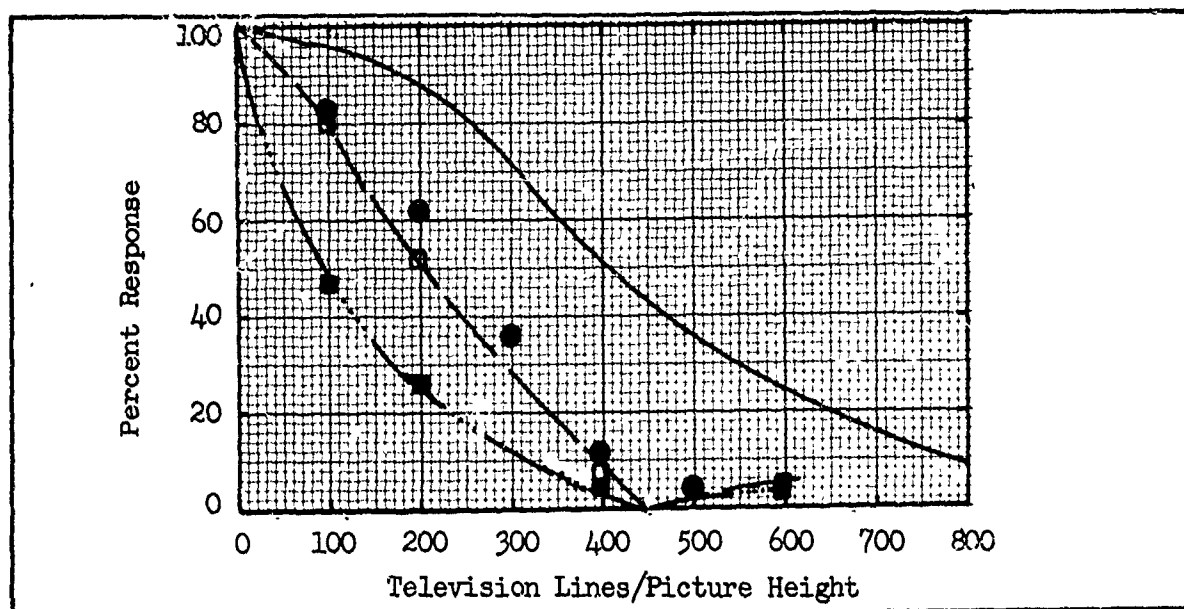


Fig. 68 Dynamic Amplitude Response for Pattern Speed of 10 Seconds/Picture Width $\square V_T = 20V$, $\bullet V_T = 7.5V$ for WX 31841 - Solid Curve Static Case \bullet Theoretical

$\approx 47\%$), the measured result is on the average 49% smaller than the calculated; the difference is the largest for the fastest target speed.

Plots of the buildup and decay values are shown in Fig. 69. To within the experimental accuracy the sum of the two values at a given target voltage is unity. If γ is the fraction of charge neutralized during one readout, then as is shown in Ref. (2), the buildup lag $= \gamma(5 - \gamma)/4$ and the decay lag $= (4 - \gamma)(1 - \gamma)/4$. In Fig. 70, a plot of γ is shown as a function of target voltage which was obtained for buildup lag using the data from Ref. (2). From Fig. 70, it is seen that $\gamma \approx \ln V_T$.

For the above, the buildup and decay lag are defined as follows. A small spot of light is imaged onto the center of the input to the camera tube and the resulting signal current as a series of pulses, one for each successive field, is displayed on an oscilloscope. The occurrence of a

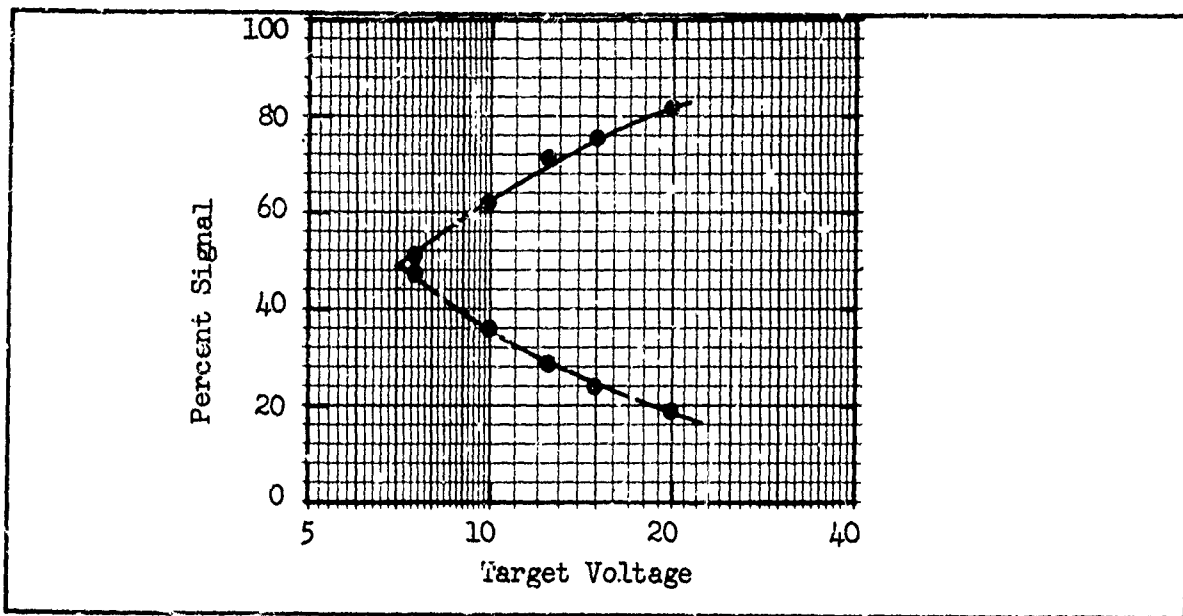


Fig. 69 Build Up Lag ●, Decay Lag ○ As a Function of Target Voltage for WX 31911

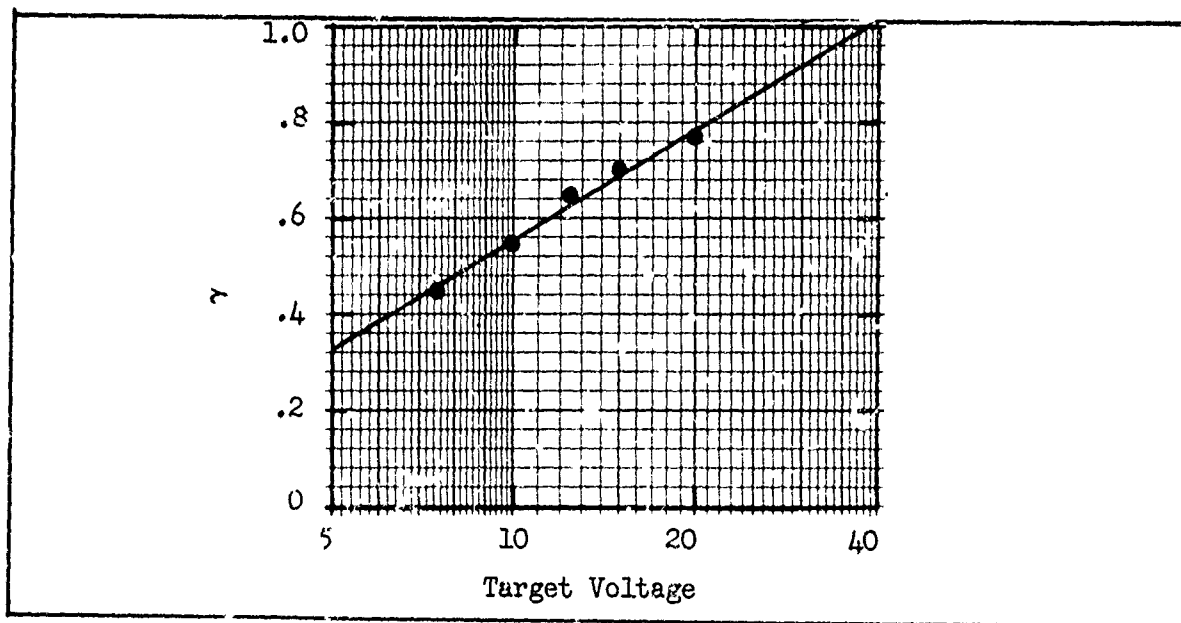


Fig. 70 Gamma, γ for Different Target Voltages for WX 31911

pulse is mid-time between the beginning and end of any field. This time is given a field designation. At the same time during a vertical flyback the illumination is turned on. The field prior to this is designated zero and that following the onset of illumination is denoted one. Thus, the illumination is turned on mid-time between the zero and first field readouts. The light remains on for a sufficient number of fields to permit a steady state to occur and then mid-time between two successive field readouts the illumination is removed for an equal number of fields. The build up lag is defined as the ratio of the third field current (after turn on of the light) to the steady state value times 100 and the decay lag is defined as the ratio of the third field current (after turn off of the light) to the steady state value times 100.

Similar to the measurement of dynamic amplitude response, measurements were made of the tube dynamic limiting resolution by imaging a 100% contrast Westinghouse vertical bar resolution chart on the camera tube and determining the minimum illumination required to permit perception of various resolution line numbers. For these tests the tube was operated with target voltages of 7.5 and 20 volts with the chart stationary and moving at speeds of 60, 20, 10 and 5 seconds per picture width. All measurements were made with a photocathode potential of -10Kv and a video bandwidth of 12 MHz. From the resulting data, curves of limiting resolution as a function of photocathode illumination for the various rates of image motion were generated. These are presented in Fig. 71 for a target voltage of 20 volts and Fig. 72 for a target voltage of 7.5 volts.

Curves similar to those shown in Figs. 71 and 72 were generated using 35% contrast patterns and are shown in Figs. 73 and 74. One image speed

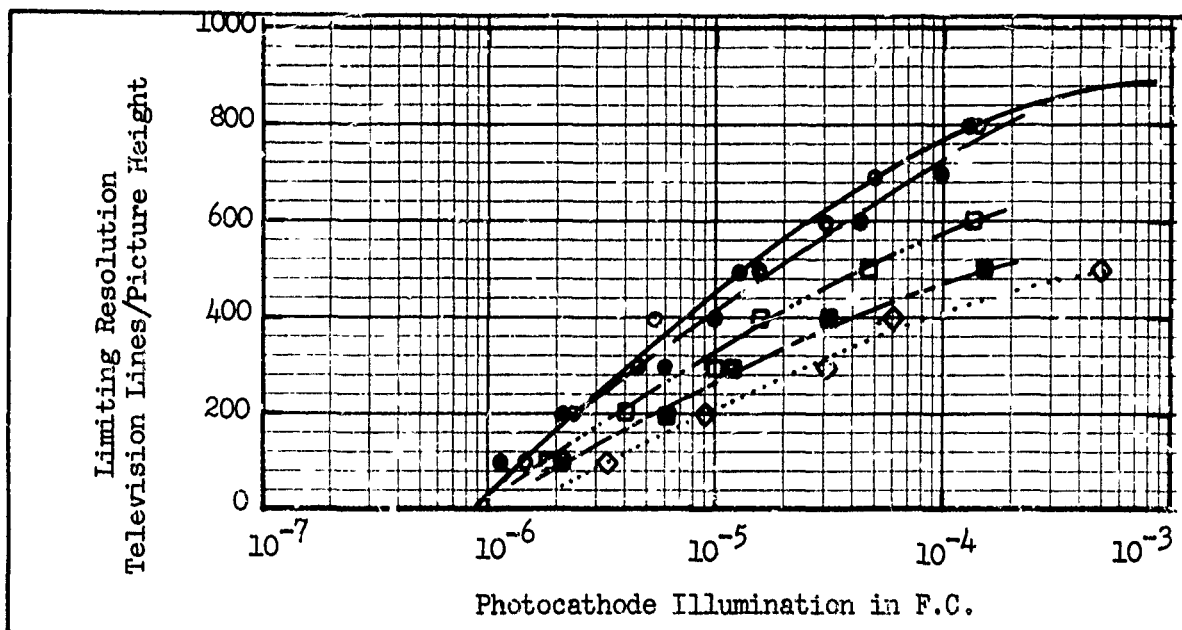


Fig. 71 Dynamic Sensitivity for 100% Contrast Pattern, $V_T = 20$ volts
 ○ Static, ● 60 Sec/P.W., □ 20 Sec/P.W., ■ 10 Sec/P.W., ◇ 5 Sec/P.W., Bandwidth 12MHz

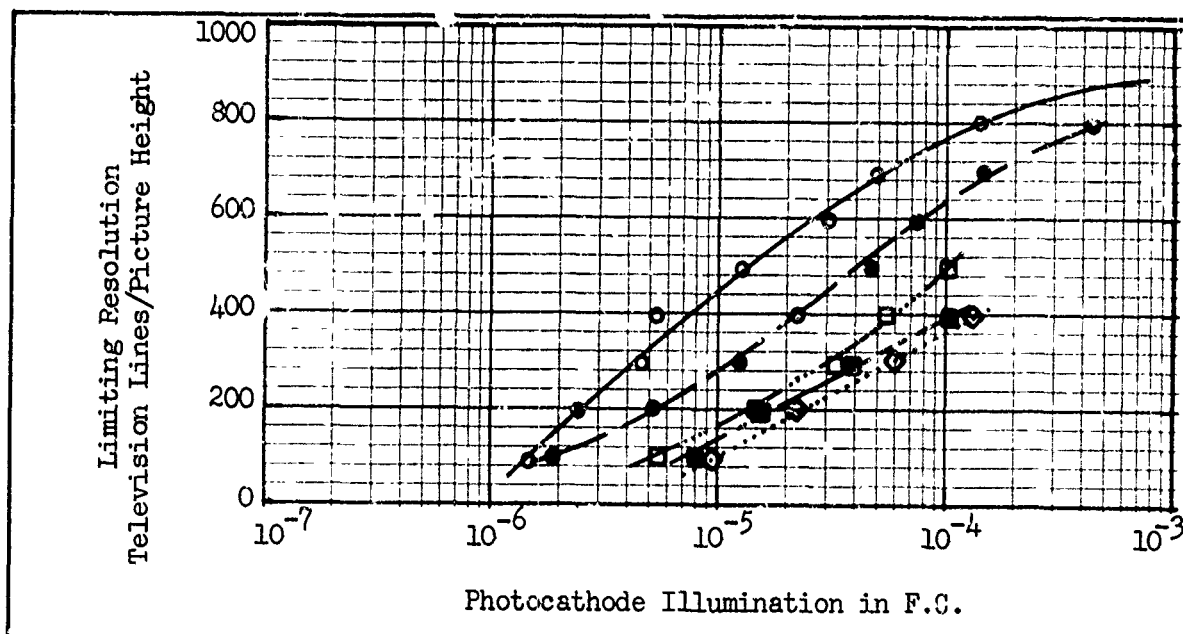


Fig. 72 Dynamic Sensitivity for 100% Contrast Pattern, $V_T = 7.5$ volts
 ○ Static, ● 60 Sec/P.W., □ 20 Sec/P.W., ■ 10 Sec/P.W., ◇ 5 Sec/P.W., Bandwidth 12 MHz

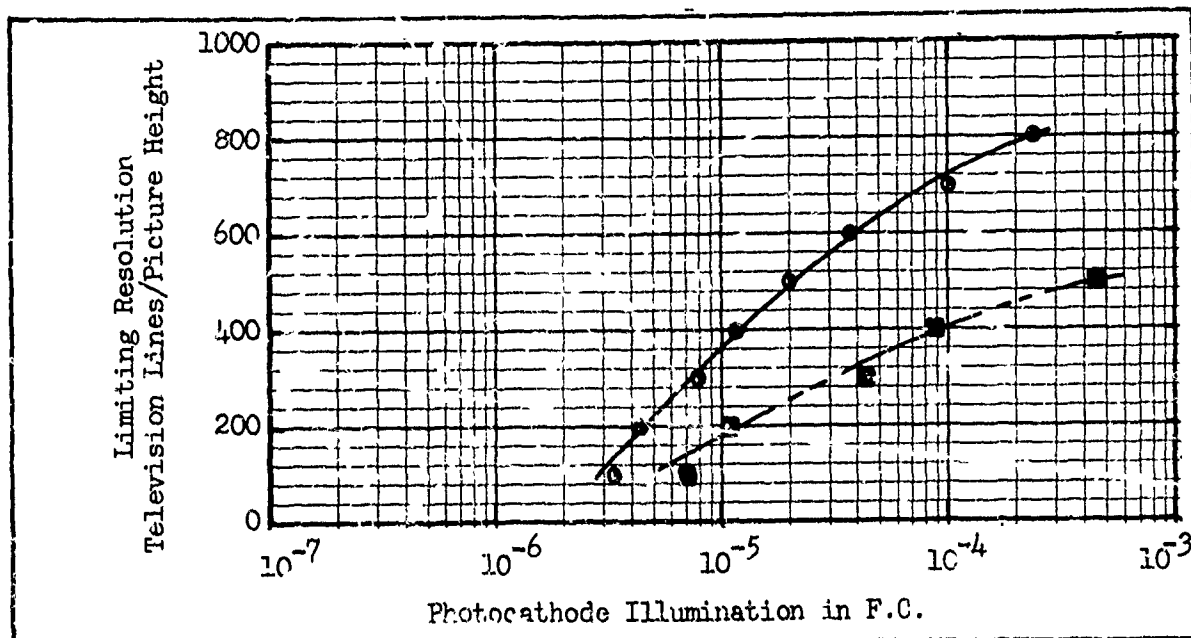


Fig. 73 Dynamic Sensitivity for 35% Contrast Pattern, $V_T = 20$ volts
 ○ Static, ■ 10 Sec/P.W., Bandwidth 12 MHz

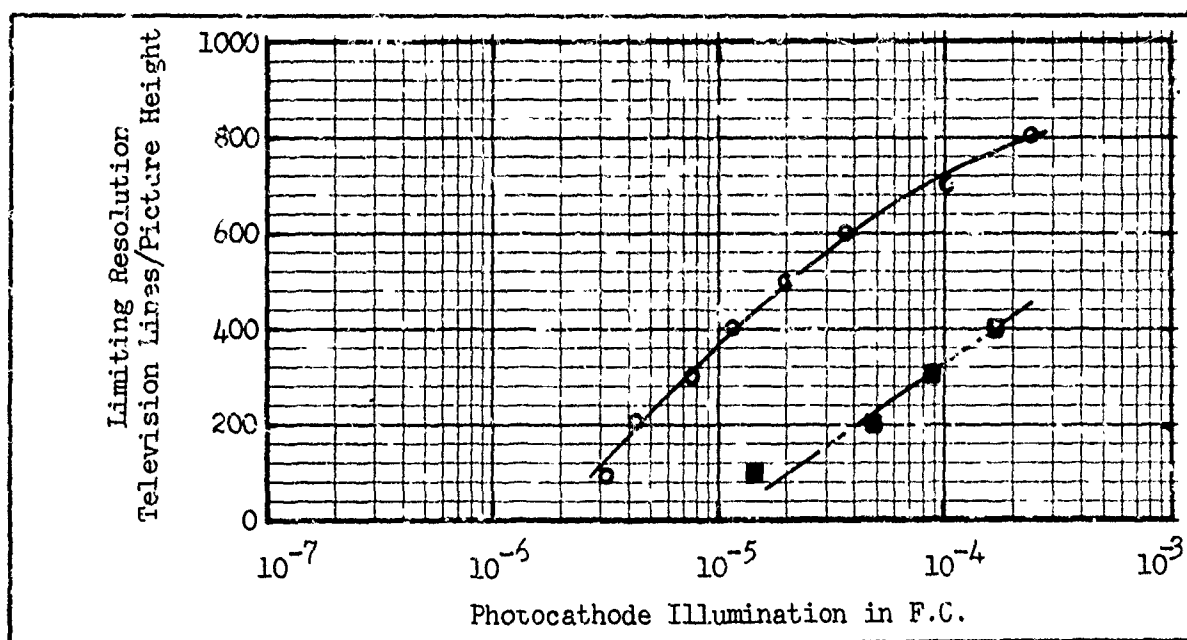


Fig. 74 Dynamic Sensitivity for 35% Contrast Pattern $V_T = 7.5$ volts
 ○ Static, ■ 10 Sec/P.W., Bandwidth 12 MHz

was used, 10 seconds per picture width and the two target voltages used were 20 and 7.5 volts. For each target voltage with the 35% contrast pattern, the loss in sensitivity due to motion is approximately the same as that measured for the same speed with the 100% contrast pattern.

Assume that the threshold SNR_{D-T} , for the low lag situation is a constant, independent of pattern speed. Then, for a given pattern speed, the increase in light level that is required for a given line number should be inversely proportional to the dynamic flux factor. Let the pattern speed be v and the line number N . Statically, the required light level is E_S and dynamically, the required light level is E_{vS} . If the static flux factor is $R_{SF}(N)$ and the dynamic flux factor $R_{vSF}(N)$ then, if linear motion alone accounts for the change in light level, we have that

$$\frac{R_{vSF}(N)}{R_{SF}(N)} = \frac{E_S}{E_{vS}} \quad (155)$$

For the calculation of $R_{SF}(N)$ and $R_{vSF}(N)$, the static and dynamic sine wave response is used, respectively. The dynamic sine wave response is calculated from the dynamic square wave response as discussed above. Our assumption of constant SNR_{D-T} , independent of pattern velocity is found to be only approximately true. The departures are the largest at high line number and high pattern speeds, and increases in E_S of a factor of 2 larger than that expected by Eq. (155) are found. The results are further off for the high lag case, an added increase in the photocathode illumination from 2 to 3 times over that used for the low lag case were found. Thus for high lag, discrepancies (increases) as high as a factor of 5 or more greater than that expected from just linear motion and sensor integration are required.

5.0 Psychophysical Experiments Involving Sensor MTF

In most of the previous psychophysical experiments, the effects of sensory system MTF's were avoided by using electronically generated imagery or a high resolution TV camera and, test images whose details were large enough to preclude serious image smearing effects. In Section 3, we discussed general theories concerning the effects of sensor MTF's on periodic and aperiodic test objects. While the theory is believed to be sound and has been shown to account for most of the first order effects observed experimentally, specific psychophysical experiments have not been performed in the past to verify the theory in detail. It should be observed that certain of the effects are not strong variables and because of the statistical nature of the psychophysical experiments, difficulty in verifying the theory with high confidence may be expected. However, the experiments performed and discussed herein do tend to confirm the general theory.

The experimental set-up of Fig. 15 was used to perform the psychophysical experiments. The test images are projected on the faceplate of a high resolution 1-1/2" vidicon operated at highlight video signal-to-noise ratios of 50:1 or better. The camera and TV monitor were operated at 25 frames/second with 875 scanning lines (825 active). Band-limited white noise of Gaussian distribution was mixed with the camera generated signals. Both the signals and noise were passed through identical filters (noise equivalent bandwidth of 12.5 MHz) prior to mixing in the monitor. The monitor luminance was approximately 1 ft. Lambert unless otherwise specified. The displayed picture height was 8" and the observer-display distance was 28".

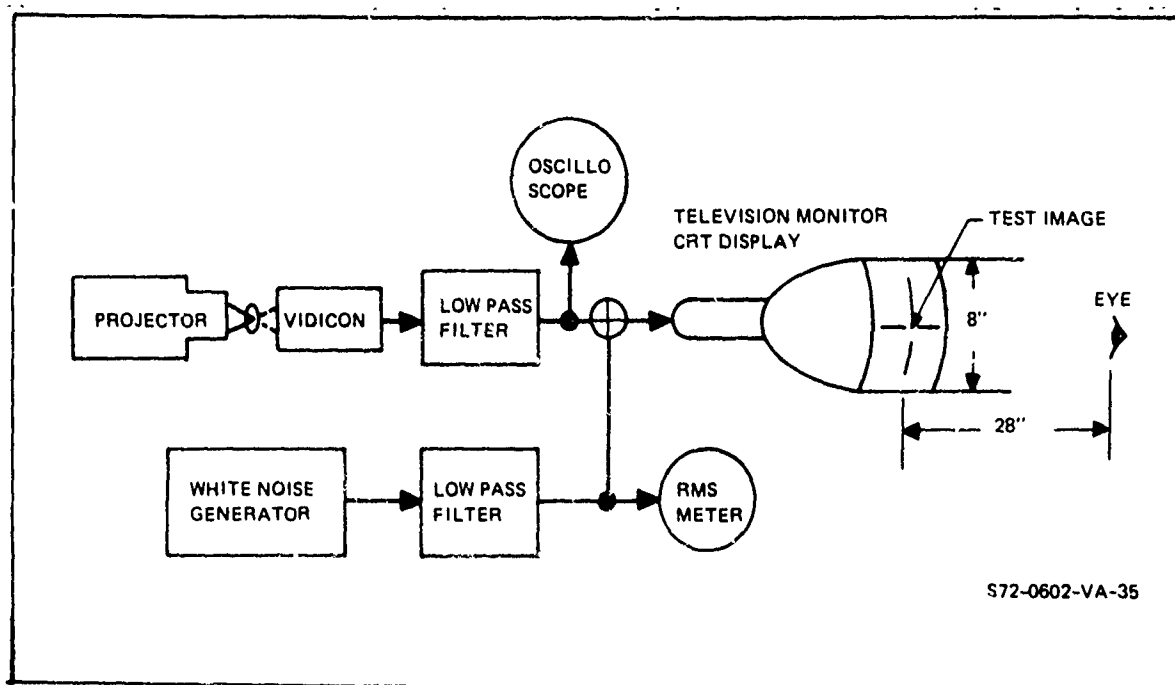


Fig. 75 Experimental Set-up for the Television Camera Generated Imagery

The MTF of the set-up (vidicon and lens) was changed by defocusing the lens. In Fig. 76 the overall MTF's that corresponded to three experimental conditions are shown. For Case A, the lens was in focus, for Case B, the lens is somewhat out of focus, and for Case C, the lens is very much out of focus. The values of N_{eT} and N_{eL} , for the three cases are listed in Table 8 where N_{eT} and N_{eL} are calculated from Eqs. (5 and 6). N_{eLT} is the overall N_e as calculated from Fig. 76.

Most of the experiments were performed using the MTF of either Case A or Case C. The method of limits described in Ref. (2) was used to take the data. The camera viewed a transparency which contained a number of patterns of different frequency. The video signal-to-noise ratios were systematically varied in 1 db steps up and down, and at each step the subject

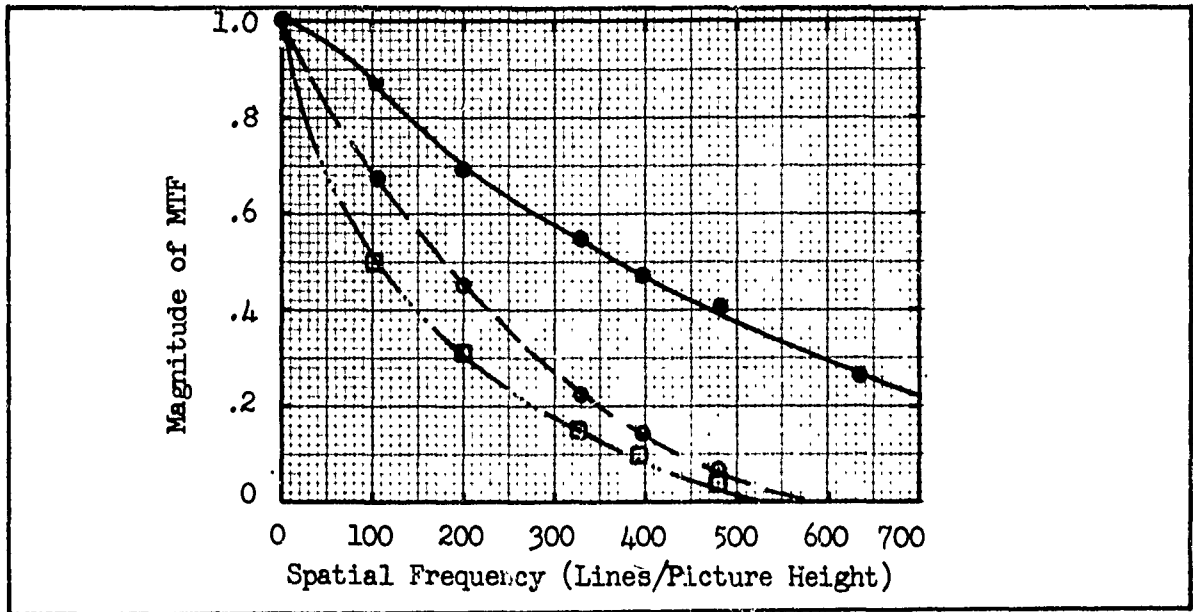


Fig. 76 Modulation Transfer Functions for Case A ● , Case B ○ , and Case C □ - Lens and Camera Combined

Case	N_{eT}	N_{eL}	N_{eLT}
A	261	1266	252
B	261	123	110
C	261	72	69

Table 8 Value of N_{eT} and N_{eL} and Overall N_{eLT} for Three Cases

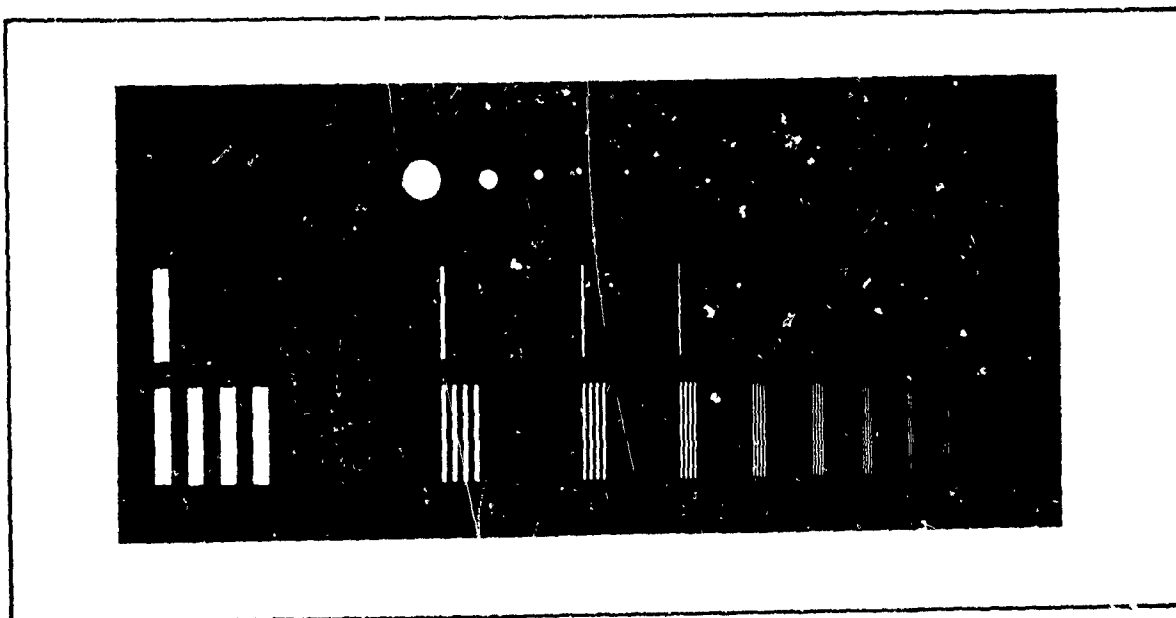


Fig. 77 Bar Patterns of Variable Aspect, Isolated Bars and Isolated Circles Used for Experiments

was required to specify the highest frequency pattern which could be barely resolved. Four different images were used, isolated circles, isolated bars, bar patterns of variable aspect, and bar patterns of constant aspect (5:1). A photograph of the isolated circles, isolated bars and bar patterns of variable aspect is shown in Fig. 77 and in Fig. 78 a photograph of the constant aspect bar patterns is shown. Table 9 lists the line number, N , for the various images calculated from

$$N = \left(\frac{H}{x_o} \right) = \frac{Y}{\Delta x} \quad (156)$$

where H is the effective height of the transparency (that which is projected onto the photocathode of height $.6 D_{pc} = Y$ where D_{pc} is the photocathode diameter) and x_o is the width of a bar. Δx is the bar width on the photocathode. Also listed in Table 9 is the bar length/width ratio, n_v . For

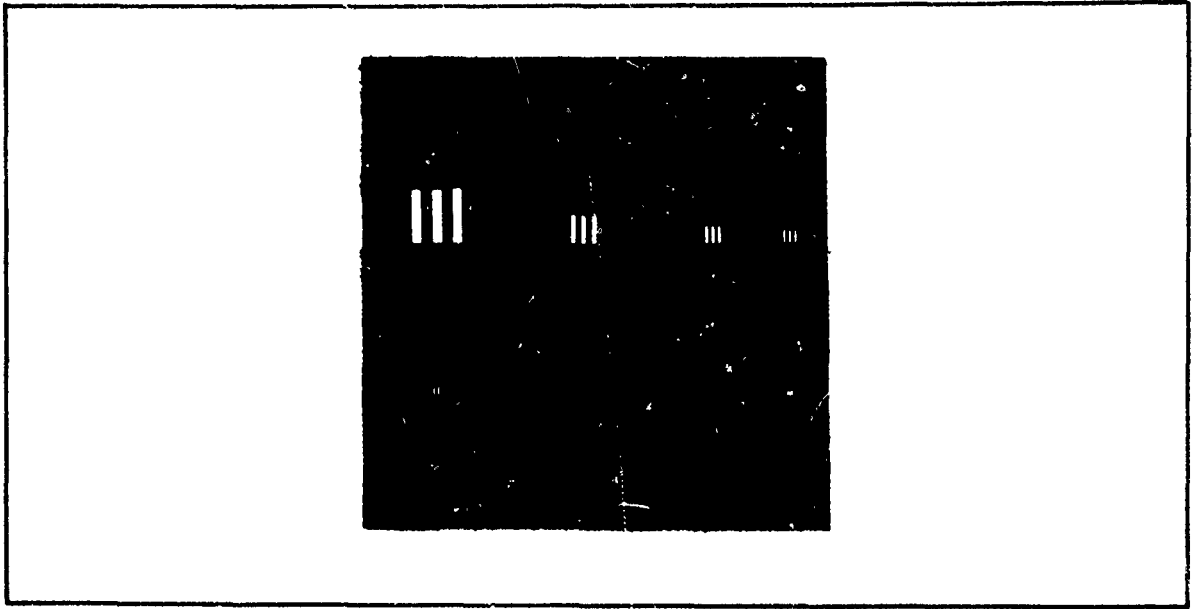


Fig. 78 Bar Patterns of Constant Aspect Used for Experiments

the isolated circles, an equivalent square is assumed, one whose area is the same as that of the circle, e.g.

$$x_0 = \left(\frac{D^2}{4} \right)^{\frac{1}{2}}, \quad (157)$$

where D is the diameter of the circle.

For bar patterns, SNR_{DI} is calculated on the basis of the total area of a bar. Specifically, the equation

$$\text{SNR}_{\text{DI}} = \left[\frac{2t n_v \Delta f_v}{\alpha} \right]^{\frac{1}{2}} \frac{R_{\text{SF}}(N)}{N \xi_y^{\frac{1}{2}}} \left(\frac{\Delta i}{I_n} \right), \quad (158)$$

is used. In the above, Δi is the peak-to-peak signal current for a broad area pattern (unity modulation transfer function) and I_n is the rms noise that is added to the camera generated image. Real cameras, of course,

Pattern							
Isolated Circles		Isolated Bars		Variable Aspect Bar Patterns		Constant Aspect Bar Patterns	
N	n_v	N	n_v	N	n_v	N	n_v
37	1	74	5.3	74	5.3	104	5
71	1	261	19.0	261	19.0	200	5
121	1	357	25.8	357	25.8	329	5
184	1	494	35.6	494	35.6	396	5
300	1	625	45.1	625	45.1	482	5
314	1	760	54.8	760	54.8	635	5
866	1	900	65.0	900	65.0	729	5
		1090	78.6	1090	78.6	800	5
		1205	88.6	1205	88.6		
		1605	116.0	1605	116.0		
		1780	125.0	1780	125.0		

Table 9 Line Number and Bar Aspect for Various Patterns

have a response that is a function of frequency and the value of Δi in the video channel for square wave inputs becomes Δi_{p-p} , the peak-to-peak value of the video signal when the frequency effects are included. That is,

$$\Delta i_{p-p} = \Delta i R_{SQ}(N), \quad (159)$$

and

$$SNR_{DI} = \left[\frac{2t n_v \Delta f_v}{\alpha} \right]^{\frac{1}{2}} \left(\frac{1}{N} \right) \frac{R_{SF}(N)}{R_{SQ}(N) \xi_y^{\frac{1}{2}}} \frac{\Delta i_{p-p}}{I_N}, \quad (160)$$

where $R_{SF}(N)$ is the value of the flux factor at N , $R_{SQ}(N)$ is the value of the square wave response at N and Δi_{p-p} the value of the peak-to-peak signal corresponding to N as measured in the output of the video channel. Alternately, one could measure Δi for a broad area pattern and use Eq. (158).

In any event, ξ_y is given by

$$\xi_y = \left[1 + \left(\frac{N}{n_v N_{eL}} \right)^2 + \left(\frac{N}{n_v N_{eT}} \right)^2 \right]^{\frac{1}{2}} \quad (161)$$

where

$$N_{eL} = \int |R_{oL}(N)|^2 dN \quad (162)$$

and

$$N_{eT} = \int |R_{oT}(N)|^2 dN \quad (163)$$

For calculation purposes, t , the integration time of the eye is taken to be 0.1 sec and α , the picture aspect ratio is 4/3. At low spatial frequencies the displayed images approach a square wave while at high spatial frequencies, above about 300 lines/picture height for Case A the

displayed images were nearly pure sine waves.

For the isolated bars and circles, the aperiodic object form of the signal-to-noise ratio should be used for calculating SNR_{DI} and it is repeated here as

$$SNR_{DI} = \left(\frac{2n_v t \Delta f}{\alpha} \right)^{\frac{1}{2}} \frac{1}{\xi_{xy}^{\frac{1}{2}}} \frac{1}{N} \frac{\Delta i}{I_n} \quad (164)$$

where

$$\xi_{xy} = \left[1 + \left(\frac{N}{N_{eL}} \right)^2 + \left(\frac{N}{N_{eT}} \right)^2 \right]^{\frac{1}{2}} \cdot \left[1 + \left(\frac{N}{n_v N_{eL}} \right)^2 + \left(\frac{N}{n_v N_{eT}} \right)^2 \right]^{\frac{1}{2}} \quad (165)$$

For the first experiment (called experiment #1), the constant aspect bar patterns were used. The experimental conditions were the same as those used previously (10 months earlier) which were reported in AFAL-TR-72-229 and the purpose of the present experiment was to establish a "bench mark" between the previous and the new results. Experimental conditions are listed in Table 10. Five subjects participated. In Fig. 79, the data from the present experiment is shown by the open circle points, o, and the original data by the solid circle points, •. A comparison of the two shows that there is nearly a constant percentage reduction in the threshold SNR_{DI} at a given line number for the new data. This difference was quite unexpected. In the original and the present experiment, the brightness of the room surrounding the monitor was approximately the same, .05 ft.Lambert.

The experiment was repeated with the same subjects with the room brightness surrounding the monitor equal to 1 ft. Lambert and the data is plotted in Fig. 80 with the threshold SNR_{DI} values plotted in Fig. 79 by

Exp. No.	Test Images	(1) L _O	(2) L _B	(3) MTF Shape	(4) No. of Obs.	(5) No. of Trials	(6) No. of Scan Lines	(7) Frames/Second	Figure No.
1	Constant Aspect	1	0.05	A	1	210	875	25	79
2	Constant Aspect	1	1	A	5	1230	875	25	80,88
3	Constant Aspect-Critical	1	1	A	1	217	875	25	81
4	Electronic Squares	1	0.05	A	4	720	525	30	82,83
5	Constant Aspect	1	1	B	5	1080	875	25	84,85 88
6	Constant Aspect	1	1	C	5	953	875	25	86,87 88
7	Constant Length	1	1	A	6	1730	875	25	89,91
8	Constant Length	1	1	C	5	1400	875	25	91
9	Isolated Bars	1	1	A	6	1730	875	25	92
10	Isolated Bars	1	1	C	5	1400	875	25	92
11	Isolated Circles	1	1	A	6	1730	875	25	93
12	Isolated Circles	1	1	C	5	1400	875	25	93
13	Tactical Targets	1	1	A	5	1000	875	25	93,94 95
14	Tactical Targets	1	1	C	5	1000	875	25	93
15	Tactical 10 Sec/PW	1	1	D	3	600	875	25	--

Table 10 Experimental Conditions

NOTES:

- (1) Average Monitor Luminance, ft-L
- (2) Average Background Luminance, ft-L
- (3) MTF Case A, B, or C Used
- (4) Total Number of Observers
- (5) Total Number of Trials
- (6) Number of Scan Lines per Picture Height, Interlaced
- (7) Number of Frames per Second Noise Bandwidth 12.5 MHz, Viewing Distance 28 inches, 8-inch High Monitor

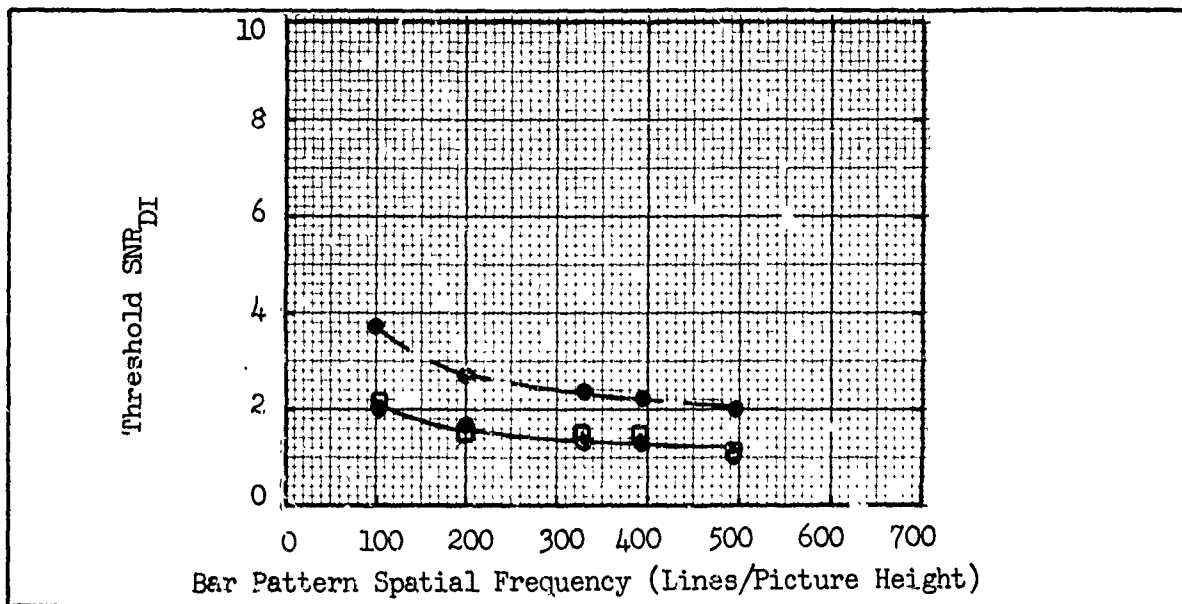


Fig. 79 Exp. No. 1 and 2. Threshold SNR_{DI} for ● Original Data and Present Data ○ Minimum Illumination Background □ 1 ft-Lambert Background - Constant Aspect Pattern Case A MTF

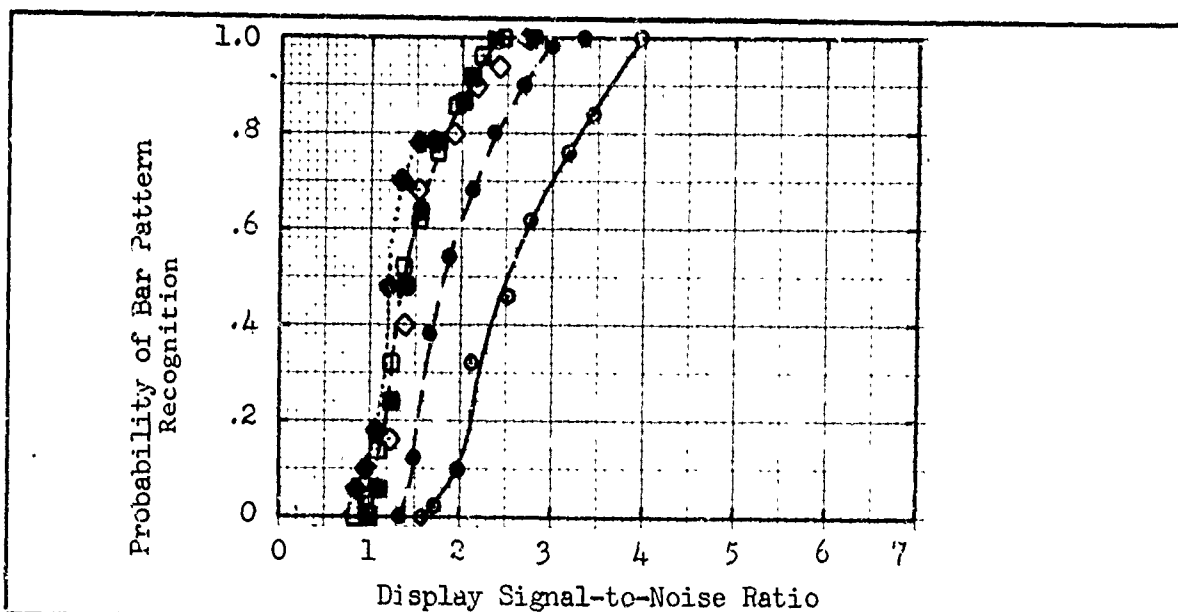


Fig. 80 Exp. No. 2 Probability of Bar Pattern Recognition Versus Display Signal to Noise Ratio for Case A MTF, 1 ft-lambert Monitor and 1 ft-Lambert Background Bar Pattern Spatial Frequency ○ 104, ● 200, □ 329, ■ 396, ◇ 482, ◆ 635 AF 5 Bar

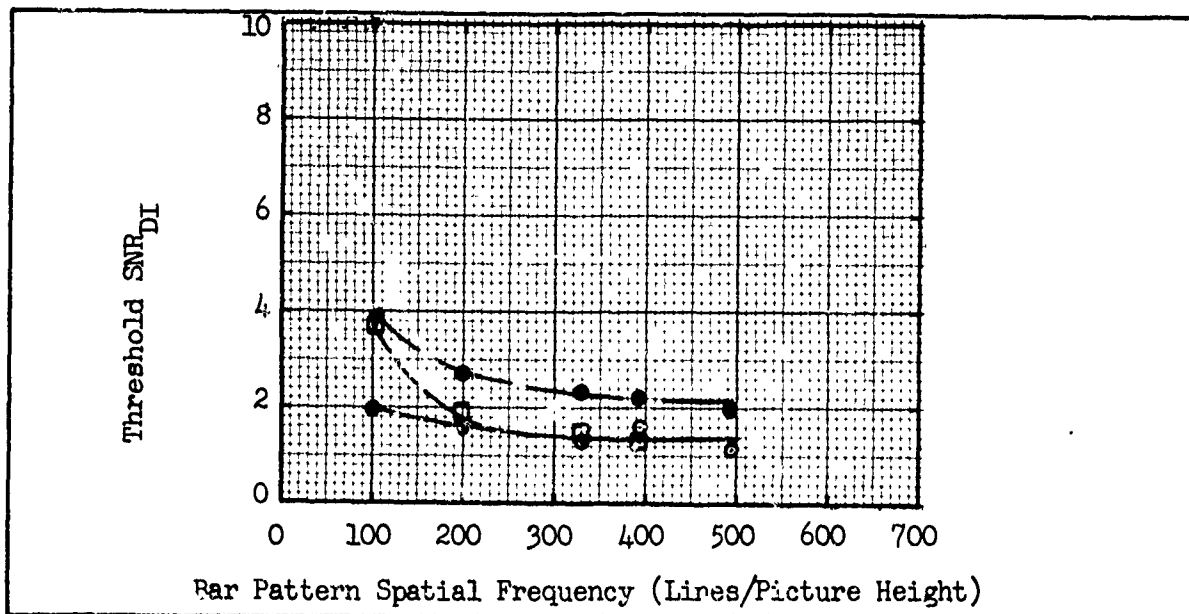


Fig. 81 Exp. No. 3. Threshold SNR_{DI} for ● Original Data and Present Data 1 ft.-Lambert Background ○ Normal □ Very Critical Threshold Judgment - Constant Aspect Pattern Case A MTF

the square data points, □ . As can be seen from a comparison of the squares and open circle of Fig. 79, the effect of the surrounding brightness was negligible but, again lower threshold values of SNR_{DI} were obtained than were obtained on the previous program.

After carefully checking the experimental set-up, recalibrating meters and oscilloscopes, checking terminations, lens focus, camera MTF, and signal currents, a third experiment was performed with one observer in which an attempt was made to be much more critical in establishing the criteria for resolving or not resolving of the bar pattern. The background was at 1 ft. Lambert. The threshold SNR_D results are shown in Fig. 81 by the square data points and then for experiment #1, by the open circles and, again for comparison, the original data from Ref. (2) is shown by solid circles. It was hypothesized that a more critical criteria for bar pattern

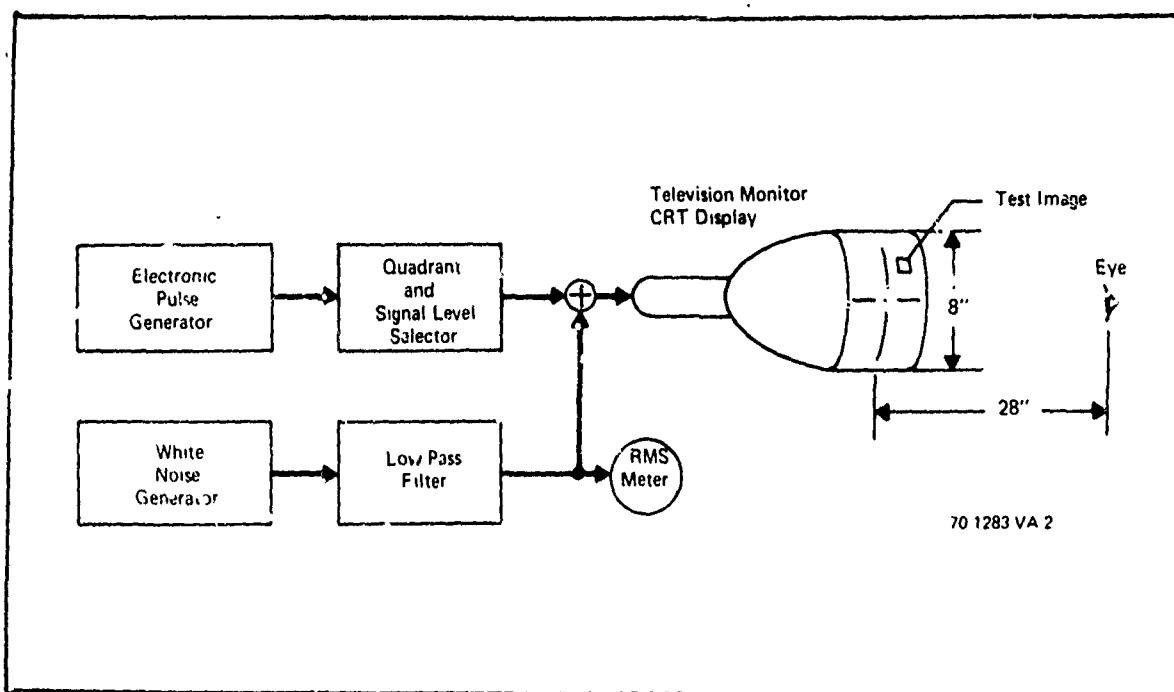


Fig. 82 The Display Signal-to-Noise Ratio Experiment

recognition would correspond with increased SNR_{DI} values and indeed, as is seen in Fig. 81 at low line numbers, this hypothesis is born out. However, virtually no change is observed at higher line numbers. A conscious change in the threshold does not account for the change in the experimental results. Why then are the present results different?

For both of the present experiments and the previous ones a more or less constant pool of about 10 people were used. All of these people were involved in numerous other resolution experiments between the old program and the new and it is postulated that the difference in the curves reflect the learning curves of the subjects. Time did not permit rerunning of the experiments with untrained subjects.

As a final check of the calibration of our equipment, an experiment was run using the set-up shown in Fig. 82. The set-up involved replacing

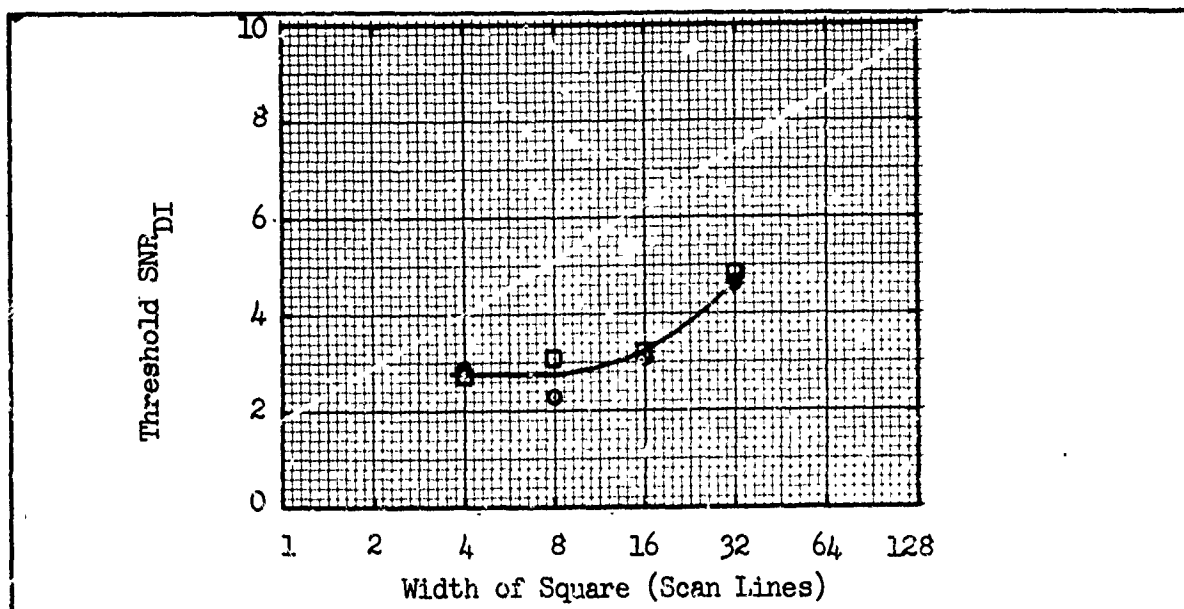


Fig. 83 Exp. No. 4. Threshold SNR_{DI} for Electronically Generated Squares \circ New Data \square Old Data

the vidicon by the electronic pulse generator and operating the monitor at the lower scan rate. The subject had to say in which quadrant of the display the electronically generated square was. Position, size, and SNR_D were randomly varied. In Fig. 83, the threshold values of SNR_{DI} as a function of square width (expressed in number of raster scan lines for convenience), is shown for the present experiment by the open circle points, \circ , and the results from the previous experiment [Ref. (2)], performed a year earlier by the open squares, \square . No difference between the two results can be seen and it is concluded that the experimental set-up is correctly calibrated and that, most likely, the differences which were observed for the bar patterns recognition experiments were due to observer training.

Part of the problem with the bar pattern experiments is that there

way to judge the correctness of the observer's response. An
 erver said he could resolve a given pattern but this is highly subjective,
 and, apparently the criterion (be it unconscious) changed with training.
 For the detection of squares, we know if the subject was right or not and,
 indeed we can correct for random guesses. Bar pattern recognition could be
 made less subjective if an element of correctness/wrongness was introduced
 such as having a break in a bar and asking where the break was or maybe
 using different size Landolt C's with the position of the break randomly
 varied and again asking where the break was. Time did not permit testing
 of either of these hypotheses. A comparison of the new data discussed
 above and that which will be discussed below does show that a high degree
 of consistency exists for similar experiments and we believe that valid
 conclusions can be drawn from these experiments.

For the fifth experiment, set-up B for the MTF was used. Again the
 constant aspect pattern was utilized and in Fig. 84, the probability versus
 SNR_{DI} is plotted as a function of different spatial frequencies. In Fig. 85,
 the threshold SNR_{DI} values are plotted versus spatial frequency. A
 comparison of Figs. 80 and 85 shows that nearly the same SNR_{DI} values are
 obtained for the two MTF cases with slightly closer agreement being obtained
 at the lower frequencies than at the higher frequencies. Finally, experiment
 six was performed with case C's MTF and the constant aspect pattern.
 Probability versus SNR_{DI} for this case is plotted in Fig. 86 and threshold
 SNR_{DI} versus spatial frequency is plotted in Fig. 87. Comparing Figs. 80
 and 87, we see that again for low frequencies, the results are nearly the
 same for Case A and Case C MTF's but for higher frequencies, lower values
 of threshold SNR_{DI} is obtained for Case C than for Case A. The above

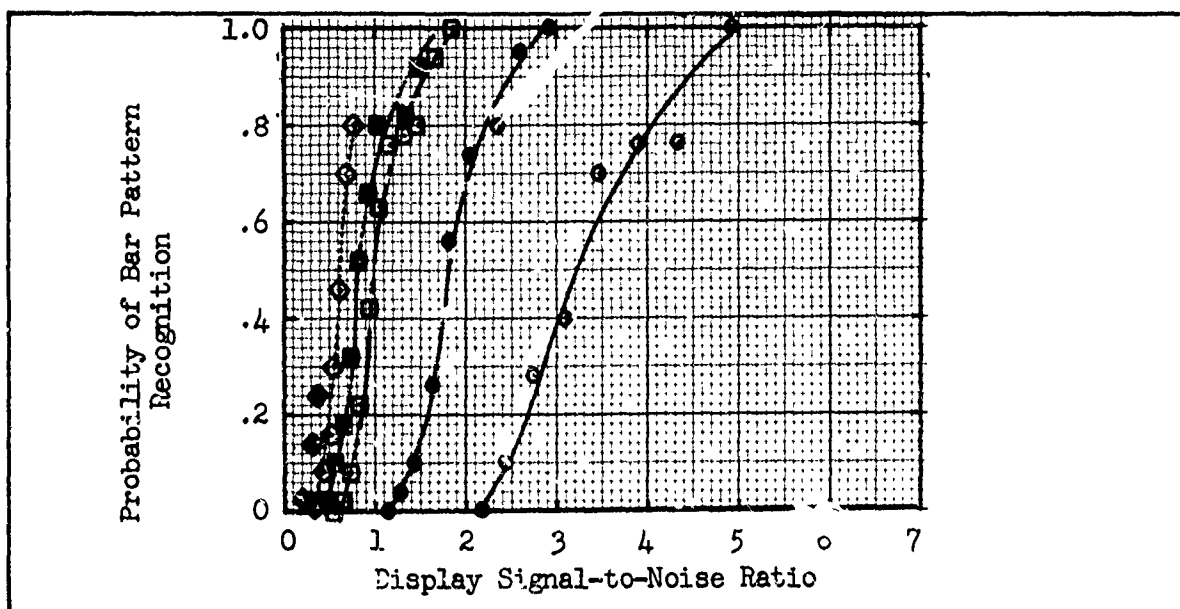


Fig. 84 Exp. No. 5. Probability of Bar Pattern Recognition-
Constant Aspect Bars - Case B MTF Spatial Frequency
○ 104, ● 200, □ 329, ■ 396, ◇ 482, ◆ 635

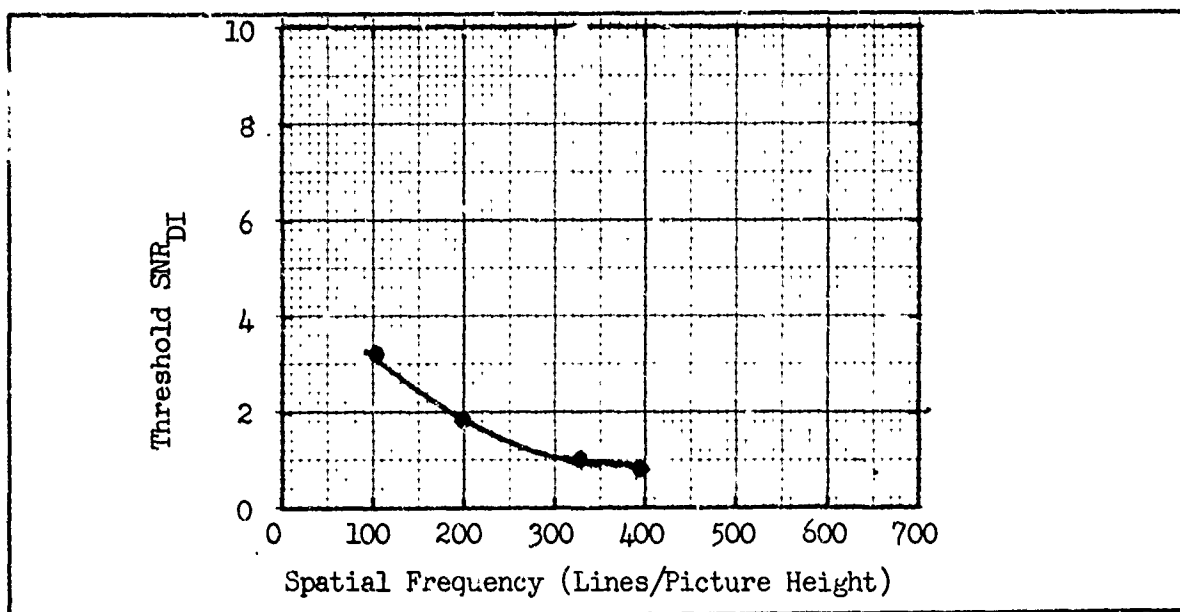


Fig. 85 Exp. No. 5. Threshold SNR_{DI} for Constant Aspect
Bar Patterns Case B MTF

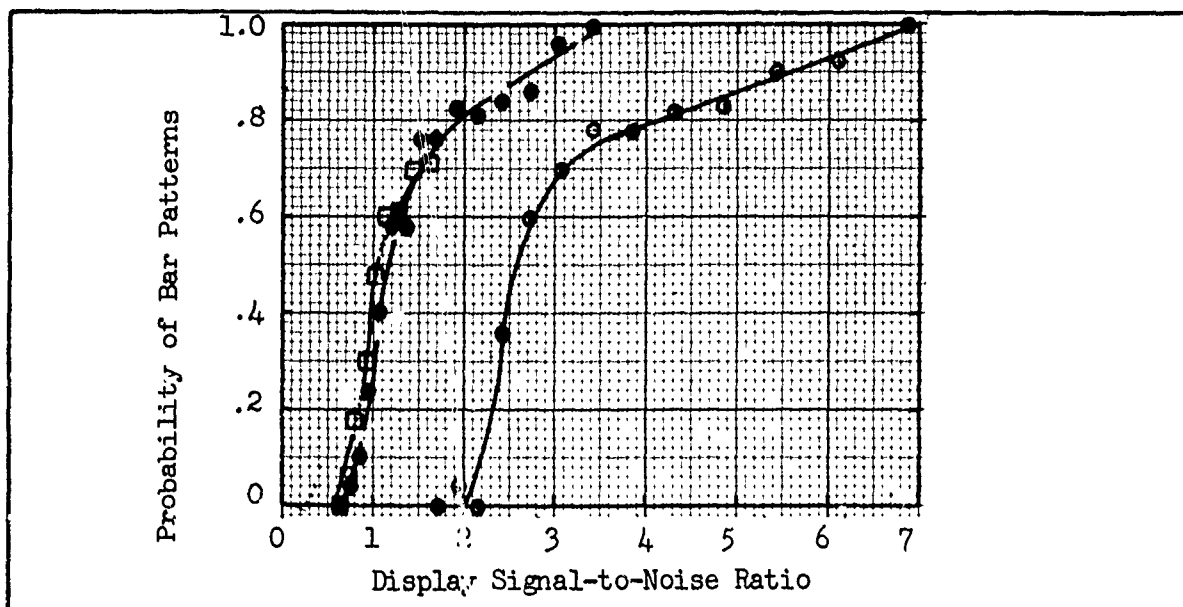


Fig. 86 Exp. No. 6. Probability of Bar Pattern Recognition for Case C, Constant Aspect Bar Patterns Spatial Frequency \circ 104, \bullet 200, \square 329

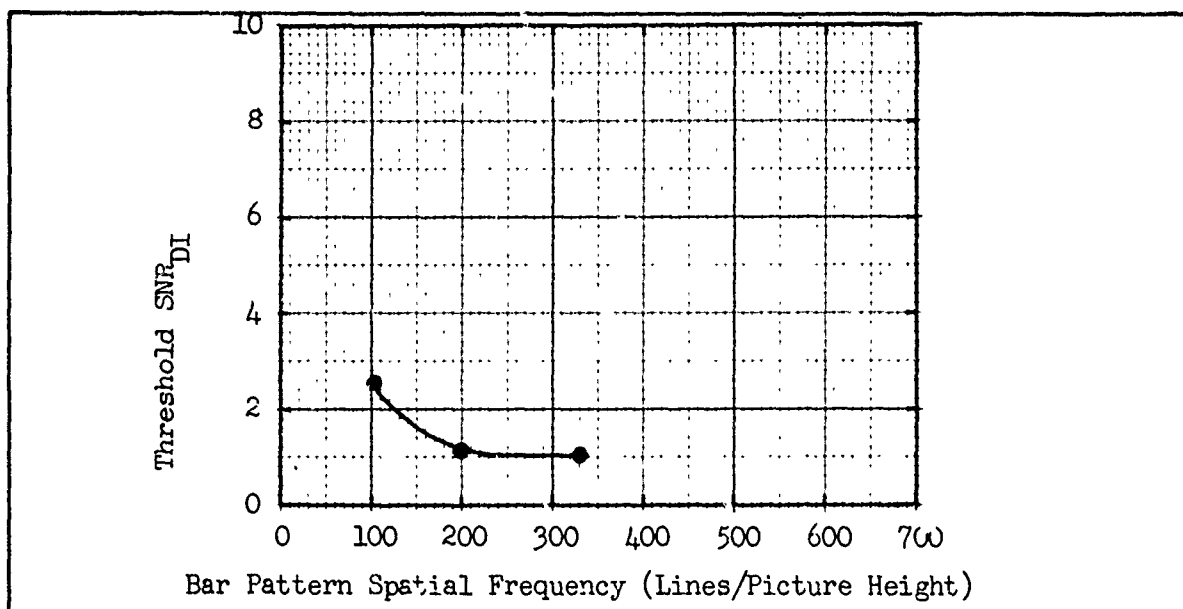


Fig. 87 Exp. No. 6. Threshold SNR_{DI} for Case C, Constant Aspect Pattern

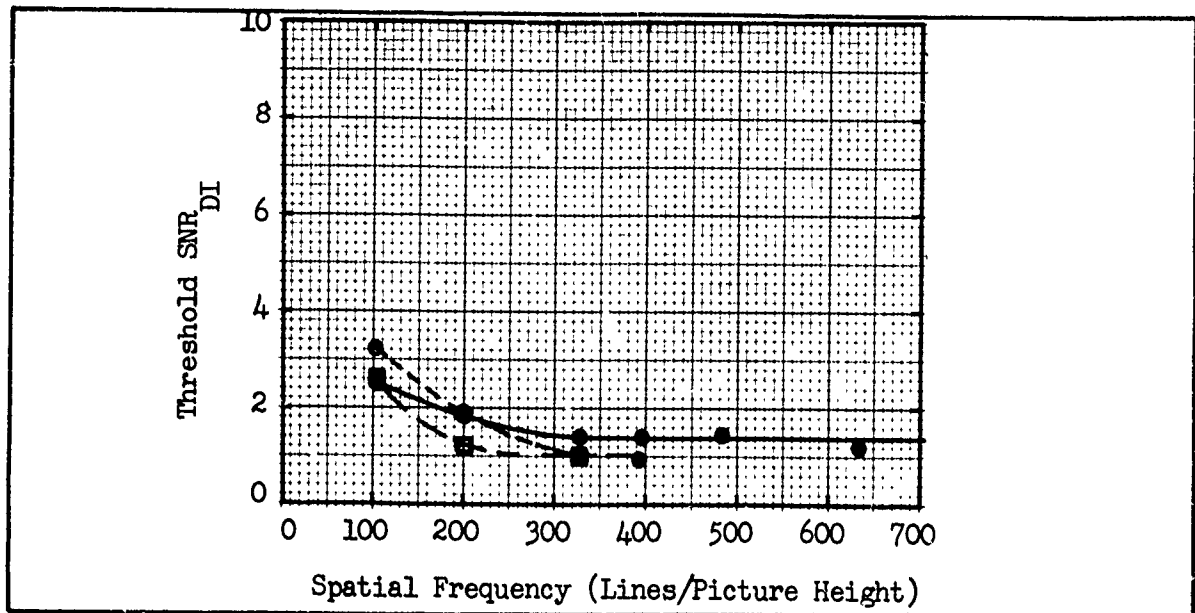


Fig. 88 Threshold SNR_{DI} for AF 5 Bar Pattern Case A \bullet ,
Case B \circ , Case C \square MTF's

results are summarized in Fig. 88 for the constant aspect patterns for Case A, B, and C MTF's. The values of SNR_{DI} are somewhat lower for Case B and C than A for higher spatial frequencies. One must be careful in concluding that lower SNR_{DI} values are obtained with poor MTF. Comparing the spread in the data at low frequencies where the experimental accuracy is the best shows a fairly large spread in the data so the difference is probably not very significant.

It must be also kept in mind that the calculation of SNR_D includes the MTF's effect on signal and on noise. For a given line number and SNR_D value, a much higher video signal-to-noise ratio is required for Case C MTF than for Case A MTF. The experimentally determined threshold values of SNR_D are somewhat lower for Case C's MTF than those for Case A's and as was mentioned the differences may be reflecting experimental error. More likely, we believe,

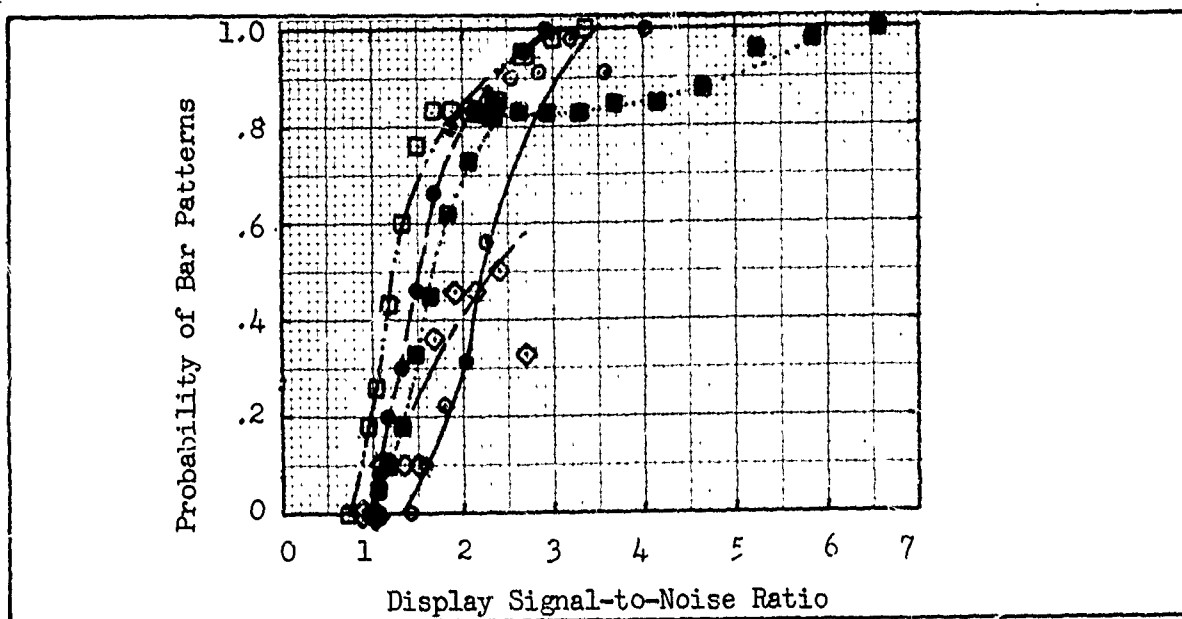


Fig. 89 Probability of Bar Pattern Recognition for
Constant Length Bar Patterns - Case A MTF

is that for poor MTF's, our formulation for SNR_D is rather pessimistic, that is, the MTF's do not degrade the images detectability as much as theory would indicate. In any event, for the same broad area video signal-to-noise ratio, the better the MTF is, the more detectable the image is.

Experiment 7 used Case A MTF with the bar patterns of variable aspect and the experimental results are shown in Figs. 89 and 90. For comparison, the results with the constant aspect patterns are also shown in Fig. 90 and as is seen, the two cases are very similar for all but the highest line numbers.

Experiment 8 utilized the variable aspect pattern with Case C MTF and the threshold SNR_D vs spatial frequency curves for Case A and C are plotted in Fig. 91. A somewhat lower result was obtained for Case C than for Case A.

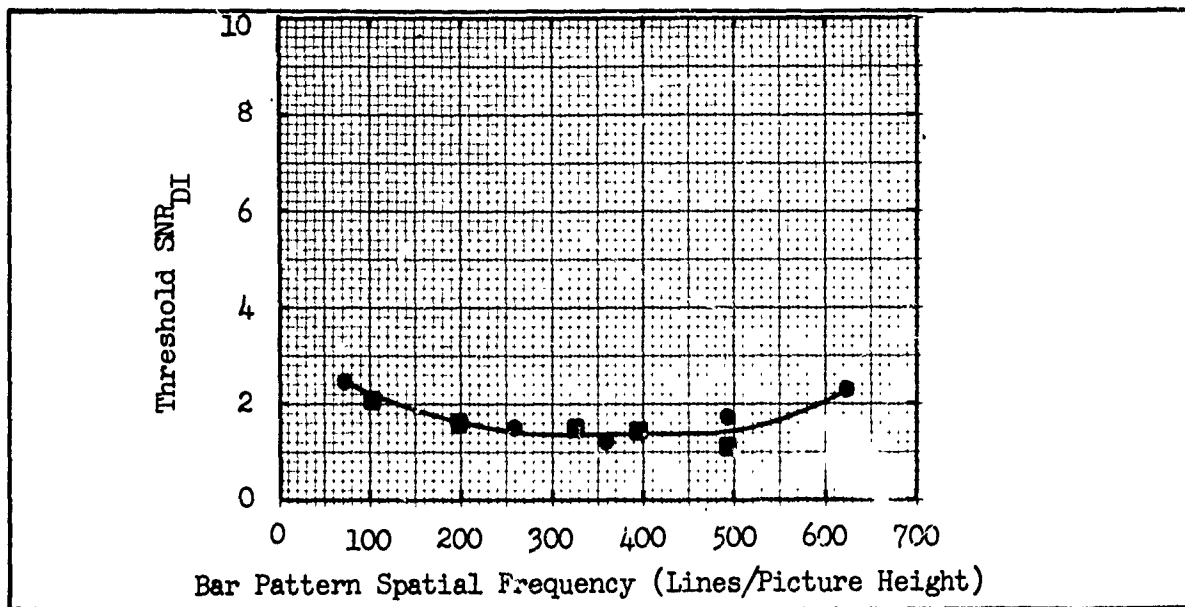


Fig. 90 Exp. No. 7. Comparison of Threshold SNR_{DI} for Case A MTF, ● Constant Length, ■ Constant Aspect Bar Patterns

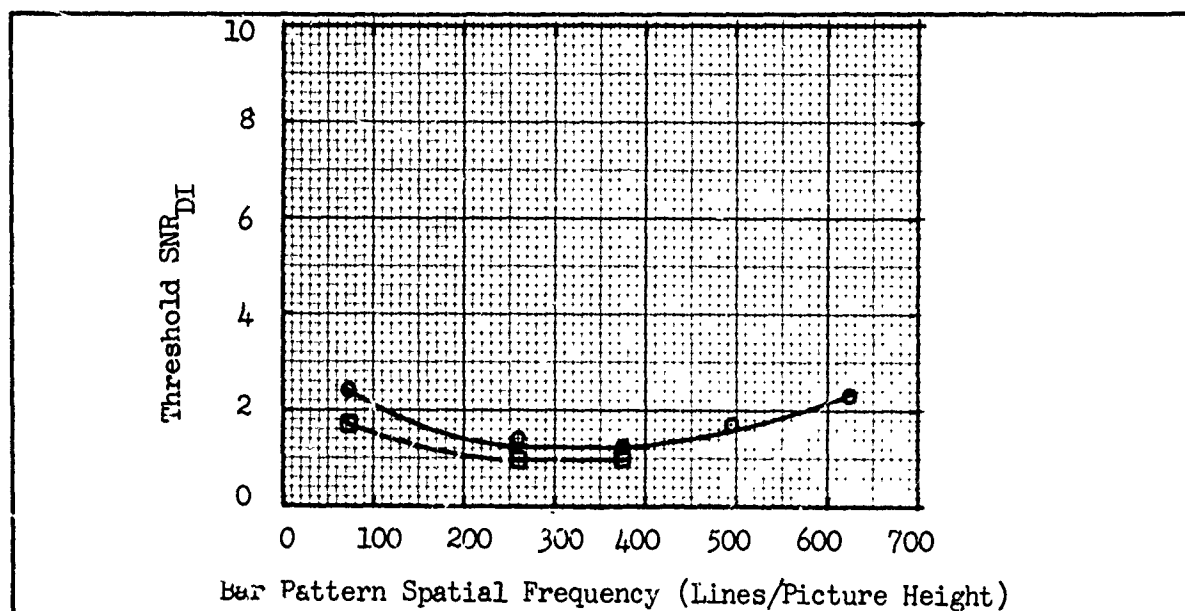


Fig. 91 Exp. No. 7 and 8. Comparison of Threshold SNR_{DI} for Constant Length Bar Patterns Case A ○, Case C □ MTF's

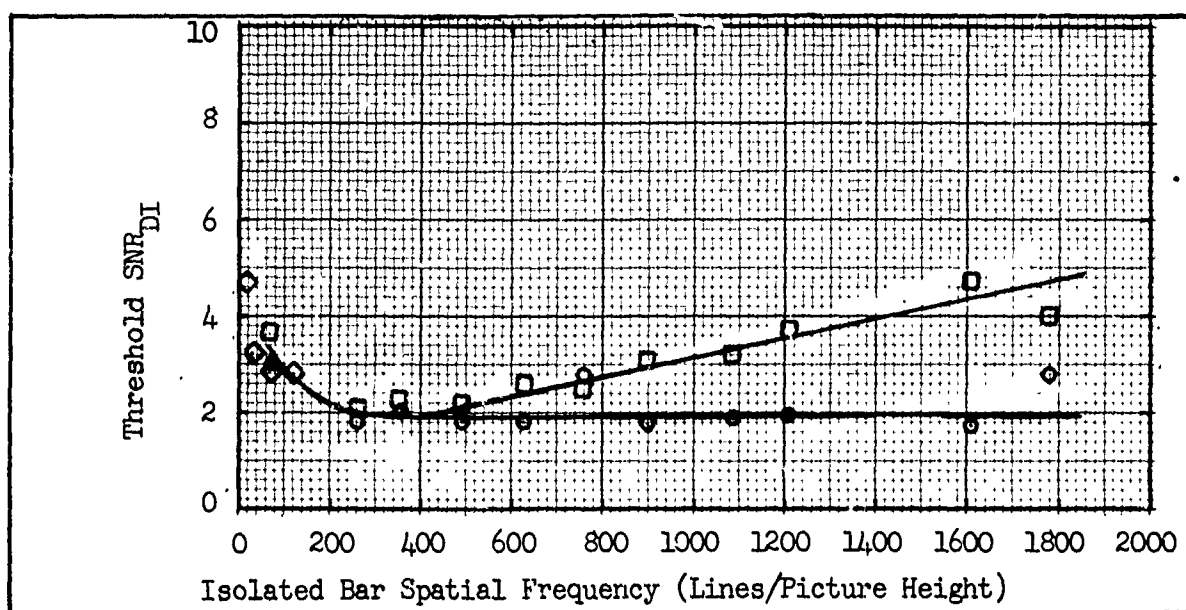


Fig. 92. Exp. No. 9 and 10, Threshold SNR_{DI} for Isolated Bars for Case A \circ , Case C \square MTF's, \diamond Electronically Generated Squares

The pattern with the isolated bars was used for the next two experiments, Case A MTF in experiment 9 and Case C MTF in experiment 10. The threshold SNR_{DI} versus spatial frequency plots for the two cases is shown in Fig. 92. The data is actually the same up to a spatial frequency of about 500 lines/picture height and then the data for Case C rises at a nearly constant rate. A rise in the threshold curve for Case A MTF is suggested at very high line numbers, $N = 1780$. A comparison of the data from Fig. 83 for the electronically generated squares and that for isolated bars of Fig. 92 shows that the two sets of data are similar at low line numbers, the Case A MTF data being nearly the same as that for the electronic generated squares. This of course is not a surprise. At low line number for Case A, aperture effects are minimized and the results should be similar to those measured for the electronically generated squares where aperture effects are

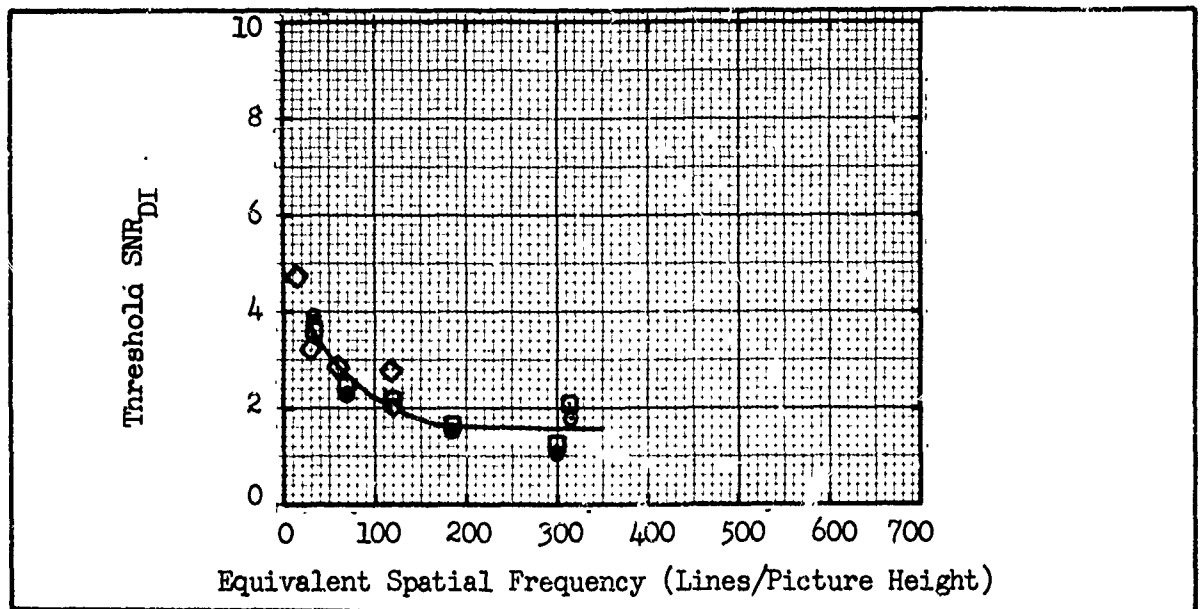


Fig. 93 Exp. No. 11 and 12. Threshold SNR_{DI} for Isolated Circles for Case A \circ , Case C \square MTF's, \diamond Electronically Generated Squares

negligible. This is further evidence that the present experimental set-up is functioning correctly.

The pattern with the isolated circles was also used with Case A MTF and Case C MTF and the threshold SNR_{DT} is plotted versus spatial frequency for the two cases in Fig. 93. Again, it is found that the data is consistent with that measured with the aperture free, electronic-target generator.

For aperiodic targets, from the comparison of the experiments with isolated bars and circles and those of the aperture free squares, it is seen that the theory as given by Eqs. (164) and (165) is confirmed, within experimental accuracy, for MTF's that are quite different from one another ($N_e = 252$ for Case A and $N_e = 69$ for Case C). Furthermore, it is seen that for bar patterns, the theory as given by Eqs. (160), (161), (162), and (163),

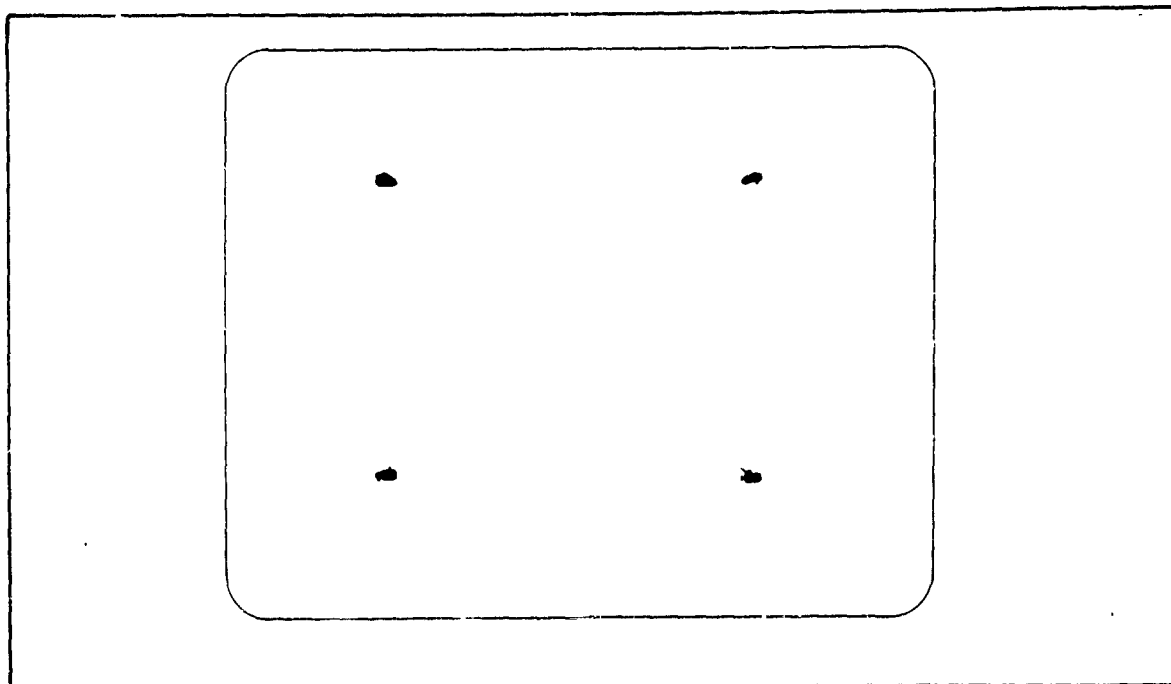


Fig. 94 Photographs of Models Used for Recognition Experiments - Upper Left, Tank; Upper Right, Van Truck; Lower Left, Half Track with Antenna; and Lower Right, Derrick Half Track.

gives a somewhat pessimistic result (smaller SNR_{DI}) for poor MTF's than it does for good MTF's. In effect, a system of poor MTF would actually perform somewhat better than the theory would suggest. The differences are in such a direction as to help the system designer.

Using the experimental set-up of Fig. 1, experiments were performed on tactical target recognitions using Case A and Case C to establish the impact of MTF's on real target recognition. The transparencies which were used were made from high quality photographs of vehicles amid a uniform white background. The photographs were taken at a depression angle of 45° from the horizontal and perpendicular to the vehicle's longitudinal axis, i.e., the sides and tops of the vehicles were imaged as is shown in Fig. 94. The vehicles included a tank, a van truck, a half track with top-mounted radar antenna and a tracked bulldozer with derrick. The areas of the

various vehicles were approximately 0.057 in^2 on the $8'' \times 10.7''$ display and subtended angles of about 0.34° by 0.68° at the observer's eye. The vehicle types and video SNR were randomly varied; and the probabilities of recognition, corrected for change, were determined. The SNR_{DI} 's for the various images were calculated on the basis of the area of a bar whose length and width are equal to the length of the vehicle's image and the width of the vehicle's image divided by 8. This is in accord with the equivalent bar pattern concept discussed in AFAL-TR-72-229. We note, however, one difference between the calculations for the bar pattern and the vehicular image's SNR_{DI} . In the case of the vehicular image, the signal amplitude was measured from the background signal level which was approximately constant, to the peak object signal level. For the "equivalent bar patterns," the signal levels were measured in terms of the mean signal excursion within the bar pattern area in the periodic direction. Had the peak-to-peak excursions about the average signal within the vehicle area been used (when the object is imaged against a uniform background), the thresholds SNR_{DI} would have been somewhat lower.

These difficulties result from the necessity of defining an image area and a signal excursion in order to calculate an SNR_{DI} threshold. In this connection, we observe that the criterion for bar pattern recognition is that the observer must be able to discern a modulation within the bar pattern whereas for vehicle image recognition, the vehicle's outline must be discerned. This outline may have periodic features but is more likely to be aperiodic.

Specifically, the SNR_{DI} was calculated from

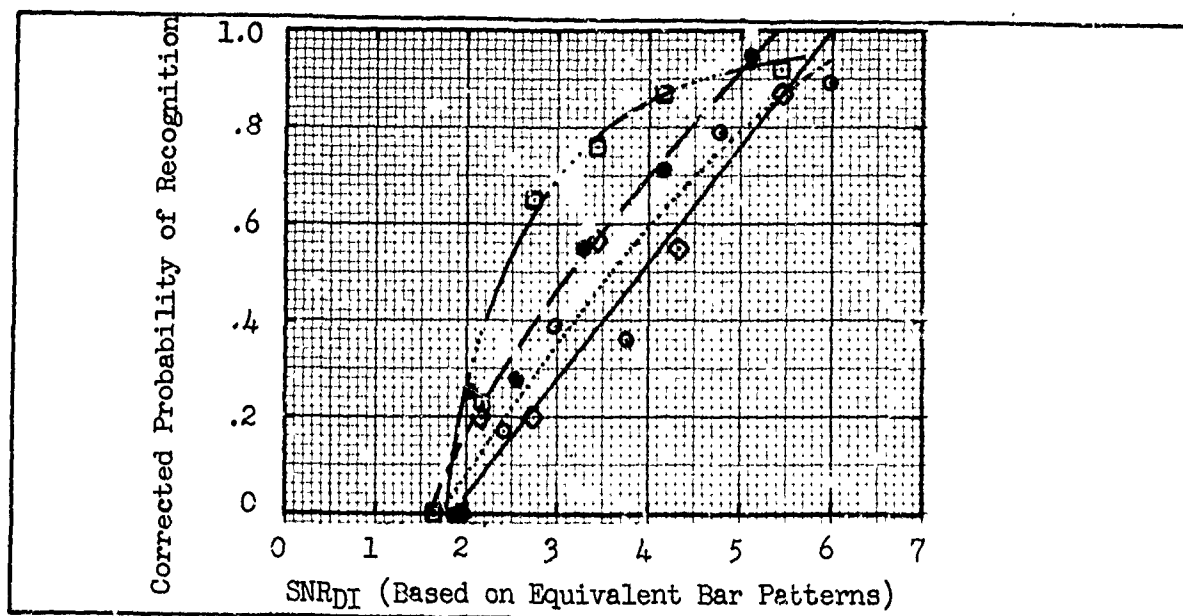


Fig. 95 Exp. No. 13. Tactical Target Recognition for Case A MTF
 ○ Tank, ● Derrick, □ Truck, ◇ Radar Truck

$$\text{SNR}_{DI} = \left[2t\Delta f_V \frac{a}{8A} \right]^{\frac{1}{2}} \text{SNR}_V \quad (166)$$

where SNR_V was the largest zero to peak voltage in a frame of the image divided by the RMS value of the noise. The value of a/A that was used was the actual area of the image, a , on the transparency divided by the total area of the transparency, A , that was viewed. The factor of 8 in Eq. (166), comes from the assumption that we are to calculate SNR_{DI} on an equivalent bar pattern basis, that is, for recognition, one whose bars are each $a/8$ in area. In Figs. 95 and 96, the probability versus SNR_{DI} is plotted for tactical target recognition for Case A and Case C, respectively. For Case A, the average threshold SNR_{DI} is 3.2 where as for Case C, the average threshold SNR_{DI} is 4.3; a value that is 34% higher than that for Case A.

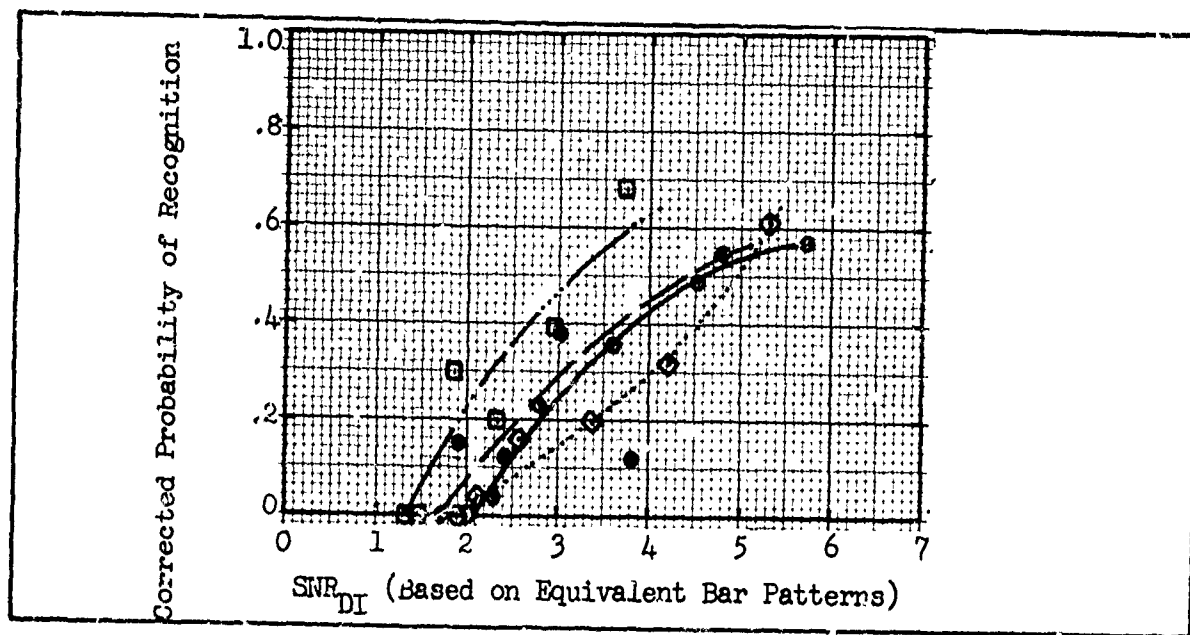


Fig. 96 Exp. No. 14. Tactical Target Recognition for Case C MTF
 ○ Tank, ● Derrick, □ Truck, ◇ Radar Truck

In Fig. 97, we show the signal excursions for the tracked bulldozer on selected horizontal lines from the top to the bottom of the vehicle with line 1 being just above the object and line 17 just below. The MTF which was used was Case A. These traces were taken on every other line from a line selector oscilloscope. The dominant features of the bulldozer shown pictorially in Fig. 94 can be located in the traces of Fig. 97. The boom arm is in traces 3 through 6, the cab in 6 through 8 and the bulldozer blade in 9 through 13. The boom appeared to be the most characteristic feature and the width was of the order of 1/8 width of the bulldozer.

Strictly speaking, the tactical targets are not either periodic or aperiodic in structure. However, as is discussed in the section on motion, if the aperiodic form of the SNR_{DI} equation is used together with the assumption that the original dimension, x_o , y_o can be associated with an

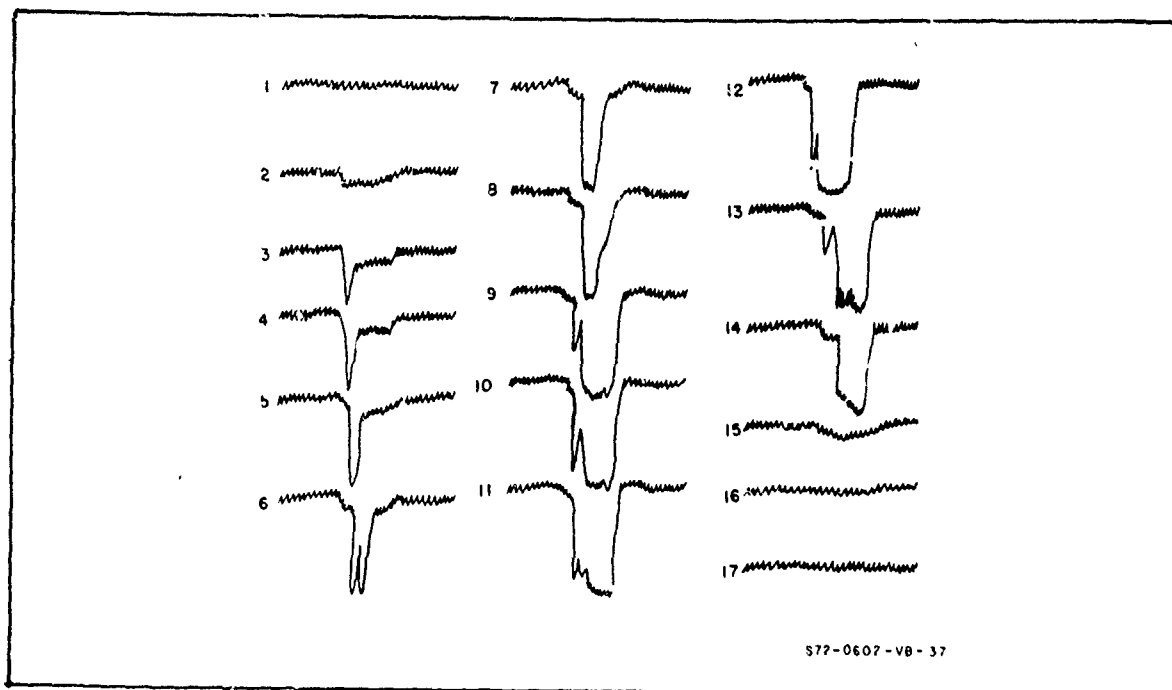


Fig. 97 Waveform of Derrick Half Track Along the Horizontal as a Function of Vertical Position of Scan Lines.

equivalent bar pattern (e.g. with bars y_o long and $x_o/8$ wide for recognition) then the static and motion results can be accounted for by the same threshold SNR_{DI} value. Furthermore, as we will now show, the same value SNR_D also holds for widely different MTF characteristics as well.

The value of aperiodic SNR_{DI} is calculated from

$$SNR_{DI} = \left[\frac{2t\Delta f_V x_o y_o}{\xi_{x_{LT}} \xi_{y_{LT}} 8A} \right]^{\frac{1}{2}} SNR_V \quad (167)$$

where

$$\xi_{x_{LT}} \xi_{y_{LT}} = \left[1 + \left(\frac{\delta_L}{x_o} \right)^2 + \left(\frac{\delta_T}{x_o} \right)^2 \right]^{\frac{1}{2}} \left[1 + \left(\frac{\delta_L}{y_o} \right)^2 + \left(\frac{\delta_T}{y_o} \right)^2 \right]^{\frac{1}{2}} \quad (168)$$

and

$$\delta_L = \frac{1}{N_{eL}} \quad (169)$$

$$\delta_T = \frac{1}{N_{eT}} \quad (170)$$

Using Eqs. (167), (168), (169), and (170), we have that for Case A $SNR_{DI} = 2.2$ whereas for Case C, $SNR_{DI} = 1.7$ and the two values of SNR_{DI} are somewhat closer in magnitude than those obtained ignoring MTF effects. The fact that the SNR_{DI} for poor MTF's is smaller may indicate that the effects of the poor MTF's are not quite as bad as the SNR_D equations would suggest. A similar result was obtained for bar patterns and we tentatively conclude that our theory is too pessimistic for very poor MTF's. Much more experimental data needs to be taken for different MTF cases to establish the limits of our theories.

6.0 Measures of Image Quality

There has been considerable interest by researchers in the optical and electro-optical field in finding a single measure of image quality. Such a number might be useful in comparing and specifying electro-optical components and may also be used in the design of the components. A specific design example is the shape of an MTF curve. In many cases, an MTF can be optimized for either a maximum low frequency response such as curve A of Fig. 98, or for a maximum high frequency response at the expense of the low frequency response as shown by curve B of the same figure. With the curve A, aperiodic signal levels will be generally higher than with curve B while with curve B, high frequency periodic patterns can be discerned that cannot be seen at all with an MTF corresponding to curve A.

To resolve fine image details, a sensor's MTF, projected into object space must be sufficiently high relative to the scene objects of interest. While a high MTF is a necessary condition, it is not sufficient. A fine grain photographic film may produce very high resolution of a day-lighted scene but be next to useless in a dimly lit cathedral. For the indoor scene, the photographer may need to select a coarser grain film of higher sensitivity. Similarly, a high resolution vidicon cannot compete with a moderately low resolution, low light level television at night but on the other hand, the high resolution vidicon camera will far outclass the LLLTV by day. It is thus readily evident that picture

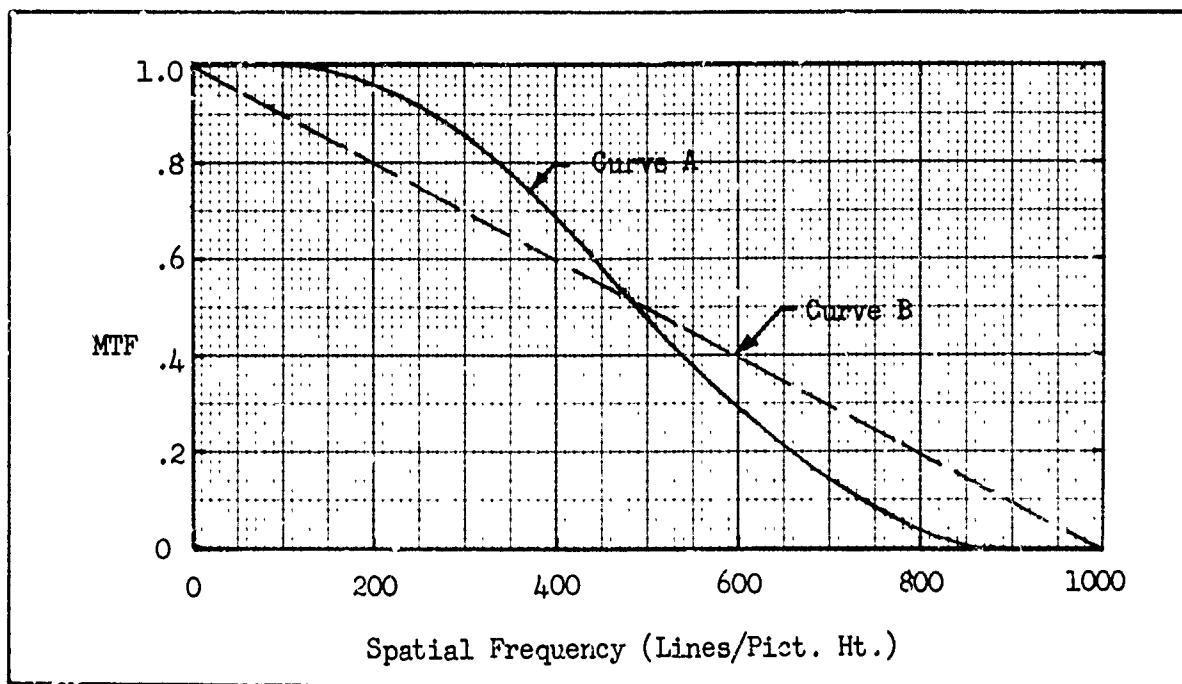


Fig. 98 Two Modulation Transfer Functions. Curve A Illustrates a High, Low Frequency Response While Curve B Illustrates a High, High Frequency Response.

quality is a function of both resolution limiting parameters such as the sensor MTF's and the sensor sensitivity. The picture quality can also be a function of the sensor's dynamic range and the scene itself.

To begin this discussion, we will first discuss the MTF related parameters and their effect on image quality. These factors have been the object of the most concern from a historical point of view.

6.1 MTF Related Image Quality Parameters

In 1881, Lord Rayleigh proposed a resolution measure for optical devices using two point source images. As discussed in Section 2, a lens images a point as a blur. As two point images are brought closer together, a point will be reached where they are no longer resolved as two points, but as one. Lord Rayleigh's criterion, however, demands

that the two images be resolved and the criteria was set so that the minimum signal excursion between the peaks of the two points and the valley between be 19% or more. This criterion is judged by many to be too severe, e.g., that the points can be resolved as two with a much smaller signal excursion. However, as we have noted above other factors must be considered. With test point images of low intensity, a 19% signal excursion may not be enough.

The modulation transfer curves such as those shown in Fig. 98 have been used in a similar manner. The "limit of resolution" has often been taken to be that spatial frequency at which the MTF has fallen to some low value such as 5% or 2%. The 2% figure is especially popular since it is often assumed that the eye cannot detect image contrasts below about 2%. However, image contrasts lower than 2% can be discerned by the unaided eye under many conditions. Also in many electro-optical sensors, the displayed contrast may be many times higher than the scene contrast. This is particularly true for FLIR equipments in the 8 - 13 μ band. With inherent scene contrasts of only a few percent, the displayed image contrast will usually be near 100%. Thus the eye's 2% "contrast limit" has little merit as a criterion when the displayed image contrast is variable.

However, the modulation transfer function has a strong effect on picture quality. As we have shown in Sections 2 and 3, the modulation transfer function can both decrease perceived signal and increase perceived noise. It also limits the size of the small scene detail that can be seen. We note again before proceeding, that the smallest detail that can be seen is not only a function of the MTF but also of

the signal and noise levels and therefore a good sensor MTF alone does not guarantee high resolution. On the other hand, a high resolution or scene detail will not be obtained without a high MTF.

An MTF is synonymous with the frequency response of an electrical filter. As is well known, a wide frequency response is need to transmit short pulses and similarly a wide MTF is need to transmit point or line images. Electrical engineers are fond of the concept of equivalent bandwidth which is defined as the width of a rectangle whose area is the same as the area under the MTF curve. Since the value of the MTF at zero frequency is unity, the width of the rectangle (or equivalent bandwidth) is equal to

$$N_b = \int_0^{\infty} |R_o(N)| dN \quad (171)$$

Corresponding to N_b , there will be an equivalent impulse response width, δ_b , where

$$\delta_b = \frac{1}{N_b} \quad (172)$$

As is evident, the larger the bandwidth N_b , the smaller will be the equivalent impulse response width. Since the displayed image's detail is the convolution of the input image with the sensor's impulse response, a wide impulse response width will result in a loss of image detail.

The Eq. (171) can be written in two-dimensional form as

$$N_b(x,y) = \int_0^{\infty} \int_0^{\infty} |R_o(N_x N_y)| dN_x dN_y \quad (173)$$

This equation has been related directly to the Strehl measure of image

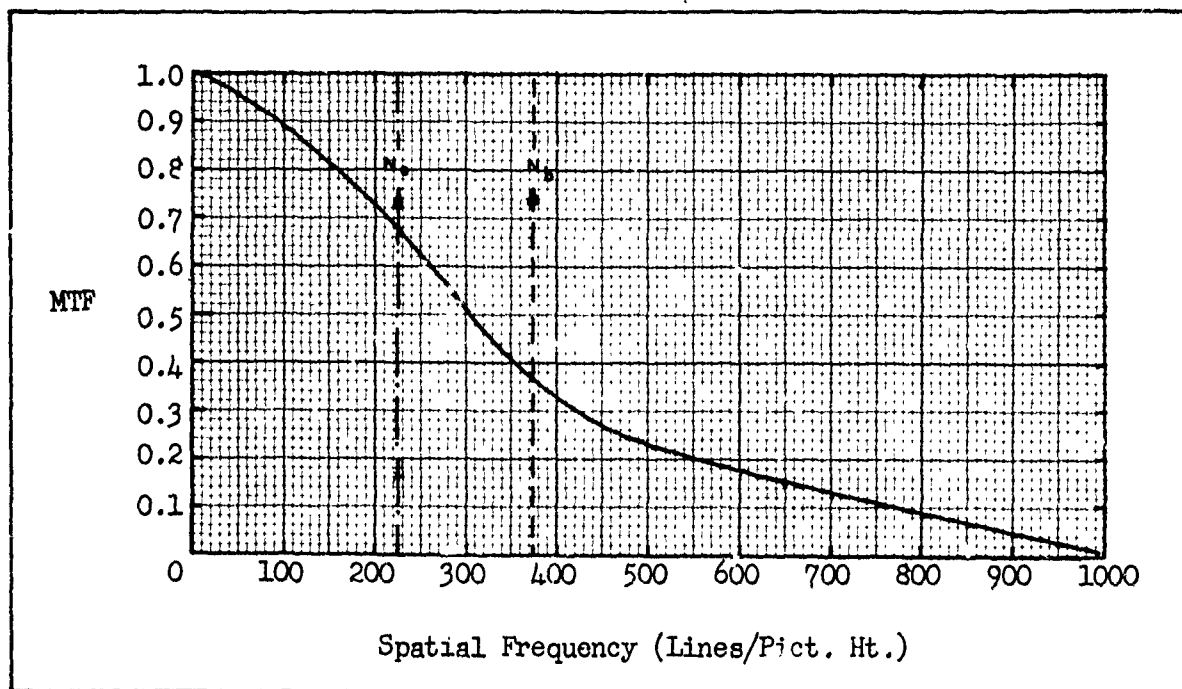


Fig. 99 MTF, Equivalent Bandwidth N_b and Noise Equivalent Bandwidth vs Spatial Frequency for a Typical 40/40/25 I-EBSICON Camera Tube.

quality (Ref. 9).

Schade (Ref. 9) has proposed the noise equivalent bandwidth, N_e , as a summary measure of quality where

$$N_e = \int_0^\infty |R_o(N)|^2 dN \quad (174)$$

Since $R_o(N)$ has a maximum value of one at zero frequency (for a linear system) and falls off with frequency, Schade's measure weighs the low frequency response more heavily than Eq. (171). The equivalent and noise equivalent bandwidths are shown for a typical MTF in Fig. 99.

Another figure of merit that has been extensively used is the acutance of an image (Ref. 10). The acutance is obtained in the following manner. A sensitive surface is partially covered with a knife

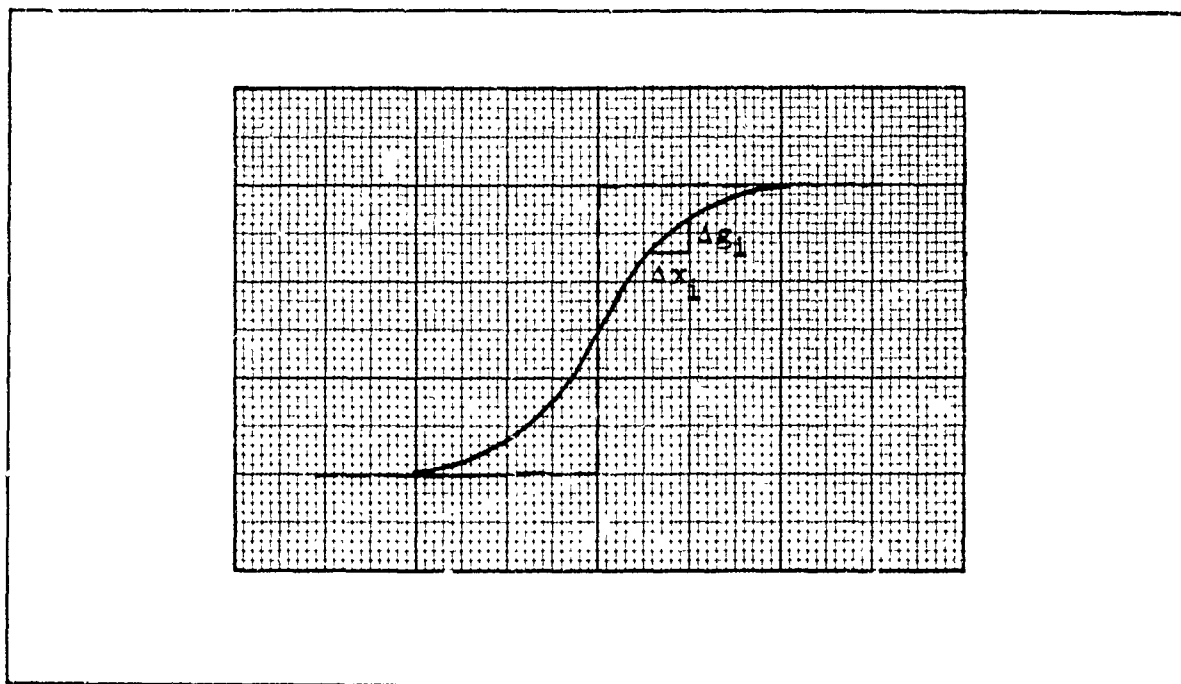


Fig. 100 Output Waveshape (—) for a Step Function Input (---). Slope of Output Waveshape, $\Delta g_i / \Delta x_i$ is used to Find Image Acutance.

edge and exposed to light. The light in the illuminated area does not stop at the knife edge but is diffused into the shielded region by reason of reflection, refraction, diffraction and scattering within the surface. Thus, the distribution of photoelectrons generated (or density of exposed grains in a photograph) instead being a step function assumes the typical S shape shown in Fig. 100. The slope of the S-shaped curve at any point is $\Delta g(x_i) / \Delta x_i$. The slope is determined for every position on the curve at equally spaced increments Δx_i and summed to give the expression

$$\bar{g}_x^2 = \Sigma (\Delta g_i / \Delta x_i)^2 / n , \quad (175)$$

where n is the total number of Δx increments. The acutance is defined as

$$\text{Acutance} = \frac{\bar{g}_{x_1}^2}{I_s}, \quad (176)$$

where I_s is the magnitude of the step in exposure. Acutance has been found to correlate with image sharpness.

Acutance bears a strong resemblance to Schade's N_e . The derivative of the unit step function $r_{-1}(x)$ is the impulse response $r_0(x)$, i.e.,

$$\begin{aligned} r_0(x) &= \frac{d}{dx} [r_{-1}(x)] \\ &\sim \frac{\Delta r_{-1}(x_1)}{\Delta x_1} \end{aligned} \quad (177)$$

and

$$\begin{aligned} \Sigma \frac{[\Delta r_{-1}(x_1)]^2}{\Delta x_1} &\sim \frac{1}{nI_s} \Sigma \frac{\Delta g_1^2}{\Delta x_1} \\ &\sim \int_{-\infty}^{\infty} r_0^2(x) dx ; \end{aligned} \quad (178)$$

and by Parseval's theorem,

$$N_e = \int_0^{\infty} |R_0^2(N)| dN = \int_{-\infty}^{\infty} r_0^2(x) dx \quad (179)$$

as can be seen N_e is equivalent to, if not exactly the same as acutance.

Hufnagel (Ref. 9) evaluated 4 measures consisting of the one and two dimensional forms of N_e and N_b . He notes that none of

the functions meet his test for a measure "that is not invalid." (Hufnagel rates a measure "not invalid" if the objective vs subjective rankings of image quality plot as a rising straight line.) However, he claims the best results for the Strehl measure for photographs with substantially zero grain. For photographs with grain, he found a quantity Q_4^2 where

$$Q_4^2 = \frac{\iint_0^\infty |R_o(N_x N_y)| dN_x dN_y}{1 + \beta \iint_0^\infty |R_o(N_x N_y)|^2 F(N_x N_y) dN_x dN_y} \quad (180)$$

which he dubs a grain modified Strehl measure. The above equation has the form of a signal-to-noise ratio for an aperiodic image.

Most of the work in defining picture quality measures has been performed using photographs. The usual procedure is to make photographs with lenses of different MTF's (but MTF's which are similar in shape). Observers are asked to grade the resulting pictures in order of "quality." It is not surprising that the pictures taken with the lenses of highest MTF proved to be the best or that the integral of the highest MTF (whether squared or not) has the largest numerical value.

A measure based on MTF alone applies only when the image, and the eye observing the image, is completely noiseless. Note also, that it may be necessary to include the observer's MTF in certain image quality determinations even if the noise is essentially negligible. However, no photoconversion process is completely noise-free and under many conditions, picture quality may be primarily limited by noise

rather than MTF. Indeed, much of the apparent lack of straight line correlation between image quality and a summary measure based on MTF alone may be due to the neglect of the noise.

In any event there is a growing belief that a summary measure of image quality must be based on signal-to-noise ratio and efforts in this direction are being made.

6.2 Signal-to-Noise Ratio Related Image Quality Parameters

As a first step in defining an image quality measure based on signal-to-noise ratio, Snyder (Ref. 9) has proposed that the measure be the integral of the display signal-to-noise ratio above the observer's threshold (SNR_{DT}) as illustrated in Fig. 101. The solid curves represent the image signal-to-noise ratio obtainable from the sensor's display at two different light levels and the dashed curve represents the observer's threshold signal-to-noise ratio requirement. The area is that between a given solid line and the dashed line.

Mathematically, the enclosed SNR_D area, called the MTF_A is given by

$$MTF_A = \int_0^{\infty} [SNR_D(N) - SNR_{DT}(N)] dN \quad . \quad (181)$$

SNR_D , for periodic bar patterns, is proportional to $R_{SF}(N)$ the square wave flux response and is inversely proportional to N , the spatial frequency, i.e.,

$$SNR_D \propto \frac{R_{SF}(N)}{N} \quad , \quad (182)$$

as N approaches zero, SNR_D approaches infinity. Even at low N , SNR_D

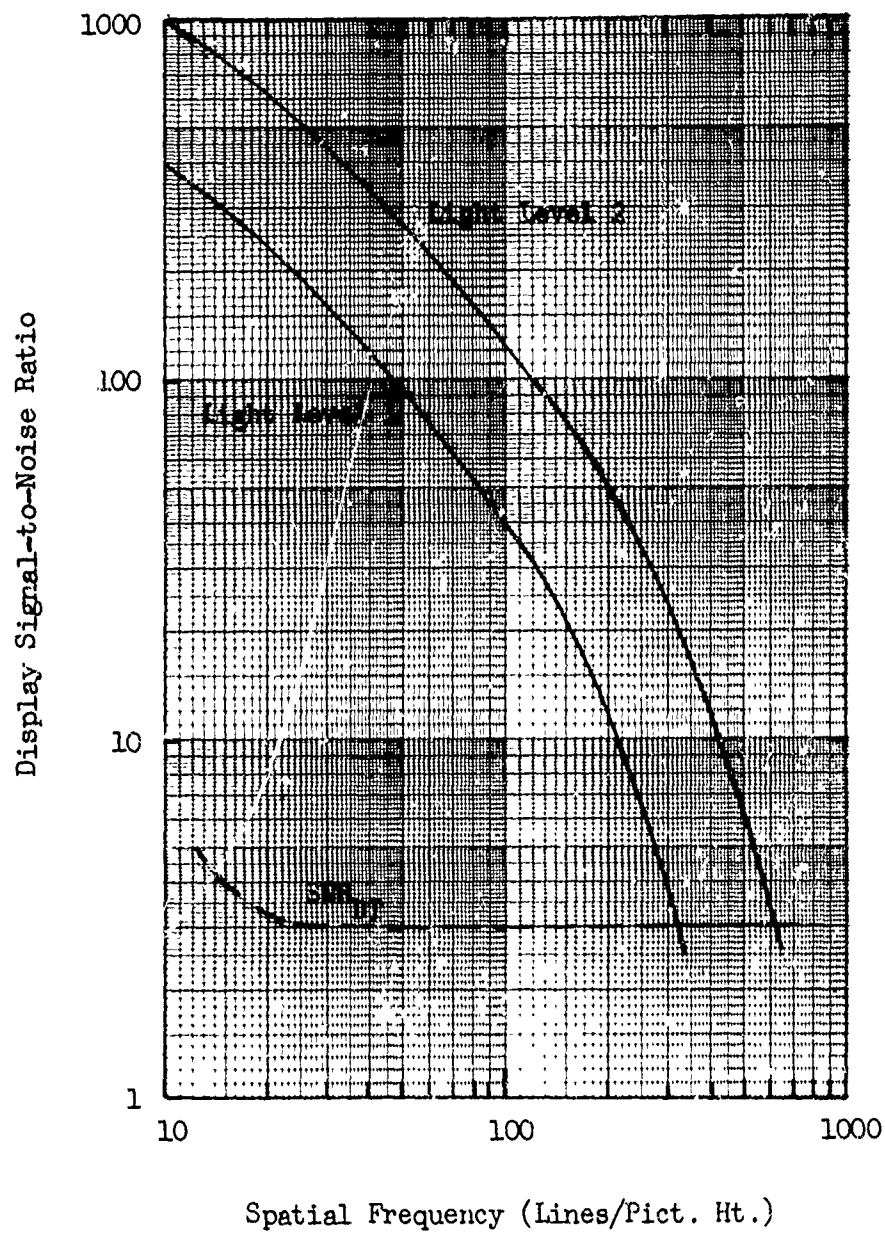


Fig. 101 Display Signal-to-Noise Ratio Obtainable (—) and Required (---) for Two Light Levels as a Function of Spatial Frequency.

becomes very large. However, the SNR_{DT} also increases at low spatial frequencies and thus integral of Eq. (181) should have a finite value. MTF is, of course, a function of the observer viewing distance since viewing distance influences the lowest spatial frequency observable.

MTF_A , generally weighs low spatial frequency response even more heavily than does N_e and the heavy weight of N_e on low frequency response has been one of the major criticisms of N_e . Schade (Ref. 4) also notes that MTF_A while generally a valid guide for systems with similar MTF's and noise characteristics is inappropriate for systems with dissimilar characteristics. In Schade's new measure, the balanced threshold resolution becomes the image quality criterion. By balanced resolution, Schade means the average of resolution calculated for periodic and aperiodic test patterns. Since periodic pattern detection weighs high spatial frequency response more heavily, the balanced resolution concept would presumably remove some of the heavy low spatial frequency response bias of N_e .

The goal of many researchers has been to find a single unitary measure of image quality. As we have shown, a single unitary measure is unlikely because of the dependence of image quality on image exposure and on noise. Rather than a single unitary measure, a function will result. It is agreed that the function should be based on image signal-to-noise ratio but that integral measures such as MTF_A may not result in the most useful form.

We currently favor the threshold resolution approach. An image quality measure such as MTF_A may show the relative "goodness" of two systems but the measure cannot be used to predict system performance in

the field. Threshold resolution incorporates all of the system parameters including image exposure time, light level, image stability, sensitivity, photoconversion noise, system generated noises, MTF and etc. Also, it can be used directly to estimate field performance -- at least on a first cut basis. The previous complaint was that threshold resolution only applied to periodic bar patterns. The balanced resolution concept which has been discussed at some length in Section 2 circumvents this difficulty since it includes aperiodic objects. However, the method of weighing the aperiodic and periodic resolutions remain as an issue. We note that Schade's balanced resolution concept includes dynamic range (grey shades) which has not been included in the discussion of Section 2.

REFERENCES

1. Rosell, F. A., and Willson, R. H., "Performance Synthesis-Electro-Optical Sensors," Tech. Rept. No. AFAL-TR-71-137, Air Force Avionics Laboratory, WPAFB, Ohio, May 1971.
2. Rosell, F. A., and Willson, R. H., "Performance Synthesis-Electro-Optical Sensors," Tech. Rept. No. AFAL-TR-72-229, Air Force Avionics Laboratory, WPAFB, Ohio, August 1972.
3. Johnson, J., "Analysis of Image Forming System," Image Intensifier Symposium, Ft. Belvoir, Va., AD220 160, October 1958.
4. Schade, O. Sr., "Resolving Power Functions and Integrals of High Definition Television and Photographic Cameras--A New Concept of Image Evaluation," RCA Review, Vol. 32, December 1971.
5. Middleton, W. E. K., "Vision Through the Atmosphere," University of Toronto Press, Canada 1952.
6. Levi, I., "Motion Blurring with Decaying Detector Response," Applied Optics, Vol. 10, No. 1, Jan. 1971.
7. DeVries, H. L., Physica X, No. 7, July 1943.
8. Goodman, J. W., "Introduction to Fourier Optics," McGraw-Hill, 1968.
9. Eiberman, et. al., "Preception of Displayed Information," Plenum Press, 1973.
10. Perrin, F. H., "Methods of Appraising Photographic Systems," Part 1, SMPTE, Vol. 69, March 1960.

UNCLASSIFIED

Security Classification

DOCUMENT CONTROL DATA - R&D		
(Security classification of title, body of abstract and indexing annotation must be entered when the overall report is classified)		
1 ORIGINATING ACTIVITY (Corporate author) Westinghouse Defense and Space Center Aerospace Division, Baltimore, Maryland		2a REPORT SECURITY CLASSIFICATION Unclassified
		2b GROUP None
3 REPORT TITLE Performance Synthesis of Electro-Optical Sensors		
4 DESCRIPTIVE NOTES (Type of report and inclusive dates) Final Report		
5 AUTHOR(S) (Last name, first name, initial) Rosell, Frederick A. Willson, Robert H.		
6 REPORT DATE July 1973	7a. TOTAL NO OF PAGES 180	7b. NO. OF REFS 10
8a. CONTRACT OR GRANT NO. F33615-70C-1461	9a. ORIGINATOR'S REPORT NUMBER(S)	
b. PROJECT NO 698DF	9b. OTHER REPORT NO(S) (Any other numbers that may be assigned this report) AFAL-TR-73-260	
c.		
d.		
10 AVAILABILITY/LIMITATION NOTICES Distribution limited to United States government agencies only; test and evaluation; 31 August 1973. Other requests for this document must be referred to Air Force Avionics Laboratory (NVA-698DF), Wright-Patterson Air Force Base, Ohio 45433.		
11 SUPPLEMENTARY NOTES		12. SPONSORING MILITARY ACTIVITY Air Force Avionics Laboratories Wright-Patterson AFB, Ohio 45433
13 ABSTRACT <p>This effort is a continuation of the Performance Synthesis Study (Electro-Optical Sensors) reported in Technical Report AFAL-TR-72-229, dated August 1972. Analytical models were further developed and refined to include image motion and aperturing effects. Psychophysical experiments were performed as tests of the theories and it was found that the theory is reasonably accurate. A concept of balanced resolution is discussed which combines a system's performance for both aperiodic and periodic imagery. The question of a single figure of merit for a system is also discussed.</p>		

DD FORM 1473
JAN 64

UNCLASSIFIED

Security Classification

UNCLASSIFIED

Security Classification

14. KEY WORDS	LINK A		LINK B		LINK C	
	ROLE	WT	ROLE	WT	ROLE	WT
Synthesis						
698DF						
Low-Light-Level Television						
Model						
Range						
Electro-Optics						
Sensors						
Video						
Perception						
Vision						
Signal-to-Noise Ratio Display						
Motion						
Apertures						

UNCLASSIFIED

Security Classification